

# UC Berkeley

## UC Berkeley Electronic Theses and Dissertations

### Title

Synthesis and reactivity of reduced niobium imido complexes

### Permalink

<https://escholarship.org/uc/item/7423j648>

### Author

Gianetti, Thomas Lucien

### Publication Date

2014

Peer reviewed|Thesis/dissertation

# Synthesis and Reactivity of Reduced Niobium Imido Complexes

By

Thomas Lucien Gianetti

A dissertation submitted in partial satisfaction of the requirements  
for the degree of Doctor of Philosophy  
in  
CHEMISTRY  
in  
the Graduate Division  
of the  
University of California, Berkeley

Committee in charge:  
Professor John Arnold, Chair  
Professor Robert G. Bergman  
Professor Christopher D. Vulpe

Spring 2014



## Abstract

# Synthesis and Reactivity of Reduced Niobium Imido Complexes

By

Thomas Lucien Gianetti  
Doctor of Philosophy in Chemistry  
University of California, Berkeley  
Professor John Arnold, Chair

**Chapter I.** The discovery of a Nb(III)-mediated catalytic hydrogenation of internal alkynes to *Z*-alkenes is reported and found to proceed through an unprecedented mechanism. The mechanistic proposal involves initial reduction of the alkyne by the Nb(III) complex (BDI)Nb(N<sup>t</sup>Bu)(CO)<sub>2</sub> to provide a Nb(V) metallacyclopropene, itself capable of  $\sigma$ -bond metathesis reactivity with H<sub>2</sub>. The resulting alkenyl hydride species then undergoes reductive elimination to provide the *Z*-alkene product and regenerate a metal complex in the Nb(III) oxidation state. Support for the proposed mechanism is derived from *i*) the dependence of product selectivity on the relative concentrations of CO and H<sub>2</sub>, *ii*) the isolation of complexes closely related to those proposed to lie on the catalytic cycle, *iii*) H/D crossover experiments, and *iv*) DFT studies on multiple possible reaction pathways.

**Chapter II.** Monometallic niobium arene complexes [Nb(BDI)(N<sup>t</sup>Bu)(R-C<sub>6</sub>H<sub>5</sub>)] (R = H and Me, BDI = N,N'-diisopropylbenzene- $\beta$ -diketiminate) were synthesized and were found to slowly convert into the dinobium inverted arene sandwich complexes [[(BDI)Nb(N<sup>t</sup>Bu)]<sub>2</sub>( $\mu$ -RC<sub>6</sub>H<sub>5</sub>)] (R = H and Me) in solution. The kinetics of this reaction were followed by <sup>1</sup>H NMR spectroscopy, and is in agreement with a dissociative mechanism. These compounds showed a lack of reactivity towards small molecules – even at elevated temperatures – which is unusual in the chemistry of inverted sandwich complexes. However, protonation of the BDI ligands occurred readily on treatment with [H(OEt<sub>2</sub>)] [B(C<sub>6</sub>F<sub>5</sub>)<sub>4</sub>], resulting in the mono-protonated cationic inverted sandwich complex [[(BDI<sup>#</sup>)Nb(N<sup>t</sup>Bu)][(BDI)Nb(N<sup>t</sup>Bu)]( $\mu$ -C<sub>6</sub>H<sub>5</sub>)] [B(C<sub>6</sub>F<sub>5</sub>)<sub>4</sub>] and the dicationic complex [[(BDI<sup>#</sup>)Nb(N<sup>t</sup>Bu)]<sub>2</sub>( $\mu$ -RC<sub>6</sub>H<sub>5</sub>)] [B(C<sub>6</sub>F<sub>5</sub>)<sub>4</sub>]<sub>2</sub> (BDI<sup>#</sup> = (ArNC(Me))<sub>2</sub>CH<sub>2</sub>). NMR and UV-vis spectroscopies were used to characterize this unique series of diamagnetic molecules as a means of determining how best to describe the Nb–arene interactions. The X-ray crystal structures, UV-visible spectra, arene <sup>1</sup>H NMR chemical shifts and large *J*<sub>CH</sub> coupling constants provide evidence for donation of electron density from the Nb d-orbitals into the antibonding  $\pi$  system of the arene ligands. However, the lack of sp<sup>3</sup> hybridization of the arene carbon indicate that the Nb→arene donation is not accompanied by an increase in formal oxidation state, and suggest that 4d<sup>2</sup> electronic configurations are appropriate to describe the Nb atoms in all four complexes.

**Chapter III.** Inverted sandwich complexes have seen interesting recent developments both in the nature of their bonding and in their use as chemical reactants. Although discussions concerning the electronic delocalization lend credit to their use as potential electronic and spintronic devices, mixed valent inverted sandwich complexes are rarely reported. We show in this work that the selective single electron oxidation of a neutral

benzene inverted sandwich complex of niobium leads to an isolable cationic mixed valent benzene inverted sandwich complex. The latter complex shows unique structural features elucidated through studies with an arsenal of physical methods, including cyclic voltammetry,  $^1\text{H}$  NMR, UV-Vis, magnetism, EPR spectroscopies, in addition to DFT calculations. These analyses indicate that although delocalization is allowed over the benzene ring from both niobium atoms, the single electron is unequally shared between the two metal centres. Under certain conditions, this complex reforms the neutral benzene complex along with a highly reactive Nb(IV) species, which is of great interest for potential chemical reactivity.

**Chapter IV.** All three C-F bonds in  $\text{CF}_3$ -substituted arenes are activated by a niobium imido complex, driven by the formation of strong Nb-F bonds. The mechanism of this transformation was studied by NMR spectroscopy which revealed the involvement of Nb(III). Attempts to extend this chemistry to non-aromatic  $\text{CF}_3$  groups led to intramolecular reactivity. The mechanism of activation of C-F bonds in fluoroarenes using a well-defined niobium (III) imido complex has been investigated.

**Chapter V.** The Nb(III) arene species  $[\text{BDI}]\text{Nb}(\text{N}^t\text{Bu})(\eta^6\text{-C}_6\text{H}_6)$ , (BDI =  $\beta$ -diketimate), reacts stoichiometrically with fluoroarenes to yield niobium (V) aryl fluorides. Spectroscopic analysis supported by DFT calculations revealed the critical involvement of a Nb(III) fluoroarene-bound species. In contrast to previous reports of related reactivity, we found that perfluorinated arenes (i.e. those normally assumed to bear more ‘activated’ C-F bonds) are, in the present system, much less reactive towards C-F bond cleavage than mono- or difluoro-substituted arenes. In addition to demonstrating stoichiometric hydrodefluorination reactions, we also describe an efficient and mild hydrodefluorination of mono- and di-fluoroarenes that is catalytic in niobium.

# Synthesis and Reactivity of Reduced Niobium Imido Complexes

## Table of Contents

<b>Acknowledgments</b>	<b>iii</b>
<b>Curriculum Vitae</b>	<b>v</b>
<b>Chapter I. Z-selective, Catalytic, Internal-Alkyne Semi-Hydrogenation under H<sub>2</sub>:CO Mixtures by a Niobium(III) Imido Complex</b>	<b>1</b>
Introduction	2
Results and Discussions	3
Conclusions	10
Experimental	10
References	17
<b>Chapter II. Diniobium Inverted Sandwich Complexes with <math>\mu</math>-<math>\eta^6</math>:<math>\eta^6</math>-arene Ligands: Synthesis, Kinetics of Formation, and Electronic Structure</b>	<b>20</b>
Introduction	21
Results and Discussions	22
Conclusions	37
Experimental	37
References	48
<b>Chapter III. Synthesis, Electronic Structure and Reactivity of a Mixed-Valence Benzene Inverted-Sandwich Diniobium Complex</b>	<b>51</b>
Introduction	52
Results and Discussions	53
Conclusions	66
Experimental	66
References	74
<b>Chapter IV. Dis-assembly of a Benzylic CF<sub>3</sub> Group Mediated by a Niobium (III) Imido Complex</b>	<b>77</b>
Introduction	78
Results and Discussions	78
Conclusions	89
Experimental	89

References	96
<b>Chapter V. Carbon-Fluorine Bond Cleavage in Fluoroarenes via a Niobium (III) Imido Complex: From Stoichiometric to Catalytic Hydrodefluorination</b>	<b>98</b>
Introduction	99
Results and Discussions	100
Conclusions	116
Experimental	116
References	126
<b>Appendix A. DFT Calculation for Chapter I</b>	<b>130</b>
<b>Appendix B. Stoichiometric Carbon-Carbon Bond Formation Mediated by Well-defined Nb(III) Complexes</b>	<b>141</b>
Introduction	142
Results and Discussions	142
Conclusions	147
Experimental	148
References	152
<b>Appendix C. DFT Calculation for Chapter IV and V</b>	<b>154</b>

## Acknowledgements

First and foremost, I would like to thank my advisors, John Arnold and Bob Bergman, for their direction through graduate school. I have learned such a great deal from each of you about the world of chemistry. The contribution of your respective methods and demeanors to my intellectual development has been untold.

Apart from the advisors, their administrative assistants Rain Simar and Anneke Runtupalit deserve special mention. I will always appreciate how both Rain and Anneke seemed ever ready with a smile and words of encouragement. Their good nature was always a welcome sight.

None of this work would have been possible without a great number of other staff at the college of chemistry. In particular, I would also like to acknowledge the crystallographers who have guided me through problems big and small: Dr. Antonio DiPasquale. Their expertise and patience made a significant portion of this work possible. I would also like to acknowledge my collaborators, Drs Gregory Nocton, Stefan G. Minasian, Neil C. Tomson, David K. Shuh, Tolek Tyliczyczak, A. L. David Kilcoyne, and Stosh A. Kozimor.

On a personal level, I have been fortunate to become friends with a number of talented, engaging and kind individuals. Pete LaPierre, my original labmate and a good friend, set an example of dedication to his work that was inspiring. Ashleigh Ward, Dan Kallenberger and Heather Buckley whom joined the Arnold group the same year than I did, were of great support, especially during my first year. Ben Kriegel, Drs Andreas Obenhuber and Clement Camp. Finally, I would like to acknowledged all the bright undergraduate students that I have been fortunate to mentor and who made my work go significantly faster, Mark Abubekеров, Xavier Berrebi, Leonard Eymann, and Michael Nechayev. Thank you all, and to those I've failed to mention – my apologies, but thank you, too.

Beyond these people, a great many others made the day-to-day of graduate school enjoyable, fruitful, and challenging. In particular, my roommates Andre Carrel and Sebastian Guerrero, whom were always available to enjoy a beer and relaxing time after a long day at work.

Finally, I would be remiss to not mention the unending support of my parents, Antoine Gianetti and Nicole Marciano, my sister Audrey Gianetti and my best friend Remi Cossu. A thousand thank you's for all of your love, encouragement and support. This one's for you. "Je vous aime".



## Curriculum Vitae

### Thomas Lucien Gianetti

---

#### Education

*Ph.D. Inorganic Chemistry*- **University of California**, Berkeley, CA **2009 – 2014**  
*B.S. and M.S. in Chemistry* -**CPE Lyon**, Lyon, France **2003 – 2009**

#### Research Experience

**University of California, Berkeley**, Berkeley CA, USA

*Graduate Student Researcher* **2009 – 2014**

- *Advisors:* Professors John Arnold and Robert G. Bergman
- *Thesis:* “Low valent niobium imido complexes supported by  $\beta$ -diketiminato ligand: toward making and breaking bonds”

*Visiting Scholar* **2008 – 2009**

- *Advisor:* Prof. T. Don Tilley
- *Master thesis:* “Developing synthesis route in order to access  $O=V[OTi(OR)_3]_3$ ”

**Johnson Matthey Catalyst**, Middlesborough, UK.

*Laboratory Technician* **2007 – 2008**

- *Advisor:* Dr. Calum McIntosh
- *Internship thesis:* “Catalyst design for polymerization of PolyEtheleneTerephatalete (PET)”

**IRCE /CNRS, CPE Lyon**, Lyon, France

*Undergraduate Student Researcher* **2006 – 2007**

- *Advisors:* Dr. Christophe Coperet and Dr. Henry Chermett
- *Bachelor thesis:* “Computational analysis of zirconium active site in heterogeneous catalytic hydrogenation of ketones”

#### Publications

10. **Gianetti, T. L.**; Bergman, R. G.; Arnold, J. “Stoichiometric carbon-carbon bond formation mediated by well defined Nb(III) complexes.” *Manuscript accepted, invited issue in Polyhedron*.

9. Arnold, J.; **Gianetti, T. L.**; Kastan, Y. “Thorium lends a fiery hand” *Nat. Chem.* **2014**, 6, 2.

8. **Gianetti, T. L.**; Bergman, R. G.; Arnold, J. “Carbon-Fluorine Bond Cleavage in Fluoroarenes via a Niobium (III) Imido Complex: From Stoichiometric to Catalytic Hydrodefluorination.” *Chem. Science* **2014**, DOI: 10.1039/c4sc00006d.

7. Obenhuber, A.; **Gianetti, T. L.**; Berrebi, X.; Bergman, R. G.; Arnold, J. “Reactivity Study of Organic Azides on Reversing NacNac Cleavage in a Bis(Imido) Nb(V) Complex: Azide Activation via “hidden  $d^2$ -Niobium” Species” *J. Am. Chem. Soc.* **2014**, 136, 2994.

6. **Gianetti, T. L.**; La Pierre, H. S.; Arnold, J. “Group 5 Imides and Bis(imide)s as Selective Hydrogenation Catalysts.” *Eur. J. Inorg. Chem.* **2013**, 22-23, 3771.

5. **Gianetti, T. L.**; Bergman, R. G.; Arnold, J. “Dis-assembly of Benzylic CF<sub>3</sub> group mediated by a Niobium (III) Imido Complex.” *J. Am. Chem. Soc.* **2013**, *135*, 8145.
4. **Gianetti, T. L.**; Nocton, G.; Minasian, S. G.; Tomson, N. C.; Kilcoyne, A. L. D.; Kozimor, S. A.; Shuh, D. K.; Tylliszczak, T.; Bergman, R. G.; Arnold, J. “Diniobium Inverted Sandwich Complexes with m-h<sup>6</sup>:h<sup>6</sup>-Arene Ligands: Synthesis, Kinetics of Formation, and Electronic Structure.” *J. Am. Chem. Soc.* **2013**, *135*, 3224.
3. Abubekerov, M.; **Gianetti, T. L.**; Arnold, J. “Synthesis and Characterization of Coordinatively Unsaturated Nickel (II) and Manganese (II) Alkyl Complexes Supported by the Hydrotris (3-phenyl-5-methylpyrazolyl) borate (Tp<sup>Ph,Me</sup>) Ligand.” *Dalton Trans.* **2013**, *42*, 10525.
2. Kunishita, A.; **Gianetti, T. L.**; Arnold, J. “Structures, Physicochemical Properties, and Reactivities of Cobalt(II) Complexes Supported by a Homoscorpionate (Tris(pyrazolyl)borate) Ligand Tp<sup>Ph,Me</sup>.” *Organometallics* **2012**, *31*, 372.
1. **Gianetti, T. L.**; Tomson, N. C.; Arnold, J.; Bergman, R. G. “Z-Selective, Catalytic Internal Alkyne Semihydrogenation under H<sub>2</sub>/ CO Mixtures by a Niobium(III) Imido Complex” *J. Am. Chem. Soc.* **2011**, *133*, 14904.

## Manuscript

4. **Gianetti, T. L.**; Nocton, G.; Minasian, S. G.; Kaltzoyannis, N.; Kilcoyne, A. L. D.; Kozimor, S. A.; Shuh, D. K.; Tylliszczak, T.; Bergman, R. G.; Arnold, J. “Synthesis of a Mixed Valence  $\mu$ - $\eta^2$ : $\eta^4$ -Benzene Diniobium Inverted Sandwich Complexes Nb(III)/Nb(IV).” **manuscript in preparation** intended to *Nat. Chem.*
3. Nechayev, M.; Kriegel, B.; **Gianetti, T. L.**; Bergman, R. G.; Arnold, J. “Halo, Alkyl, Aryl Complexes of Niobium Supported by the  $\beta$ -Diketiminato Ligand”. **manuscript in preparation** invited issue in *Inorg. Chim. Acta*
2. Obenhuber, A.; **Gianetti, T. L.**; Bergman, R. G.; Arnold, J. “Regioselective [2+2] and [4+2] Cycloaddition Reactivity in an asymmetric Niobium(bis-imido) Moiety towards Unsaturated Organic Molecules” **manuscript in preparation** intended to *Chem. Comm.*
1. Abubekerov, M.; **Gianetti, T. L.**; Eymann, L.; Arnold, J. “Insertion of Unsaturated Small Molecule into a Coordinatively Unsaturated Nickel (II) Alkyl Complexes Supported by the Hydrotris (3-phenyl-5-methylpyrazolyl) borate (Tp<sup>Ph,Me</sup>) Ligand.” **manuscript in preparation** intended to *Organometallics*

## Presentations

3. “Niobium-mediated disassembly of benzylic CF<sub>3</sub> groups”. Presentation at the ACS international conference, Dallas, TX, USA, **2014**. Paper ID: 20773.
2. “Synthesis and electronic structure of diamagnetic  $\mu$ - $\eta^6$ : $\eta^6$ -arene diniobium inverted sandwich complexes”. Presentation at the ACS international conference, New Orleans, LA, USA, **2013**. Paper ID: 23311
1. “Z-selective, catalytic, internal-alkyne semihydrogenation under H<sub>2</sub>:CO mixtures by a niobium(III) imido complex”. Presentation at the ACS international conference, San Diego, CA, USA, **2012**. Paper ID: 19533.

## **Award and Distinctions**

### **Outstanding Graduate Student Instructor Award**

**Spring 2012**

Department of Chemistry, University of California, Berkeley, CA, USA

### **Howard W. Crandall Fellowship**

**Spring 2010**

Department of Chemistry, University of California, Berkeley, CA, USA

### **Glaxo Smith Klein Organic Synthesis Award**

**Spring 2007**

Department of Chemistry and Chemical Engineering, CPE Lyon, Lyon, France

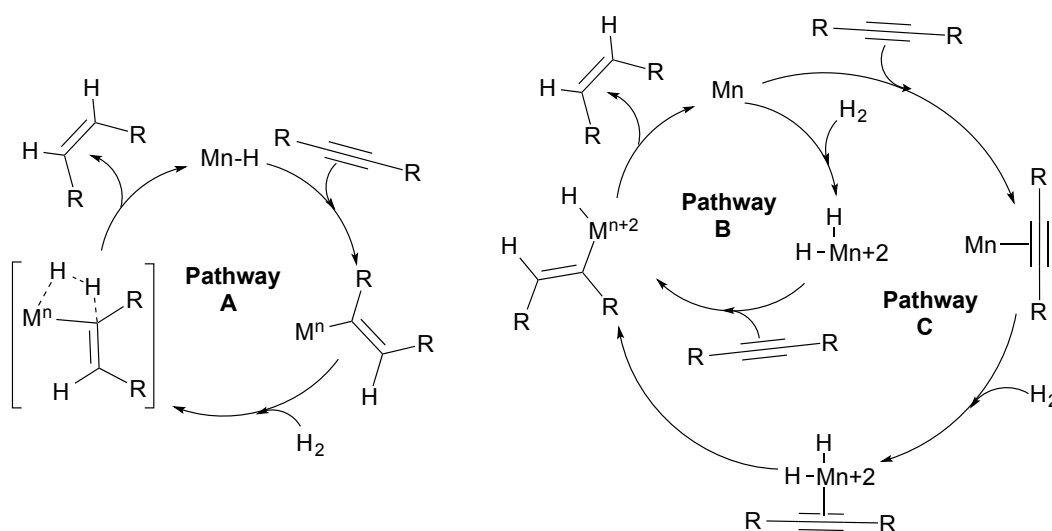
## **Chapter I**

# **Z-selective, Catalytic, Internal-Alkyne Semi-Hydrogenation under H<sub>2</sub>:CO Mixtures by a Niobium(III) Imido Complex**

## Introduction

Homogeneous hydrogenation reactions catalyzed by transition metal complexes are some of the most extensively studied in organometallic chemistry. Many of these systems operate via one of two common mechanisms, namely the monohydride and dihydride mechanisms shown in Scheme 1.1.<sup>1</sup> The development of new catalysts able to access alternative hydrogenation pathways constitutes an attractive area of research for discovering reagents capable of providing control over selectivity and substrate scope. The selective conversion of alkynes to *Z*-alkenes, typically accomplished by the heterogeneous Lindlar's catalyst,<sup>2</sup> is difficult to achieve due to *E/Z* isomerization and over-hydrogenation.<sup>1-3</sup> The development of effective molecular catalysts for this transformation remains an area of intense study with recent notable successes.<sup>1,4</sup> Here we report the mechanistic investigation of a selective semihydrogenation reaction catalyzed by a  $d^2$  transition metal under a mixture of  $H_2$  and CO. Considering that most of the hydrogen produced industrially must be separated from CO, the lack of hydroformylation reactivity of the catalyst presented herein constitutes an interesting step in designing effective hydrogenation catalysts that are able to function in the presence of unpurified syngas.<sup>5</sup>

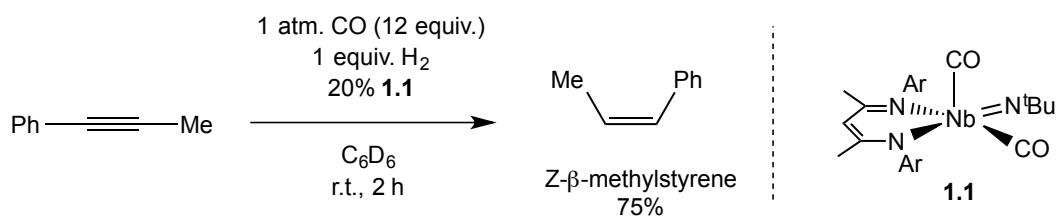
Many low valent early transition metals, such as  $d^2$  metal complexes, are known to oxidatively couple alkynes to form metallacyclopentadiene species.<sup>3,6</sup> Because of this reactivity, the use of  $d^2$  transition metal complexes as hydrogenation catalysts is rare.<sup>7</sup> Only one  $d^2$  system, reported by Boncella *et al.*, efficiently catalyzes hydrogenation of an unsaturated substrate (internal alkene),<sup>8</sup> but the mechanism of this  $d^2$  molybdenum imido-catalyzed reaction has not been reported. We have recently shown that treatment of the Nb(III) dicarbonyl complex (BDI)Nb(N<sup>t</sup>Bu)(CO)<sub>2</sub> (**1.1**) with 1-phenyl-1-propyne does not result in alkyne-alkyne coupling but instead yields the metallacyclopropene complex (BDI)Nb(N<sup>t</sup>Bu)( $\eta^2$ -MeC $\equiv$ CPh)(CO) (**1.2**).<sup>9</sup> Acidification of the alkyne adduct in methanol led to the formation of *Z/E*- $\beta$ -methylstyrene along with the starting alkyne in a 2 : 1 ratio. The formation of  $\beta$ -methylstyrene focused our attention on the potential use of (BDI)Nb(N<sup>t</sup>Bu)(CO)<sub>2</sub> as a hydrogenation catalyst.



**Scheme 1.1** Monohydride (path A) and dihydride mechanisms (path B and C).

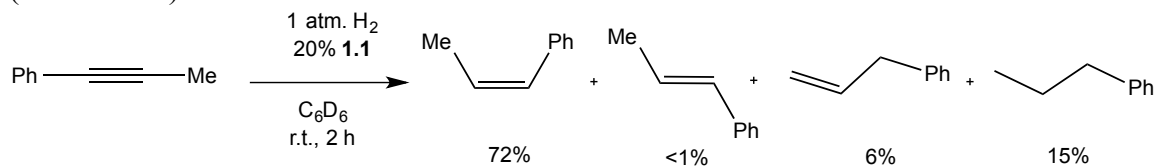
## Results and discussions

**Hydrogenation of 1-phenyl-1-propyne.** Catalytic hydrogenation of 1-phenyl-1-propyne to *Z*- $\beta$ -methylstyrene (2 h, 1.0 equiv. H<sub>2</sub>, 75% yield) was achieved in the presence of **1.1** (20 mol %) and an excess of CO (12 equiv.) in benzene at room temperature (Scheme 1.2). Increasing the H<sub>2</sub>-loading to 3.0 equiv led to a marginal increase in the yield of *Z*- $\beta$ -methylstyrene (85%) and produced trace amounts of *n*-propyl-benzene (<sup>*n*</sup>PrPh, 3%). Higher CO loadings (40 equiv.) led to a drop in catalytic activity but no decrease in selectivity, providing *Z*- $\beta$ -methylstyrene in 45% yield after 2 h. Previous reports of both CO-exchange on (BDI)Nb(N<sup>*t*</sup>Bu)(CO)<sub>2</sub> (**1.1**) and the isolation of the *tris*(isocyanide)Nb(III) complex (BDI)Nb(N<sup>*t*</sup>Bu)(CNXyl)<sub>3</sub> (Xyl = 2,6-Me<sub>2</sub>-C<sub>6</sub>H<sub>3</sub>) suggest that higher CO-loadings result in the formation of the electronically- and coordinatively-saturated tricarbonyl complex (BDI)Nb(N<sup>*t*</sup>Bu)(CO)<sub>3</sub>.



**Scheme 1.2** Hydrogenation of 1-phenyl-1-propyne with 0.2 equiv of [Nb] under H<sub>2</sub>/CO atmosphere (1:12 ratio).

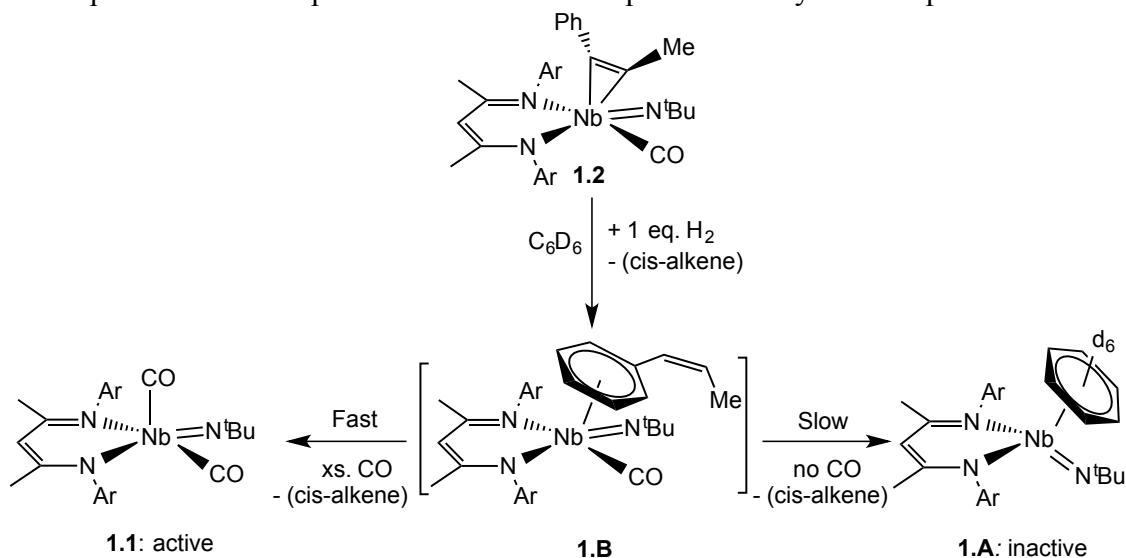
Decreasing the CO loading also resulted in lower yields of *Z*- $\beta$ -methylstyrene (*ca.* 12%) but concurrently led to the formation of both <sup>*n*</sup>PrPh (*ca.* 16%) and allylbenzene (*ca.* 6%) (Scheme 1.3).



**Scheme 1.3** Hydrogenation of 1-phenyl-1-propyne with 0.2 equiv of **1.1** under 1 atmosphere of H<sub>2</sub>.

Under these conditions, <sup>1</sup>H NMR spectroscopic monitoring of the reaction mixture indicated that the catalytic activity stops after 2 h, at which time the metal complex had converted into a new, catalytically inactive species, complex **1.A**. Analysis by <sup>1</sup>H and <sup>2</sup>H NMR spectroscopy led to the assignment of **1.A** as a C<sub>6</sub>D<sub>6</sub>-coordinated complex (Scheme 1.4), based in part on the presence of a characteristic singlet at 3.7 ppm in the <sup>2</sup>H NMR spectrum. A related  $\eta^6$ -arene Mo complex was observed by Boncella and co-workers.<sup>8</sup> Over the course of the reaction leading to **1.A**, another intermediate complex **1.B** was also observed. The latter species displays three resonances with a 1 : 2 : 2 ratio between 3.6 – 4.1 ppm. This pattern is consistent with a mono-substituted arene ligand bound to the metal center; **1.B** was therefore assigned to a product-catalyst- $\pi$ -complex (Scheme 1.4), similar to **1.A**. The presence of this  $\eta^6$ -arene intermediate in hydrogenation mechanisms is not unusual and has been observed with several catalysts.<sup>7-8,10</sup> Separate experiments have shown that treatment of (BDI)Nb(N<sup>*t*</sup>Bu)(CO)<sub>2</sub> with *Z*- $\beta$ -methylstyrene provides no observable reaction;

thus, the excess CO required for efficient catalysis may be needed to drive catalyst turnover *via* displacement of the product alkene from the product-catalyst- $\pi$ -complex.



**Scheme 1.4** Role of CO to maintain a high reactivity and selectivity

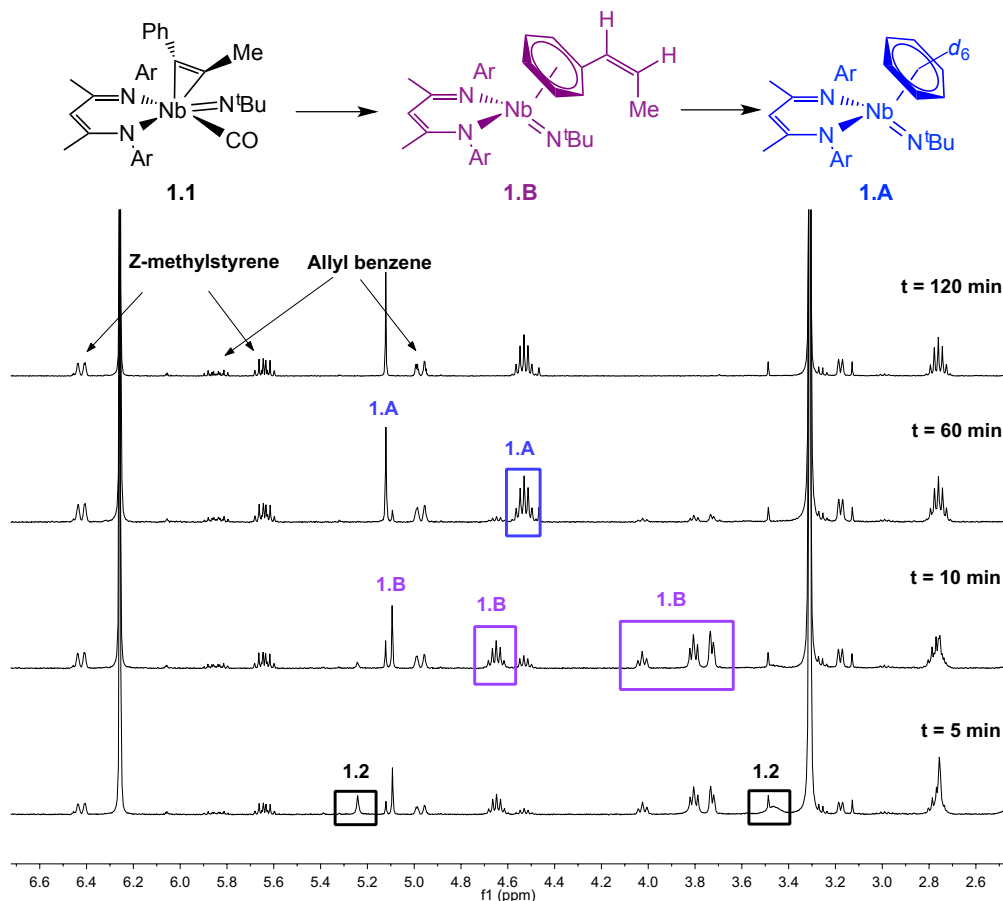
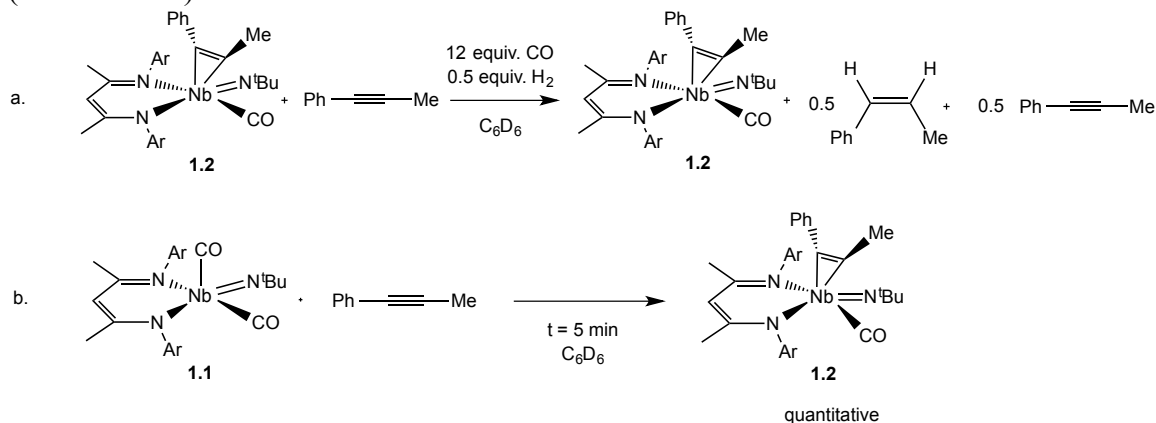


**Figure 1.1**  $^1\text{H}$  NMR spectra of hydrogenation reaction in absence of CO, which shows the lack of selective in the product distribution and the conversion of the metal center into a new species.

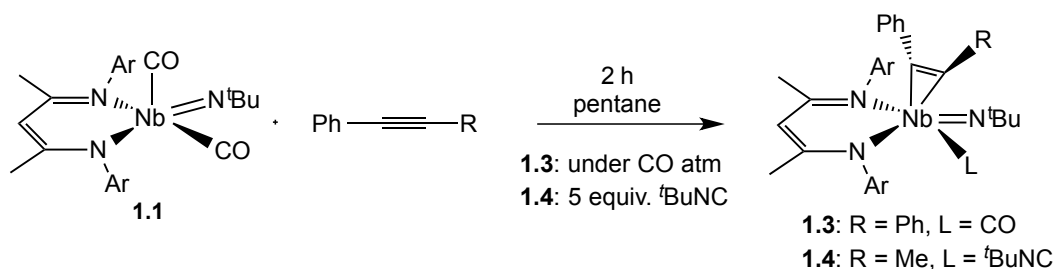
**Mechanistic Study.** Monitoring the course of the most-selective and highest-yielding catalytic reaction (12 : 1 ratio of CO : H<sub>2</sub>) by NMR spectroscopy allowed us to observe that the metallacyclopropene complex maintained a constant concentration, suggesting this complex is the resting state of the catalytic cycle. A half turnover experiment supports this hypothesis, whereby the treatment of **1.2** with 1.0 equiv. of alkyne and 0.5 equiv. of H<sub>2</sub> results in 0.5 equiv. of *Z*- $\beta$ -methylstyrene, 0.5 equiv. of alkyne and 1.0 equiv. of **1.2** (Scheme 1.5a). We note that the formation of **1.2** from the treatment of **1.1** with 1-phenyl-1-propyne is rapid within the concentration range used during catalysis and that complex **1.2** is the only transition metal-containing species observed in solution during the course of the reaction (Scheme 1.5b).



**Scheme 1.5**

Obtaining structural information on **1.2** was hampered by its thermal instability, but closely-related analogues were isolable. The treatment of (BDI)Nb(N<sup>t</sup>Bu)(CO)<sub>2</sub> with 1,2-diphenylacetylene yielded the metallacyclopropene complex **1.3** (BDI)Nb(N<sup>t</sup>Bu)( $\eta^2$ -PhC≡CPh)(CO) in 71% yield (Scheme 1.6). The higher  $\nu_{\text{CO}}$  absorption frequency for **1.3** ( $\nu_{\text{CO } 1.3} = 2052 \text{ cm}^{-1}$ ) compared to that of (BDI)Nb(N<sup>t</sup>Bu)( $\eta^2$ -PhC≡CMe)(CO) ( $\nu_{\text{CO } 1.2} = 2039 \text{ cm}^{-1}$ ) correlates with the  $\pi$ -acidity of the two alkynes, but the high  $\nu_{\text{CO}}$  for both complexes (free CO:  $\nu_{\text{CO}} = 2143 \text{ cm}^{-1}$ ) suggests little  $\pi$ -backbonding from the metal into the  $\pi^*$  orbitals of CO, consistent with a high oxidation state at the metal center. Complexes **1.2** and **1.4** comprise two of the few examples of CO coordinated to a formally  $d^0$  group 5 transition metal complex.<sup>11</sup> Substitution of the CO on (BDI)Nb(N<sup>t</sup>Bu)( $\eta^2$ -PhC≡CMe)(CO) by the more  $\sigma$ -donating ligand <sup>t</sup>BuNC yielded the thermally-stable complex (BDI)Nb(N<sup>t</sup>Bu)( $\eta^2$ -PhC≡CMe)(CN<sup>t</sup>Bu) (**1.4**, Scheme 1.6) in 52% yield. Similar to complex **1.1**, weak-to-non-existent  $\pi$ -back donation from the metal to the isocyanide in **1.4** was indicated by IR spectroscopy ( $\nu_{\text{CN } 1.4} = 2167 \text{ cm}^{-1}$ ,  $\nu_{\text{CN}}(\text{free } ^t\text{BuCN}) = 2125 \text{ cm}^{-1}$ ). The crystal structures of **1.3** and **1.4** exhibit distorted square-based pyramidal geometries (Figure 1.2,  $\tau_{1.3} = 0.32$  and  $\tau_{1.4} = 0.33$ ).<sup>12</sup> In both structures the C<sub>1</sub>-C<sub>2</sub> bond lengths of the metallacyclopropene unit show significant elongation from those of the uncoordinated alkyne to values consistent with C-C double bonds (C<sub>1</sub>-C<sub>2</sub>(**1.3**): 1.308(4) Å and C<sub>1</sub>-C<sub>2</sub>(**1.4**): 1.309(3) Å, C(sp<sup>2</sup>)-C(sp<sup>2</sup>): 1.31-1.34 Å).<sup>13</sup> The Nb-C distances (Nb-C<sub>1</sub>(**1.3**): 2.144(3) Å, Nb-C<sub>2</sub>(**1.3**): 2.175(3) Å; Nb-C<sub>1</sub>(**1.4**): 2.144(2) Å, Nb-C<sub>2</sub>(**1.4**): 2.143(2) Å) are within the range of Nb(V)-C(alkyl) bonds reported previously.<sup>14</sup> Because both complexes **1.3** and **1.4** exhibit considerable metallacyclopropene-Nb(V) character, the oxidative addition of H<sub>2</sub> to such formally oxidized complexes (**1.2**, **1.3** and **1.4**) is unlikely.





**Scheme 1.6** Synthesis of complexes **1.3** and **1.4**.

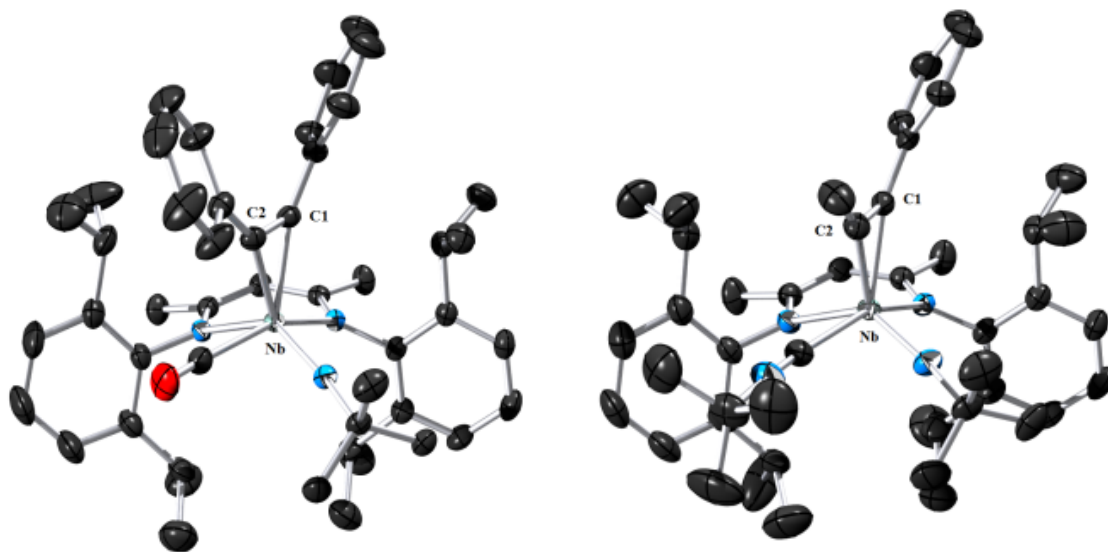
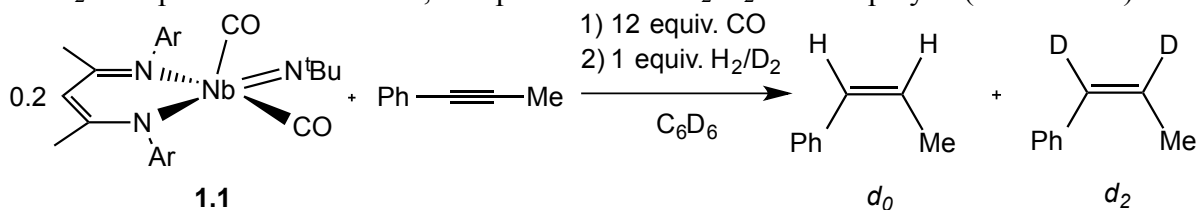


**Figure 1.2** Molecular structure of **1.3** (left) and **1.4** (right) determined by single crystal X-ray diffraction study. The hydrogen atoms were omitted for clarity; the thermal ellipsoids are 50% probability level.

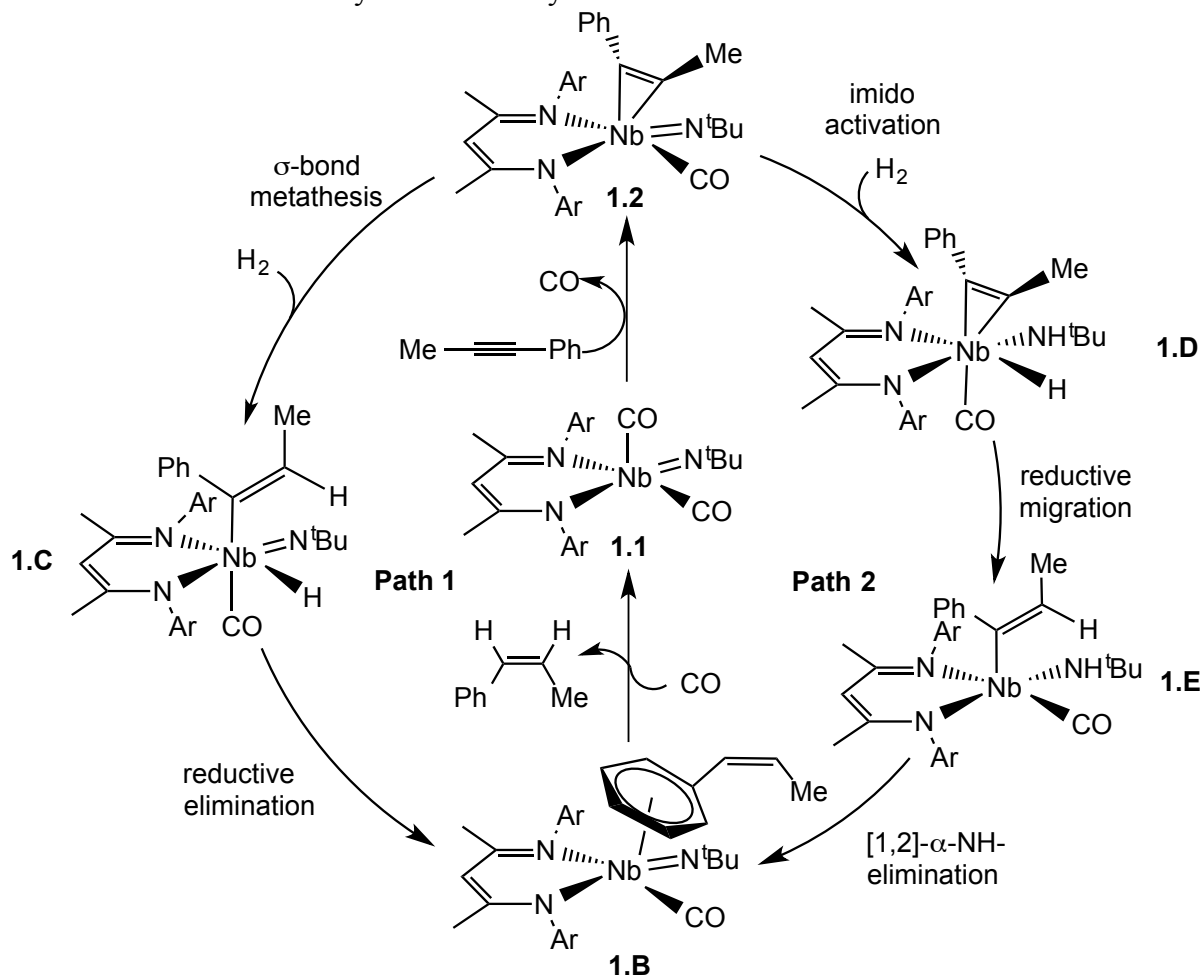
Performing the hydrogenation reaction with mixtures of  $\text{H}_2$  and  $\text{D}_2$  under the conditions found to exclusively produce *Z*- $\beta$ -methylstyrene (12 : 1 ratio of  $\text{CO} : \text{H}_2$ ) revealed that only the  $d_0$ - and  $d_2$ -isotopomers were formed, irrespective of the  $\text{H}_2:\text{D}_2$  ratio employed (Scheme 1.7).



**Scheme 1.7** Crossover experiment with a 1 : 1 mixture of  $\text{H}_2 : \text{D}_2$ .

This finding is consistent with a mechanism that involves the hydrogenation of one molecule of alkyne by one molecule of dihydrogen. This contrasts with many early-metal hydrogenation mechanisms (Scheme 1.1, path A) in which two separate molecules of  $\text{H}_2$  formally provide one hydrogen atom a piece when reducing an unsaturated hydrocarbon by one bond order. The mechanisms for late-metal-mediated hydrogenation reactions typically involve oxidative addition of  $\text{H}_2$  to the metal center (Scheme 1.1, path B and C). While  $(\text{BDI})\text{Nb}(\text{N}^t\text{Bu})(\text{CO})_2$  appears to serve as a catalyst for the formation of HD from mixtures of  $\text{H}_2$  and  $\text{D}_2$  when in the absence of an alkyne substrate, no HD was observed during the course

of the hydrogenation reaction under the conditions described above for selective alkyne reduction. A mechanism involving initial H<sub>2</sub> oxidative addition to the metal center is therefore deemed unlikely under the catalytic conditions.<sup>15</sup> Thus, both the metal-hydride mechanism common to early metal hydrogenation catalysts and the oxidative addition mechanisms common to late metal catalysts are unlikely in this case.



**Scheme 1.8** Proposed mechanisms

We propose two possible mechanisms, both of which are consistent with our data (Scheme 1.8). In the first pathway (Scheme 1.8, Pathway 1), the alkyne substrate oxidizes the metal center of complex **1.1** to give the Nb(V) metallacyclopropene complex **1.2**. Subsequent  $\sigma$ -bond metathesis of one of the Nb-C bonds with H<sub>2</sub> forms an alkenyl Nb(V) hydride complex (**1.C**). Reductive elimination of the alkene generates the catalyst-product adduct **1.B**, from which external CO may replace the alkene to regenerate **1.1**. The second proposed mechanism (Scheme 1.8, Pathway 2) involves the same initial addition of an alkyne to **1.1** as a means of generating **1.2**, but H<sub>2</sub> addition in this case would occur across the Nb=N<sup>t</sup>Bu bond to form the amido niobium hydride complex **1.D**.<sup>4b</sup> Insertion of the coordinated alkyne into the newly-formed M-H bond yields an amino alkenyl complex **1.E**, from which [1,2]- $\alpha$ -NH-elimination would result in the same catalyst-product adduct – complex **1.B** – described for Pathway 1. We currently favor Pathway 1 based on our computational investigations (see below) as well as the following precedents: *i*) The Nb(V) dimethyl complex

(BDI)Nb(N<sup>t</sup>Bu)Me<sub>2</sub> was observed to react rapidly and cleanly with H<sub>2</sub> in THF to give a product whose identity strongly suggested a Nb(III) intermediate.<sup>9c</sup> *ii*) Reaction site-selectivity studies on related neutral and cationic alkylNb(V) and alkylTa(V) imido complexes indicated a preference for both polar and non-polar substrates to undergo reactivity at the alkyl group as opposed to the imido group.<sup>16</sup>

**DFT calculation.** Calculations were performed to probe the potential energy surface describing the interaction of (BDI')Nb(NMe)(CO)<sub>2</sub> (**I-1**, BDI' = HC[C(Me)NPh]<sub>2</sub>) with MeC≡CPh and H<sub>2</sub> (see Appendix A).<sup>17</sup> At this level of theory, the rate-determining step (r.d.s.) of pathway 1, **TS-3a-1**, which corresponds to the  $\sigma$ -bond metathesis of the Nb-C( $\alpha$ -CH<sub>3</sub>) bond with H<sub>2</sub>, was favored by *ca.* 30 kcal/mol over the r.d.s. of Pathway 2, **TS-3c**, itself comprising the [1,2] addition of H<sub>2</sub> across the Nb=N<sup>t</sup>Bu bond (Figures 1.3 and 1.4). Alternative pathways were considered, including both a five membered ring transition state formed by interaction of the alkyne and the imido group as well as  $\sigma$ -bond metathesis with the Nb-C( $\alpha$ -Ph), but they were all found to lie significantly higher in energy than **TS-3a-1** (Appendix A). The CO moiety, which was displaced during **TS-3a-1** to a *trans* position relative to the alkyne in **I-4**, was found to relax to a basal position (**I-5**) prior to C-H reductive elimination. The proximity of CO and the hydride led to a nonproductive CO-insertion pathway to generate a formyl alkenyl complex (**I-8b**). However, the small calculated energy differences between **I-5** and **I-8a/b** suggest that formation of the latter may be reversible and difficult to detect. Whether C-C reductive elimination from **I-8a/b** is kinetically or thermodynamically disfavored is not currently known, but we find no experimental evidence for hydroformylation products under the studied conditions. Finally, the calculations suggest that the product-metal adduct, **I-7**, and a hypothetical four-coordinate monocarbonyl Nb(III) complex (BDI')Nb(NMe)(CO) (**I-9s**, S = 0<sup>18</sup>) are essentially equi-energetic (See Appendix A).<sup>12,18</sup>

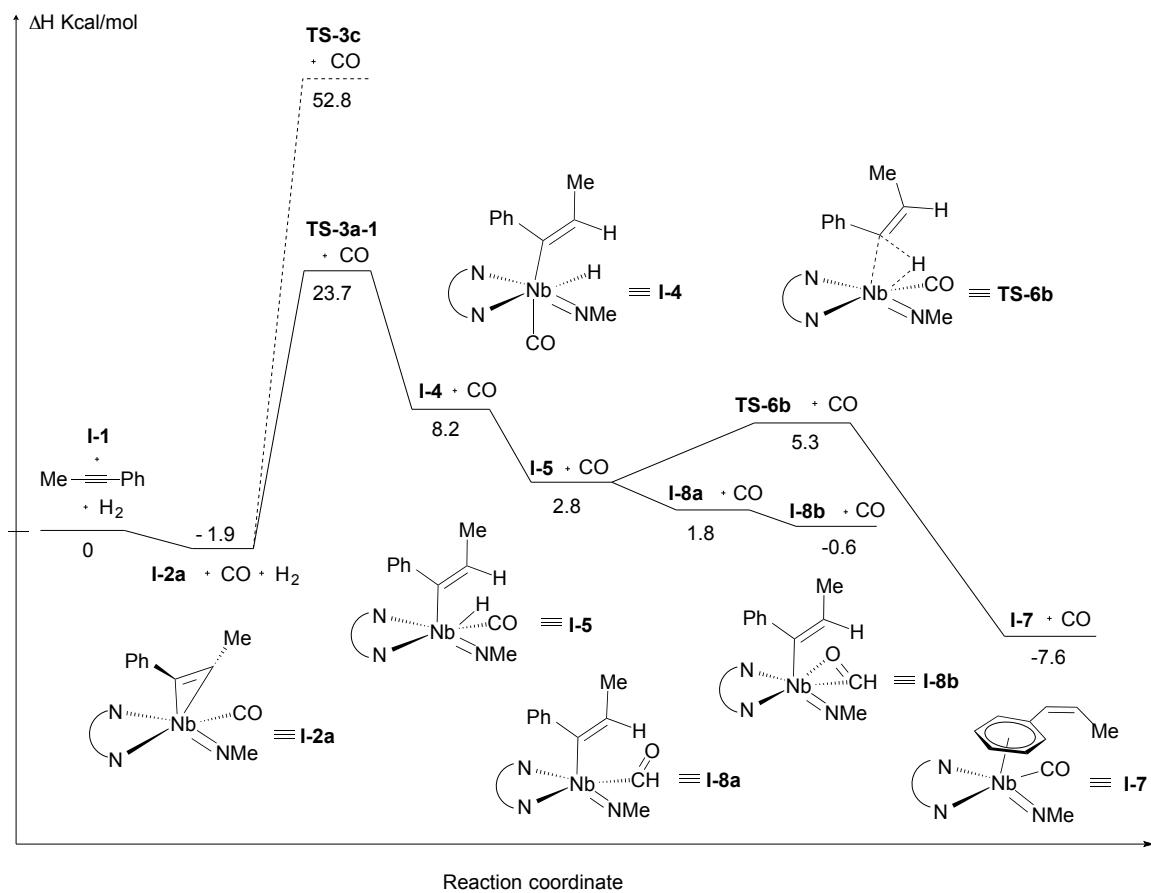


**Figure 1.3** Free enthalpy of the hydrogenation mechanism.

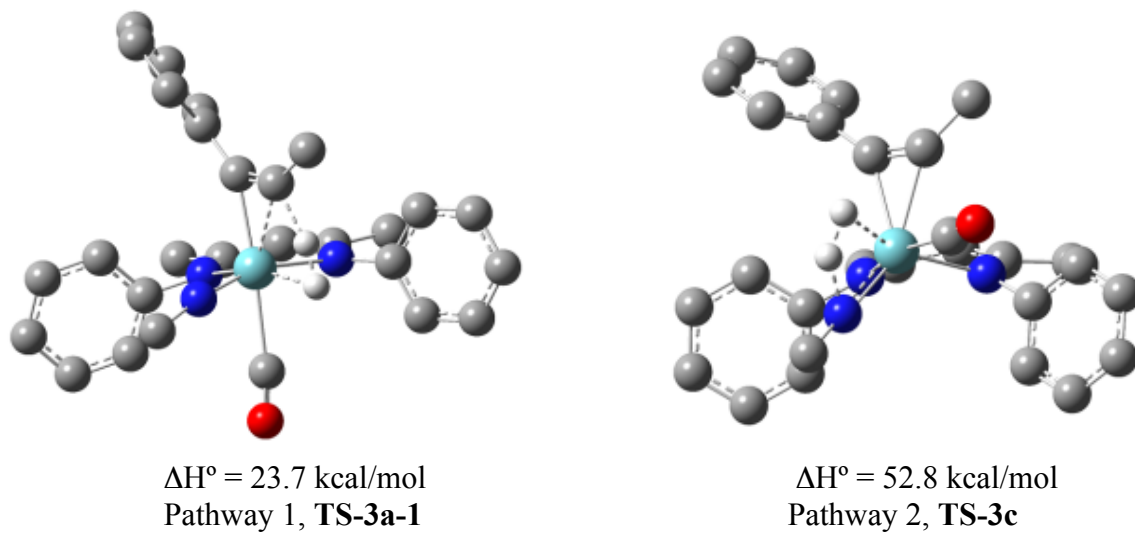


**Figure 1.4** Theoretical calculation on the transition state of the rate-limiting step of each proposed mechanism.

## Conclusion

In summary, we have presented in this chapter the efficient and selective catalytic semihydrogenation of 1-phenyl-1-propyne into *Z*- $\beta$ -methylstyrene by a  $d^2$  niobium complex under H<sub>2</sub> : CO mixtures. The experimental data are supported by DFT calculations, which suggest a novel mechanism for the hydrogenation reaction, involving coordination of an alkyne to form a metallacyclopropene Nb(V) complex **1.2**, followed by  $\sigma$ -bond metathesis with H<sub>2</sub> and subsequent reductive elimination to yield the product *Z*-alkene. An excess of CO is required for catalyst stability and proposed to function as a means of displacing the product alkene from a Nb(III) intermediate for achieving catalyst turnover. We are currently performing further synthetic, mechanistic and kinetic studies in order to support our preliminary results on the mechanism and intermediates involved in this reaction (See Appendix B).

## Experimental

**General Considerations.** Unless otherwise noted, all reactions were performed using standard Schlenk line techniques, or in an MBraun glovebox under an atmosphere of purified nitrogen (<1 ppm O<sub>2</sub>/H<sub>2</sub>O). Glassware, cannulae, and Celite were stored in an oven at *ca.* 180 °C; molecular sieves (4 Å) were activated by heating to 200 °C for 8 h under vacuum prior to storage in a glovebox. *n*-Pentane, *n*-hexane, Et<sub>2</sub>O, THF, toluene, and benzene were purified by passage through a column of activated alumina, stored over molecular sieves, and degassed prior to use.<sup>19</sup> Deuterated solvents (C<sub>6</sub>D<sub>6</sub>, C<sub>7</sub>D<sub>8</sub>) were dried over sodium/benzophenone, vacuum transferred to a storage flask containing molecular sieves, and degassed by three freeze-pump-thaw cycles before being stored in the dry box. PhC≡CMe was stored over molecular sieves and degassed by three freeze-pump-thaw cycles. PhC≡CPh was recrystallized from Et<sub>2</sub>O and dried under vacuum over night. 1,3,5-trimethoxybenzene was sublimed under static vacuum. *N,N'*-bis-(2,6-diisopropylphenyl)- $\beta$ -DiketIminate (BDI),<sup>20</sup> Li(BDI)·Et<sub>2</sub>O,<sup>21</sup> (BDI)pyCl<sub>2</sub>Nb(N<sup>t</sup>Bu),<sup>9</sup> (BDI)(Me)<sub>2</sub>Nb(N<sup>t</sup>Bu),<sup>9</sup> (BDI)(CO)<sub>2</sub>Nb(N<sup>t</sup>Bu) (**1.1**)<sup>14</sup> and (BDI)( $\eta^2$ -PhC≡CPh)(CO)Nb(N<sup>t</sup>Bu) (**1.2**)<sup>9</sup> were prepared using literature procedures. All other reagents were acquired from commercial sources and used as received. NMR spectra were recorded on 300, 400, 500, or 600 MHz Bruker NMR spectrometers. <sup>1</sup>H and <sup>13</sup>C NMR assignments were routinely confirmed by <sup>1</sup>H-<sup>1</sup>H (COSY, NOESY) or <sup>1</sup>H-<sup>13</sup>C (HSQC and HMBC) experiments. GC/MS analysis were performed using a Agilent 6890 N Network GC system coupled to a 5973 Network mass selective detector. Elemental analyses were performed in the College of Chemistry microanalytic facility, University of California, Berkeley.

**(BDI)( $\eta^2$ -PhC≡CPh)(CO)Nb(N<sup>t</sup>Bu) (**1.3**).** PhC≡CPh (81.3 mg, 0.456 mmol, 1 equiv.) was added to a solution of (BDI)(CO)<sub>2</sub>Nb(N<sup>t</sup>Bu) (**1.1**) (0.292 g, 0.458 mmol, 1 equiv.) in *n*-pentane (30 ml). Gas evolution was observed immediately as the solution lost its initial dark green color, turning first orange and then bright yellow, color of the product (BDI)( $\eta^2$ -PhC≡CPh)(CO)Nb(N<sup>t</sup>Bu). After being stirred for 2 h, the reaction mixture was slowly concentrated by bubbling CO through the solution until bright yellow crystals began to form. Concentration of the solution in this fashion is important due to the instability of solutions of **1.1** toward CO-loss when subjected to a dynamic vacuum. The flask was subsequently stored under a CO atmosphere at room temperature for 12 h, during which time additional crystals

formed. The yellow crystalline material was collected by filtration, and residual solvent was removed under vacuum. The crystalline material can be stored under vacuum without decomposition. Yield: 255 mg, 0.323 mmol, 71 %. <sup>1</sup>H NMR (500 MHz, C<sub>7</sub>D<sub>8</sub>, 293 K) δ(ppm) 7.56 (broad, 2 H), 7.34 (broad, 2 H), 7.16 (broad), 5.31 (s, 1 H, HC(C(Me)NAr)<sub>2</sub>), 3.70 (broad, 1 H), 3.42 (broad, 2 H), 2.62 (broad, 1 H), 1.86 (broad, 6 H), 1.46 (broad, 20 H), 1.13 (broad, 16 H), 0.86 (broad, 28 H), 0.72 (broad, 6 H), 0.62 (broad, 6 H). <sup>1</sup>H NMR (500 MHz, C<sub>7</sub>D<sub>8</sub>, 243 K) δ(ppm) 7.65 (d, 2 H, *o*-PhC≡CPh', <sup>3</sup>J<sub>HH</sub> = 7.2 Hz), 7.39 (t, 2 H, *m*-PhC≡CPh', <sup>3</sup>J<sub>HH</sub> = 7.0 Hz), 7.14 (m, 3 H, Ar and PhC≡CPh'), 6.85 (t, 1 H, *p*-PhC≡CPh', <sup>3</sup>J<sub>HH</sub> = 6.5 Hz, <sup>3</sup>J<sub>HH</sub> = 2.0 Hz), 5.25 (s, 1 H, HC(C(Me)NAr)<sub>2</sub>), 3.75 (sept, 1 H, CHMe<sub>2</sub>, <sup>3</sup>J<sub>HH</sub> = 6.8 Hz), 3.42 (m, 2 H, CHMe<sub>2</sub>), 2.60 (sept, 1 H, CHMe<sub>2</sub>, <sup>3</sup>J<sub>HH</sub> = 7.0 Hz), 1.86 (s, 3 H, HC(C(Me)NAr)<sub>2</sub>), 1.54 (d, 3 H, CHMe<sub>2</sub>, <sup>3</sup>J<sub>HH</sub> = 6.8 Hz), 1.49 (s, 3 H, HC(C(Me')NAr)<sub>2</sub>), 1.46 (d, 3 H, CHMe<sub>2</sub>, <sup>3</sup>J<sub>HH</sub> = 6.8 Hz), 1.16 (d, 3 H, CHMe<sub>2</sub>, <sup>3</sup>J<sub>HH</sub> = 6.8 Hz), 1.13 (d, 3 H, CHMe<sub>2</sub>, <sup>3</sup>J<sub>HH</sub> = 6.8 Hz), 0.98 (d, 6 H, CHMe<sub>2</sub>, <sup>3</sup>J<sub>HH</sub> = 7.1 Hz), 0.93 (s, 9 H, <sup>t</sup>BuN), 0.78 (d, 3 H, CHMe<sub>2</sub>, <sup>3</sup>J<sub>HH</sub> = 6.8 Hz), 0.65 (d, 3 H, CHMe<sub>2</sub>, <sup>3</sup>J<sub>HH</sub> = 6.8 Hz). <sup>13</sup>C{<sup>1</sup>H} NMR (125 MHz, C<sub>7</sub>D<sub>8</sub>, 293 K) δ(ppm) 178.4, 169.1 (C, (HC(C(Me)NAr)<sub>2</sub>), 164.2 (C, (HC(C'(Me)NAr)<sub>2</sub>), 152.6, 150.3, 143.1, 142.6, 141.8 and 139.2 (C, Ar and PhC≡CPh), 100.8 (CH, (HC(C(Me)NAr)<sub>2</sub>), 68.2 (C, Nb=N<sup>t</sup>Bu, C<sub>α</sub>), 31.7 (CH<sub>3</sub>, Nb=N<sup>t</sup>Bu, C<sub>β</sub>) 28.9, 28.8, 28.02 and 27.3 (CH, CHMe<sub>2</sub> of C=NAr), 226.2, 25.5, 25.4, 24.9, 24.8, 24.7, 24.4, 24.1 and 23.8 (CH<sub>3</sub>, CHMe<sub>2</sub> of C=NAr). IR (KBr, nujol, cm<sup>-1</sup>): 2052 (s). Anal. Calcd for C<sub>48</sub>H<sub>60</sub>N<sub>3</sub>NbO: C, 73.17; H, 7.67; N, 5.33 %. Found: C, 72.82; H, 7.80; N, 5.34 %. M.p.: 80-82 °C (decomp).

**(BDI)(η<sup>2</sup>-PhC≡CMe)(<sup>t</sup>BuN≡C)Nb(N<sup>t</sup>Bu) (1.4).** PhC≡CMe (98 ml, 0.78 mmol, 1 equiv.) was added to a solution of (BDI)(CO)<sub>2</sub>Nb(N<sup>t</sup>Bu) (**1.1**) (0.51 g, 0.78 mmol, 1 equiv.) in pentane (20 ml). Gas evolution and a change in the color of the solution from dark green to bright yellow were observed immediately, corresponding to the formation of the (BDI)(η<sup>2</sup>-PhC≡CMe)(CO)Nb(N<sup>t</sup>Bu). After 20 min, a solution of *t*-butyl isocyanide (440 mL, 3.90 mmol, 5 equiv.) in pentane (5 mL) was added dropwise, causing the solution to effervesce and the color to change from bright yellow to light orange. The CO formed in this reaction was removed by applying a dynamic vacuum for 3 × 30 s. The reaction mixture was then stirred for an additional 12 h before all the volatile materials were removed under vacuum. The remaining residue was triturated with Et<sub>2</sub>O (2 × 15 ml), extracted with *n*-hexane (20 ml), concentrated, and stored at -40 °C overnight. The orange crystals that precipitated were collected by filtration, and the residual solvent was removed under vacuum. Yield: 316 mg, 0.406 mmol, 52 %. <sup>1</sup>H NMR (400 MHz, C<sub>6</sub>D<sub>6</sub>, 293 K) δ(ppm) 7.68 (d, 2 H, *o*-PhC≡CMe, <sup>3</sup>J<sub>HH</sub> = 7.2 Hz), 7.39 (t, 2 H, *m*-PhC≡CMe, <sup>3</sup>J<sub>HH</sub> = 7.0 Hz), 7.11-7.10 (m, 4 H, Ar and *p*-PhC≡CMe), 7.04 (dd, 2 H, *o*-Ar', <sup>3</sup>J<sub>HH</sub> = 6.5 Hz, <sup>3</sup>J<sub>HH</sub> = 2.0 Hz), 7.00 (t, 2 H, *m*-Ar', <sup>3</sup>J<sub>HH</sub> = 6.0 Hz), 6.91 (dd, 1 H, *p*-Ar', <sup>3</sup>J<sub>HH</sub> = 6.2 Hz, <sup>3</sup>J<sub>HH</sub> = 1.6 Hz), 5.29 (s, 1 H, HC(C(Me)NAr)<sub>2</sub>), 3.84 (broad, 1 H, CHMe<sub>2</sub>, <sup>3</sup>J<sub>HH</sub> = 6.8 Hz), 3.70 (broad, 1 H, CHMe<sub>2</sub>), 3.49 (broad, 1 H, CHMe<sub>2</sub>), 2.87 (s, 3 H, PhC≡CMe), 2.68 (sept, 1 H, CHMe<sub>2</sub>, <sup>3</sup>J<sub>HH</sub> = 6.8 Hz), 1.89 (s, 3 H, HC(C(Me)NAr)<sub>2</sub>), 1.63 (d, 3 H, CHMe<sub>2</sub>, <sup>3</sup>J<sub>HH</sub> = 6.8 Hz), 1.54 (s, 3 H, HC(C(Me')NAr)<sub>2</sub>), 1.44 (d, 3 H, CHMe<sub>2</sub>, <sup>3</sup>J<sub>HH</sub> = 6.8 Hz), 1.31 (d, 3 H, CHMe<sub>2</sub>, <sup>3</sup>J<sub>HH</sub> = 6.8 Hz), 1.21 (d, 3 H, CHMe<sub>2</sub>, <sup>3</sup>J<sub>HH</sub> = 6.8 Hz), 1.02 (d, 6 H, CHMe<sub>2</sub>, <sup>3</sup>J<sub>HH</sub> = 6.8 Hz), 0.90 (s, 24 H, <sup>t</sup>BuN/<sup>t</sup>BuNC/ CHMe<sub>2</sub> (isopropyl)). <sup>13</sup>C{<sup>1</sup>H} NMR (100 MHz, C<sub>6</sub>D<sub>6</sub>, 293 K) δ(ppm) 168.72 (C, (HC(C(Me)NAr)<sub>2</sub>), 163.49 (C, (HC(C'(Me)NAr)<sub>2</sub>), 154.5 (C, Ar), 152.4 (C, Ar), 145.5 (C, PhC≡CMe), 143.4, 142.7 and 142.2 (C, Ar), 131.22 (CH, *o*-PhC≡CMe), 128.0 (CH, *m*-PhC≡CMe), 125.2 (CH, PhC≡CMe), 124.8, 124.7, 124.6, 123.7, 123.6 and 122.9 (CH, Ar), 100.2 (CH,

(HC(C(Me)NAr)<sub>2</sub>, 67.2 (C, Nb=N<sup>t</sup>Bu, C<sub>a</sub>), 56.36 (C, Nb-C≡N<sup>t</sup>Bu, C<sub>a</sub>), 32.37 (CH<sub>3</sub>, Nb-C≡N<sup>t</sup>Bu, C<sub>β</sub>), 30.21 (CH<sub>3</sub>, Nb=N<sup>t</sup>Bu, C<sub>β</sub>) 29.4, 28.8, 28.3 and 27.6 (CH, CHMe<sub>2</sub> of C=NAr), 26.3 (CH<sub>3</sub>, CHMe<sub>2</sub> of C=NAr), 25.8 (CH<sub>3</sub>, PhC≡CMe), 25.6, 25.4, 25.1, 24.5 and 24.3 (CH<sub>3</sub>, CHMe<sub>2</sub> of C=NAr). IR (KBr, nujol, cm<sup>-1</sup>): 2167 (s). Anal. Calcd for C<sub>47</sub>H<sub>67</sub>N<sub>4</sub>Nb: C, 72.29; H, 8.65; N, 7.18 %. Found: C, 72.25; H, 8.45; N: 7.11 %. M.p.: 131-132 °C.

**General Procedure for Catalytic Hydrogenation of PhC≡CMe.** Inside a glove box, PhC≡CMe (6.8 ml, 55 mmol, 5 equiv.) was added to a stock solution of **1.1** (0.011 M, 1 equiv.) and trimethoxybenzene (0.011 M, 1 equiv.) in C<sub>6</sub>D<sub>6</sub> (1 ml). Several reactions were performed using the same batch of stock solution, but the solution was renewed every 3 days. Addition of PhC≡CMe caused the solution to rapidly effervesce as the color turned from dark green to bright yellow. The resulting solution was transferred inside the glove box to either a 10 mL or 40 mL flask equipped with a vacuum stopcock, then sealed, taken out of the dry box, and quickly cooled with liquid nitrogen. The flask was fitted with a known-volume bulb equipped with a stopcock (V = 8.3 ml, 19.6 ml or 63.4 ml). The atmosphere above the stopcock to the flask and the headspace above the frozen sample were evacuated sequentially, then the flask was closed under vacuum and allowed to warm to room temperature. As the solution began to thaw, the headspace was refilled with an atmosphere of CO (or N<sub>2</sub> or H<sub>2</sub>). The bottom of the known-volume bulb was then closed, evacuated and refilled with x equivalents of H<sub>2</sub> (for V = 8.3 ml, 122 mmHg, 0.055 mmol for x = 1 equiv.; or 370 mmHg, 0.165 mmol for x = 3 equiv.). The thawed solution was stirred rapidly at room temperature while the bottom of the bulb was slowly opened. The solution was stirred for 2 h at room temperature, then the flask was sealed and taken into a glove box. An aliquot of the solution was taken for analysis by <sup>1</sup>H NMR spectroscopy, and the yield of *Z*-β-methylstyrene was evaluated based on integration vs. the trimethoxybenzene internal standard (6.26 ppm, 3 H). Determinations of the identity and yield of the various products were based on the vinyl protons of both *E/Z*-β-methylstyrene and allylbenzene and on the benzylic protons of the *n*-propylbenzene. These signals were chosen for their clarity in the <sup>1</sup>H NMR spectrum. <sup>1</sup>H NMR (500 MHz, C<sub>6</sub>D<sub>6</sub>, 293 K), δ(ppm), **trimethoxybenzene**: 6.26 (s, 3 H, benzene ring); ***Z*-β-methylstyrene**: 6.42 (dd, 1 H, PhC(H)=C(H)Me, <sup>3</sup>J<sub>HHvinyl</sub> = 11.5 Hz, <sup>3</sup>J<sub>HHphenyl</sub> = 2 Hz); ***E*-β-methylstyrene**: 6.03 (m, 1 H, PhC(H)=C(H)Me); **allylbenzene**: 4.97 (broad d, 2 H, PhCH<sub>2</sub>C(H)=CH<sub>2</sub>, <sup>3</sup>J<sub>HH</sub> = 13.2 Hz.); ***n*-propylbenzene**: 2.42 (t, 2 H, PhCH<sub>2</sub>CH<sub>2</sub>CH<sub>3</sub>, <sup>3</sup>J<sub>HH</sub> = 7.5 Hz). This experiment was repeated in the presence of liquid Hg<sup>0</sup> (300 equiv., 665 mg) and no poisoning was observed. Formation of the catalyst 1, and the resting state 2.

**Half-Turnover Experiment.** Using the general procedure described above, PhC≡CMe (22.0 ml, 0.204 mmol, 2 equiv.) was added to a solution of **1.1** (74.8 mg, 0.111 mmol, 1 equiv.) in C<sub>6</sub>D<sub>6</sub>, resulting in 1 equiv. of complex **1.2** and 1 equiv. of free PhC≡CMe. H<sub>2</sub> (8.3 ml, 0.055 mmol, P<sub>H2</sub> = 120 mmHg, 0.5 equiv.) was then diffused into the solution through an atmosphere of CO. After 2 h, the reaction mixture was analyzed by <sup>1</sup>H NMR spectroscopy, the formation of 0.5 equiv. of *Z*-β-methylstyrene and 0.5 equiv. of unreacted PhC≡CMe along with the regeneration of (BDI)(η<sup>2</sup>-PhC≡CMe)(CO)Nb(N<sup>t</sup>Bu) (**1.2**) was observed. The choice of half of an equivalent of hydrogen was used to simplify the analysis of a single-turnover experiment by decreasing the amount of excess alkyne present in solution.

**H<sub>2</sub>/D<sub>2</sub> Crossover Experiments.** The catalytic hydrogenation procedure described above was used for this experiment. D<sub>2</sub> (0.5 atm) and H<sub>2</sub> (0.5 atm) were admitted into an isolated vacuum manifold and allowed to equilibrate for 15 min prior to addition to a known-volume bulb. The H<sub>2</sub> : D<sub>2</sub> mixture (8.3 ml, 0.055 mmol, P<sub>H<sub>2</sub></sub> = 120 mmHg, 1 equiv.) was then diffused through the CO atmosphere. The <sup>1</sup>H NMR spectrum of the reaction mixture exhibited a sharp and distinctive doublet for *Z*-PhC(*H*)=C(*H*)Me and doublet of quartets for *Z*-PhC(*H*)=C(*H*)Me. The <sup>2</sup>H NMR spectrum revealed two broad signals of equal intensity with chemical shifts identical to those observed for the vinylic protons in the <sup>1</sup>H NMR spectrum. The volatile products were isolated from the metal complex by vacuum transfer and diluted with 1 mL of Et<sub>2</sub>O for GC/MS analysis. The GC/MS spectrum revealed the absence of the *d*<sub>1</sub>-isotopomer (Figure 1.3). In order to compensate for any kinetic isotope effect, the crossover experiment was repeated using a 9 : 1 ratio of D<sub>2</sub> : H<sub>2</sub>, which again gave no indication for formation of the *d*<sub>1</sub>-isotopomer.

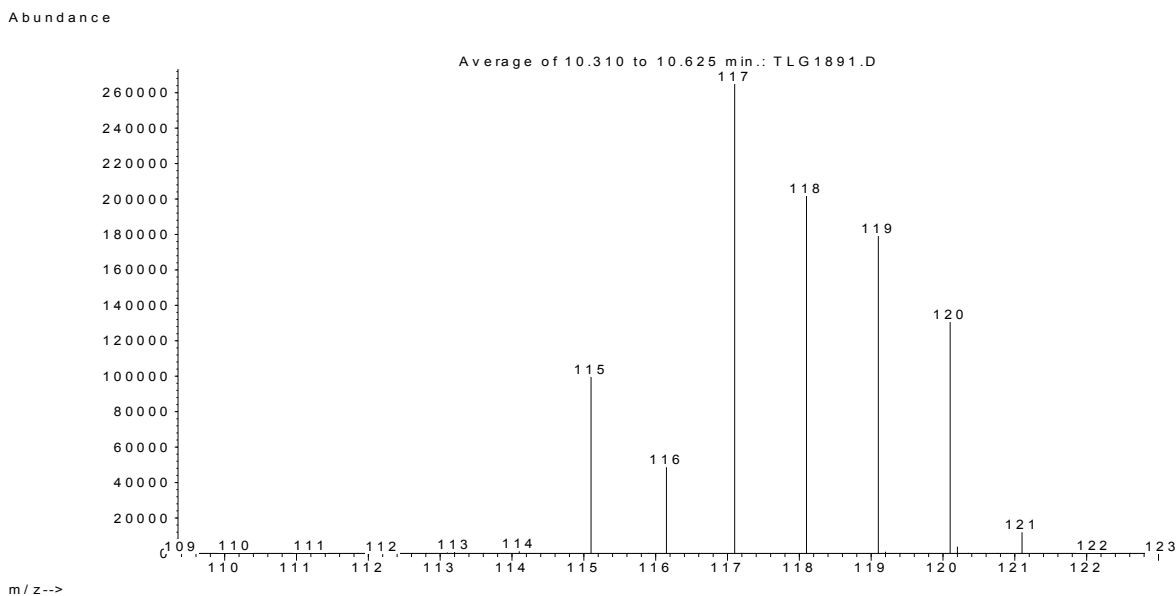


**Figure 1.5** MS of the product formed under H<sub>2</sub>:D<sub>2</sub> mixture.



## Monitoring the hydrogenation of 1-phenyl-1-propyne in the presence of CO by $^1\text{H}$ NMR spectroscopy.

### Special equipment:

- The internal volume of a specialty, large-volume J-Young tube was measured by the difference in weight between the empty tube and the tube filled with several solvents of varying densities (acetone, water and isopropanol). The internal volume was determined to be  $16.7 \pm 0.1$  mL.
- A smaller known-volume bulb for a J-Young tube was made using fresh butyl tubing, a glass J-Young tube adaptor, and a glass stopcock. The internal volume was again measured solvents of varying densities, giving an internal volume of  $2.8 \pm 0.1$  mL.

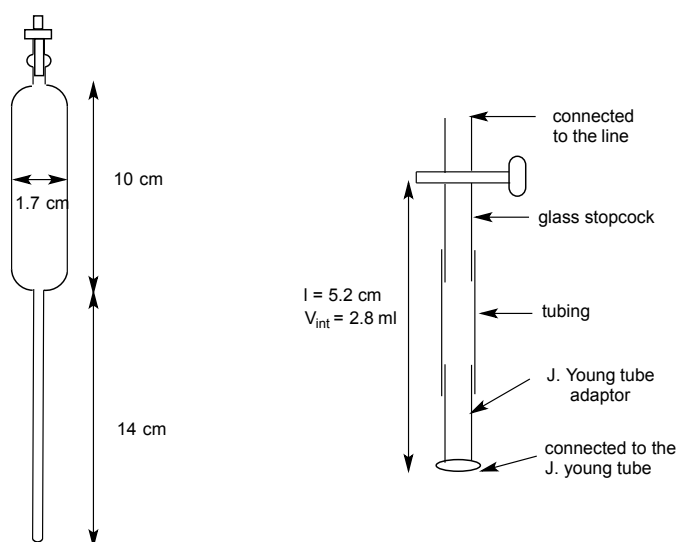


**Figure 1.6** Large-volume J-Young tube (left) and known-volume bulb (right).

General procedure.  $\text{PhC}\equiv\text{CMe}$  (6.8 ml, 55 mmol, 5 equiv.) was added to a solution of  $(\text{BDI})(\text{CO})_2\text{Nb}(\text{N}^t\text{Bu})$  (0.011 M, 1 equiv.) and trimethoxybenzene (0.011 M, 1 equiv.) in  $\text{C}_6\text{D}_6$  (1 mL). The solution was transferred to a J-Young NMR tube with a Teflon cap (16.7 mL), then the tube was sealed and removed from the glovebox for analysis by NMR spectroscopy. The  $^1\text{H}$  NMR spectrum taken at this point (80 % of free alkynes and 20 % of **1.2**) represents  $t = 0$  in the analyzed data. The solution was subsequently subjected to three freeze-pump-thaw cycles, then refilled with 1 atm of CO (15.7 mL, 0.61 mmol, 60 equiv.). The NMR tube was sealed and the CO atmosphere was condensed into the tube cooled with liquid nitrogen for 10 min. Meanwhile, the homemade known volume bulb was filled with  $\text{H}_2$  ( $P_{\text{H}_2} = 430$  mmHg in 2.8 mL; 0.066 mmol, 6 equiv.) and the glass stopcock was closed. The Teflon cap of the NMR tube was opened, allowing  $\text{H}_2$  to equilibrate within the apparatus. After 2 min the Teflon cap was re-closed, the mixture was allowed to warm to room temperature (in  $V = 15.7$  mL, new  $P_{\text{H}_2} = 65$  mmHg, 0.055 mmol, 5 equiv.).  $^1\text{H}$  NMR spectra were taken at regular intervals showing the clean conversion of the alkyne into Z-alkene as well as the constant concentration of the complex **1.2**.

**Monitoring of the hydrogenation of 1-phenyl-1-propyne in the absence of CO by  $^1\text{H}$  NMR spectroscopy.**  $\text{PhC}\equiv\text{CMe}$  (6.8 ml, 55 mmol, 5 equiv.) was added to a solution of **1.1** (0.011 M, 1 equiv.) and trimethoxybenzene (0.011 M, 1 equiv.) in  $\text{C}_6\text{D}_6$  (1 mL). The resulting solution was transferred to a J-Young NMR tube with a Teflon stopcock (3.5 mL). The solution was subjected to three freeze-pump-thaw cycles, then the tube was refilled with 1 atm of  $\text{H}_2$  (2.5 mL, 0.102 mmol, 10 equiv.) and sealed. The J-Young tube was allowed to warm to room temperature, and the progress of the reaction was monitored by  $^1\text{H}$  NMR spectroscopy (Figure 1.1).

Characterization of  $(\text{BDI})(\text{C}_6\text{H}_6)\text{Nb}(\text{N}^t\text{Bu})$ , **1.A**:  $^1\text{H}$  NMR (500 MHz,  $\text{C}_6\text{D}_6$ , 298 K):  $\delta$  (ppm) 5.12 (s, 1H,  $\text{HC}(\text{C}(\text{Me})\text{NAr})_2$ ), 4.53 (sept, 2H,  $\text{CHMe}_2$ ), 2.76 (sept, 2H,  $\text{CHMe}_2$ ), 1.73 (s, 6H,  $\text{HC}(\text{C}(\text{Me})\text{NAr})_2$ ), 1.44 (s, 9H,  $t\text{Bu}$ ), 1.37 (d, 6H,  $\text{CHMe}_2$ ), 1.04 (m, 12H,  $2 \times \text{CHMe}_2$ ), 0.99 (d, 6H,  $\text{CHMe}_2$ ).  $^2\text{H}$  NMR (MHz,  $\text{C}_6\text{D}_6$ , 298 K):  $\delta$  (ppm) 3.6 (s,  $\text{C}_6\text{D}_6$ ). Performing the reaction in  $\text{C}_6\text{H}_6$  and analyzing the reaction mixture by  $^1\text{H}$  NMR (with 10 %  $\text{C}_6\text{D}_6$  to lock) allowed for the observation of a new signal at  $\delta$  3.69 (s, 6H,  $\text{C}_6\text{H}_6$ ).

Characterization of  $(\text{BDI})(\eta^6\text{-PhC}(\text{H})=\text{C}(\text{H})\text{Me})(\text{CO})\text{Nb}(\text{N}^t\text{Bu})$ , **1.B**: This compound was observed as an intermediate during the formation of **1.A** (Figure 1.1). Due to the presence of other aryl-containing organic and organometallic products, the regions between 7 - 5.5 and 2.5 - 0.5 ppm could not be assigned.  $^1\text{H}$  NMR (500 MHz,  $\text{C}_6\text{D}_6$ , 298 K):  $\delta$  (ppm) 5.09 (s, 1 H,  $\text{HC}(\text{C}(\text{Me})\text{NAr})_2$ ), 4.65 (sept, 2 H,  $\text{CHMe}_2$ ), 4.03 (t, 1 H,  $p\text{-PhCH}=\text{CHMe}$ ), 3.81 (t, 2 H,  $m\text{-PhCH}=\text{CHMe}$ ), 3.73 (d, 2 H,  $o\text{-PhCH}=\text{CHMe}$ ), 2.77 (sept, 2 H,  $\text{CHMe}_2$ ).

**X-Ray crystallography studies.** The X-ray structural determinations were performed on a Bruker SMART 1000 or SMART APEX diffractometer. Both are 3-circle diffractometers that couple a CCD detector<sup>22</sup> with a sealed-tube source of monochromated Mo  $\text{K}\alpha$  radiation ( $\lambda = 0.71073 \text{ \AA}$ ). A crystal of appropriate size was coated in Paratone-N oil and mounted on a Kapton<sup>®</sup> loop. The loop was transferred to the diffractometer, centered in the beam, and cooled by a nitrogen flow low-temperature apparatus that had been previously calibrated by a thermocouple placed at the same position as the crystal. Preliminary orientation matrices and cell constants were determined by collection of 60 x 10 s frames, followed by spot integration and least-squares refinement. The reported cell dimensions were calculated from all reflections with  $I > 10 \sigma$ . The data were corrected for Lorentz and polarization effects; no correction for crystal decay was applied. An empirical absorption correction based on comparison of redundant and equivalent reflections was applied using SADABS.<sup>23</sup> All software used for diffraction data processing and crystal-structure solution and refinement are contained in the APEX2 program suite (Bruker AXS, Madison, WI).<sup>24,25</sup> Thermal parameters for all non-hydrogen atoms were refined anisotropically. For all structures,  $R_1 = \Sigma(|F_o| - |F_c|)/\Sigma(|F_o|)$ ;  $wR_2 = [\Sigma\{w(F_o^2 - F_c^2)^2\}/\Sigma\{w(F_o^2)^2\}]^{1/2}$ . ORTEP diagrams were created using the ORTEP-3 software package and POV-ray.<sup>25</sup>

**Table 1.1.** Crystallographic data for compounds **1.3** and **1.4**.

Compound	<b>1.3</b>	<b>1.4</b>
Formula	C <sub>48</sub> H <sub>60</sub> N <sub>3</sub> NbO	C <sub>47</sub> H <sub>67</sub> N <sub>4</sub> Nb
Formula weight (amu)	787.90	780.96
Space Group	P2 <sub>1</sub> /n	P2 <sub>1</sub> /c
<i>a</i> (Å)	15.246(5)	12.702(3)
<i>b</i> (Å)	18.113(6)	17.670(4)
<i>c</i> (Å)	15.847(5)	20.776(5)
$\alpha$ (°)	90°	90°
$\beta$ (°)	98.388(7)°	100.094(3)°
$\gamma$ (°)	90°	90°
<i>V</i> (Å <sup>3</sup> )	4329(3)	4590.6(18)
<i>Z</i>	4	4
$\rho_{\text{calcd}}$ (g/cm <sup>3</sup> )	1.209	1.130
F <sub>000</sub>	1672	1672
$\mu$ (mm <sup>-1</sup> )	0.315	0.295
T <sub>min</sub> /T <sub>max</sub>	0.8583/0.9875	0.9140/0.9218
No. rflns measured	33201	75656
No. indep. rflns	7628	8411
<i>R</i> <sub>int</sub>	0.0460	0.0381
No. obs. ( <i>I</i> > 2.00σ( <i>I</i> ))	7628	8411
No. variables	491	486
<i>R</i> <sub>1</sub> , <i>wR</i> <sub>2</sub>	0.0385/0.0748	0.0319/0.0760
<i>R</i> <sub>1</sub> (all data)	0.0598	0.0449
GoF	1.047	1.062
Res. peak/hole (e <sup>-</sup> /Å <sup>3</sup> )	0.323/-0.436	0.645/-0.237

**General remarks for DFT calculations.** All structures and energies were calculated using the Gaussian09 suite of programs.<sup>26</sup> Self-consistent field computations were performed with tight convergence criteria on ultrafine grids, while geometry optimizations were converged to tight geometric convergence criteria for all compounds. Spin expectation values  $\langle S \rangle^2$  indicated that spin contamination was not significant in any result. Frequencies were calculated analytically at 298.15 K and 1 atm. Structures were considered true minima if they did not exhibit imaginary vibration modes and were considered as transition states when only one imaginary vibration mode was found. Intrinsic Reaction Coordinates (IRC) calculations were performed to ensure the transition state geometries connected the reactants and the products. Optimized geometries were compared using the sum of their electronic and zero-point energies. In order to reduce the computational time, the system was structurally simplified by replacing 2,6-diisopropylphenyl groups by phenyl groups and the N<sup>t</sup>Bu imido group by a NMe imido group.

The B3LYP hybrid functional was used throughout this computational study.<sup>27,28</sup> For geometry optimizations and frequency calculations, the light atoms (H, C, N and O) were treated with Pople's 6-31G(d) double- $\zeta$  split-valence basis,<sup>29,30</sup> whereas the niobium atom was treated with LANL2DZ.<sup>31-33</sup> A 5d diffusional function was used for the H, C, N and O atoms, no polarization functions were added for H.

## References

- (1) *Handbook for Homogeneous Hydrogenation*; de Vries, J. G., Elsevier, C. J., Ed.; Wiley-VCH, Weinheim, 2007; Vol. 1.
- (2) Lindlar, H. *Helvet. Chim. Acta.* **1952**, *35*, 446.
- (3) *Organotransition Metal Chemistry, From Bonding to Catalysis*; Hartwig, J., Ed.; University Science Books, 2010.
- (4) (a) Hauwert, P.; Maestri, G.; Sprengers, J. W.; Catellani, M.; Elsevier, C. J. *Angew. Chem. Int. Edit.* **2008**, *47*, 3223. (b) La Pierre, H. S.; Arnold, J.; Toste, F. D. *Angew. Chem. Int. Edit.* **2011**, *50*, 3900. (c) Hauwert, P.; Boerleider, R.; Warsink, S.; Weigand, J. J.; Elsevier, C. J. *J. Am. Chem. Soc.* **2010**, *132*, 16900. (d) Warsink, S.; Chang, I. H.; Weigand, J. J.; Hauwert, P.; Chen, J. T.; Elsevier, C. J. *Organometallics* **2010**, *29*, 4555.
- (5) (a) A mixture of H<sub>2</sub>:CO has recently been used to form N-H bond from N<sub>2</sub> via CO induced-cleavage followed by hydrogenation. (b) Knobloch, D. J.; Lobkovsky, E.; Chirik, P. J. *J. Am. Chem. Soc.* **2010**, *132*, 15340.
- (6) (a) Miller, A. D.; Mcbee, J. L.; Tilley, T. D. *J. Am. Chem. Soc.* **2008**, *130*, 4992. (b) Smith, D. P.; Strickler, J. R.; Gray, S. D.; Bruck, M. A.; Holmes, R. S.; Wigley, D. E. *Organometallics* **1992**, *11*, 1275. (c) Reichard, H. A.; Micalizio, G. C. *Angew. Chem. Int. Edit.* **2007**, *46*, 1440.
- (7) (a) However, some group 5 and 6 transition metal complexes show a tendency to form stable h<sup>2</sup>-alkyne/alkene adducts; their reactivity has also been studied. (b) Biasotto, F.; Etienne, M.; Dahan, F. *Organometallics* **1995**, *14*, 1870. (c) Etienne, M.; Carfagna, C.; Lorente, P.; Mathieu, R.; de Montauzon, D. *Organometallics* **1999**, *18*, 3075. (d) Hirpo, W.; Curtis, M. D. *Organometallics* **1994**, *13*, 2706. (e) Ison, E. A.; Abboud, K. A.; Boncella, J. M. *Organometallics* **2006**, *25*, 1557.
- (8) Ortiz, C. G.; Abboud, K. A.; Cameron, T. M.; Boncella, J. M., *Chem. Commun.* **2001**, 247.

- (9) (a) BDI: *N,N'*-bis-(2,6-diisopropylphenyl)- $\beta$ -DiketIminate. (b) Tomson, N. C.; Arnold, J.; Bergman, R. G. *J. Am. Chem. Soc.* **2008**, *130*, 11262. (c) Tomson, N. C.; Arnold, J.; Bergman, R. G. *Organometallics* **2010**, *29*, 5010.
- (10) (a) Giernoth, R.; Heinrich, H.; Adams, N. J.; Deeth, R. J.; Bargon, J.; Brown, J. M. *J. Am. Chem. Soc.* **2000**, *122*, 12381. (b) Giernoth, R.; Huebler, P.; Bargon, J. *Angew. Chem. Int. Edit.* **1998**, *37*, 2473.
- (11) (a) Burckhardt, U.; Tilley, T. D. *J. Am. Chem. Soc.* **1999**, *121*, 6328. (b) Sabo-Etienne, S.; Rodriguez, V.; Donnadiou, B.; Chaudret, B.; el Makarim, H. A.; Barthelat, J. C.; Ulrich, S.; Limbach, H. H.; Moise, C. *New J. Chem.* **2001**, *25*, 55. (c) La Pierre, H. S.; Arnold, J.; Bergman, R. B.; Toste, F. D. *Angew. Chem. Int. Ed.*, **2011**, *50*, 3900 (d) An alternative description of these complexes would be that of a  $d^2$  metal center with both the CO and the alkyne as strong  $\pi$ -accepting ligands. However, a complex with this latter electronic structure would likely exhibit both shorter carbon-carbon bonds and more linear R-C-C (R = Me, Ph) angles for the alkyne, as well as a more reduced  $\nu_{CO}$  and the presence of strong p-bonding interaction between CO and the metal center in the occupied molecular orbitals of the complex **I-2a** calculated by DFT (see Appendix B).
- (12) Determined using the continuous symmetry parameter  $\tau = (\alpha - \beta)/60$ , where  $\alpha$  and  $\beta$  are the largest and second largest angles about the metal center, respectively: Addison, A. W.; Rao, T. N.; Reedijk, J.; van Rijn, J.; Verschoor, G. C. *J. Chem. Soc., Dalton Trans.* 1984, 1349.
- (13) *Modern Physical Organic Chemistry*; Anslyn, E. V., Dougherty, D. A., Ed.; University Science Books, Weinheim, 2006; p 22.
- (14) Tomson, N. C.; Arnold, J.; Bergman, R. G. *Organometallics* **2010**, *29*, 2926.
- (15) In addition to this result, DFT calculations showed that the dihydride intermediate **I-10** is +27.5 kcal/mol from the dicarbonyl complex **1** and thus +3.8 kcal/mol from the s-bond metathesis transition state (see Appendix B).
- (16) Tomson, N. C.; Arnold, J.; Bergman, R. G., *Dalton Trans.* **2011**.
- (17) All structures were fully optimized using the Gaussian09 program using the B3LYP hybrid functional. The LANL2DZ basis set was used for the metal center and the 6-31G\* basis sets with a 5d diffusional were used for the H, C, N and O atoms. All optimized geometries were compared using their Zero Point Energies (ZPE). For computational expediency, the aryl groups of the BDI ligand were replaced with phenyl groups and the tBu imido ligand was replaced by a methylimido group.
- (18) The triplet state was found to be 9.4 kcal/mol higher in energy.
- (19) Alaimo, P. J.; Peters, D. W.; Arnold, J.; Bergman, R. G. *J. Chem. Educ.* **2001**, *78*, 64.
- (20) Feldman, J.; McLain, S. J.; Parthasarathy, A.; Marshall, W. J.; Calabrese, J. C.; Arthur, S. D. *Organometallics* **1997**, *16*, 1514.
- (21) Budzelaar, P. H. M.; van Oort, A. B.; Orpen, A. G. *Eur. J. Inorg. Chem.* **1998**, 1485.
- (22) SMART: Area-Detector Software Package; Bruker Analytic X-ray Systems, I., Madison, WI, 2001-2003, Ed.
- (23) SADABS: Bruker-Nonius Area Detector Scaling and Absorption V2.05 Bruker Analytical X-ray Systems, I., Madison, WI, 2003.
- (24) Sheldrick, G. M. *Acta Crystallogr. A* **2008**, *64*, 112.
- (25) Farrugia, L. J., *J. Appl. Crystallogr.* 1997, *30*, 565., Ed.
- (26) Frisch, M. J.; Trucks, G. W.; Schlegel, H. B.; Scuseria, G. E.; Robb, M. A.; Cheeseman, J. R.; Scalmani, G.; Barone, V.; Mennucci, B.; Petersson, G. A.; Nakatsuji, H.; Caricato, M.;

Li, X.; Hratchian, H. P.; Izmaylov, A. F.; Bloino, J.; Zheng, G.; Sonnenberg, J. L.; Hada, M.; Ehara, M.; Toyota, K.; Fukuda, R.; Hasegawa, J.; Ishida, M.; Nakajima, T.; Honda, Y.; Kitao, O.; Nakai, H.; Vreven, T.; J. A. Montgomery, J.; Peralta, J. E.; Ogliaro, F.; Bearpark, M.; Heyd, J. J.; Brothers, E.; Kudin, K. N.; Staroverov, V. N.; Kobayashi, R.; Normand, J.; Raghavachari, K.; Rendell, A.; Burant, J. C.; Iyengar, S. S.; Tomasi, J.; Cossi, M.; Rega, N.; Millam, J. M.; Klene, M.; Knox, J. E.; Cross, J. B.; Bakken, V.; Adamo, C.; Jaramillo, J.; Gomperts, R.; Stratmann, R. E.; Yazyev, O.; Austin, A. J.; Cammi, R.; Pomelli, C.; Ochterski, J. W.; Martin, R. L.; Morokuma, K.; Zakrzewski, V. G.; Voth, G. A.; Salvador, P.; Dannenberg, J. J.; Dapprich, S.; Daniels, A. D.; Farkas, Ö.; Foresman, J. B.; Ortiz, J. V.; Cioslowski, J.; Fox, D. J. Gaussian09, Revision A.2; Gaussian, Inc.: Wallingford, CT, 2009.

(27) Becke, A. D. *Phys. Rev. A* **1988**, 38, 3098.

(28) Lee, C. T.; Yang, W. T.; Parr, R. G. *Phys. Rev. B* **1988**, 37, 785.

(28) Harihara.Pc; Pople, J. A. *Theor. Chim. Acta.* **1973**, 28, 213.

(30) Harihara.Pc; Pople, J. A. *Mol. Phys.* **1974**, 27, 209.

(31) Hay, P. J.; Wadt, W. R. *J. Chem. Phys.* **1985**, 82, 270.

(32) Wadt, W. R.; Hay, P. J. *J. Chem. Phys.* **1985**, 82, 284.

(33) Hay, P. J.; Wadt, W. R. *J. Chem. Phys.* **1985**, 82, 299.

## **Chapter II.**

### **Diniobium Inverted Sandwich Complexes with $\mu$ - $\eta^6$ : $\eta^6$ - arene Ligands: Synthesis, Kinetics of Formation, and Electronic Structure**

## Introduction

Arene complexes of low-valent metal ions are an intriguing class of molecules because of the high variability in metal-arene interactions.<sup>1-3</sup> Facially-bound arene ligands are known to bind to a wide range of metals in unusual oxidation states using a variety of bonding interactions. In 1983, Krüger *et al.* reported the first dinuclear C<sub>6</sub>H<sub>6</sub> complex, in which a benzene ligand was bound by two CpV moieties in an  $\mu\text{-}\eta^6\text{:}\eta^6$  fashion.<sup>4</sup> Although the inverted arene sandwich motif remains very rare, similar molecules have been found with s-,<sup>5</sup> d-,<sup>4,6-12</sup> and f-block<sup>13-24</sup> metal ions. Typically, these molecules are synthesized by the reduction of metal-halide precursors in aromatic solvents. Upon formation of electron-rich metal centers, coordination of an aromatic solvent molecule provides chemical stability by mixing of the occupied metal d-manifold with the vacant  $\pi^*$  system of the arene ring. Important questions remain, however, regarding the bonding in these compounds, such as how to assign formal oxidation states and how electron density is shared between the metal and the arene. Support for reduction of the arene to form an anionic ligand can be derived from detailed structural investigations, which have revealed elongation<sup>4-24</sup> of the average C-C distances and disruption of arene planarity.<sup>6-7,9-10,13,16-17,19-20</sup> However, evaluating arene charge based on these structural distortions can be challenging because both neutral<sup>4,6-11</sup> and anionic<sup>5,12-24</sup> configurations have been assigned previously.<sup>25</sup> In addition, questions regarding the mechanism of formation of these bimetallic complexes have also not been resolved fully. In a report on the hafnium species Hf<sub>2</sub>I<sub>4</sub>(PMe<sub>2</sub>Ph)<sub>2</sub>( $\mu\text{-}\eta^6\text{:}\eta^6$ -arene), Cotton and coworkers proposed the intermediacy of the monometallic HfI<sub>2</sub>(PMe<sub>2</sub>Ph)<sub>2</sub>( $\eta^6$ -arene).<sup>6</sup> More recently, P. Arnold, L. Maron *et al.* provided computational and experimental evidences for formation of U<sup>3+</sup> inverted sandwich complexes *via* a monometallic arene intermediate.<sup>23</sup>

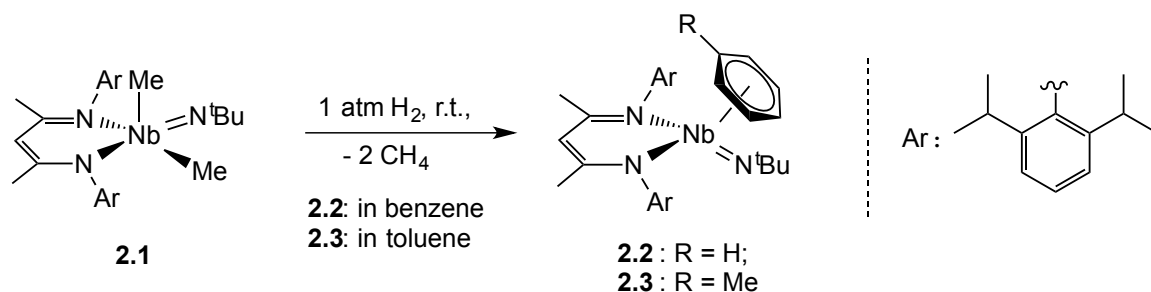
In the previous chapter (e.g. chapter I), in an effort to explore the catalytic potential of low-valent niobium, we reported the catalytic, Z-selective hydrogenation of internal alkynes by the Nb(III) complex [Nb(BDI)(N<sup>t</sup>Bu)(CO)<sub>2</sub>] (**1.1**) (BDI = N,N'-2,6-diisopropylphenyl- $\beta$ -diketiminato).<sup>26</sup> While performing these catalytic studies in aromatic solvents, we became intrigued by the observation of arene complexes (e.g. **1.A** and **1.B**). These complexes formed in the absence of CO, presumably by trapping a low coordinate trivalent niobium complex "Nb(BDI)(N<sup>t</sup>Bu)", which was proposed to be an active species of the catalytic cycle. The study of low-valent, Group 5 transition metals such as Nb could lead to new chemical transformations and catalytic processes. In earlier work, remarkable reactivity and redox behavior has been reported for monomeric low-valent Nb(III) complexes that were isolated or generated *in situ*, spanning activation of small molecules<sup>27-32</sup> hydrogenation,<sup>26,33</sup> C-C coupling,<sup>34-38</sup> and C-H bond activation reactions.<sup>39-44</sup> The study presented here describes the synthesis and characterization of several new Nb arene complexes, including the kinetics of formation of the first bimetallic  $\mu\text{-}\eta^6\text{:}\eta^6$ -arene inverted sandwich complexes<sup>45</sup> from the parent  $\eta^6$ -arene monometallic species. Protonation of the BDI ligands afforded the mono- and dicationic  $\mu\text{-}\eta^6\text{:}\eta^6$ -benzene complexes. All four inverted sandwich complexes were subjected to a suite of characterization methods, including single-crystal X-ray diffraction as well as UV-visible. Each of the four inverted-sandwich complexes also bears a diamagnetic electronic configuration, which provides an unusual opportunity to undertake an in-depth <sup>1</sup>H and <sup>13</sup>C (1D and 2D) NMR spectroscopic study of the metal-arene interactions. The combined experimental data provide new insight into the electronic structure of d-block metal-arene complexes.



## Results and discussions

### Monometallic arene complexes

The Nb(V) complex  $[\text{Nb}(\text{BDI})(\text{N}^t\text{Bu})\text{Me}_2]$  (**2.1**)<sup>46</sup> reacts with  $\text{H}_2$  in benzene or toluene at room temperature to form two complexes,  $[\text{Nb}(\text{BDI})(\text{N}^t\text{Bu})(\text{R}-\text{C}_6\text{H}_5)]$  ( $\text{R} = \text{H}$ , **2.2** or  $\text{Me}$ , **2.3**), as diamagnetic red powders in high purities and very good yields (93%, Scheme 2.1). Initial efforts to obtain X-ray quality crystals of **2.2** and **2.3** were thwarted by their propensity to form mixtures with their bimetallic counterparts upon isolation (see below). Nevertheless, rapid crystallization of **2.2** from a mixture of toluene/hexanes formed material suitable for X-ray crystallographic analysis (Figure 2.1).



**Scheme 2.1** Synthesis of complexes **2.2** and **2.3**

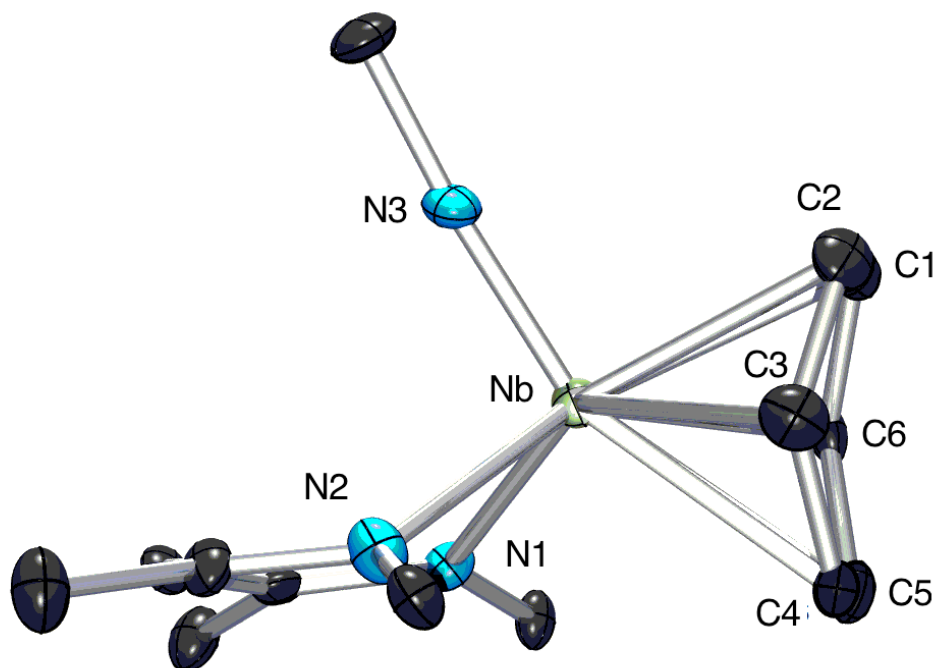
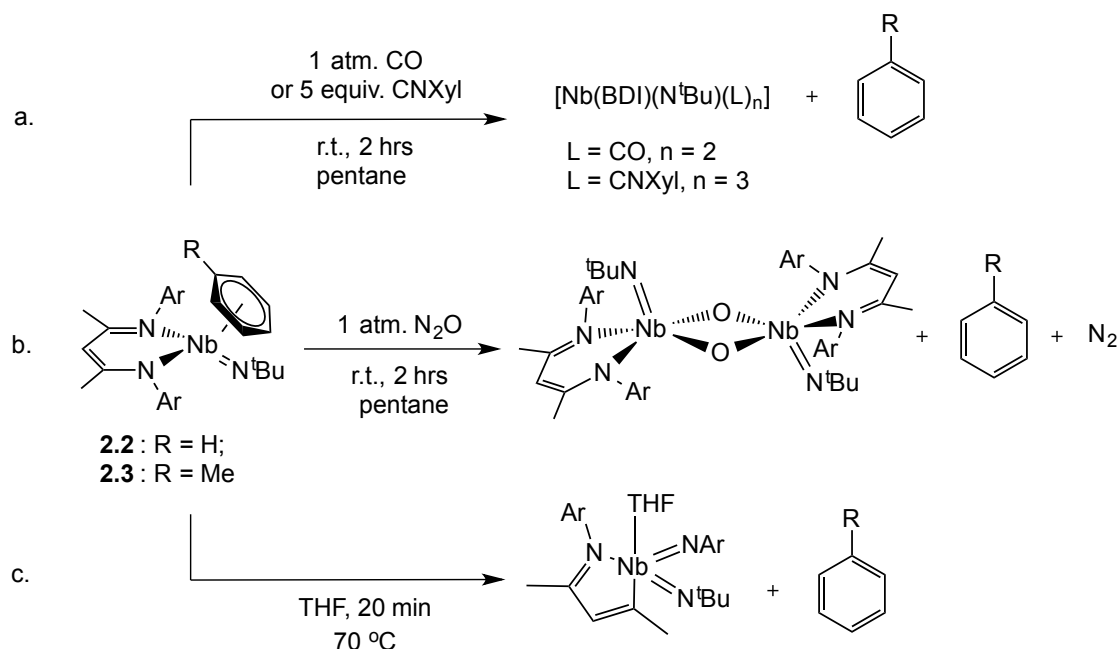


**Figure 2.1** Thermal ellipsoid plot of the complex **2.2**. Diisopropyl aryl groups of the BDI ligand have been removed and  $t\text{Bu}$  moieties have been truncated for clarity. Structural parameters are presented in the experimental part in Table 2.2.

Although several niobium arene complexes have been reported,<sup>47-62</sup> to the best of our knowledge **2.2** is the first niobium-benzene complex that has been structurally characterized. In **2.2** the BDI and imido ligands occupy facial positions in a pseudo-octahedral geometry. The N-Nb-N angle of the BDI ligand is 81.4° and the average N-Nb-N<sub>imido</sub> angle is 98.5°. The two Nb-N<sub>BDI</sub> distances are 2.246(4) Å, which are similar to those observed in related BDI complexes of Nb(III) and Nb(V).<sup>32,44,46</sup> The Nb-N<sub>imido</sub>-CMe<sub>3</sub> bond angle (175.3(4)°) is close to linear and the Nb-N<sub>imido</sub> distance is 1.775(3) Å, which is also typical of values reported in the literature.<sup>32,44,46</sup> The C<sub>6</sub>H<sub>6</sub> ligand of **2.2** is puckered, which is a characteristic of niobium-arene complexes.<sup>47-50,52-53,57,62</sup> The fold angle at C3···C6 is 22.8°, such that the Nb(1)-C(3) (2.280(5) Å) and Nb(1)-C(6) (2.284(5) Å) distances are shorter than observed for the other four Nb-C bonds (average 2.471(4) Å). These Nb-C distances compare well with Nb-C distances observed previously for arene compounds (from 2.198(5) Å to 2.513(4) Å).<sup>47-62</sup> The C-C bond lengths of the benzene ring vary, with C(1)-C(2) (1.337(6) Å) and C(4)-C(5) (1.384(6) Å) being significantly shorter than bonds involving the C(3) and C(6) atoms (average of 1.450(5) Å).

The <sup>1</sup>H NMR spectrum of the η<sup>6</sup>-benzene complex [Nb(BDI)(N<sup>t</sup>Bu)(η<sup>6</sup>-C<sub>6</sub>H<sub>6</sub>)], **2.2**, shows 12 signals, corresponding to a C<sub>s</sub>-symmetric Nb(N<sup>t</sup>Bu)(BDI) moiety, with a singlet (6 H) at high-field (3.60 ppm) for the six equivalent benzene protons. The toluene complex [Nb(BDI)(N<sup>t</sup>Bu)(η<sup>6</sup>-Me-C<sub>6</sub>H<sub>5</sub>)], **2.3**, presents similar <sup>1</sup>H NMR spectroscopic features, with three sharp resonances at δ = 3.93, 3.71, 3.59 ppm that were assigned to the aromatic toluene protons and one at δ = 2.0 ppm corresponding to the methyl group of the coordinated toluene. The η<sup>6</sup> aromatic rings of **2.2** and **2.3** exchange with C<sub>6</sub>D<sub>6</sub> (in C<sub>6</sub>D<sub>6</sub> solution) within 120 min and 20 min, respectively, at room temperature. The <sup>2</sup>H NMR spectrum of **2.2-d<sub>6</sub>** also shows a singlet at 3.60 ppm, in accordance with the proposed structure. These <sup>1</sup>H NMR data are consistent with the presence of an averaged η<sup>6</sup>-arene adduct in solution (Scheme 2.1).

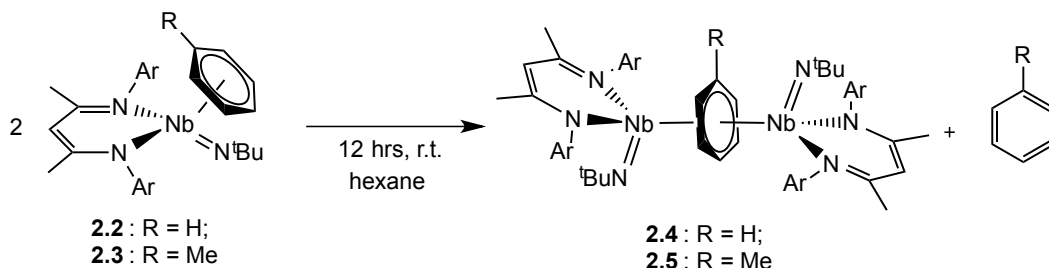
Consistent with this behavior, the coordinated arene rings of **2.2** and **2.3** were found to be readily displaced by carbon monoxide or 2,6-xylyl-isocyanide, leading to the previously reported [Nb(BDI)(N<sup>t</sup>Bu)(CO)<sub>2</sub>]<sup>44</sup> and [Nb(BDI)(N<sup>t</sup>Bu)(CNXyl)<sub>3</sub>]<sup>32</sup> complexes, respectively (Scheme 2.2a). Reactivity studies also confirm that the coordinated arene ligands in **2.2** and **2.3** serves to stabilize the Nb(BDI)(N<sup>t</sup>Bu) moiety, which can be oxidized by two electrons with suitable substrates. For example, exposure of a benzene solution of **2.2** or a toluene solution of **2.3** to N<sub>2</sub>O (1 atm.) quickly leads to the formation of the previously reported μ-oxo dinuclear complex [Nb(BDI)(N<sup>t</sup>Bu)(μ-O)]<sub>2</sub> (Scheme 2.2b).<sup>32</sup> In the absence of an external oxidant, loss of the arene via thermolysis of either **2.2** and **2.3** in THF leads to formation of the bis-imido Nb(V) complex (Scheme 2.2c), where the BDI ligand has been reductively cleaved. This latter compound has been observed previously following hydrogenolysis of [Nb(BDI)(N<sup>t</sup>Bu)Me<sub>2</sub>] in THF, via cleavage of the BDI ligand in the related Nb(III) species [Nb(BDI)(N<sup>t</sup>Bu)(THF)].<sup>32</sup>



**Scheme 2.2** Reactivity of complexes **2.2** and **2.3**

### *Bimetallic arene complexes*

**Synthesis and kinetic studies.** In an attempt to hinder arene exchange in solution,  $^1\text{H}$  NMR spectra of **2.2** and **2.3** were recorded in  $\text{C}_6\text{D}_{12}$ . Unexpectedly, collecting additional  $^1\text{H}$  NMR spectra of these solutions after 3 d revealed the clean formation of new diamagnetic arene species that were subsequently formulated as  $\mu\text{-}\eta^6\text{:}\eta^6\text{-arene}$  dinuclear inverted sandwich complexes  $[[(\text{BDI})\text{Nb}(\text{N}^t\text{Bu})]_2(\mu\text{-}\eta^6\text{:}\eta^6\text{-RC}_6\text{H}_5)]$  ( $\text{R} = \text{H}$ , **2.4** or  $\text{Me}$ , **2.5**; Scheme 2.3). Red crystals were obtained on a preparative scale in good yields from saturated, dark red, hexanes solutions of either **2.2** or **2.3**.



**Scheme 2.3** Formation of complexes **2.4** and **2.5**

To the best of our knowledge, experimental evidence for the formation of an arene bridged dinuclear complex from a parent, mononuclear species has only been reported once,<sup>23</sup> although related mechanisms have been suggested since the early 90s.<sup>6</sup> The relatively slow rate of conversion from **2.2** to **2.4** provides an opportunity to follow the kinetics of this process by  $^1\text{H}$  NMR spectroscopy. The experiment was performed in  $\text{C}_6\text{D}_{12}$  with 0.07 M **2.2** and 4.90 mM internal standard at 334 K. In the absence of benzene, the kinetic data cannot be fitted to a rate law that is either first order or second order in **2.2** because the concentration of

free benzene is changing during the experiments. Introducing an excess of benzene (from 4 to 30 equivalents) yields data that are consistent with a dissociative mechanism, and a rate law that is second order in **[2.2]** and inverse first order in benzene (Figure 2.2 and Appendix C). The rate law for the formation of **2.4** predicted for the dissociative mechanism illustrated in Scheme 2.4 is included at the bottom of the Scheme. When benzene is in a large excess, the condition  $k_{-1}[\text{Benz}] \gg k_2[\mathbf{2.2}]$  is satisfied. Therefore, the formation of complex **2.4** follows second order kinetics, consistent with P. Arnold report,<sup>23</sup> with  $k_{\text{obs}}$  being inversely proportional to the initial benzene concentration, where  $\frac{k_1 k_2}{k_{-1}}$  is  $0.0723 \text{ min}^{-1}$  at 334 K (Figure 2.2).

Knowing the rate law, an Eyring analysis was performed in the presence of a large excess of benzene (0.593 M, 8 equivalents) over the temperature range 313 – 344 K, at 5 K intervals (Figure 2.3 and Appendix C). The large enthalpy of activation ( $28.8(4) \text{ kcal.mol}^{-1}$ ) is consistent with the slow conversion of **2.2** to **2.4** at room temperature. The large positive entropy of activation ( $56(2) \text{ cal.mol}^{-1}.\text{K}^{-1}$ ), must be interpreted carefully due to the relatively small temperature range of the study. However, the large positive value further supports a dissociative mechanism in which the first step corresponds to the formation of a 3-coordinate species and free benzene (Scheme 2.4).

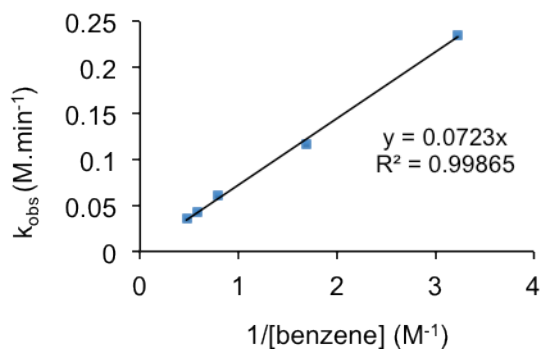
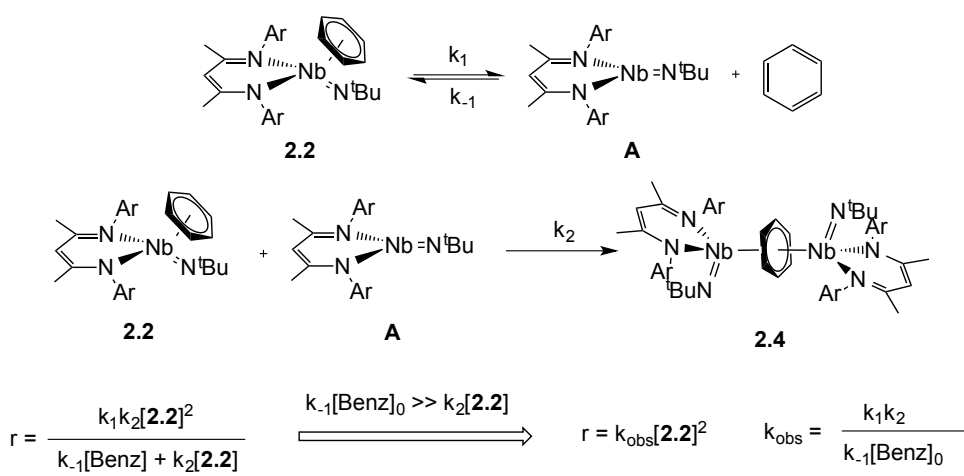
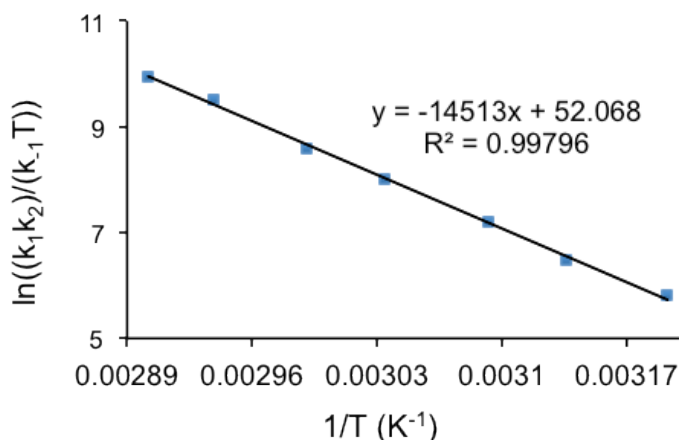


**Figure 2.2** Benzene dependence on the observed 2<sup>nd</sup> order rate constant of the formation of **2.2**



**Scheme 2.4** Reactions of the formation of complex **2.2** and kinetic law derivation.



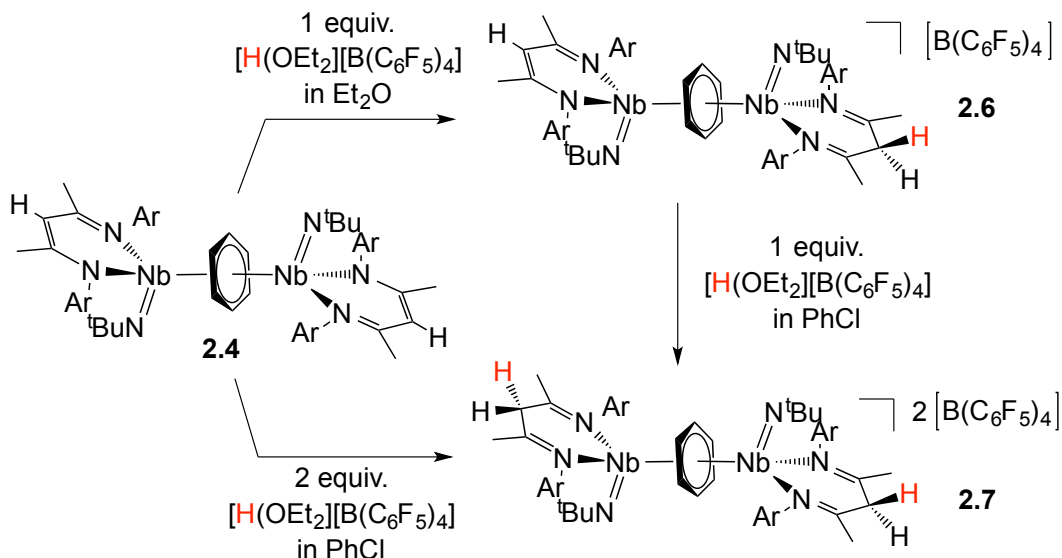
$$(\Delta H_1^\ddagger - \Delta H_{-1}^\ddagger) + \Delta H_2^\ddagger = 28.8 (4) \text{ kcal.mol}^{-1}$$

$$(\Delta S_1^\ddagger - \Delta S_{-1}^\ddagger) + \Delta S_2^\ddagger = 56 (2) \text{ cal.mol}^{-1}.\text{K}^{-1}$$

**Figure 2.3** Eyring plot for the formation of complex **2.2** (top). Activation parameters derived from the Eyring plot (bottom).

**Reactivity of 2.4.** Unlike the monometallic complexes **2.2** and **2.3** discussed above, and relative to other inverted sandwich molecules reported in the literature,<sup>4,6-8,10-12,14-23</sup> the bridged arenes of **2.4** and **2.5** did not exchange with deuterated benzene, toluene, or strong p-acidic ligands such as carbon monoxide or isocyanide, even at temperatures up to 110 °C. To our knowledge, only two other inverted sandwich complex did not show exchange with solvent molecules at reasonable temperatures.<sup>9,23</sup> Complexes **2.4** and **2.5** also did not react with small molecules such as Ph<sub>2</sub>N<sub>2</sub>, Ph<sub>2</sub>S<sub>2</sub>, N<sub>2</sub>O, organic azides, alkynes, CO<sub>2</sub> and H<sub>2</sub> within a temperature range of 20 to 110 °C, unlike many other inverted sandwich complexes.<sup>4,8,10,14-17,19,23</sup> In contrast, treatment of complex **2.4** with either 1 or 2 equivalents of [H(OEt<sub>2</sub>)] [B(C<sub>6</sub>F<sub>5</sub>)<sub>4</sub>] produced two products that were formulated as new inverted sandwich complexes, [[(BDI<sup>#</sup>)Nb(N<sup>t</sup>Bu)][(BDI)Nb(N<sup>t</sup>Bu)](μ-η<sup>6</sup>:η<sup>6</sup>-C<sub>6</sub>H<sub>6</sub>)] [B(C<sub>6</sub>F<sub>5</sub>)<sub>4</sub>] (**2.6**) and [[(BDI<sup>#</sup>)Nb(N<sup>t</sup>Bu)]<sub>2</sub>(μ-η<sup>6</sup>:η<sup>6</sup>-C<sub>6</sub>H<sub>6</sub>)] [B(C<sub>6</sub>F<sub>5</sub>)<sub>4</sub>]<sub>2</sub> (**2.7**) in which one (**2.6**) or two (**2.7**) BDI ligands have been protonated (Scheme 2.5, BDI<sup>#</sup> = (ArNC(Me))<sub>2</sub>CH<sub>2</sub>).

Compounds **2.6** and **2.7** have been synthesized in diethyl ether and chlorobenzene, respectively, and can both be isolated on a preparative scale in good yields. The lack of reactivity at the coordinated benzene ligand may be evidence of a neutral C<sub>6</sub>H<sub>6</sub> configuration; however, it is difficult to rule out the possibility that the ancillary ligands are providing steric protection (see Figure 2.4, bottom).



**Scheme 2.5** Synthesis of complexes **2.6** and **2.7**

**X-Ray Crystal Structure Descriptions.** Thermal ellipsoid plots of complexes **2.4**, **2.5**, **2.6** and **2.7** are shown in Figures 2.4 and 2.5, and bond distances and angles are summarized in Table 2.1 (see also the Tables 2.2 and 2.3 in the experimental part for crystallographic parameters). In each of the four inverted-sandwich complexes **2.4**, **2.5**, **2.6** and **2.7**, the BDI and imido ligands occupy facial positions in a pseudo-octahedral geometry. Complexes **2.4**, **2.6**, and **2.7** adopt geometries with dihedral angles between the two imido groups of  $114.3^\circ$ ,  $132.3^\circ$ ,  $117.9^\circ$  respectively, which minimizes steric repulsion between the aryl rings of the BDI ligands. The BDI-aryls are distorted away from the central toluene ligand in **2.4**, resulting in a smaller dihedral angle of  $40.6^\circ$  (Figure 2.5). Average Nb- $\text{N}_{\text{BDI}}$  distances are  $2.249(2)$  Å and  $2.258(3)$  Å in **2.4** and **2.5**, and  $2.311(2)$  Å in **2.7**. Because **2.6** is dissymmetric, two different sets of average Nb- $\text{N}_{\text{BDI}}$  distances are observed:  $2.317(2)$  Å on the side with the protonated BDI ligand, and  $2.203(2)$  Å on the other.

The C–C distances of the arene rings in **2.4**, **2.5**, **2.6** and **2.7** are all very similar, and provide an average C–C distance of  $1.45$  Å for all four complexes with a standard deviation of  $0.02$  Å (see Table 2.1). These distances are slightly longer than those reported for free benzene and toluene ( $1.397(1)^{63}$  Å and  $1.39(1)^{64}$  Å) but in the range of the reported values found for m- $\text{h}^6\text{:h}^6$ -arene ligands in the literature.<sup>4-24</sup> In the four complexes **2.4**, **2.5**, **2.6** and **2.7** the bridging arenes are non-planar. Observed Nb–C bond distances vary widely for **2.4** ( $2.2673(17)$  to  $2.6291(19)$  Å), **2.5** ( $2.286(4)$  to  $2.636(4)$  Å), and **2.7** ( $2.277(2)$  to  $2.620(2)$  Å). The benzene centroid is nearly equidistant from both niobium atoms in **2.4**, **2.5**, and **2.7**, with average Nb–centroid bond distances of  $1.958$  Å (**2.4**),  $1.944$  Å (**2.5**), and  $1.939$  Å (**2.7**). For complex **2.6**, in which one of the BDI ligands is protonated, the benzene ligand lies closer to the Nb bearing the protonated ligand (Nb(1)–C range  $2.256(2)$  to  $2.607(2)$  Å; Nb(1)–centroid  $1.919$  Å) than it does to Nb atom with the unprotonated ligand (Nb(2)–C range  $2.202(2)$  to  $2.835(2)$  Å; Nb(2)–centroid  $2.089$  Å). The Nb(1)–Nb(2) distances decrease by  $0.046(5)$  Å from the  $\text{C}_6\text{H}_6$  complex **2.4** ( $3.914(2)$  Å) to  $\text{C}_7\text{H}_8$  complex **2.5** ( $3.868(4)$  Å), which could be a consequence of changes in bonding or an increase in steric pressure in **2.5**. However, the Nb(1)–Nb(2) distances also decrease by  $0.038(2)$  Å from neutral **2.4** ( $3.914(2)$  Å) to twice-

protonated **2.7** (3.876(2) Å), which is clearer evidence that protonation disrupts the BDI-Nb interaction and enhances bonding between the arene ligand and Nb atoms.

The mean deviation of the arene rings from planarity is 0.051 Å, 0.052 Å, 0.050 Å and 0.053 Å respectively, while the largest distortions from the mean plane are 0.170 Å (**2.4**) and 0.147 Å (**2.5**), 0.159 Å (**2.6**) and 0.163 Å (**2.7**) (Figure 2.6). The deviation from planarity was also measured from the different dihedral angles of the ring, with average distortions of 14.4° (**2.4**), 15.1° (**2.5**), 15.2° (**2.6**) and 15.2° (**2.7**) (Figure 2.7). Such deformations of the  $\eta^6, \eta^6$ -arene ring have been described in the literature,<sup>6-7,9-10,13,16-17,19-20</sup> and support three possible conclusions: i) the arene ring is significantly reduced, such that there is a disruption of aromaticity and the carbon atoms are best regarded as  $sp^3$ -hybridized; ii) the distortions are sterically-induced; or iii) both these electronic and steric factors are at work. Therefore, additional measurements were performed to understand whether the origin of these structural deformations is inherent to the electronic structure of these complexes.

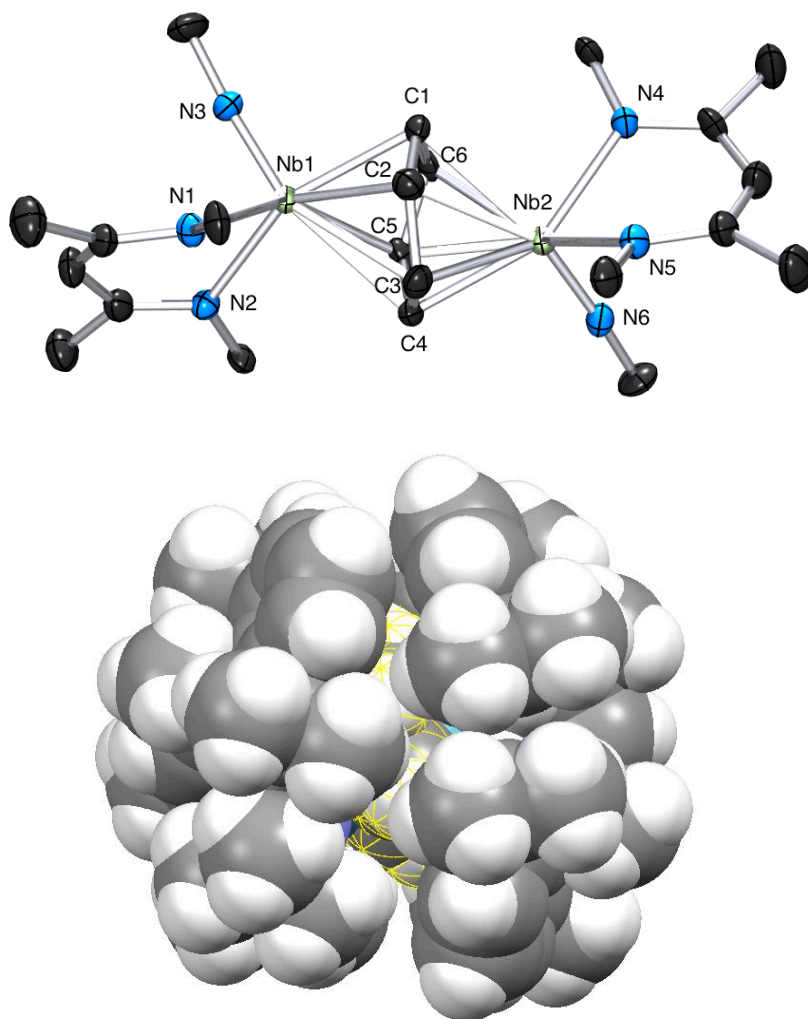


**Figure 2.4** Thermal ellipsoid plots (top, diisopropyl aryl groups of the BDI ligand and hydrogens have been removed and <sup>t</sup>Bu moieties have been truncated for clarity) and spacefill view (bottom, the benzene moiety is highlighted in yellow) of **2.4**.

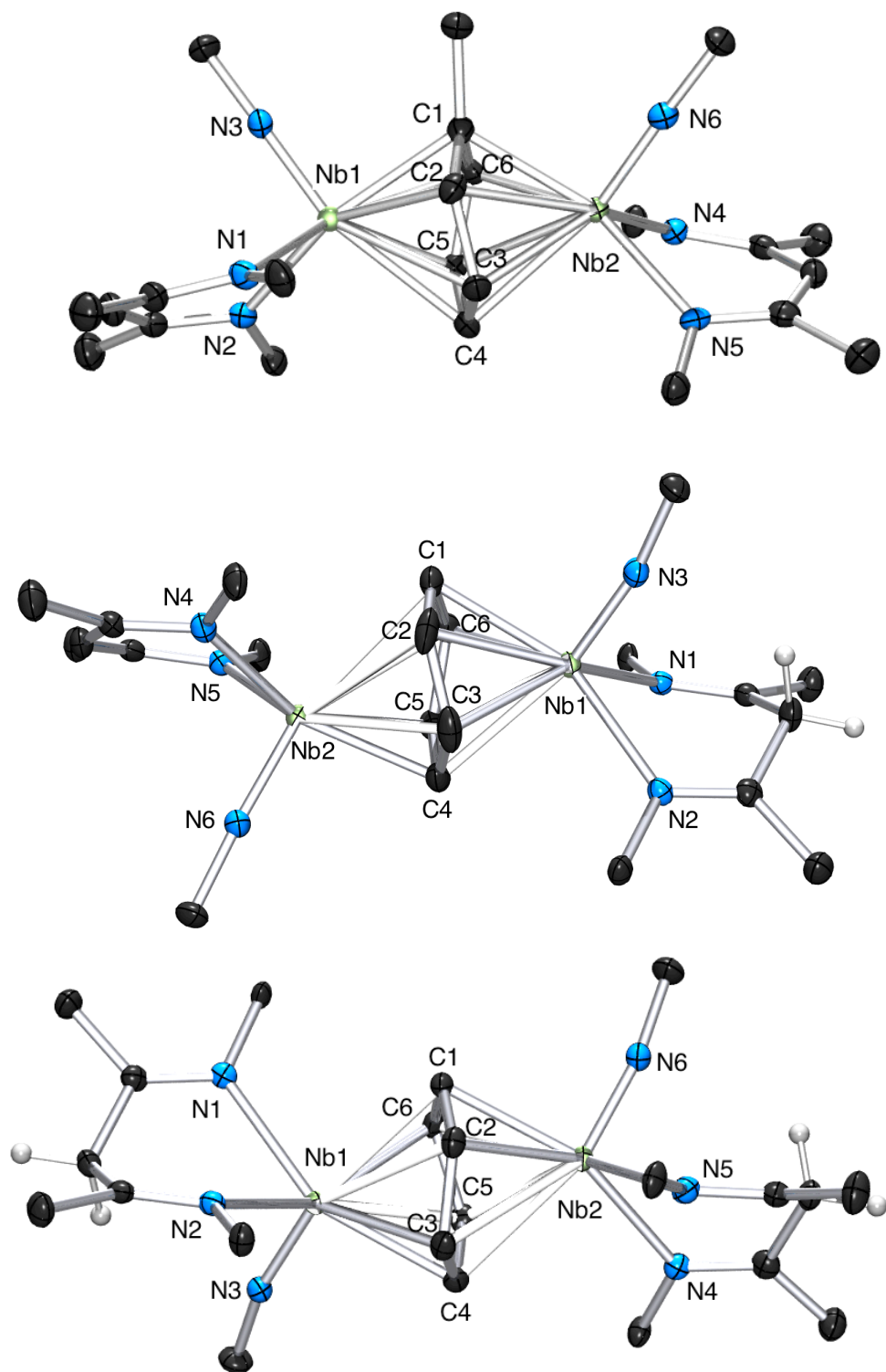


**Figure 2.5** Thermal ellipsoid plots of the complexes **2.5** (first), **2.6** (second) and **2.7** (third). Diisopropyl aryl groups of the BDI ligand and B(C<sub>6</sub>F<sub>5</sub>)<sub>4</sub> have been removed and 'Bu moieties have been truncated for clarity.



**Table 2.1** Selected bond distances (in Å) for complexes **2.4**, **2.5**, **2.6** and **2.7**.

	<b>2.4</b>	<b>2.5</b>	<b>2.6</b>	<b>2.7</b>
C(1)–C(2)	1.452(3)	1.462(4)	1.474(3)	1.444(3)
C(2)–C(3)	1.451(3)	1.476(4)	1.464(3)	1.461(3)
C(3)–C(4)	1.453(3)	1.422(5)	1.424(4)	1.452(4)
C(4)–C(5)	1.447(3)	1.451(5)	1.432(4)	1.453(3)
C(5)–C(6)	1.473(3)	1.443(4)	1.426(3)	1.443(3)
C(6)–C(1)	1.450(3)	1.475(4)	1.463(3)	1.465(3)
average C–C	1.454	1.455	1.447	1.453
Nb(1)–C(1)	2.2599(16)	2.304(4)	2.607(2)	2.301(2)
Nb(1)–C(2)	2.478(2)	2.296(4)	2.504(2)	2.620(2)
Nb(1)–C(3)	2.3273(19)	2.630(5)	2.256(2)	2.511(2)
Nb(1)–C(4)	2.5526(17)	2.518(4)	2.371(2)	2.325(2)
Nb(1)–C(5)	2.6291(19)	2.324(4)	2.325(2)	2.482(2)
Nb(1)–C(6)	2.3324(19)	2.446(3)	2.305(2)	2.277(2)
Nb(2)–C(1)	2.5533(18)	2.286(4)	2.345(2)	2.605(2)
Nb(2)–C(2)	2.3302(19)	2.449(3)	2.202(2)	2.308(2)
Nb(2)–C(3)	2.4785(18)	2.328(4)	2.501(2)	2.297(2)
Nb(2)–C(4)	2.2673(17)	2.527(5)	2.528(2)	2.460(2)
Nb(2)–C(5)	2.324(2)	2.636(4)	2.748(2)	2.294(2)
Nb(2)–C(6)	2.6197(19)	2.289(3)	2.835(2)	2.493(2)
Nb(1)–Nb(2)	3.914	3.868	3.989	3.876
Nb(1)–Cent	1.957	1.944	1.919	1.947
Nb(2)–Cent	1.959	1.945	2.089	1.932
average Nb(1)–C	2.430	2.420	2.395	2.419
average Nb(2)–C	2.429	2.419	2.527	2.409
average Nb–C	2.429	2.419	2.461	2.414
Nb(1)–N(1)	2.2764(16)	2.249(3)	2.3236(18)	2.289(2)
Nb(1)–N(2)	2.2136(17)	2.271(3)	2.3109(17)	2.3226(19)
Nb(1)–N(3)	1.7770(15)	1.776(3)	1.7860(18)	1.774(2)
Nb(2)–N(4)	2.2787(16)	2.241(3)	2.2209(18)	2.2983(19)
Nb(2)–N(5)	2.2266(15)	2.271(3)	2.2055(18)	2.3287(19)
Nb(2)–N(6)	1.7815(15)	1.782(3)	1.7718(19)	1.7819(19)

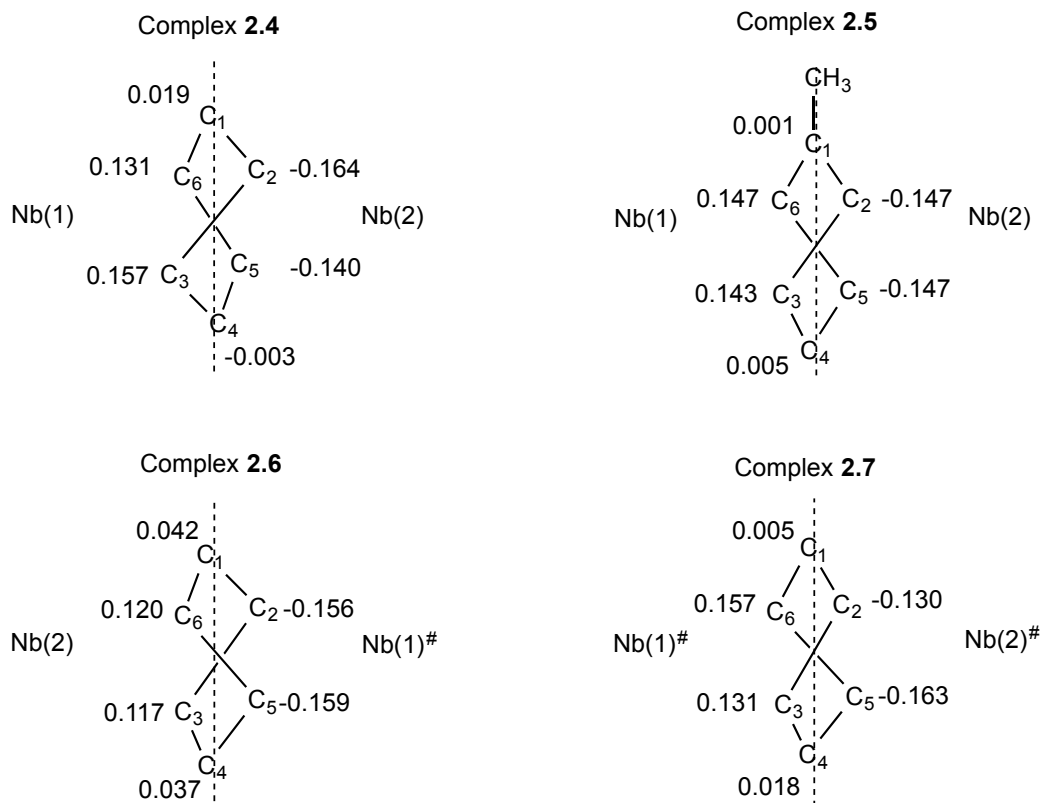
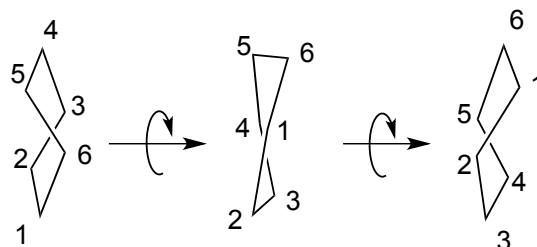


**Figure 2.6** Mean deviations were estimated by summing the deviation from each carbon and the mean plane formed by the arene moiety (in Å).



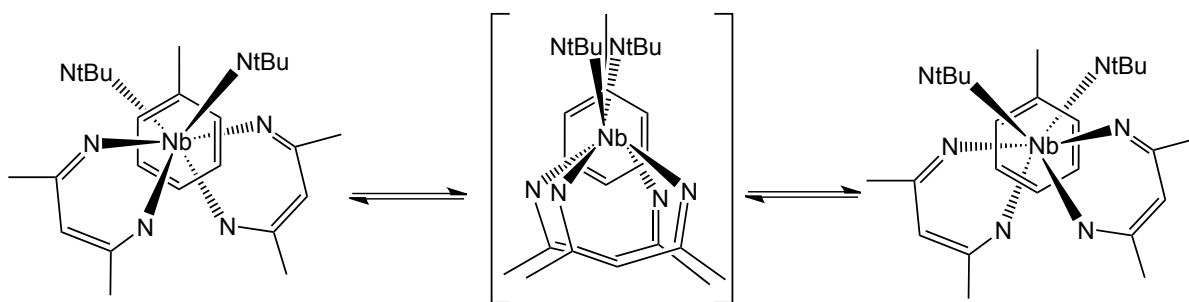
Complexes	Angle (°) 3456 $\angle$ 3216	Angle (°) 1234 $\angle$ 1654	Angle (°) 2165 $\angle$ 2345	Average distortion (°)
<b>2.4</b>	19.04	4.92	18.56	14.06
<b>2.5</b>	20.37	4.74	20.13	15.08
<b>2.6</b>	21.95	7.02	16.71	15.22
<b>2.7</b>	20.82	4.92	19.99	15.24

**Figure 2.7** The average distortion angles were estimated by averaging the three dihedral angles formed between the 6 planes of the arene moiety (e.g. 1234  $\angle$  1654 reads angle between plane 1234 and 1654)

**NMR Spectroscopy.** The  $^1\text{H}$  NMR spectrum of **2.4** exhibits one singlet for the methyl groups of both the BDI ligands, one singlet for the equivalent  $^t\text{Bu}$  groups of the imido ligands, and one singlet ( $\delta = 2.21$  ppm) for the benzene ring. These data are consistent with free rotation of the  $(\text{BDI})\text{Nb}(\text{N}^t\text{Bu})$  moieties in solution around the  $\text{Nb}\cdots\text{Nb}$  axis, resulting in an average  $C_{2v}$  symmetry on the  $^1\text{H}$  NMR time-scale at room temperature (see Scheme 2.6).

Although the spectrum of the benzene complex **2.4** remains unchanged down to 213 K in  $\text{C}_7\text{D}_8$ , lowering the temperature to 213 K for the toluene derivative **2.5** results in a  $^1\text{H}$  NMR spectrum that reflects the same  $C_2$ -symmetric coordination environment observed in the solid state, thus implying that the dynamic motion has been frozen on the  $^1\text{H}$  NMR time scale. Variable temperature  $^1\text{H}$  NMR data collected between 213 K and 383 K provided a coalescence temperature of  $T_c = 300(2)$  K (Figure 2.8). Thermodynamic parameters for this geometrical rearrangement were also measured via a Selective Inversion Recovery (SIR) experiment, yielding  $\Delta H^\ddagger = 13.9(6)$  kcal mol $^{-1}$  and  $\Delta S^\ddagger = -4(2)$  cal K $^{-1}$  mol $^{-1}$  (Figure 2.8 and Figure 2.9).

As expected, the room-temperature  $^1\text{H}$  NMR spectrum of complex **2.6** reflects a lower symmetry coordination environment than **2.4** and **2.5**, involving two singlets (6 H) for the methyl groups of the two different BDI ligands, two singlets (9 H) for each of the  $^t\text{Bu}$  substituents on the two imido groups and a singlet for the  $\text{C}_6\text{H}_6$  ligand ( $\delta = 2.40$  ppm). Complex **2.7**, which has two protonated BDI ligands, exhibits two singlets for the methyl groups of the BDI ligands, one singlet for the  $^t\text{Bu}$  groups and a singlet for the benzene ring ( $\delta = 2.55$  ppm). This indicates that the dynamic motion in this complex is slow on the  $^1\text{H}$  NMR time scale at room temperature. Although **2.7** undergoes slow decomposition at temperatures higher than 335 K, a variable temperature experiment (295 K to 330 K) provided a coalescence temperature ( $T_c = 320(2)$  K) which was higher than for complex **2.5** ( $T_c = 300(2)$  K). A SIR experiment was not possible due to the small chemical shift difference of the exchanging peaks. The coalescence temperature trend measured for the geometrical rearrangement of **2.4**, **2.5**, **2.6** and **2.7** ( $T_c < 213$  K,  $T_c = 300$  K,  $T_c < 230$  K and  $T_c = 320$  K, respectively) is not strictly consistent with what would be expected from steric considerations. Rather, the solution data suggest that the interaction between the arene and the metal centers is stronger in **2.7** relative to both **2.4** and **2.5**, resulting in higher activation barrier of the geometric rearrangement.



**Scheme 2.6** Dynamic motion of complex **2.5**

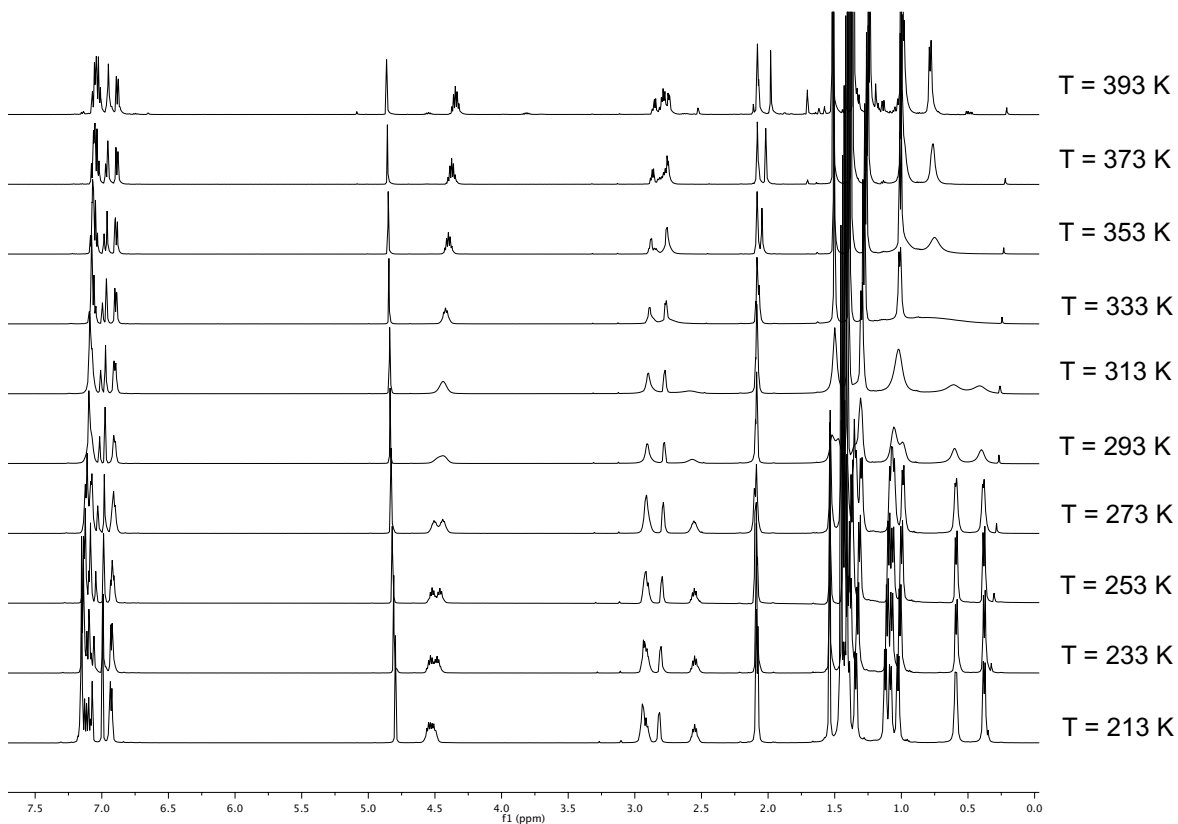


**Figure 2.8.**  $^1\text{H}$  NMR Variable temperature spectra from 213 K to 383 K of complex **2.5**

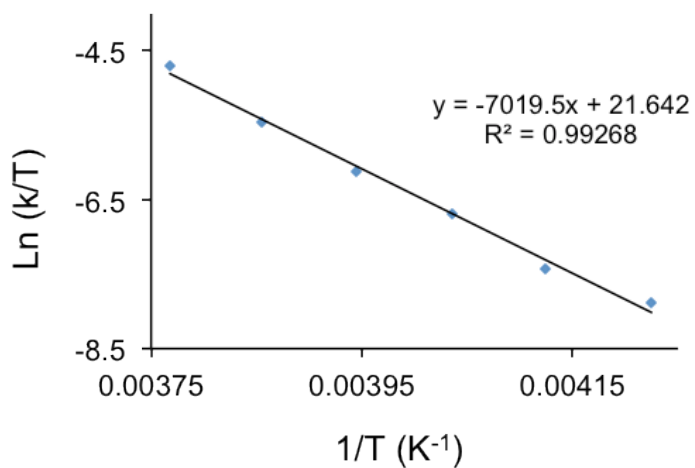


**Figure 2.9** Eyring plots for the dynamic processes observed by  $^1\text{H}$  NMR in toluene- $d_8$  for complex **2.5**.

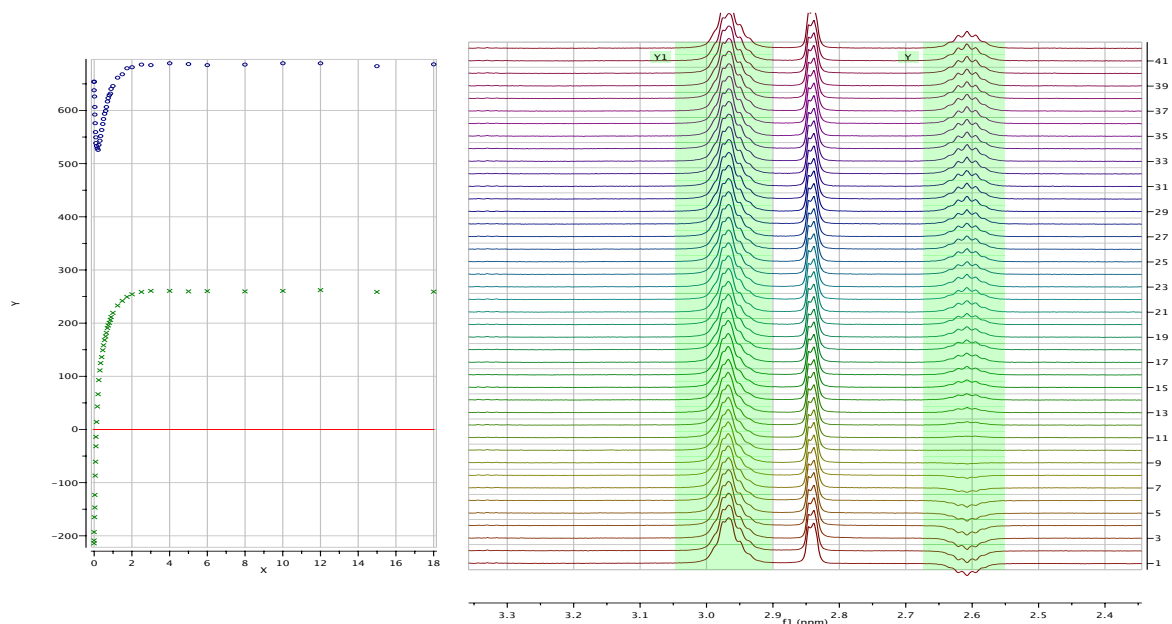


**Figure 2.10**  $^1\text{H}$  NMR spectra of complex **2.5** at different mixing time from the SIR experiment at  $T = 253$  K (right). Observed integral of the exchange resonance (top left, blue) and of the saturated resonance (bottom left, green) from the SIR experiment at  $T = 253$  K.

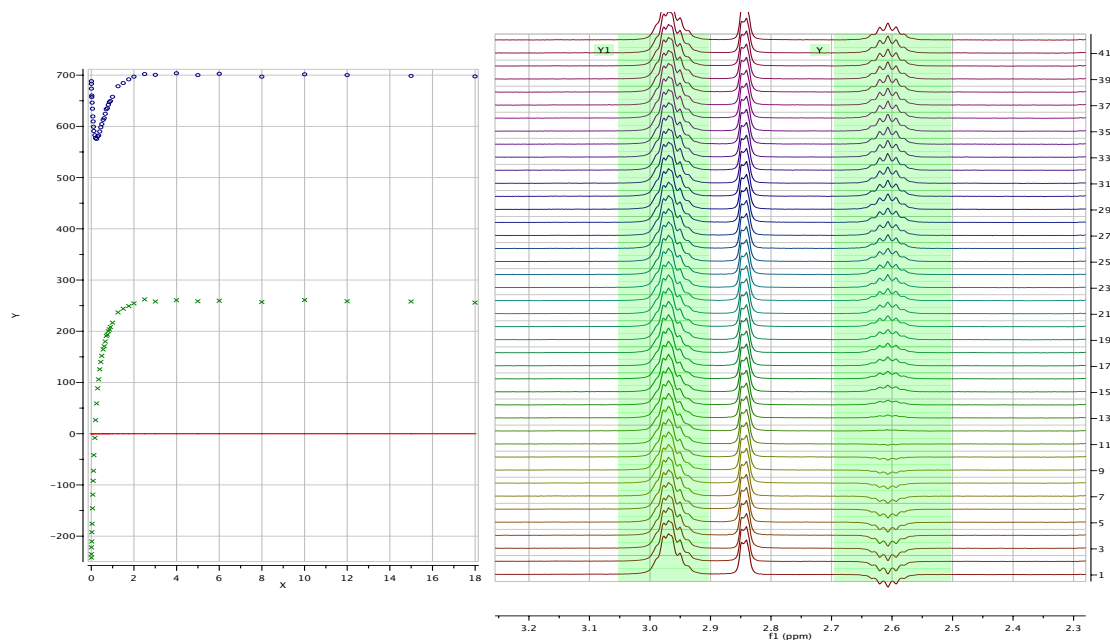


**Figure 2.11**  $^1\text{H}$  NMR spectra of complex **2.5** at different mixing time from the SIR experiment at  $T = 263$  K (right). Observed integral of the exchange resonance (top left, blue) and of the saturated resonance (bottom left, green) from the SIR experiment at  $T = 263$  K.

The  $^1\text{H}$  NMR resonances of the bridging arene rings of **2.4**, **2.5**, **2.6** and **2.7** are all found in the 2-3 ppm range, which is consistent with data provided for a diamagnetic, Hf inverted-sandwich of toluene (3.12 to 3.34 ppm).<sup>6</sup> The chemical shifts of the benzene rings observed in **2.4** (2.21 ppm) were slightly more shielded than those observed for **2.7** (2.53 ppm). Shifts to higher field from the free arene could result from either  $\text{sp}^3$ -hybridization of the carbon due to covalent bonding with the metal centers or from strong shielding effect from the flanking rings on the BDI ligand.

Proton-coupled  $^{13}\text{C}$  NMR spectroscopy was performed to determine  $^1J_{\text{CH}}$  values and further refine the bonding models proposed above. The coupling constants were found to be  $J_{\text{CH}} = 178.2(6)$  Hz for **2.4**,  $J_{\text{CH}} = 178.9(7)$  Hz for complex **2.6** and  $J_{\text{CH}} = 184.5(6)$  Hz for **2.7**. A similar experiment performed on the monometallic complex **2.2** gave a  $J_{\text{CH}}$  value of 170.5(6) Hz. These differ from the corresponding parameters for aromatic  $\text{sp}^2$  carbons (160(1) Hz) by approximately +20 Hz for bimetallic complexes **2.4**, **2.6** and **2.7** and by +10 Hz for complex **2.2**.<sup>65</sup> Such increases in coupling strength are inconsistent with a decrease in s-character relative to an  $\text{sp}^2$ -hybridized aromatic carbon and suggest that coordination of the Nb atoms does not result in a formal  $\text{sp}^3$ -hybridization of the bridging arene-ring atoms. Taken together, the NMR data lead us to conclude that the upfield chemical shifts of the benzene ring are due to shielding induced by the ligand set. This effect has been previously observed in the Nb(BDI)(N<sup>t</sup>Bu) system.<sup>44</sup>

As an additional note, the amplitude of the observed coupling constant  $J_{\text{CH}}$  is also proportional to the electron density located on the atom.<sup>66</sup> Hence, the magnitude of the increase in  $J_{\text{CH}}$  is due to electron density donated from the niobium metal centers to the arene ligands in **2.2**, **2.4**, **2.6** and **2.7**. The relative amount of donation may be evaluated by consideration of the  $J_{\text{CH}}$  coupling constants in a manner related to the accepted practice of using shifts in  $\nu_{\text{CO}}$  as a measure of the metal-based electron density in carbonyl complexes.<sup>67</sup> In the present case, the  $^1\text{H}$  NMR data indicate that Nb→benzene donation increases in the order **2.2** < **2.4** ≈ **2.6** < **2.7**. These solution data are also correlated with the slight decrease observed in Nb(1)–Nb(2) distances in the solid-state for **2.4** (3.914(2) Å) relative to **2.6** (3.876(4) Å).

**Optical Spectroscopy.** UV-visible spectra were recorded to further investigate the electronic structure of monometallic **2.2** and **2.3**, and bimetallic **2.4**, **2.5**, **2.6** and **2.7** (Figure 2.12, top). Each of the bimetallic complexes has one band at high energy (340-360 nm, 27700-29410  $\text{cm}^{-1}$ ) that gradually decreases in intensity in the order **2.4** = **2.5** > **2.6** > **2.7**. These bands are assigned to intra-ligand transitions and show a decrease in intensity upon protonation of the BDI ligands in **2.6** and **2.7**, which disrupts the conjugation of the BDI p-system. The spectra also exhibit broad d-d bands at around 460 nm for **2.2**, **2.3**, **2.4** and **2.5**, and 425 nm for **2.7** (Figure 2.12, bottom). Complex **2.6** shows two bands at 460 nm and 580 nm, which is in agreement with the dissymmetric structure. Spectral intensities ( $\epsilon$ ) in this region are unusually large for d-d transitions ( $\epsilon \approx 2000 \text{ cm}^{-1} \cdot \text{M}^{-1}$  for the monometallic species and  $4000 < \epsilon < 8000 \text{ cm}^{-1} \cdot \text{M}^{-1}$  for the bimetallic species). Large values of  $\epsilon$  can be explained by a mixture of d- and p-character in the final state orbital that is involved in the transition.<sup>68</sup> These transitions are therefore partially Laporte allowed, which results in unusually high intensities for d-d transitions. This concept of metal-arene mixed transitions has been described previously, and supports Nb–arene mixing in the inverted sandwich complexes.<sup>21</sup> The absorption spectroscopy data reinforce the bonding picture developed above with the  $J_{\text{CH}}$  analysis, which

suggests that coordination of a second Nb atom to form a bimetallic Nb–arene–Nb interaction enhances Nb–C orbital mixing.

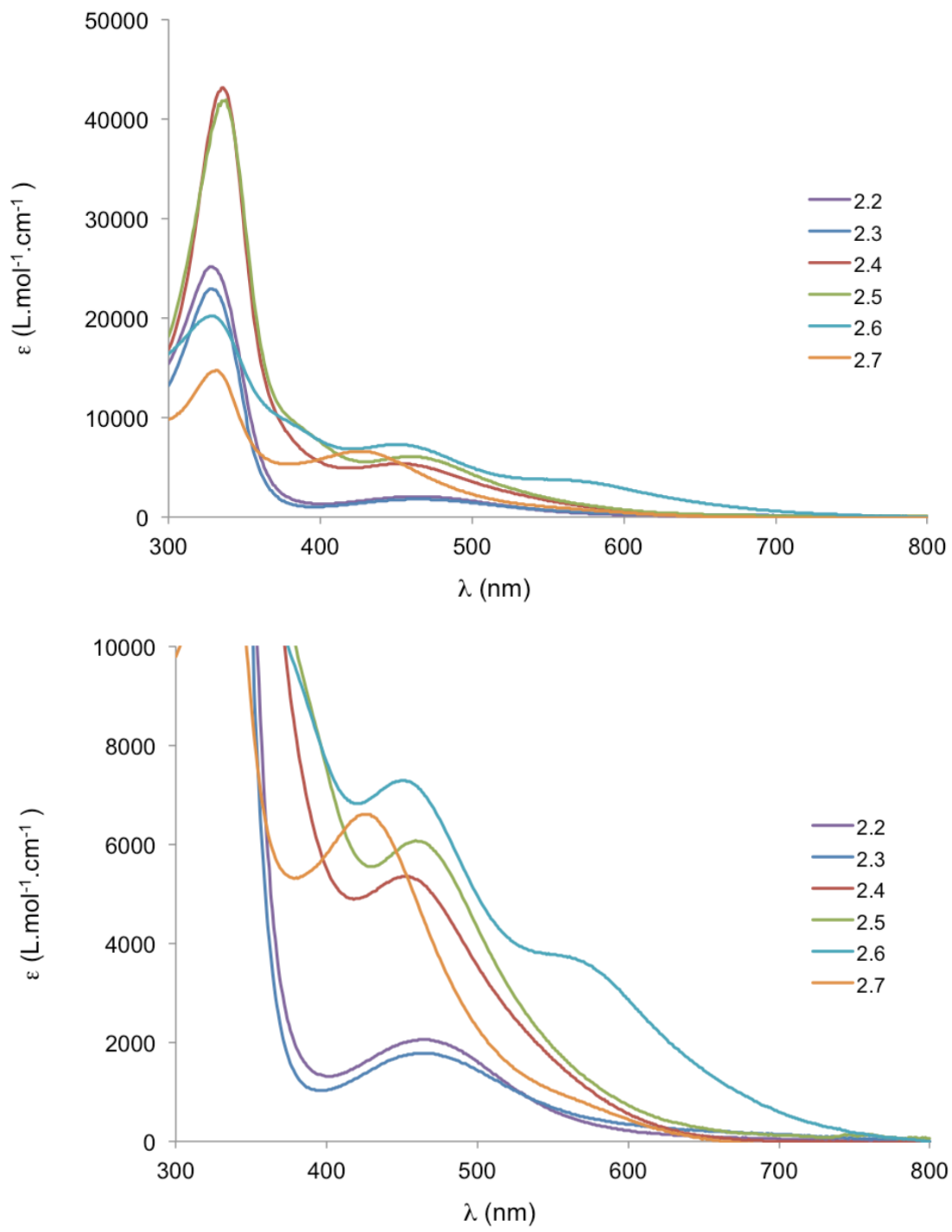


**Figure 2.12** Electronic absorbance spectrum of 87.8 mM solution of **2.2** in benzene, 76.0 mM solution of **2.3** in toluene, 47.8 mM solution of **2.4** in benzene, 56.2 mM solution of **2.5** in toluene, 61.3 mM solution of **2.6** and 36.4 mM solution of **2.7** in  $\alpha,\alpha,\alpha$ -trifluorotoluene. Full spectrum (top), zoom on the visible area (bottom).

## Conclusion

Described here are high-purity syntheses of four diniobium, inverted-sandwich compounds,  $[[(\text{BDI})\text{Nb}(\text{N}^t\text{Bu})_2(\mu\text{-RC}_6\text{H}_5)]$  (**2.4**: R = H and **2.5**: R = Me), monocationic **2.6**  $[[(\text{BDI}^\#)\text{Nb}(\text{N}^t\text{Bu})][(\text{BDI})\text{Nb}(\text{N}^t\text{Bu})](\mu\text{-C}_6\text{H}_5)]^{1+}$ , and dicationic **2.7**  $[[(\text{BDI}^\#)\text{Nb}(\text{N}^t\text{Bu})]_2(\mu\text{-RC}_6\text{H}_5)]^{2+}$  ( $\text{BDI}^\# = (\text{ArNC}(\text{Me}))_2\text{CH}_2$ ). Both the neutral complexes **2.4** and **2.5** were synthesized directly from their monometallic precursors **2.2** and **2.3**, which is a new approach to access the chemistry of inverted sandwich compounds. The kinetics of formation of **2.4** from **2.2** were determined using  $^1\text{H}$  NMR spectroscopy and suggest that the reaction follows a dissociative mechanism that may involve a transient three-coordinate “(BDI)Nb=N<sup>t</sup>Bu” intermediate.

The combined structural, reactivity and spectroscopic data provide new insight into the nuanced bonding interactions that are involved in bimetallic complexes with bridging arene ligands. X-ray crystal structures reveal bridging arene ligands that are distorted from planarity, with carbon atoms deviating from the average plane by as much as 0.16 Å. However, these distortions cannot be ascribed to a disruption of arene aromaticity resulting from Nb→arene donation because of the undefined role of steric strain, which may also be impacting arene reactivity. The  $^1\text{H}$  NMR spectra also show increases in the arene  $^1J_{\text{CH}}$  coupling constants relative to those for the free arene, which is inconsistent with an  $\text{sp}^3$ -hybridization of the bridging-arene C atoms. Taken together, there is little support for a model based on a reduced arene or oxidized Nb atoms. However, the magnitudes of the increase in  $^1J_{\text{CH}}$  also indicate that some Nb→arene donation is present and increases in the order **2.2** < **2.4** < **2.7** – a conclusion that is also reached upon examination of the variable temperature  $^1\text{H}$  NMR data, UV-visible spectra, and the bridged Nb–Nb distances. The Nb→arene donation is not accompanied by a change in formal oxidation state, which is consistent with earlier reports of inverted sandwich complexes based on d-block metals.<sup>4,6-11</sup> Finally, we conclude that the lack of reactivity at the arene ligands in **2.4** and **2.5** may be a kinetic effect due to the steric bulk of the BDI ligands. Future work will be focused on efforts to further refine our understanding of electronic structure with computational modeling, and will include extensions of this chemistry to a wider range of metal systems and ligand sets.

## Experimental

**General considerations.** Unless otherwise noted, all reactions were performed either using standard Schlenk line techniques or in an MBraun inert atmosphere glove box under an atmosphere of purified nitrogen (<1 ppm O<sub>2</sub>/H<sub>2</sub>O). Glassware, cannulae, and Celite were stored in an oven at *ca.* 160 °C for at least 12 hrs prior to use. *n*-Pentane, hexanes, Et<sub>2</sub>O, THF, toluene and benzene were purified by passage through a column of activated alumina, stored over 3 or 4 Å molecular sieves, and degassed prior to use.<sup>77</sup>  $\alpha,\alpha,\alpha$ -trifluorotoluene, dichloroethane and chlorobenzene were dried over P<sub>2</sub>O<sub>5</sub>, distilled under reduced pressure, degassed and stored over 4 Å molecular sieves. Deuterated solvents (C<sub>6</sub>D<sub>6</sub>, C<sub>7</sub>D<sub>8</sub> and C<sub>6</sub>D<sub>12</sub>) were dried over sodium/benzophenone, and C<sub>6</sub>D<sub>5</sub>Cl was dried over CaH<sub>2</sub>. The deuterated solvents were then vacuum transferred to a storage flask and degassed before being stored in the dry box. C<sub>6</sub>D<sub>6</sub>, C<sub>7</sub>D<sub>8</sub> and C<sub>6</sub>D<sub>5</sub>Cl were stored over activated molecular sieves. *N,N'*-bis-(2,6-diisopropylphenyl)- $\beta$ -diketiminate (BDI),<sup>78</sup> Li(BDI)·Et<sub>2</sub>O,<sup>79</sup> (BDI)pyCl<sub>2</sub>Nb(N<sup>t</sup>Bu)<sup>44</sup> and (BDI)(Me)<sub>2</sub>Nb(N<sup>t</sup>Bu) (**2.1**)<sup>44</sup> were prepared using literature procedures. All other reagents were acquired from commercial sources and used as received. NMR spectra were recorded on



Bruker AV-300, AVQ-400, AVB-400, DRX-500, AV-500, and AV-600 spectrometers. Chemical shifts were measured relative to residual solvent peaks, which were assigned relative to an external TMS standard set at 0.00 ppm.  $^1\text{H}$  and  $^{13}\text{C}$  NMR assignments were routinely confirmed by  $^1\text{H}$ - $^1\text{H}$  (COSY, NOESY) and  $^1\text{H}$ - $^{13}\text{C}$  (HSQC and HMBC) experiments. Samples for UV-vis-NIR spectroscopy were prepared in a Schlenk-adapted quartz cuvette and analyzed on a Varian Cary 50 scanning spectrophotometer. The uncorrected melting points were determined using sealed capillaries prepared under nitrogen on an Optmelt SRS. Elemental analyses were performed at the College of Chemistry Microanalytical Laboratory, University of California, Berkeley. The X-ray structural determinations were performed at CHEXRAY, University of California, Berkeley on Bruker SMART 1000 or SMART APEX diffractometers.

**(BDI)Nb(N<sup>t</sup>Bu)( $\eta^6$ -C<sub>6</sub>H<sub>6</sub>) (2.2).** Benzene (30 mL) was added to a 100-mL Schlenk flask containing **2.1** (0.548 g, 0.90 mmol, 1.0 equiv.) at room temperature. The clear yellow solution was degassed with two freeze-pump-thaw cycles. While warming the solution during the second cycle, the headspace of the flask was filled with 1 atm of H<sub>2</sub> (70 mL, 2.8 mmol, 3.0 equiv.) and the solution was stirred vigorously. The color of the solution turned to dark red within 5 min. After 12 hrs, the volatile materials were removed under reduced pressure to yield a red powder. Yield: 530 mg, 93%. X-ray suitable crystals were obtained by rapid crystallization from a mixture of toluene/hexanes (30 mg of **2.2** in 0.1 mL of solvent at -40 °C for 6 hrs).  $^1\text{H}$  NMR (500MHz, C<sub>6</sub>D<sub>6</sub>, 293 K):  $\delta$ (ppm) 7.10 (t, 2 H, *p*-Ar,  $^3J_{\text{HH}} = 7.6$  Hz), 6.97 (d, 2 H, *m*-Ar,  $^3J_{\text{HH}} = 7.2$  Hz), 5.13 (s, 1 H, HC(C(Me)NAr)<sub>2</sub>), 4.53 (sept, 2 H, CHMe<sub>2</sub>,  $^3J_{\text{HH}} = 6.6$  Hz), 3.71 (s, 6 H, C<sub>6</sub>H<sub>6</sub>), 2.77 (sept, 2 H, CHMe<sub>2</sub>,  $^3J_{\text{HH}} = 6.9$  Hz), 1.73 (s, 6 H, HC(C(Me)NAr)<sub>2</sub>), 1.45 (s, 9 H, <sup>t</sup>Bu), 1.37 (d, 6 H, CHMe<sub>2</sub>,  $^3J_{\text{HH}} = 6.9$  Hz), 1.05 (d, 6 H, CHMe<sub>2</sub>,  $^3J_{\text{HH}} = 6.6$  Hz), 1.04 (d, 6 H, CHMe<sub>2</sub>,  $^3J_{\text{HH}} = 6.6$  Hz), 1.00 (m, 6 H, CHMe<sub>2</sub>,  $^3J_{\text{HH}} = 6.9$  Hz).  $^{13}\text{C}\{^1\text{H}\}$  NMR (125.8 MHz, C<sub>6</sub>D<sub>6</sub>, 293 K)  $\delta$ (ppm) 168.56 (C, HC(C(Me)NAr)<sub>2</sub>), 153.15 (C, Ar), 143.08 (C, Ar), 141.31 (C, Ar), 125.71 (CH, Ar), 125.63 (CH, Ar), 124.06 (CH, Ar), 105.21 (broad, CH, C<sub>6</sub>H<sub>6</sub>), 103.56 (CH, HC(C(Me)NAr)<sub>2</sub>), 33.04 (CH<sub>3</sub>, Nb=N<sup>t</sup>Bu, C <sub>$\beta$</sub> ), 28.46 (CH, CHMe<sub>2</sub> of C=NAr), 27.39 (CH, CHMe<sub>2</sub> of C=NAr), 25.92 (CH<sub>3</sub>, CHMe<sub>2</sub> of C=NAr), 25.71 (CH<sub>3</sub>, CHMe<sub>2</sub> of C=NAr), 25.07 (CH<sub>3</sub>, CHMe<sub>2</sub> of C=NAr), 24.79 (CH<sub>3</sub>, CHMe<sub>2</sub> of C=NAr), 24.70 (CH<sub>3</sub>, HC(C(Me)NAr)<sub>2</sub>).  $^{13}\text{C}$  NMR (100 MHz, C<sub>6</sub>D<sub>6</sub>, 293 K)  $\delta$ (ppm) 105.2 (d, CH, C<sub>6</sub>H<sub>6</sub>,  $^1J_{\text{CH}} = 170$  Hz).  $^1\text{H}$  NMR (500MHz, C<sub>6</sub>D<sub>12</sub>, 293 K):  $\delta$ (ppm) 7.12 (dd, 2 H, *m*-Ar,  $^3J_{\text{HH}} = 7.6$  Hz,  $^4J_{\text{HH}} = 1.6$  Hz), 7.00 (t, 2 H, *p*-Ar,  $^3J_{\text{HH}} = 7.6$  Hz), 6.92 (dd, 2 H, *m*'-Ar,  $^3J_{\text{HH}} = 7.6$  Hz,  $^4J_{\text{HH}} = 1.6$  Hz), 5.16 (s, 1 H, HC(C(Me)NAr)<sub>2</sub>), 4.45 (sept, 2 H, CHMe<sub>2</sub>,  $^3J_{\text{HH}} = 6.8$  Hz), 3.61 (s, 6 H, C<sub>6</sub>H<sub>6</sub>), 2.73 (sept, 2 H, CHMe<sub>2</sub>,  $^3J_{\text{HH}} = 6.8$  Hz), 1.77 (s, 6 H, HC(C(Me)NAr)<sub>2</sub>), 1.35 (s, 9 H, <sup>t</sup>Bu), 1.26 (d, 6 H, CHMe<sub>2</sub>,  $^3J_{\text{HH}} = 6.4$  Hz), 1.03 (d, 6 H, CHMe<sub>2</sub>,  $^3J_{\text{HH}} = 6.8$  Hz), 1.00 (d, 6 H, CHMe<sub>2</sub>,  $^3J_{\text{HH}} = 6.4$  Hz), 0.98 (m, 6 H, CHMe<sub>2</sub>,  $^3J_{\text{HH}} = 6.8$  Hz). Anal. Calcd for C<sub>39</sub>H<sub>59</sub>N<sub>3</sub>Nb<sub>1</sub> powders: C, 70.99; H, 8.56; N, 6.37. Found: C, 69.61; H, 8.45; N, 6.33. m.p.: 85-86 °C (decomp).

**(BDI)Nb(N<sup>t</sup>Bu)( $\eta^6$ -C<sub>6</sub>D<sub>6</sub>) (2.2-*d*<sub>6</sub>).** Benzene-*d*<sub>6</sub> (10 mL) was added to a 50-mL Schlenk flask containing **2.1** (0.219 g, 0.36 mmol, 1.0 equiv.) at room temperature. The clear yellow solution was degassed with two freeze-pump-thaw cycles. While warming the solution during the second cycle, the headspace of the flask was filled with 1 atm of H<sub>2</sub> (40 mL, 1.6 mmol, 4.5 equiv.) and the solution was stirred vigorously overnight. The volatile materials were removed under reduced pressure to yield a bright red powder (210 mg, 86% yield). The  $^1\text{H}$  and  $^{13}\text{C}$  NMR spectra were similar to those of complex **2.2** with the exception of the

resonance assigned to the coordinated benzene.  $^2\text{H}$  NMR (92 MHz,  $\text{C}_6\text{D}_6$ , 293 K):  $\delta(\text{ppm})$  3.60 (br, s, 6D);  $^{13}\text{C}$  NMR (125 MHz,  $\text{C}_6\text{D}_6$ , 293 K):  $\delta(\text{ppm})$  79.96 (t, CD,  $\text{C}_6\text{D}_6$ ,  $^1J_{\text{CD}} = 27.5$  Hz). m.p.: decomp 84-85 °C.

**(BDI)Nb(N<sup>t</sup>Bu)( $\eta^6$ -C<sub>7</sub>H<sub>8</sub>) (2.3).** Toluene (30 mL) was added to a 100 mL Schlenk flask containing **2.1** (0.509 g, 0.83 mmol, 1 equiv.) at room temperature. The clear yellow solution was degassed with two freeze pump-thaw cycles. While warming the solution during the second cycle, the headspace of the flask was filled with 1 atm of H<sub>2</sub> (70 mL, 2.8 mmol, 3 equiv.) and the solution was vigorously stirred. The solution rapidly turned dark red within 5 min and was stirred for 12 h at room temperature. The volatile materials were removed under reduced pressure to yield a red powder (620 mg, 91%).  $^1\text{H}$  NMR (500MHz,  $\text{C}_7\text{D}_8$ , 293 K):  $\delta(\text{ppm})$ : 7.19 (dd, 2 H, *m*-Ar,  $^3J_{\text{HH}} = 8.0$  Hz,  $^3J_{\text{HH}} = 2.0$  Hz), 7.09 (t, 2 H, *p*-Ar,  $^3J_{\text{HH}} = 7.6$  Hz), 6.97 (dd, 2 H, *m'*-Ar,  $^3J_{\text{HH}} = 7.6$  Hz,  $^4J_{\text{HH}} = 1.2$  Hz), 5.07 (s, 1 H, HC(C(Me)NAr)<sub>2</sub>), 4.61 (sept, 2 H, CHMe<sub>2</sub>,  $^3J_{\text{HH}} = 6.5$  Hz), 3.93 (t, 1 H, *p*-C<sub>7</sub>H<sub>8</sub>,  $^3J_{\text{HH}} = 7.5$  Hz), 3.71 (t, 2 H, *m*-C<sub>7</sub>H<sub>8</sub>,  $^3J_{\text{HH}} = 7.2$  Hz), 3.59 (d, 2 H, *o*-C<sub>7</sub>H<sub>8</sub>,  $^3J_{\text{HH}} = 5.0$  Hz), 2.74 (sept, 2 H, CHMe<sub>2</sub>,  $^3J_{\text{HH}} = 7.0$  Hz), 1.70 (s, 6 H, HC(C(Me)NAr)<sub>2</sub>), 1.45 (s, 9 H, <sup>t</sup>Bu), 1.37 (d, 6 H, CHMe<sub>2</sub>,  $^3J_{\text{HH}} = 6.6$  Hz), 1.15 (d, 6 H, CHMe<sub>2</sub>,  $^3J_{\text{HH}} = 6.0$  Hz), 1.40 (s, 3 H, CH<sub>3</sub> of C<sub>7</sub>H<sub>8</sub>), 1.02 (d, 12 H, CHMe<sub>2</sub>,  $^3J_{\text{HH}} = 6.6$  Hz).  $^{13}\text{C}\{^1\text{H}\}$  NMR (125.8 MHz,  $\text{C}_7\text{D}_8$ , 293 K)  $\delta(\text{ppm})$  166.6 (C, HC(C(Me)NAr)<sub>2</sub>), 152.3 (C, Ar), 143.9 (C, Ar), 141.1 (C, Ar), 124.7 (CH, Ar), 124.6 (CH, Ar), 124.0 (CH, Ar), 102 (broad, CH, C<sub>7</sub>H<sub>8</sub>), 101.5 (CH, HC(C(Me)NAr)<sub>2</sub>), 33.4 (CH<sub>3</sub>, Nb=N<sup>t</sup>Bu, C<sub>β</sub>), 29.4 (CH, CHMe<sub>2</sub> of C=NAr), 27.2 (CH, CHMe<sub>2</sub> of C=NAr), 26.4 (CH<sub>3</sub>, CHMe<sub>2</sub> of C=NAr), 25.9 (CH<sub>3</sub>, CHMe<sub>2</sub> of C=NAr), 25.4 (CH<sub>3</sub>, CHMe<sub>2</sub> of C=NAr), 24.8 (CH<sub>3</sub>, CHMe<sub>2</sub> of C=NAr), 24.50 (CH<sub>3</sub>, HC(C(Me)NAr)<sub>2</sub>), 23.2 (broad, CH<sub>3</sub>, C<sub>7</sub>H<sub>8</sub>).  $^1\text{H}$  NMR (500MHz,  $\text{C}_6\text{D}_{12}$ , 293 K):  $\delta(\text{ppm})$  7.14 (dd, 2 H, *m*-Ar,  $^3J_{\text{HH}} = 7.5$  Hz,  $^4J_{\text{HH}} = 1.8$  Hz), 7.01 (t, 2 H, *p*-Ar,  $^3J_{\text{HH}} = 7.5$  Hz), 6.93 (dd, 2 H, *m'*-Ar,  $^3J_{\text{HH}} = 7.8$  Hz,  $^4J_{\text{HH}} = 1.5$  Hz), 5.12 (s, 1 H, HC(C(Me)NAr)<sub>2</sub>), 4.54 (sept, 2 H, CHMe<sub>2</sub>,  $^3J_{\text{HH}} = 6.6$  Hz), 3.81 (q, 1 H, *p*-C<sub>7</sub>H<sub>8</sub>,  $^3J_{\text{HH}} = 4.5$  Hz), 3.59 (d, 4 H, *o,m*-C<sub>7</sub>H<sub>8</sub>,  $^3J_{\text{HH}} = 4.5$  Hz), 2.70 (sept, 2 H, CHMe<sub>2</sub>,  $^3J_{\text{HH}} = 6.9$  Hz), 1.88 (s, 6 H, HC(C(Me)NAr)<sub>2</sub>), 1.37 (s, 9 H, <sup>t</sup>Bu), 1.29 (d, 6 H, CHMe<sub>2</sub>,  $^3J_{\text{HH}} = 6.9$  Hz), 1.26 (s, 3 H, CH<sub>3</sub> of C<sub>7</sub>H<sub>8</sub>), 1.12 (d, 6 H, CHMe<sub>2</sub>,  $^3J_{\text{HH}} = 6.6$  Hz), 1.04 (d, 6 H, CHMe<sub>2</sub>,  $^3J_{\text{HH}} = 6.9$  Hz), 1.00 (m, 6 H, CHMe<sub>2</sub>,  $^3J_{\text{HH}} = 6.6$  Hz). Anal. Calcd for C<sub>40</sub>H<sub>61</sub>N<sub>3</sub>Nb<sub>1</sub> powders: C, 71.30; H, 8.68; N, 6.24. Found: C, 69.59; H, 8.33; N, 6.18. m.p.: decomp 92-93 °C.

**[(BDI)Nb(N<sup>t</sup>Bu)]<sub>2</sub>( $\mu$ - $\eta^6$ : $\eta^6$ -C<sub>6</sub>H<sub>6</sub>) (2.4).** Hexanes (50 mL) was added to a 100-mL Schlenk flask containing (BDI)( $\eta^6$ -C<sub>6</sub>H<sub>6</sub>)Nb(N<sup>t</sup>Bu) (**2.2**) (0.378 g, 0.575 mmol). The dark red solution was stirred for 12 hrs. The volatile materials were removed under reduced pressure to yield a red powder, which was dissolved in pentane and concentrated to ca. 10 mL. The solution was stored at -40 °C, and the bright red crystals that formed within 1 day were filtered and residual solvent was removed under reduced pressure. One molecule of pentane remained present in the crystal lattice, as confirmed by elemental analysis and  $^1\text{H}$  NMR spectroscopy. X-ray suitable crystals were obtained by recrystallization from Et<sub>2</sub>O. Yield: 0.305 g, 80%.  $^1\text{H}$  NMR (500MHz,  $\text{C}_6\text{D}_6$ , 293 K):  $\delta(\text{ppm})$  7.10 (t, 4 H, *p*-Ar,  $^3J_{\text{HH}} = 7.6$  Hz), 6.97 (dd, 4 H, *m*-Ar,  $^3J_{\text{HH}} = 7.6$  Hz,  $^4J_{\text{HH}} = 1.6$  Hz), 4.92 (s, 2 H, HC(C(Me)NAr)<sub>2</sub>), 4.13 (sept, 4 H, CHMe<sub>2</sub>,  $^3J_{\text{HH}} = 6.8$  Hz), 3.05 (sept, 4 H, CHMe<sub>2</sub>,  $^3J_{\text{HH}} = 6.8$  Hz), 2.41 (s, 6 H, C<sub>6</sub>H<sub>6</sub>), 1.68 (s, 12 H, HC(C(Me)NAr)<sub>2</sub>), 1.27 (d, 12 H, CHMe<sub>2</sub>,  $^3J_{\text{HH}} = 8.0$  Hz), 1.26 (s, 18 H, <sup>t</sup>Bu), 1.23 (m, 6H, pentane), 1.153 (d, 12 H, CHMe<sub>2</sub>,  $^3J_{\text{HH}} = 6.4$  Hz), 1.145 (d, 12 H, CHMe<sub>2</sub>,  $^3J_{\text{HH}} = 6.8$  Hz), 1.08 (d, 12 H, CHMe<sub>2</sub>,  $^3J_{\text{HH}} = 6.8$  Hz), 0.83 (t, 6H, pentane).  $^{13}\text{C}\{^1\text{H}\}$  NMR (125.8 MHz,  $\text{C}_6\text{D}_6$ , 293 K)  $\delta(\text{ppm})$  168.37 (C, HC(C(Me)NAr)<sub>2</sub>), 151.77 (C, Ar), 142.53 (C, Ar), 142.05 (C, Ar),

125.96 (CH, Ar), 125.47 (CH, Ar), 123.93 (CH, Ar), 101.59 (CH, HC(C(Me)NAr)<sub>2</sub>), 79.96 (CH, C<sub>6</sub>H<sub>6</sub>), 34.45 (*pentane*), 32.82 (CH<sub>3</sub>, Nb=N<sup>t</sup>Bu, C<sub>β</sub>), 28.94 (CH, CHMe<sub>2</sub> of C=NAr), 27.21 (CH, CHMe<sub>2</sub> of C=NAr), 25.95 (CH<sub>3</sub>, CHMe<sub>2</sub> of C=NAr), 25.86 (CH<sub>3</sub>, CHMe<sub>2</sub> of C=NAr), 25.73 (CH<sub>3</sub>, CHMe<sub>2</sub> of C=NAr), 25.70 (CH<sub>3</sub>, CHMe<sub>2</sub> of C=NAr), 25.06 (CH<sub>3</sub>, HC(C(Me)NAr)<sub>2</sub>), 22.72 (*pentane*), 14.25 (*pentane*). <sup>13</sup>C NMR (125.8 MHz, C<sub>6</sub>D<sub>6</sub>, 293 K) δ(ppm) 79.96 (d, CH, C<sub>6</sub>H<sub>6</sub>, <sup>1</sup>J<sub>CH</sub> = 178.2 Hz). <sup>1</sup>H NMR (500MHz, C<sub>6</sub>D<sub>12</sub>, 293 K): δ(ppm) 7.04 (dd, 4 H, *m*-Ar, <sup>3</sup>J<sub>HH</sub> = 7.6 Hz, <sup>4</sup>J<sub>HH</sub> = 1.6 Hz), 6.97 (t, 4 H, *p*-Ar, <sup>3</sup>J<sub>HH</sub> = 7.6 Hz), 6.84 (dd, 4 H, *m'*-Ar, <sup>3</sup>J<sub>HH</sub> = 7.6 Hz, <sup>4</sup>J<sub>HH</sub> = 1.6 Hz), 4.93 (s, 2 H, HC(C(Me)NAr)<sub>2</sub>), 3.98 (sept, 4 H, CHMe<sub>2</sub>, <sup>3</sup>J<sub>HH</sub> = 6.8 Hz), 2.91 (sept, 4 H, CHMe<sub>2</sub>, <sup>3</sup>J<sub>HH</sub> = 6.8 Hz), 2.27 (s, 6 H, C<sub>6</sub>H<sub>6</sub>), 1.69 (s, 12 H, HC(C(Me)NAr)<sub>2</sub>), 1.13 (d, 12 H, CHMe<sub>2</sub>, <sup>3</sup>J<sub>HH</sub> = 6.8 Hz), 1.06 (s, 18 H, <sup>t</sup>Bu), 0.995 (d, 12 H, CHMe<sub>2</sub>, <sup>3</sup>J<sub>HH</sub> = 7.2 Hz), 0.96 (d, 12 H, CHMe<sub>2</sub>, <sup>3</sup>J<sub>HH</sub> = 7.4 Hz), 0.94 (d, 12 H, CHMe<sub>2</sub>, <sup>3</sup>J<sub>HH</sub> = 7.5 Hz). Anal. Calcd for C<sub>77</sub>H<sub>118</sub>N<sub>6</sub>Nb<sub>2</sub>: C, 70.41; H, 9.05; N, 6.40. Found: C, 70.33; H, 9.11; N, 6.51. m.p.: 117.9-119.4°C.

**[(BDI)Nb(N<sup>t</sup>Bu)]<sub>2</sub>(μ-η<sup>6</sup>:η<sup>6</sup>-C<sub>6</sub>D<sub>6</sub>) (2.4-d<sub>6</sub>).** The complex **2.2-d<sub>6</sub>** (57.1 mg, 0.086 mmol) was stirred in hexanes (20 mL) for 12 hrs. The dark red solution was then concentrated to ca. 10 mL and stored at -40 °C to form bright red crystals which were filtered and residual solvent was removed under reduced pressure (43.2 mg, 76% yield). The <sup>1</sup>H and <sup>13</sup>C NMR spectra were similar to those of complex **2.4**. <sup>2</sup>H NMR (92 MHz, C<sub>6</sub>D<sub>6</sub>, 293 K): δ(ppm) 2.2 (br, s, 6D); <sup>13</sup>C NMR (125 MHz, C<sub>6</sub>D<sub>6</sub>, 293 K): δ(ppm) 79.96 (t, CD, C<sub>6</sub>D<sub>6</sub>, <sup>1</sup>J<sub>CD</sub> = 27.45 Hz).

**[(BDI)Nb(N<sup>t</sup>Bu)]<sub>2</sub>(μ-η<sup>6</sup>:η<sup>6</sup>-C<sub>7</sub>H<sub>8</sub>) (2.5).** Hexanes (20 mL) was added to a 50-mL flask containing the complex (BDI)(η<sup>6</sup>-C<sub>7</sub>H<sub>8</sub>)Nb(N<sup>t</sup>Bu) (**2.3**) (0.104 g, 0.11 mmol). The red solution was stirred overnight and the volatile materials were removed under reduced pressure to yield a dark red powder, which was recrystallized from hexanes at -40 °C (10 mL), yielding red crystals that were collected by filtration and residual solvent was removed under reduced pressure (0.057 mg, 72%). One molecule of pentane remained present in the lattice of the crystal, as confirmed by elemental analysis and <sup>1</sup>H NMR spectroscopy. Recrystallization from toluene at -40 °C yielded X-ray suitable crystals within 2 days. <sup>1</sup>H NMR (500MHz, C<sub>7</sub>D<sub>8</sub>, 293 K): δ(ppm) 7.10 (broad, Ar + C<sub>7</sub>D<sub>8</sub>), 6.90 (dd, 4 H, *m*-Ar, <sup>3</sup>J<sub>HH</sub> = 6.4 Hz, <sup>4</sup>J<sub>HH</sub> = 2.4 Hz), 4.84 (s, 2 H, HC(C(Me)NAr)<sub>2</sub>), 4.5 (broad, 4 H, CHMe<sub>2</sub>, <sup>3</sup>J<sub>HH</sub> = 7.0 Hz), 2.88 (broad, 2 H, *o*-C<sub>7</sub>H<sub>8</sub>), 2.83 (broad, 1 H, *p*-C<sub>7</sub>H<sub>8</sub>), 2.76 (broad, 6 H, *m*-C<sub>7</sub>H<sub>8</sub> and CHMe<sub>2</sub>), 1.50 (broad, 12 H, HC(C(Me)NAr)<sub>2</sub>), 1.41 (s, 18 H, <sup>t</sup>Bu), 1.31 (d, 12 H, CHMe<sub>2</sub>, <sup>3</sup>J<sub>HH</sub> = 6.4 Hz), 1.14 (d, 6 H, CHMe<sub>2</sub>, <sup>3</sup>J<sub>HH</sub> = 6.8 Hz), 1.04 (d, 18 H, CHMe<sub>2</sub>, <sup>3</sup>J<sub>HH</sub> = 7.0 Hz), 0.61 (broad, 6 H, CHMe<sub>2</sub>), 0.40 (broad, 6 H, CHMe<sub>2</sub>). (500MHz, C<sub>7</sub>D<sub>8</sub>, 353 K): δ(ppm) 7.10 (broad, Ar + C<sub>7</sub>D<sub>8</sub>), 6.90 (d, 4 H, *m*-Ar, <sup>3</sup>J<sub>HH</sub> = 7.6 Hz), 4.86 (s, 2 H, HC(C(Me)NAr)<sub>2</sub>), 4.39 (sept, 4 H, CHMe<sub>2</sub>, <sup>3</sup>J<sub>HH</sub> = 7.0 Hz), 2.88 (broad, 2 H, *o*-C<sub>7</sub>H<sub>8</sub>), 2.83 (broad, 1 H, *p*-C<sub>7</sub>H<sub>8</sub>), 2.76 (broad, 6 H, *o*-C<sub>7</sub>H<sub>8</sub> and CHMe<sub>2</sub>), 2.04 (s, 3 H, CH<sub>3</sub> of C<sub>7</sub>H<sub>8</sub>), 1.53 (s, 12 H, HC(C(Me)NAr)<sub>2</sub>), 1.38 (s, 18 H, <sup>t</sup>Bu), 1.20 (d, 12 H, CHMe<sub>2</sub>, <sup>3</sup>J<sub>HH</sub> = 6.5 Hz), 1.07 (d, 12 H, CHMe<sub>2</sub>, <sup>3</sup>J<sub>HH</sub> = 7.0 Hz), 1.05 (broad, 12 H, CHMe<sub>2</sub>), 0.77 (broad, 12 H, CHMe<sub>2</sub>). <sup>13</sup>C{<sup>1</sup>H} NMR (125.8 MHz, C<sub>7</sub>D<sub>8</sub>, 353 K) δ(ppm) 167.95 (C, HC(C(Me)NAr)<sub>2</sub>), 151.66 (C, Ar), 143.23 (C, Ar), 126.25 (CH, Ar), 124.42 (CH, Ar), 102.98 (CH, HC(C(Me)NAr)<sub>2</sub>), 87.53 (CH, C<sub>7</sub>H<sub>8</sub>), 43.06 (CH<sub>3</sub>, C<sub>7</sub>H<sub>8</sub>), 32.90 (CH<sub>3</sub>, Nb=N<sup>t</sup>Bu, C<sub>β</sub>), 28.29 (CH, CHMe<sub>2</sub> of C=NAr), 27.43 (CH, CHMe<sub>2</sub> of C=NAr), 25.95 (CH<sub>3</sub>, CHMe<sub>2</sub> of C=NAr), 26.52 (CH<sub>3</sub>, CHMe<sub>2</sub> of C=NAr), 25.73 (CH<sub>3</sub>, CHMe<sub>2</sub> of C=NAr), 25.54 (CH<sub>3</sub>, CHMe<sub>2</sub> of C=NAr), 25.29 (CH<sub>3</sub>, HC(C(Me)NAr)<sub>2</sub>). Anal. Calcd for C<sub>78</sub>H<sub>120</sub>N<sub>6</sub>Nb<sub>2</sub>: C, 70.57; H, 9.11; N, 6.33. Found: C, 70.24; H, 9.85; N, 6.20. m.p.: 132.1-133.7 °C.

**Formation of [(BDI)Nb(N<sup>t</sup>Bu)(L)<sub>x</sub>] (L = CO, x = 2 and L = XylNC, x = 3).** CO (1 atm) was added to an evacuated J-Young tube containing **2.2** (12.0 mg, 18.2 mmol) or **2.3** (17.2 mg, 25.7 mmol) in C<sub>6</sub>D<sub>12</sub>, resulting in a slow color change from dark red to green within 6 hrs or 4 hrs, respectively. Solution analysis by <sup>1</sup>H and <sup>13</sup>C NMR spectroscopies agreed with the formation of the previously reported complex (BDI)Nb(N<sup>t</sup>Bu)(CO)<sub>2</sub> (1.1).<sup>44</sup> Similarly, 5 equivalents of XylNC (10.9 mg, 83.1 mmol) were added to a J-Young tube containing **2.2** (11.2 mg, 17.8 mmol) or **2.3** (13.5 mg, 20.0 mmol) in C<sub>6</sub>D<sub>12</sub>, resulting in a fast color change from dark red to purple within 2 hrs or 40 min, respectively. The product formed was assigned by <sup>1</sup>H and <sup>13</sup>C NMR spectroscopies to the previously reported complex (BDI)Nb(N<sup>t</sup>Bu)(CNXyl)<sub>3</sub>.<sup>32</sup>

**Reaction with N<sub>2</sub>O to form [(BDI)Nb(N<sup>t</sup>Bu)(μ<sub>2</sub>-O)]<sub>2</sub>.** Addition of 1 atmosphere of N<sub>2</sub>O to a J-Young tube containing **2.2** (11.8 mg, 17.2 mmol) in C<sub>6</sub>D<sub>6</sub> or **2.3** (13.2 mg, 19.6 mmol) in C<sub>7</sub>D<sub>8</sub> resulted in a color change from dark red to bright orange within 20 min or 5 min, respectively with yellow microcrystalline material rapidly crystallizing out of the solution. This yellow material has been assigned by <sup>1</sup>H NMR spectroscopy in both cases to the previously synthesized [(BDI)Nb(N<sup>t</sup>Bu)(μ<sub>2</sub>-O)]<sub>2</sub> complex.<sup>32</sup>

**Formation of (N(Ar)C(CH<sub>3</sub>)CHC(CH<sub>3</sub>))(THF)Nb(N<sup>t</sup>Bu)(NAr).** Heating a solution of **2.2** (11.2 mg, 17.0 mmol) or **2.3** (11.9 mg, 17.8 mmol) in THF-*d*<sub>8</sub> to 70 °C for 1 hr resulted in the formation of (MAD)(THF)Nb(N<sup>t</sup>Bu)(NAr) (MAD = N(Ar)C(CH<sub>3</sub>)CHC(CH<sub>3</sub>), confirmed by <sup>1</sup>H NMR spectroscopy), which was previously synthesized via a different route.<sup>32</sup>

**[(BDI<sup>#</sup>)Nb(N<sup>t</sup>Bu)][(BDI)Nb(N<sup>t</sup>Bu)](μ-η<sup>6</sup>:η<sup>6</sup>-C<sub>6</sub>H<sub>6</sub>)[B(C<sub>6</sub>F<sub>5</sub>)<sub>4</sub>] (**2.6**).** Et<sub>2</sub>O (20 mL) was added to a 50-mL flask containing the complex [(BDI)Nb(N<sup>t</sup>Bu)]<sub>2</sub>(μ-η<sup>6</sup>:η<sup>6</sup>-C<sub>6</sub>H<sub>6</sub>) (**2.4**) (0.180 g, 0.136 mmol, 1.0 equiv.) and the red solution was cooled to -80 °C. 10 mL of a diethylether solution of [(H(OEt<sub>2</sub>))[B(C<sub>6</sub>F<sub>5</sub>)<sub>4</sub>] (97 mg, 0.143 mmol, 1.05 equiv.) was added to the red solution, and the mixture was stirred at -80 °C for 20 min, warmed to room temperature and stirred overnight. The purple microcrystalline material that formed was separated by filtration, washed with Et<sub>2</sub>O (2 x 20 mL) and extracted with DCE (10 mL). The resulting purple solution was cooled at -15 °C to yield dark purple crystals (150 mg, 61%). X-ray suitable crystals were obtained by recrystallization from DCE. <sup>1</sup>H NMR (500MHz, C<sub>6</sub>D<sub>5</sub>Cl, 293 K): δ (ppm) 7.16 - 6.87 (multiple peaks, broad, Ar + C<sub>6</sub>D<sub>5</sub>Cl), 5.05 (s, 1 H, HC(C(Me)NAr)<sub>2</sub>), 4.99 (d, 1 H, CHH'(C(Me)NAr)<sub>2</sub>), <sup>2</sup>J<sub>HH</sub> = 16.3 Hz), 3.79 (d, 1 H, CHH'(C(Me)NAr)<sub>2</sub>), <sup>2</sup>J<sub>HH</sub> = 16.2 Hz), 3.70 (sept, 2 H, CHMe<sub>2</sub>, <sup>3</sup>J<sub>HH</sub> = 7.0 Hz), 3.47 (sept, 2 H, CHMe<sub>2</sub>, <sup>3</sup>J<sub>HH</sub> = 7.0 Hz), 2.75 (sept, 2 H, CHMe<sub>2</sub>, <sup>3</sup>J<sub>HH</sub> = 7.0 Hz), 2.40 (s, 6 H, C<sub>6</sub>H<sub>6</sub>), 1.90 (sept, 2 H, CHMe<sub>2</sub>, <sup>3</sup>J<sub>HH</sub> = 7.0 Hz), 1.80 (s, 6 H, CHH'(C(Me)NAr)<sub>2</sub>), 1.63 (s, 6 H, CH(C(Me)NAr)<sub>2</sub>), 1.12 (d, 6 H, CHMe<sub>2</sub>, <sup>3</sup>J<sub>HH</sub> = 6.8 Hz), 1.08 (s, 9 H, <sup>t</sup>Bu), 1.01 (d, 6 H, CHMe<sub>2</sub>, <sup>3</sup>J<sub>HH</sub> = 6.4 Hz), 1.00 (d, 6 H, CHMe<sub>2</sub>, <sup>3</sup>J<sub>HH</sub> = 6.8 Hz), 0.95 (d, 6 H, CHMe<sub>2</sub>, <sup>3</sup>J<sub>HH</sub> = 7.0 Hz), 0.92 (d, 6 H, CHMe<sub>2</sub>, <sup>3</sup>J<sub>HH</sub> = 6.4 Hz), 0.88 (d, 6 H, CHMe<sub>2</sub>, <sup>3</sup>J<sub>HH</sub> = 6.4 Hz), 0.85 (d, 6 H, CHMe<sub>2</sub>, <sup>3</sup>J<sub>HH</sub> = 6.4 Hz), 0.84 (s, 9 H, <sup>t</sup>Bu), 0.74 (d, 6 H, CHMe<sub>2</sub>, <sup>3</sup>J<sub>HH</sub> = 6.4 Hz). <sup>13</sup>C{<sup>1</sup>H} NMR (125.8 MHz, C<sub>6</sub>D<sub>5</sub>Cl, 293 K) δ(ppm) 167.5 (C, HC(C(Me)NAr)<sub>2</sub>), 164.9 (C, HC(C(Me)NAr)<sub>2</sub>), 151.66 (C, Ar), 150.5 (C, Ar), 147.3 (C, Ar), 143.23 (C, Ar), 140.03 (CH, Ar), 138.5 (CH, Ar), 126.25 (CH, Ar), 124.42 (CH, Ar), 102.98 (CH, HC(C(Me)NAr)<sub>2</sub>), 80.6 (CH, C<sub>6</sub>H<sub>6</sub>), 68.8 (CH<sub>2</sub>, H<sub>2</sub>C(C(Me)NAr)<sub>2</sub>), 32.9 (CH<sub>3</sub>, Nb=N<sup>t</sup>Bu, C<sub>β</sub>), 31.4 (CH<sub>3</sub>, Nb=N<sup>t</sup>Bu, C<sub>β</sub>), 29-27 (CH, CHMe<sub>2</sub> of C=NAr), 25-22 (CH<sub>3</sub>, CHMe<sub>2</sub> of C=NAr). <sup>13</sup>C NMR (125.8 MHz, C<sub>6</sub>D<sub>5</sub>Cl, 293 K) δ(ppm) 80.6 (d, CH, C<sub>6</sub>H<sub>6</sub>, <sup>1</sup>J<sub>CH</sub> = 178.9 Hz). <sup>19</sup>F NMR (470.4 MHz, C<sub>6</sub>D<sub>5</sub>Cl,

293 K)  $\delta$ (ppm) -133.8, -166.1 and -169.6 (B(C<sub>6</sub>F<sub>5</sub>)<sub>4</sub>). Anal. Calcd for C<sub>96</sub>H<sub>107</sub>N<sub>6</sub>Nb<sub>2</sub>B<sub>1</sub>F<sub>20</sub>: C, 60.01; H, 5.61; N, 4.37. Found: C, 59.76; H, 5.56; N, 4.30. m.p.: 215.4-217.5 °C.

**[[B(DI<sup>#</sup>)Nb(N<sup>t</sup>Bu)]<sub>2</sub>( $\mu$ - $\eta^6$ : $\eta^6$ -C<sub>6</sub>H<sub>6</sub>)] [B(C<sub>6</sub>F<sub>5</sub>)<sub>4</sub>]<sub>2</sub> (2.7).** Chlorobenzene (20 mL) was added to a 50-mL flask containing the complex [[B(DI<sup>#</sup>)Nb(N<sup>t</sup>Bu)] [B(DI)Nb(N<sup>t</sup>Bu)] ( $\mu$ - $\eta^6$ : $\eta^6$ -C<sub>6</sub>H<sub>6</sub>)] [B(C<sub>6</sub>F<sub>5</sub>)<sub>4</sub>] (**2.6**) (0.180 g, 0.09 mmol, 1 equiv.). To the dark purple solution was added 10 mL a chlorobenzene solution of [(H(OEt<sub>2</sub>))] [B(C<sub>6</sub>F<sub>5</sub>)<sub>4</sub>] (168 mg, 0.20 mmol, 2.1 equiv.) at room temperature and the mixture was stirred overnight, resulting in a clear orange solution. The volatile materials were removed under reduced pressure to yield an orange powder, which was washed with Et<sub>2</sub>O (2 x 20 mL) and extracted with 10 mL  $\alpha,\alpha,\alpha$ -trifluorotoluene. Et<sub>2</sub>O (20 mL) was layered over the  $\alpha,\alpha,\alpha$ -trifluorotoluene solution at room temperature, yielding bright orange X-ray suitable crystals within 2 days, which were filtered and residual solvent was removed under reduced pressure (100 mg, 42%). One molecule of  $\alpha,\alpha,\alpha$ -trifluorotoluene remained present in the lattice of the crystal, as confirmed by elemental analysis, X-ray crystallography and <sup>1</sup>H NMR spectroscopy. <sup>1</sup>H NMR (500MHz, C<sub>6</sub>D<sub>5</sub>Cl, 293 K):  $\delta$  (ppm) 7.38 (broad, 2 H, Ar), 7.20 (broad, 4 H, Ar), 7.06 (broad, 2 H, Ar), 6.90 (broad, 2 H, Ar), 6.84 (broad, 2 H, Ar), 4.78 (d, 1 H, CHH'(C(Me)NAr)<sub>2</sub>), <sup>2</sup>J<sub>HH</sub> = 16.5 Hz), 3.98 (d, 1 H, CHH'(C(Me)NAr)<sub>2</sub>), <sup>2</sup>J<sub>HH</sub> = 16.2 Hz), 3.30 (broad, 2 H, CHMe<sub>2</sub>), 3.14 (broad, 2 H, CHMe<sub>2</sub>), 2.55 (s, 6 H, C<sub>6</sub>H<sub>6</sub>), 1.90 (s, 6 H, CHH'(C(Me)NAr)<sub>2</sub>), 1.83 (broad, 10 H, CH(C(Me)NAr)<sub>2</sub> + 2 CHMe<sub>2</sub>), 1.08 (broad, 12 H, CHMe<sub>2</sub>), 0.94 (broad, 12 H, CHMe<sub>2</sub>), 0.84 (s, 30 H, <sup>t</sup>Bu), 0.73 (broad, 12 H, CHMe<sub>2</sub>). <sup>13</sup>C {<sup>1</sup>H} NMR (125.8 MHz, C<sub>6</sub>D<sub>5</sub>Cl, 293 K)  $\delta$ (ppm) 167.95 (C, H<sub>2</sub>C(C(Me)NAr)<sub>2</sub>), 150.5 (C, Ar), 147.3 (C, Ar), 140.03 (CH, Ar), 138.5 (CH, Ar), 84.16 (CH, C<sub>6</sub>H<sub>6</sub>), 68.8 (CH<sub>2</sub>, H<sub>2</sub>C(C(Me)NAr)<sub>2</sub>), 31.4 (CH<sub>3</sub>, Nb=N<sup>t</sup>Bu, C <sub>$\beta$</sub> ), 29-27 (CH, CHMe<sub>2</sub> of C=NAr), 25-22 (CH<sub>3</sub>, CHMe<sub>2</sub> of C=NAr). <sup>13</sup>C NMR (125.8 MHz, C<sub>6</sub>D<sub>5</sub>Cl, 293 K)  $\delta$ (ppm) 84.2 (d, CH, C<sub>6</sub>H<sub>6</sub>, <sup>1</sup>J<sub>CH</sub> = 184.5 Hz). <sup>19</sup>F NMR (470.4 MHz, C<sub>6</sub>D<sub>5</sub>Cl, 293 K)  $\delta$ (ppm) -62.7 (PhCF<sub>3</sub>), -133.8, -166.1 and -169.6 (B(C<sub>6</sub>F<sub>5</sub>)<sub>4</sub>). Anal. Calcd for C<sub>131</sub>H<sub>120</sub>B<sub>2</sub>F<sub>43</sub>N<sub>6</sub>Nb<sub>2</sub>: C, 56.50; H, 3.69; N, 3.02. Found: C, 56.63; H, 3.81; N, 2.78. m.p.: 204.9-206.2 °C.

**Kinetic NMR Studies.** The kinetics of the reaction that transformed **2.2** to **2.4** were followed by <sup>1</sup>H NMR spectroscopy in a J-Young tube with a 0.07 M solution of **2.2** in C<sub>6</sub>D<sub>12</sub> at different temperatures and in presence of various concentrations of benzene. The rate constants determined by the disappearance of starting material and appearance of product were identical. The mass balance was conserved, with no loss of material, upon time in each experiment. When the C<sub>6</sub>D<sub>12</sub> was stored over molecular sieves, the kinetic data were inconsistent and not reproducible. This was attributed to the acidity of the sieves,<sup>80</sup> which may lead to the formation of side products. Reproducible kinetic data were obtained either by using NMR solvents stored in the absence of molecular sieves or by stirring the solvent over basic alumina and filtering prior to use. Complex **2.2** was added to a J-Young tube (22.1 - 23.3 mg, 0.032 - 0.033 mmol), followed by 0.4 mL of C<sub>6</sub>H<sub>6</sub>/C<sub>6</sub>D<sub>12</sub> stock solution containing 4.92 mM internal standard (tetrakis(trimethylsilyl)silane). The concentration of each species was calculated by integrating the methyl peaks of the BDI backbone (1.77 ppm for complex **2.2** and 1.69 ppm for complex **2.4**) relative to the internal standard. All data used for the Eyring plot were obtained using the same C<sub>6</sub>D<sub>12</sub>-C<sub>6</sub>H<sub>6</sub>-internal standard stock solution to minimize experimental error (4.92 mM internal standard and 0.593 M C<sub>6</sub>H<sub>6</sub>). Temperatures inside the probe were determined as a function of the frequency difference (in Hz) between the two signals observed for a 100% ethylene glycol.<sup>81</sup>

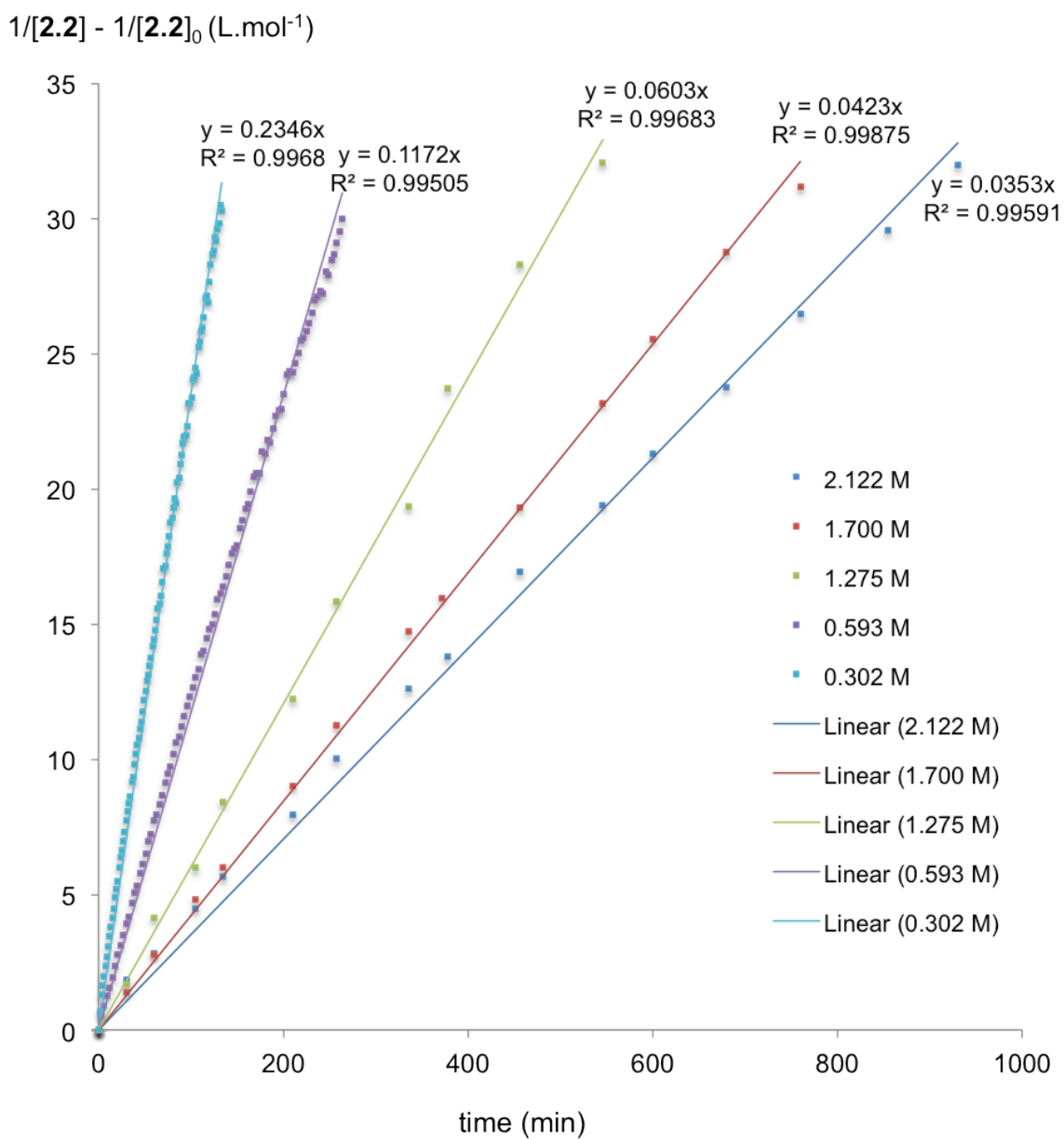


**Figure 2.13** Second order fit of the conversion of complex **2.2** into **2.4** at 330 K with different loading of benzene.

$1/[2.2] - 1/[2.2]_0$  (L.mol<sup>-1</sup>)

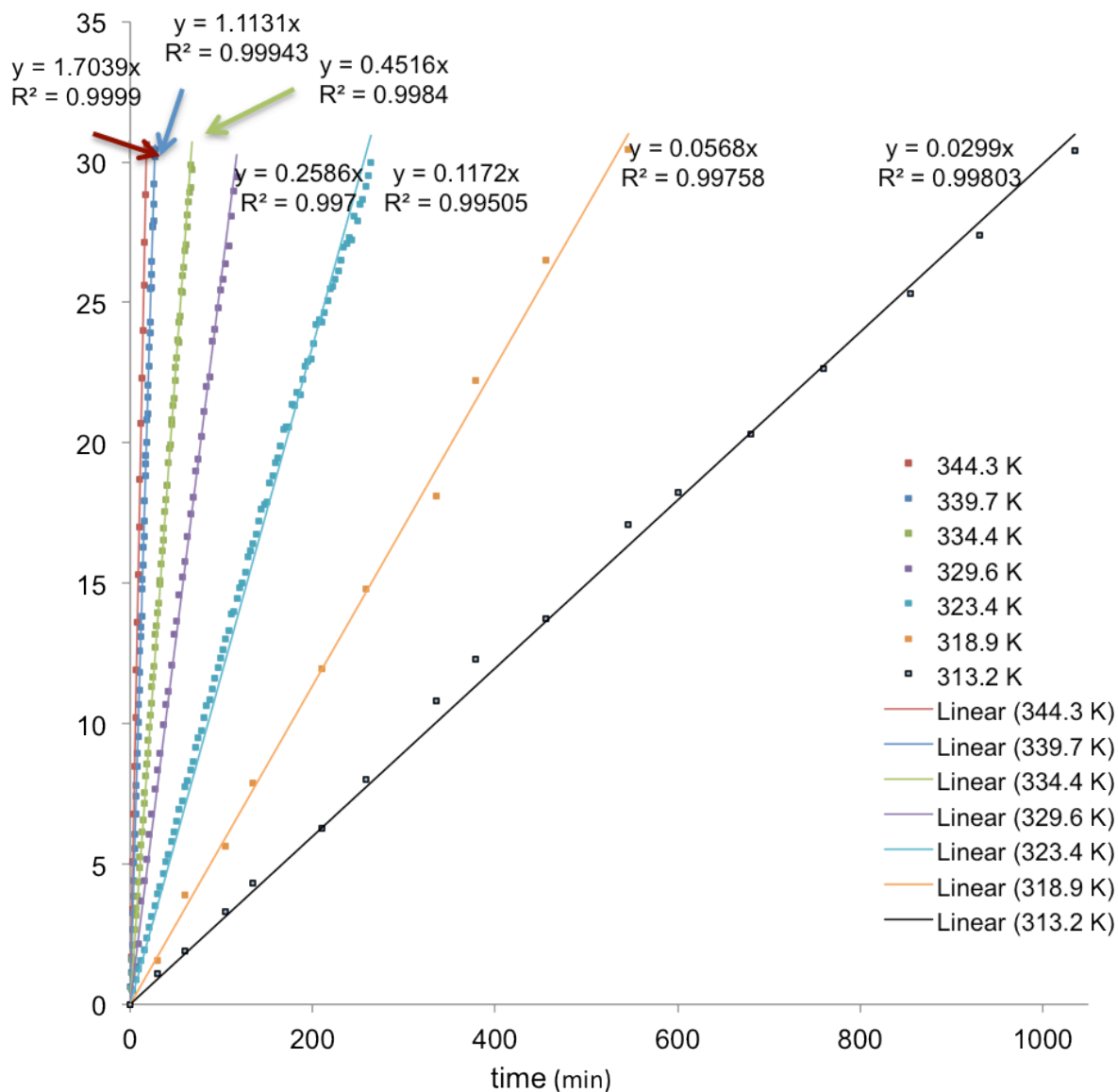


**Figure 2.14** Second order fit of the conversion of complex **2.2** into **2.4** at different temperatures [313 – 344] K.

**Selective Inversion Recovery (SIR) experiments.**<sup>82-83</sup> The kinetics of the intramolecular rearrangement reactions were studied at six different temperatures within the range of 235-265 K. Temperatures were calculated using a 100% methanol sample by measuring the separation between two peaks in Hz.<sup>81</sup> For complex 2.5, the SIR experiment was performed by saturating the resonance at 2.55 ppm, then following the exchange with the resonance at 2.95 ppm, corresponding to the CH group of the isopropyl moiety. These resonances were unambiguously assigned using a combination of COSY, TOCSY, NOESY, HSQC and HMBC experiments. Unfortunately, the latter resonance overlaps with the peaks of the meta and para protons of the bridging toluene. This was corrected by subtracting 3/5 of the value for each data point, since the signal of interest integrates for 2 H atoms and the signals for the meta and para hydrogens of toluene integrate to 3 H atoms.

**X-Ray crystallography studies.** X-ray structural determinations were performed on a Bruker SMART 1000 or SMART APEX diffractometer. Both are 3-circle diffractometers that couple a CCD detector<sup>84</sup> with a sealed-tube source of monochromated Mo K $\alpha$  radiation ( $\lambda = 0.71073$  Å). A crystal of appropriate size was coated in Paratone-N oil and mounted on a Kapton<sup>®</sup> loop. The loop was transferred to the diffractometer, centered in the beam, and cooled by a nitrogen flow low-temperature apparatus that had been previously calibrated by a thermocouple placed at the same position as the crystal. Preliminary orientation matrices and cell constants were determined by collection of 60 10 s frames, followed by spot integration and least-squares refinement. The reported cell dimensions were calculated from all reflections with  $I > 10 \sigma$ . The data were corrected for Lorentz and polarization effects; no correction for crystal decay was applied. An empirical absorption correction based on comparison of redundant and equivalent reflections was applied using SADABS.<sup>85</sup> All software used for diffraction data processing and crystal-structure solution and refinement are contained in the APEX2 program suite (Bruker AXS, Madison, WI).<sup>86</sup> Thermal parameters for all non-hydrogen atoms were refined anisotropically. For all structures,  $R_1 = \Sigma(|F_o| - |F_c|)/\Sigma(|F_o|)$ ;  $wR_2 = [\Sigma\{w(F_o^2 - F_c^2)^2\}/\Sigma\{w(F_o^2)^2\}]^{1/2}$ . Thermal ellipsoid plots were created using the ORTEP-3 software package and POV-ray.<sup>87</sup>



**Table 2.2**

Compound	<b>2.2</b>	<b>2.4•C<sub>4</sub>H<sub>10</sub>O</b>	<b>2.5•C<sub>7</sub>H<sub>8</sub></b>
Formula	C <sub>39</sub> H <sub>56</sub> N <sub>3</sub> Nb	C <sub>76</sub> H <sub>116</sub> N <sub>6</sub> Nb <sub>2</sub> O	C <sub>80</sub> H <sub>116</sub> N <sub>6</sub> Nb <sub>2</sub>
Formula weight	659.78	1313.59	1347.61
Space Group	P2 <sub>1</sub> 2 <sub>1</sub> 2 <sub>1</sub>	Pna2 <sub>1</sub>	Pna2 <sub>1</sub>
<i>a</i> (Å)	9.9013(5)	21.775(4)	23.114(5)
<i>b</i> (Å)	18.7383(11)	25.726(4)	17.957(4)
<i>c</i> (Å)	18.9322(10)	12.645(2)	17.525(4)
<i>α</i> (°)	90	90	90
<i>β</i> (°)	90	90	90
<i>γ</i> (°)	90	90	90
<i>V</i> (Å <sup>3</sup> )	3512.6(3)	7083(2)	7274(3)
<i>Z</i>	4	4	4
$\rho_{\text{calcd}}$ (g/cm <sup>3</sup> )	1.248	1.234	1.231
<i>F</i> <sub>000</sub>	1408	2816	2880
$\mu$ (mm <sup>-1</sup> )	0.373	0.370	0.361
<i>T</i> <sub>min</sub> / <i>T</i> <sub>max</sub>	0.9637/0.9852	0.9363/0.9639	0.8993/0.9892
No. rflns measured	19888	111211	142569
No. indep. rflns	6335	12991	13354
<i>R</i> <sub>int</sub>	0.0758	0.0322	0.0827
No. obs. ( <i>I</i> > 2.00σ( <i>I</i> ))	6335	13169	13354
No. variables	425	807	822
<i>R</i> <sub>1</sub> , <i>wR</i> <sub>2</sub>	0.0473, 0.0822	0.0205, 0.0500	0.0345, 0.0681
<i>R</i> <sub>1</sub> (all data)	0.0811	0.0223	0.0467
GoF	0.982	1.060	1.042
Res. peak/hole (e <sup>-</sup> /Å <sup>3</sup> )	0.365/-0.553	0.583/-0.122	0.800/-0.397

**Table 2.3**

Compound	<b>2.6</b>	<b>2.7•PhCF<sub>3</sub></b>
Formula	C <sub>96</sub> H <sub>107</sub> B <sub>1</sub> F <sub>20</sub> N <sub>6</sub> Nb <sub>2</sub>	C <sub>127</sub> H <sub>124</sub> B <sub>2</sub> F <sub>43</sub> N <sub>6</sub> Nb <sub>2</sub>
Formula weight	1921.51	2742.64
Space Group	P <sub>-1</sub>	P <sub>-1</sub>
<i>a</i> (Å)	14.834(5)	15.2951(10)
<i>b</i> (Å)	17.750(5)	19.8041(13)
<i>c</i> (Å)	17.811(5)	21.4734(15)
<i>α</i> (°)	82.109(5)	86.047(3)
<i>β</i> (°)	75.003(5)	73.864(4)
<i>γ</i> (°)	86.878(5)	74.382(3)
<i>V</i> (Å <sup>3</sup> )	4486(2)	6017.4(7)
<i>Z</i>	2	2
$\rho_{\text{calcd}}$ (g/cm <sup>3</sup> )	1.422	1.514
F <sub>000</sub>	1984	2792
$\mu$ (mm <sup>-1</sup> )	0.347	0.310
T <sub>min</sub> /T <sub>max</sub>	0.9030 / 0.9795	0.9265/0.9726
No. rflns measured	82723	95984
No. indep. rflns	16401	21919
<i>R</i> <sub>int</sub>	0.0312	0.0419
No. obs. ( <i>I</i> > 2.00σ( <i>I</i> ))	16401	21920
No. variables	1184	1627
<i>R</i> <sub>1</sub> , <i>wR</i> <sub>2</sub>	0.0304, 0.0659	0.03630, 0.0830
<i>R</i> <sub>1</sub> (all data)	0.0425	0.0505
GoF	1.012	1.035
Res. peak/hole (e <sup>-</sup> /Å <sup>3</sup> )	0.337/ -0.534	1.889/-0.847

## References

- (1) Muerterties, E. L.; Bleek, J. R.; Wucherer, E. J.; Albright, T. A. *Chem. Rev.* **1982**, *82*, 499.
- (2) Cassani, M. C.; Gun'ko, Y. K.; Hitchcock, P. B.; Lappert, M. F.; Laschi, F. *Organometallics*, **1999**, *18*, 5539.
- (3) Bochkarev, M. N. *Chem. Rev.* **2002**, *102*, 2089.
- (4) Duff, A. W.; Jonas, K.; Goddard, R.; Kraus, H. J.; Krueger, C. *J. Am. Chem. Soc.* **1983**, *105*, 5479.
- (5) Krieck, S.; Görls, H.; Yu, L.; Reiher, M.; Westerhausen, M. *J. Am. Chem. Soc.*, **2009**, *131*, 2977.
- (6) Cotton, F.A.; Kibala, P. A.; Wojtczak, W. A. *J. Am. Chem. Soc.*, **1991**, *113*, 1462.
- (7) Troyanov, S. I.; Meetsma, A.; Teuben J. H. *Inorg. Chim. Acta*, **1998**, *271*, 180.
- (8) Tsai, Y.-C.; Wang, P.-Y.; Chen, S.-A.; Chen, J.-M. *J. Am. Chem. Soc.* **2007**, *129*, 8066.
- (9) Nikiforov, G. B.; Crewdson, P.; Gambarotta, S.; Korobkov, I.; Budzelaar, P. H. M. *Organometallics* **2007**, *26*, 48.
- (10) Tsai, Y.-C.; Wang, P.-Y.; Lin, K.-M.; Chen, S.-A.; Chen, J.-M. *Chem. Commun.* **2008**, 205.
- (11) Ni, C.; Ellis, B. D.; Fettinger, J. C.; Long, G. J.; Power, P. P. *Chem. Commun.* **2008**, 1014.
- (12) Bénard, M.; Rohmer, M. M.; López, X.; Theopold, K. H. *Angew. Chem. Int. Ed.* **2008**, *47*, 5597.
- (13) Fryzuk, M. D.; Love, J. B.; Rettig, S. J. *J. Am. Chem. Soc.*, **1997**, *119*, 9071.
- (14) Diaconescu, P. L.; Arnold, P. L.; Baker, T. A.; Mindiola, D. J.; Cummins, C. C. *J. Am. Chem. Soc.* **2000**, *122*, 6108.
- (15) Diaconescu, P. L.; Cummins, C. C. *J. Am. Chem. Soc.* **2002**, *124*, 7660.
- (16) Evans, W. J.; Kozimor, S. A.; Ziller, J. W.; Kaltsoyannis, N. *J. Am. Chem. Soc.* **2004**, *126*, 14533.
- (17) Evans, W. J.; Traina, C. A.; Ziller, J. W. *J. Am. Chem. Soc.* **2009**, *131*, 17473.
- (18) Mills, D. P.; Moro, F.; McMaster, J.; van Slageren, J.; Lewis, W.; Blake, A. J.; Liddle, S. T. *Nature Chem* **2011**, *3*, 454.
- (19) Huang, W.; Khan, S. I.; Diaconescu, P. L. *J. Am. Chem. Soc.* **2011**, *133*, 10410.
- (20) Monreal, M. J.; Khan, S. I.; Kiplinger, J. L.; Diaconescu, P. L. *Chem. Commun.* **2011**, *47*, 9119.
- (21) Patel, D.; Moro, F.; McMaster, J.; Lewis, W.; Blake, A. J.; Liddle, S. T. *Angew. Chem., Int. Ed.* **2011**, *50*, 10388.
- (22) Diaconescu, P. L.; Cummins, C. C. *Inorg. Chem.* **2012**, *51*, 2902.
- (23) Arnold P. L.; Mansell, S. M.; Maron, L.; McKay D. *Nature Chem.* **2012**, *4*, 668.
- (24) Mougel, V.; Camp, C.; Pécaut, J.; Copéret, C.; Laurent Maron, L.; Kefalidis, C. E.; Mazzanti, M. *Angew. Chem. Int. Ed.* **2012**, *51*, 12280.
- (25) Minasian, S. G.; Krinsky, J. L.; Arnold, J. *Chem. Eur. J.* **2011**, *17*, 12234.
- (26) Gianetti, T. L.; Tomson, N. C.; Arnold, J.; Bergman, R. G. *J. Am. Chem. Soc.* **2011**, *133*, 14904.
- (27) Fei, P.; Khan, M. A.; Nicholas, L. M. *J. Am. Chem. Soc.* **1992**, *114*, 6579.
- (28) Fryzuk, M. D.; Kozak, C. M.; Bowdridge, M. R.; Patrick, B. O.; Rettig, S. J. *J. Am. Chem. Soc.* **2002**, *124*, 8389.

- (29) Kilgore, U. J.; Yang, X.; Tomaszewski, J.; Huffman, J. C.; Daniel J. Mindiola, D. J. *Inorg. Chem.* **2006**, *45*, 10712.
- (30) Figueroa, J. S.; Cummins, C. C. *Dalton Trans.* **2006**, 2161.
- (31) Hiromasa Tanaka, H.; Shiota, Y.; Matsuo, T.; Kawaguchi, H.; Yoshizawa, K. *Inorg. Chem.* **2009**, *48*, 3875.
- (32) Tomson, N. C.; Arnold, J.; Bergman, R. G. *Organometallics* **2010**, *29*, 5010.
- (33) Steffey, B. D.; Chesnut, R. W.; Kerschner, J. L.; Pellechia, P. J.; Fanwick, P. E.; Rothwell, I. P. *J. Am. Chem. Soc.* **1989**, *111*, 378.
- (34) Labinger, J. A.; Schwartz, J. J. *J. Am. Chem. Soc.* **1975**, *97*, 1596.
- (35) Roskamp, E. J.; Pedersen, S. F. *J. Am. Chem. Soc.* **1987**, *109*, 6551.
- (36) Etienne, M.; Biasotto, F.; Mathieu, R.; Templeton, J. L. *Organometallics* **1996**, *15*, 1106.
- (37) Antinolo, A.; Otero, A. *Organometallics* **1997**, *16*, 2601.
- (38) Obora, Y.; Kimura, M.; Ohtake, T.; Tokunaga, M.; Tsuji, Y. *Organometallics* **2006**, *25*, 2097.
- (39) Steffey, B. D.; Chesnut, R. W.; Kerschner, J. L.; Pellechia, P. J.; Fanwick, P. E.; Rothwell, I. P. *J. Am. Chem. Soc.* **1989**, *111*, 378.
- (40) Yu, J. S.; Fanwick, P. E.; Rothwell, I. P. *J. Am. Chem. Soc.* **1990**, *112*, 8171.
- (41) Yu, J. S.; Felter, L.; Potyen, M. C.; Clark, J. R.; Visciglio, V. M.; Fanwick, P. E.; Rothwell, I. P. *Organometallics* **1996**, *15*, 4443.
- (42) Veige, A. S.; Slaughter, L. M.; Lobkovsky, E. B.; Wolczanski, P. T.; Matsunaga, N.; Decker, S. A.; Cundari, T. R. *Inorg. Chem.* **2003**, *42*, 6204.
- (43) Figueroa, J. S.; Piro, N. A.; Mindiola, D. J.; Fickes, M. G.; Cummins, C. C. *Organometallics* **2010**, *29*, 5215.
- (44) Tomson, N. C.; Yan, A.; Arnold, J.; Bergman, R. G. *J. Am. Chem. Soc.* **2008**, *130*, 11262.
- (45) Only one diniobium bridged benzene is reported but exhibits a m-h<sup>2</sup>:h<sup>2</sup> structure: Veige, A. S.; Kleckley, T. S.; Chamberlin, R. M.; Neithamer, D. R.; Lee, C. E.; Wolczanski, P. T.; Lobkovsky, E. B.; Glassey, W. V. *J. Organomet. Chem.* **1999**, *591*, 194.
- (46) Tomson, N. C.; Arnold, J.; Bergman, R. G. *Organometallics* **2010**, *29*, 2926.
- (47) Churchill, M. R.; Chang, S. W. -Y; *Chem. Comm.*, **1974**, 248.
- (48) Goldberg, S. Z.; Spivack, B. D.; Stanley, G.; Eisenberg, R.; Braitsch, D. M.; Miller, J.S.; Abkowitz, M. *J. Am. Chem. Soc.*, **1977**, *99*, 110.
- (49) Stollmaier, F.; Thewalt, U. *J. Organomet. Chem.*, **1981**, *222*, 227.
- (50) Thewalt, U.; Stollmaier, F. *Angew. Chem., Int. Ed.*, **1982**, *21*, 133.
- (51) Bandy, J. A.; Prout, K.; Cloke, F. G. N.; de Lemos, H. C.; Wallis, J.M. *J. chem. Soc., Dalton Trans.*, **1988**, 1475.
- (52) Green, M. L. H.; O'Hare, D.; Watkin, J. G. *Chem. Comm.*, **1989**, 698.
- (53) Calderazzo, F.; Pampaloni, G.; Rocchi, L.; Strahle, J.; Wurst K. *J. Organomet. Chem.*, **1991**, *413*, 91.
- (54) Calderazzo, F.; Englert, U.; Pampaloni, G.; Rocchi, L. *Angew. Chem., Int. Ed.*, **1992**, *31*, 1235.
- (55) Calderazzo, F.; Gingl, F.; Pampaloni, G.; Rocchi, L.; Strahle, J. *Chem. Ber.*, **1992**, *125*, 1005.
- (56) Calderazzo, F.; De Benedetto, G. E; Pampaloni, G.; Rocchi, L.; Englert U. *J. Organomet. Chem.* **1993**, *462*, C10.
- (57) Calderazzo, F.; Pampaloni, G.; Rocchi, L.; Englert, U. *Organometallics*, **1994**, *13*, 252.

- (58) Clark, D. L.; Gordon, J. C.; McFarlan, J. T.; Vincent-Hollis, R. L.; Watkin, J. G.; Zwick, B. D. *Inorg. Chem. Acta.*, **1996**, *244*, 269.
- (59) Tayebani, M.; Feghali, K.; Gambarotta, S.; Yap, G. *Organometallics*, **1998**, *17*, 4282.
- (60) Kesanli, B.; Fettingner, J.; Eichhorn, B. *Angew. Chem., Int. Ed.*, **2001**, *40*, 2300.
- (61) Fryzuk, M. D.; Kozak, C. M.; Mehrkhodavandi, P.; Morello, L.; Patrick, B. O.; Rettig, S. *J. Am. Chem. Soc.*, **2002**, *124*, 516.
- (62) Sussman, V. J.; Ellis J. E. *Angew. Chem., Int. Ed.*, **2008**, *47*, 484.
- (63) Plíva, J.; Johns, J. W. C.; Goodman, L. J. *Mol. Spectrosc.* **1990**, *140*, 214.
- (64) Madelung, O., Ed. *Landolt-Bornstein: Numerical Data and Functional Relationships in Science and Technology*; Springer: Berlin, 1987; Vol. 15.
- (65) Maksić, J. B. *Int. J. Quantum Chem.* **1971**, *5*, 301.
- (66) Bodner, G. M.; Todd, L. J. *Inorg Chem*, **1974**, *13*, 360.
- (67) *The Organometallic Chemistry of the Transition Metals*, 4<sup>th</sup> edition, Crabtree, R. H.; Ed. John Wiley & Sons, Inc., 2005, p 87.
- (68) Da Re, R. E.; Kuehl, C. J.; Brown, M. G.; Rocha, R. C.; Bauer, E. D.; John, K. D.; Morris, D. E.; Shreve, A. P.; Sarrao, J. L. *Inorg. Chem.*, **2003**, *42*, 5551.
- (69) Pearson, D. H.; Ahn, C. C.; Fultz, B. *Physical Review B* **1993**, *47*, 8471.
- (70) Bach, D.; Schneider, R.; Gerthsen, D.; Verbeeck, J.; Sigle, W. *Microscopy and Microanalysis* **2009**, *15*, 505.
- (71) Pearson, D. H.; Fultz, B.; Ahn, C. C. *Applied Physics Letters* **1988**, *53*, 1405.
- (72) Olszta, M. J.; Wang, J.; Dickey, E. C. *Journal of Microscopy-Oxford* **2006**, *224*, 233.
- (73) Bach, D.; Stoermer, H.; Schneider, R.; Gerthsen, D.; Verbeeck, J. *Microscopy and Microanalysis* **2006**, *12*, 416.
- (74) Bach, D.; Schneider, R.; Gerthsen, D. *Microscopy and Microanalysis* **2009**, *15*, 524.
- (75) Tao, R.; Todorovic, R.; Liu, J.; Meyer, R. J.; Arnold, A.; Walkosz, W.; Zapol, P.; Romanenko, A.; Cooley, L. D.; Klie, R. F. *Journal of Applied Physics* **2011**, *110*, 124313.
- (76) Solomon, E. I.; Lever, A. B. P. *Inorganic Electronic Structure and Spectroscopy*; John Wiley & Sons: Hoboken, New Jersey, **2006**; Vol. 2.
- (77) Alaimo, P. J.; Peters, D. W.; Arnold, J.; Bergman, R. G. *J. Chem. Educ.* **2001**, *78*, 64.
- (78) Feldman, J.; McLain, S. J.; Parthasarathy, A.; Marshall, W. J.; Calabrese, J. C.; Arthur, S. D. *Organometallics* **1997**, *16*, 1514.
- (79) Budzelaar, P. H. M.; van Oort, A. B.; Orpen, A. G. *Eur. J. Inorg. Chem.* **1998**, *10*, 1485.
- (80) Anderson, L. L.; Arnold, J.; Bergman, R. G. *J. Am. Chem. Soc.* **2005**, *127*, 14541.
- (81) Amman, C.; Meier, P.; Merbach, A. E. *J. Magn. Reson.* **1982**, *46*, 319.
- (82) Bain, A. D.; Cramer, J. A. *J. Magn. Reson. A* **1996**, *118*, 21.
- (83) Mugridge, J. S.; Szigethy, G.; Bergman, R. G.; Raymond, K. N. *J. Am. Chem. Soc.* **2010**, *132*, 16256.
- (84) SMART: Area-Detector Software Package; Bruker Analytic X-ray Systems, I., Madison, WI, 2001-2003, Ed.
- (85) SADABS: Bruker-Nonius Area Detector Scaling and Absorption V2.05 Bruker Analytical X-ray Systems, I., Madison, WI, 2003.
- (86) Sheldrick, G. M. *Acta Crystallogr. A* **2008**, *64*, 112.
- (87) Farrugia, L. J., *J. Appl. Crystallogr.* 1997, *30*, 565, Ed.

## **Chapter III**

### **Synthesis, Electronic Structure and Reactivity of a Mixed-Valence Benzene Inverted-Sandwich Diniobium Complex**

## Introduction

Since the discovery of metallocenes, the bonding modes and structures of organometallic molecules have been an important facet of chemistry over the last sixty years.<sup>1-4</sup> Among these molecules, arene complexes have drawn particular attention. Species that contain an arene coordinated in between two metal ions – so-called inverted-sandwich complexes – have been highly sought since the first report of the vanadium triple decker  $[\text{CpV}]_2(\mu\text{-}\eta^6\text{:}\eta^6\text{-C}_6\text{H}_6)$  thirty years ago.<sup>5</sup> Not only they are fascinating molecules from a structural perspective, they also provide an interesting starting platform for further reactivity and open new synthetic routes for the synthesis of highly reactive complexes.<sup>6</sup> To-date, inverted sandwich complexes containing many different metal ions from the *s*-, *p*-, *d*- and *f*-block elements have been prepared and studied, and potential applications in the development of organic transformations and materials synthesis have been demonstrated.<sup>4,7</sup>

Another class of important molecules are mixed-valence dimers in which an electron may be either localized on one metal center or delocalized across both.<sup>8</sup> The initial report in 1969 by Creutz and Taube of the mixed-valence quintuply charged decaammine( $\mu$ -pyrazine) bisruthenium ion<sup>9</sup> has inspired hundreds of publications,<sup>10,11</sup> and a number of debates over the electronic structure of these types of molecules.<sup>12-13-17</sup>

Although it is certain that both the above-mentioned vanadium and ruthenium dimers have had a considerable impact, to the best of our knowledge, only three mixed-valence inverted-sandwich dimers have been reported.<sup>18-20</sup> Most arene-inverted sandwich are described as having  $\pi$ - and  $\delta$ - back donation from the metal centres to the unoccupied  $\pi$  orbitals of the arene. In this model, spin density is transferred to the arene but when oxidants react with these dimers, reductive cleavage occurs at the metal centre, so that the arene ring acts as an electron reservoir to give highly electron rich systems.<sup>6,18</sup> Recently, Arnold *et al.* provided the first example of arene functionalization using a neutral inverted sandwich complex of uranium with the report of a remarkable direct C-H borylation.<sup>21</sup> A key point in this reaction is a formal disproportionation that allows the arene to be reduced. The idea of a formal disproportionation, in which a single electron is transferred to another metal in a bimetallic process, is of great importance in inverted sandwich complexes because their high symmetry suggests that they always provide two electrons to react, one from each metal center, so that radical chemistry or single electron transfer (SET) is not expected. A way to circumvent this problem and access radical chemistry with such complexes is to synthesize electronically unsymmetrical inverted sandwiches, *i.e.* mixed valent inverted sandwiches. At this stage, the extent of delocalization of the unpaired electron and its influence on the chemical reactivity have not been addressed.<sup>18-20</sup> Notably, Mazzanti and coworkers recently showed reactivity between  $\text{K}^+$  and a neutral benzene inverted sandwich complex of uranium that disproportionates and forms a mixed valent benzene inverted sandwich complex.<sup>19</sup> In the present report, the reason for the stability of such mixed valent species, whether it comes from the nature of the bonding with the arene ring (delocalization) or from the nature of the counter-cation that provides structural and/or electronic stability, is addressed.

In the previous chapter (chapter II) we described the synthesis and kinetics of formation of a diniobium benzene inverted sandwich complex  $\{[\text{Nb}_2(\text{BDI})_2\text{N}^t\text{Bu}_2](\mu\text{-C}_6\text{H}_6)\}$ , **3.1** (Figure 3.1) that was found to be unreactive with most small molecules.<sup>22</sup> This surprising observation led us to probe its redox behaviour as a potential means to activate the molecule toward further reactivity. Here, we present the controlled one-electron oxidation of **3.1** that

leads to the formation of a stable cationic mixed-valent diniohium arene inverted sandwich complex  $\{[\text{Nb}_2(\text{BDI})_2\text{N}^t\text{Bu}_2](\mu\text{-C}_6\text{H}_6)\}^+\{\text{B}(\text{C}_6\text{F}_5)_4\}^-$ , **3.2**. X-Ray crystallography, NMR spectroscopy, cyclic voltammetry (CV), UV-Visible spectroscopy, solid-state magnetism, EPR, and DFT calculations of **3.2** are discussed and used to help understand the electronic structure of **3.2**. Furthermore, the reactivity of **3.2** sheds additional light on its electronic structure.

## Results and discussions

**Synthesis and structural studies.** The one-electron oxidation of the inverted sandwich complex **3.1** with  $[\text{Ag}][\text{B}(\text{C}_6\text{F}_5)_4]$  in  $\text{Et}_2\text{O}$  led to a colour change from deep red to deep green within 10 mins, followed by precipitation of a yellow/green microcrystalline powder within an hour. The solid residue obtained after removal of the reaction solvent was washed several times with  $\text{Et}_2\text{O}$  and extracted with  $\alpha,\alpha,\alpha$ -trifluorotoluene. Crystallization at  $-35\text{ }^\circ\text{C}$  afforded green crystals of  $\{[\text{Nb}(\text{BDI})\text{N}^t\text{Bu}]_2(\mu\text{-C}_6\text{H}_6)\}^+\{\text{B}(\text{C}_6\text{F}_5)_4\}^-$ , **3.2**, in moderate yield (68 %, Scheme 3.1). X-ray quality crystals of complex **3.2** were obtained from recrystallization in DCE at  $-15\text{ }^\circ\text{C}$  overnight (Figure 3.1).

**Scheme 3.1**

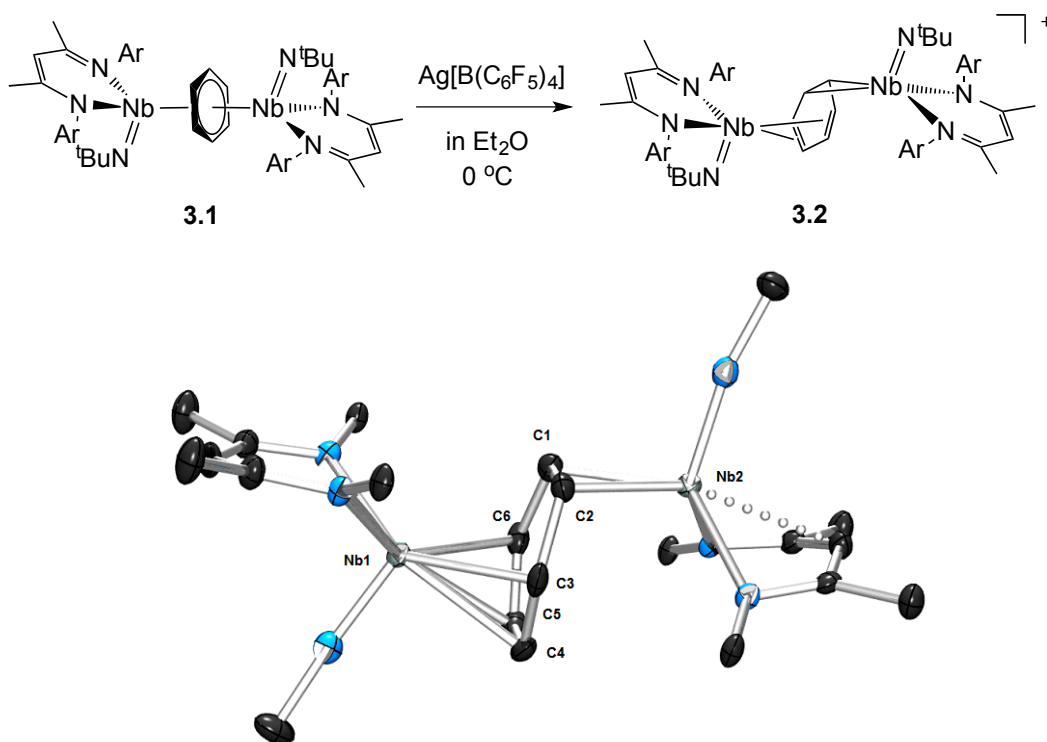


**Figure 3.1** ORTEP of the cationic part of **3.2**,  $\{[\text{Nb}_2(\text{BDI})_2\text{N}^t\text{Bu}_2](\mu\text{-C}_6\text{H}_6)\}^+$ .  $^i\text{Pr}_2\text{Ar}$  groups of BDI ligand,  $\text{CH}_3$  groups of  $^t\text{BuN}$  ligand, counter ion  $[\text{B}(\text{C}_6\text{F}_5)_4]^-$  and hydrogens have been removed for clarity. Selected bond distances in Å: Nb2-C1, 2.225(5); Nb2-C2, 2.226(5); Nb1-C3, 2.466(5); Nb1-C6, 2.384(5); Nb1-C4, 2.397(5); Nb1-C5, 2.480(5); C1-C2, 1.520(7); C2-C3, (1.460(7) Å), C3-C4, (1.390(8) Å), C4-C5, (1.446(8) Å), C5-C6, (1.382(8) Å); C6-C1 (1.454(7) Å).



Unlike **3.1**, in which the sandwiched benzene is symmetrically bound to the two metal centres via a  $\mu^2\text{-}\eta^6\text{:}\eta^6$  coordination mode, **3.2** is best described as having a  $\mu\text{-}\eta^2\text{:}\eta^4$  coordination mode, which we believe is unprecedented. This leads to a dramatic increase in the Nb-Nb distance of 4.656(4) Å as compared to 3.914(5) Å in **3.1**. The benzene ring is slightly distorted with a mean deviation from planarity of 0.07 Å, a dihedral angle of 14.9° and alternation of C-C bond distances. While C(2)-C(3), (1.460(7) Å), C3-C4, (1.390(8) Å), C(4)-C(5), (1.446(8) Å), C(5)-C(6), (1.382(8) Å) and C(6)-C(1) (1.454(7) Å) follow typical alternation of single and double bonds, C(1)-C(2) is significantly elongated (1.520(7) Å) so that Nb(1) appears to carry the single electron and interacts with a butadiene-like fragment of the arene, while Nb(2) carries the two remaining electrons and interacts with the remaining arene  $\pi$  bond at C(1)-C(2). This picture is reinforced by the short Nb(2)-C<sub>av</sub> bond length of the  $\eta^2$ - interaction (2.22 Å) compared to the longer Nb(1)-C<sub>av</sub> distance to the four C atoms engaged in the  $\eta^4$ -binding (2.43 Å). Additionally, the distortion of the BDI moiety around Nb(2) and the Nb(2)-C(31)(BDI) distance of 2.638(9) Å suggests the presence of an intramolecular donation from the  $\pi$ -system of the BDI ligand into the metal center, supporting a strong metal-arene interaction between the *d* electrons of Nb(2) atom and the empty  $\pi^*$  orbital of the C(1)-C(2) ethylene-like fragment. This intramolecular interaction between the BDI backbone and the metal center has been observed previously in Zr(IV),<sup>23-25</sup> Ti(IV),<sup>26</sup> and lanthanide complexes.<sup>27</sup> As was observed in **3.1**, the Nb=N(*t*Bu) groups are *trans* to each other in order to minimize steric interactions.

On the basis of these solid-state structural data, the one electron oxidation of **3.1** results in the formation of an asymmetric complex in which Nb(2) interacts strongly with a C2 moiety of the benzene fragment, while Nb(1) is coordinated to the remaining C4 moiety of the benzene. The Nb(1)-N(BDI) distances of 2.152(4) Å and 2.144(4) Å differ slightly from the Nb(2)-N(BDI) distances of 2.177(4) Å and 2.191(4) Å in agreement with the altered coordination environment. Even though it is clear that the two niobium centres are not identical, the Nb-C distances reported for **3.1** are close to those observed in **3.2** and it is difficult to draw conclusions concerning the electronic structure from the structural data alone.

**Cyclic Voltammetry.** Cyclic voltammetric studies were carried out on complexes **3.1** and **3.2** in  $\alpha,\alpha,\alpha$ -trifluorotoluene. For **3.1**, two features are observed (Figure 3.2). The first is a reversible process with  $E_{1/2} = -0.48$  V vs. Ag/Ag<sup>+</sup> (-0.93 V vs. Fc<sup>+</sup>/Fc) while the second is irreversible with an oxidation potential of  $E_a = +0.15$  V vs. Ag/Ag<sup>+</sup> (-0.44 V vs. Fc<sup>+</sup>/Fc). Integration of the current wave compared to an equimolar solution of **3.1** and Cp<sub>2</sub>Co is indicative of a one-electron oxidation to form a mixed valent species, while the second wave is an irreversible two-electron oxidation. Upon reduction, the cyclic voltammogram of **3.2** shows the same reversible peak at  $E_{1/2} = -0.48$  V vs. Ag/Ag<sup>+</sup>, allowing the assignment of this signal to the one-electron process that converts **3.1** to **3.2**. This half-potential is within the range reported for the reversible electrochemical oxidation of a series of isolated ( $\eta^5$ -C<sub>5</sub>H<sub>4</sub>SiMe<sub>3</sub>)<sub>2</sub>Nb(III)Cl(L) (L = phosphine or alkyne,  $E_{1/2} = [-1.69$  to  $-0.89]$  V vs. Fc<sup>+</sup>/Fc),<sup>28</sup> which suggests that the one electron event observed here is likely metal-based. Although **3.1** and **3.2** possess different structures in the solid state, it is clear from the electrochemical quasi-reversibility of the first oxidation wave that the structural rearrangement is minimal in solution and on the time scale of the CV.

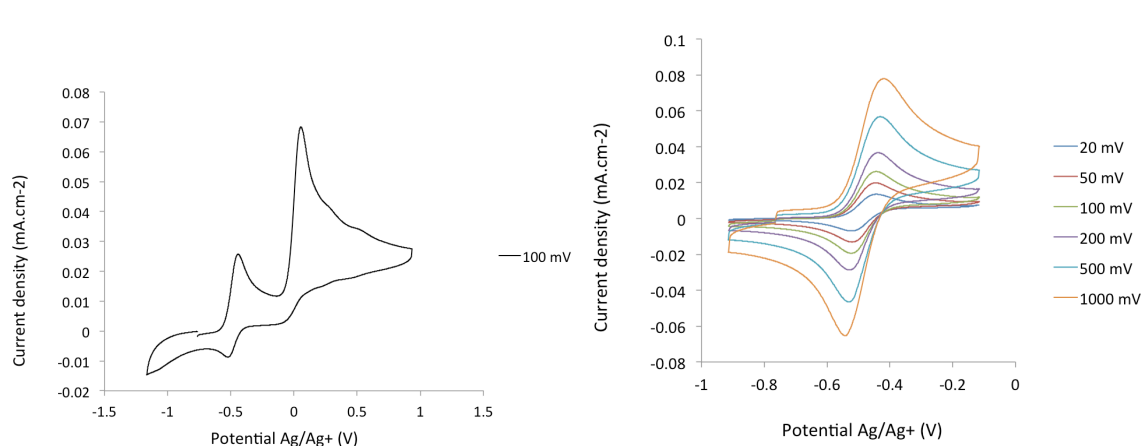


**Figure 3.2** Cyclicvoltametry of complex **3.1** in  $\alpha,\alpha,\alpha$ -trifluorotoluene

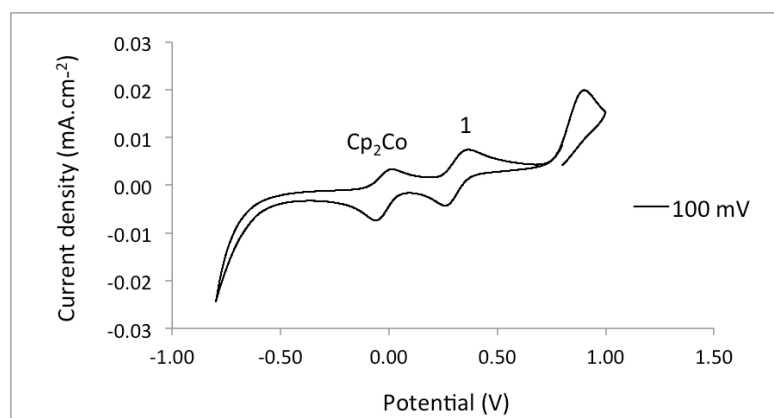


**Figure 3. 3** Cyclicvoltametry of complex **3.1** in  $\alpha,\alpha,\alpha$ -trifluorotoluene with a scan rate of 100mV/s referenced to  $[\text{Cp}_2\text{Co}]^{0/+}$  internal standard.

**NMR spectroscopy.** The  $^1\text{H}$  NMR spectrum of **3.2** in  $\text{CDCl}_3$  is unusual (see Figure 3.3). Although the peaks are broad and shifted as expected for a paramagnetic species (see below), and the temperature dependence of the chemical shift from 253 K to 373 K (see Figures 3.4 and 3.5) along with the very fast longitudinal relaxation times ( $T_1 = [5 - 12.7]$  ms, Figure S.6) further support the paramagnetic character of the analyzed species,<sup>29,30</sup> all the resonances are located close to the typical diamagnetic region (12 to -5 ppm) and the small number of peaks (8) along with their relative integrations are not consistent with the symmetry observed in the solid state. Additionally, no signals are observed in the  $^{13}\text{C}$  NMR within a reasonable accumulation time.

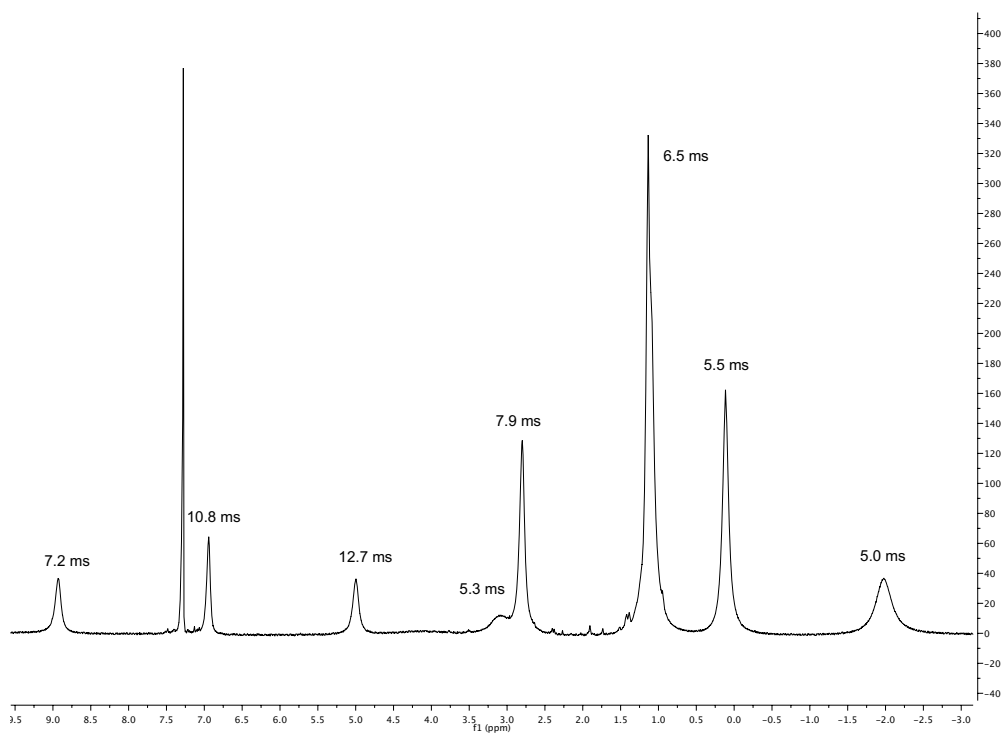


**Figure 3.4**  $^1\text{H}$  NMR spectrum of **3.2** and relaxation time of each resonance at 350 K.

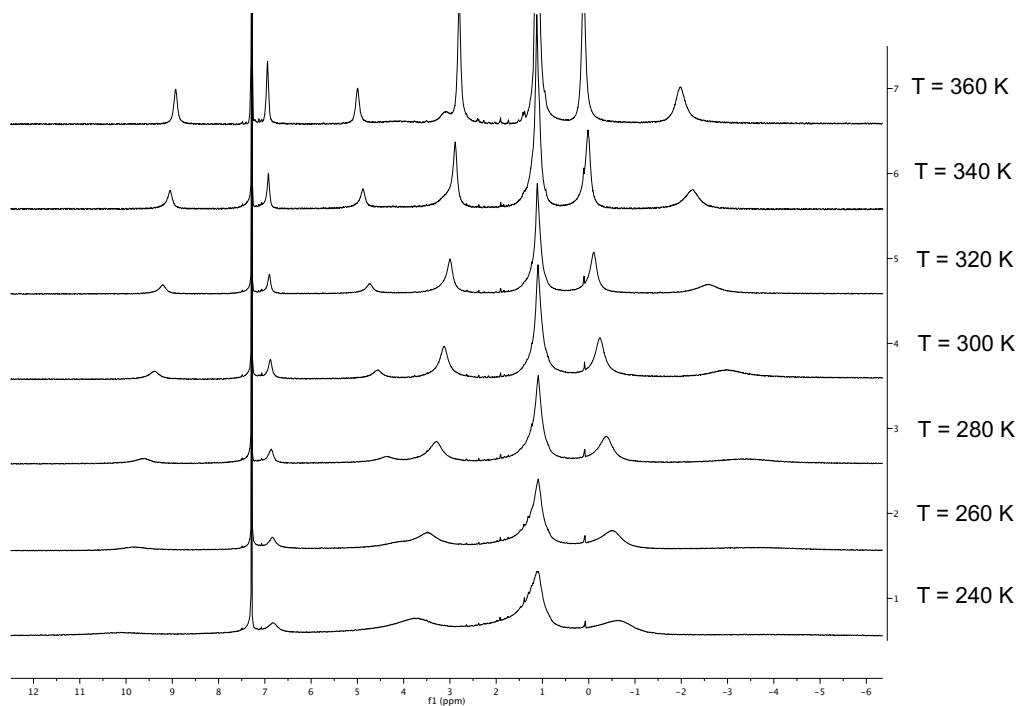


**Figure 3.5** Variable temperature  $^1\text{H}$  NMR spectroscopy of **3.2**

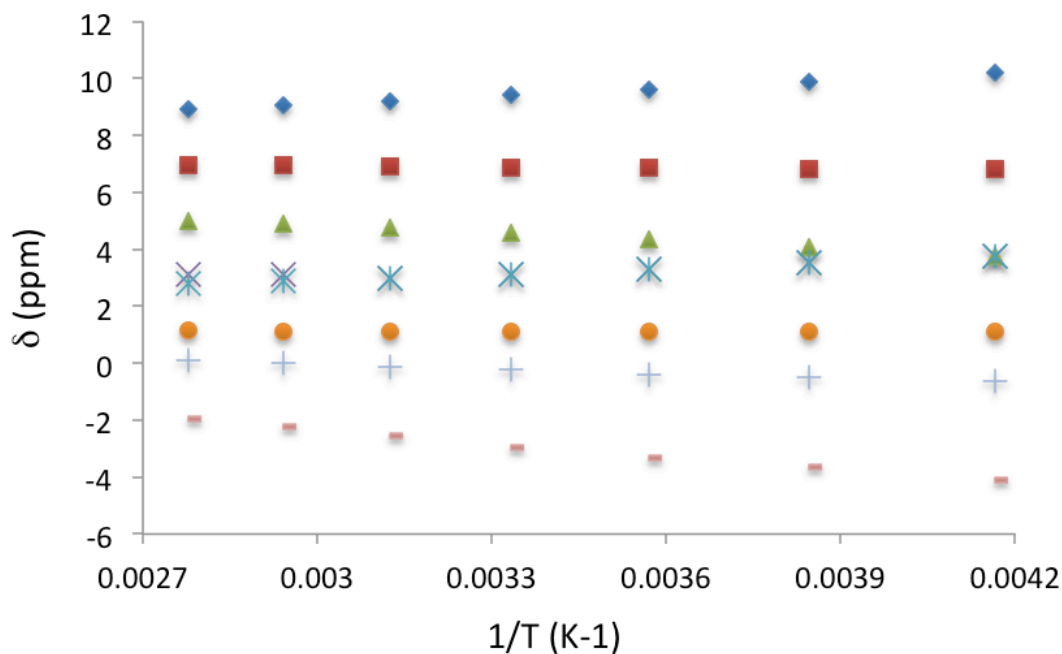


**Figure 3.6** Temperature dependence of the chemical shifts of **3.2**

In order to understand this spectrum, an equimolar mixture of **3.2** and trimethoxybenzene (used as internal standard) was analysed by  $^1\text{H}$  NMR spectroscopy. The  $^1\text{H}$  NMR signals of **3.2** were integrated and compared to those of the internal standard. This experiment revealed that only half of the number of hydrogens expected for **3.2** are observed in the  $^1\text{H}$  NMR spectrum, corresponding to a single BDI ligand and to one  $t\text{Bu}$  imido group. The other BDI ligand and  $t\text{Bu}$  imido ligand as well as the  $\mu$ -benzene are not observed. This has been further confirmed by  $^1\text{H}$  NMR analysis of the deuterated benzene analog **3.2- $d_6$** , which exhibits a similar spectrum to **3.2**, while no resonance are detected in the  $^2\text{H}$  NMR spectrum.

This behavior is in agreement with a single electron that is mostly localized on one niobium center, Nb(1), on the NMR time scale. Within this conjecture, the protons that are the closest to the paramagnetic center relax very fast and their chemical shifts are strongly shifted mostly because of the pseudo-contact term,<sup>30</sup> which results in complete broadening of their signals. On the other hand, the nuclei that lie the farthest from the paramagnetic metal center are less influenced by the pseudo-contact term and are therefore more likely to be observed in the typical diamagnetic region. The Fermi contact term is, however, important because it is clear from the EPR (see below) that the spin density of the unpaired electron is delocalized enough to cause hyperfine coupling with both metals centres.  $^1\text{H}$  NMR chemical shift calculation attempts confirmed this phenomenological observation but did not lead to satisfactory quantitative values. From this NMR analysis it is possible to conclude that the two niobium metal centres are not electronically identical, but the exact extent of the delocalization is difficult to ascertain with any degree of precision.

**UV-vis spectroscopy.** Electronic spectroscopy is often used to classify Creutz-Taube ions focusing on the presence (or absence), and intensity of the intervalence charge transfer band (IVCT).<sup>12</sup> The spectrum of **3.2** in toluene features a broad, Gaussian shaped and relatively strong band ( $\epsilon \sim 2500 \text{ cm}^{-1}\text{M}^{-1}$ ) centred at 700 nm ( $14,285 \text{ cm}^{-1}$ ) and another at 430 nm ( $23,250 \text{ cm}^{-1}$ ) (See Figure 3.6). The large absorbance of these features is not consistent with Laporte forbidden *d-d* transitions and could involve charge transfer processes.

In order to gain further insight into the nature of these transitions, TD-DFT calculations were performed on **3.2**. Two transitions are predicted at around 450 nm and are in agreement with MLCT transitions involving the benzene ligand. The presence of a similar transition in the neutral and symmetric complex **3.1** is in agreement with this assignment (Figure 3.7, blue curve). In addition, another transition is observed at 653 nm in the TD-DFT calculations and is blue shifted compared to that at 700 nm, observed in the experiment. Nevertheless, this transition can be described as an electron transfer from the SOMO (Nb(1)) into an empty *d* orbital located on the other Nb ion (Nb(2)), a formal d-d transition in which the oxidation state of Nb(2) is transferred to Nb(1) via an IVCT. In strongly delocalized systems these bands are very strong and sharp. On the other hand, they are broad and less strong in less delocalized systems. In this case, based on the experimental data, values of  $H_{ab}$  of  $1500 \text{ cm}^{-1}$  and  $\alpha^2$  of 0.011 are calculated, which classify **3.2** as a class II mixed valence system.<sup>31</sup>

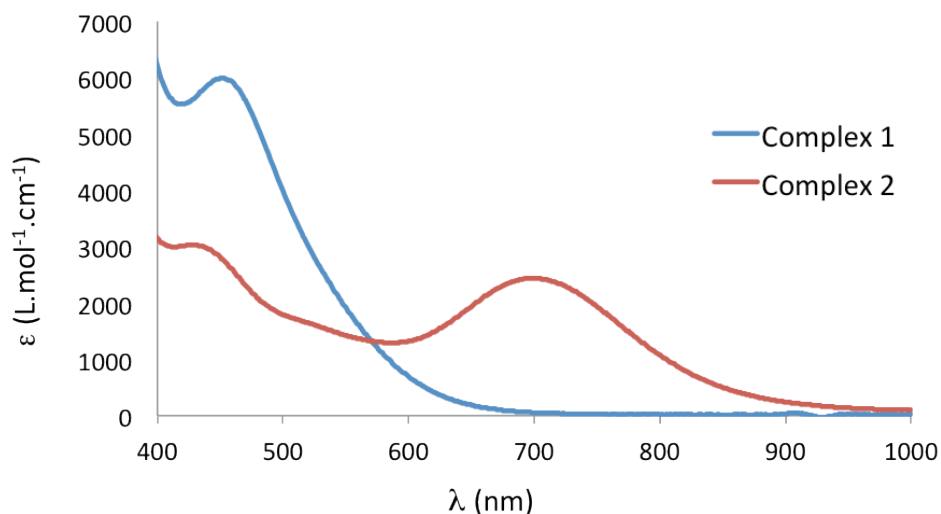


**Figure 3.7** Visible spectra of **3.1** and **3.2** in  $\alpha,\alpha,\alpha$ -trifluorotoluene at room temperature. Electronic absorbance spectrum of 47.8 mM solution of **3.1** and 38.2 mM solution of **3.2** in  $\alpha,\alpha,\alpha$ -trifluorotoluene. Complex 2: 326 nm ( $27000 \text{ cm}^{-1}\text{M}^{-1}$ ); 426 nm ( $3200 \text{ cm}^{-1}\text{M}^{-1}$ ); 704 nm ( $2430 \text{ cm}^{-1}\text{M}^{-1}$ ).

**EPR and Magnetic Studies.** Magnetic data for **3.2** were measured in the solid state using a SQUID magnetometer over the temperature range 5-300 K (see experimental, figures 3.12-3.13). The effective moment at room temperature is  $1.8 \mu_{\text{eff}}$ , in agreement with  $S=1/2$  and one unpaired electron. We then turned to EPR spectroscopy to determine the location of this spin. An X-band EPR spectrum of **3.2** was recorded in the solid state at both 298 K and 4 K (see experimental, Figure 3.14-3.15), and in a frozen solution (4K) of  $\alpha,\alpha,\alpha$ -trifluorotoluene

(Figure 3.8). Niobium has an  $I = 9/2$  nuclear spin, so a 10-line pattern is expected if the spin is located on a single metal center in an isotropic environment; in contrast, 19 equally spaced lines should be observed if the spin is delocalized over two magnetically equivalent niobiums. However, the experimental data are not in agreement with either of these two extremes, suggesting a more complex electronic structure.

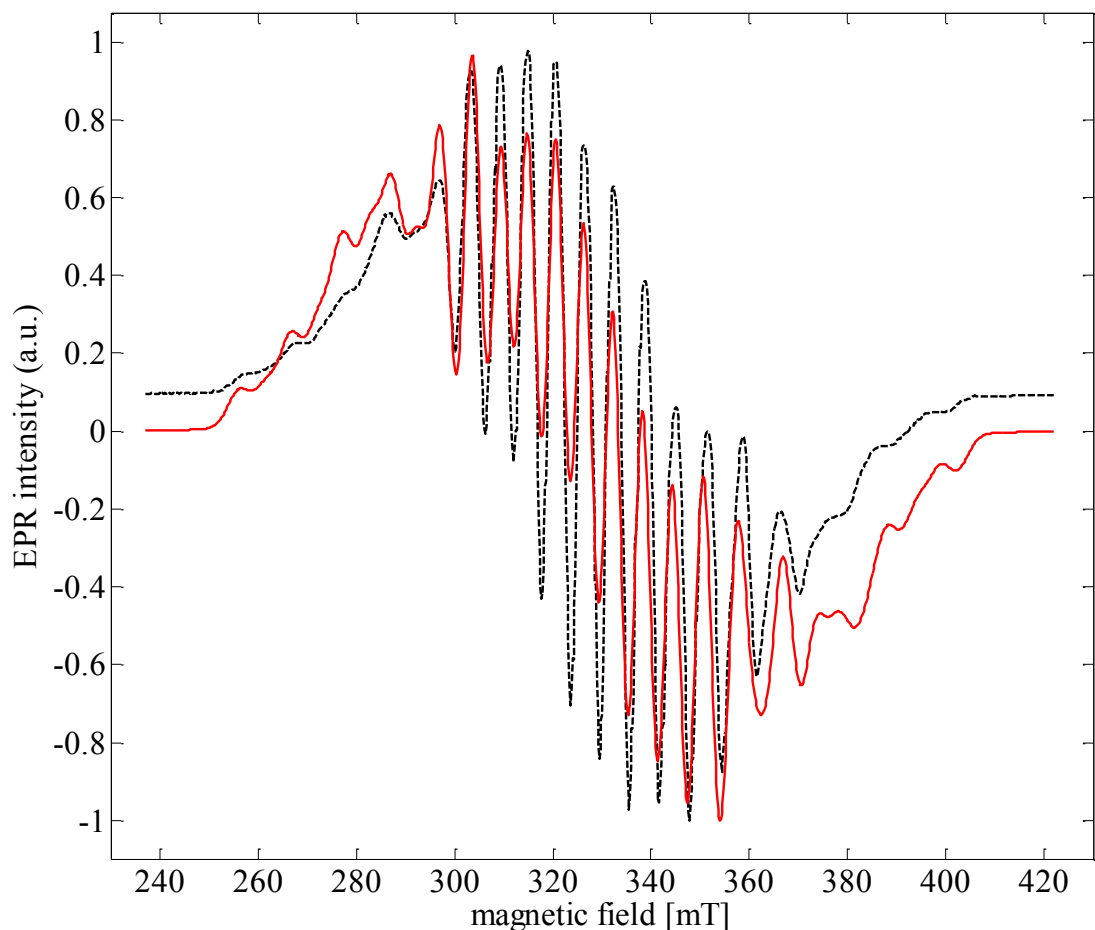


**Figure 3.8** X-Band EPR spectrum (black dashed line) of **3.1** recorded in frozen solution of  $\alpha, \alpha, \alpha$ -trifluorotoluene at 4K. The red line corresponds to the simulated data for the parameters implemented in Table 3.1.

The best simulation (Figure 3.8) of the EPR data was obtained using two niobium atoms that have different hyperfine coupling constants ( $A$   $^{93}\text{Nb}$ ) and in a slight rhombic symmetry (*viz.*  $g_1 = 1.980$ ,  $g_2 = 1.991$ ,  $g_3 = 1.997$ ). Nb(1) has a large hyperfine coupling constant of 290 MHz ( $\sim 103$  G) and two lower ones (150 and 100 MHz), while Nb(2) is isotropic (165 MHz,  $\sim 59$  G). No superhyperfine  $^{14}\text{N}$  coupling constants were used because the line shape is significantly broadened. G matrix and coupling constant calculations were carried out with the ORCA program and are in agreement with a description with only minimal differences in the hyperfine coupling constants (Table 3.1). Therefore the EPR data reinforce the bonding picture provided by the solution and solid-state data that can be

summarized as follows: complex **3.2** can be viewed as if Nb(1) carries the single electron in the  $d_{x^2-y^2}$  orbital while Nb(2) uses the filled  $d_{x^2-y^2}$  to form a bond with an  $E_{2u}$  orbital of the benzene. The sole electron delocalizes only to a small extent into the empty  $d_{xy}$  orbital of Nb(2) through the other (empty)  $E_{2u}$  benzene orbital.

**Table 3.1.** Principal experimental and calculated EPR data for complex **1** (hyperfine coupling constants,  $A$ , are give in MHz).

	$g_1, g_2, g_3$	$A \text{ } ^{93}\text{Nb}_1$	$A \text{ } ^{93}\text{Nb}_2$
<b>Exp</b>	1.980 1.991 1.997	100 150 290	165 165 165
<b>PBE0</b>	1.979 1.991 1.997	-125 -130 -295	171 171 187
<b>B3LYP</b>	1.979 1.992 2.000	-91 -90 -264	191 174 175

**DFT calculations.** Finally, DFT calculations were performed on **3.1** and **3.2**. The geometries of both complexes were optimized from their X-ray structures; a spin restricted closed shell electronic structure was assumed for **3.1** and an unrestricted open shell doublet for **3.2**. The correlation between calculated and experimental bond lengths is reasonable (see metrical parameters SI). As both complexes feature distorted benzene ligands, the energy differences between free benzene and the benzene fragments in **3.1** and **3.2** have been calculated; in the complexes the benzene rings are  $23.7 \text{ kcal.mol}^{-1}$  and  $22.7 \text{ kcal.mol}^{-1}$  less stable, respectively, than in free benzene. Moreover, the average C-C distance in the benzene ring in **3.1** is  $1.458 \text{ \AA}$  as compared to  $1.394 \text{ \AA}$  in free benzene. Taken together, these observations suggest strong Nb  $\rightarrow$  benzene charge transfer in **3.1**, which is supported by the partial atomic charge data in Table 3.2. Although the absolute values of the charges differ significantly between the different approaches, all three indicate substantial build up of electron density on the arene ligand.

**Table 3.2** Partial atomic charges on the niobium atoms and benzene fragments in **3.1** and **3.2**, calculated using the Mulliken, Hirshfeld and QTAIM approaches.

	Mulliken	Hirshfeld	QTAIM	
<b>1</b>	<b>Nb1</b>	2.89	0.63	1.88
	<b>Nb2</b>	2.90	0.63	1.87
	<b>benzene</b>	-2.46	-0.38	-1.16
<b>2</b>	<b>Nb1</b>	2.82	0.68	1.87
	<b>Nb2</b>	2.68	0.68	1.92
	<b>benzene</b>	-1.69	-0.25	-0.79

The interaction energy between the two Nb fragments and the benzene ring in **3.1** has been calculated using the Ziegler-Rauk energy decomposition scheme.<sup>36</sup> The large total bonding energy (142.9 kcal.mol<sup>-1</sup>) and the fact that the orbital interaction term contributes 47% of the overall stabilising contribution, reinforce the conclusion of a strong interaction between the arene ring and the metal centre. Consistent with such an interaction, and that it features metal → benzene charge transfer, are the canonical HOMO-1 and HOMO, shown in Figure 3.9. Both orbitals are clearly δ-backbonding.

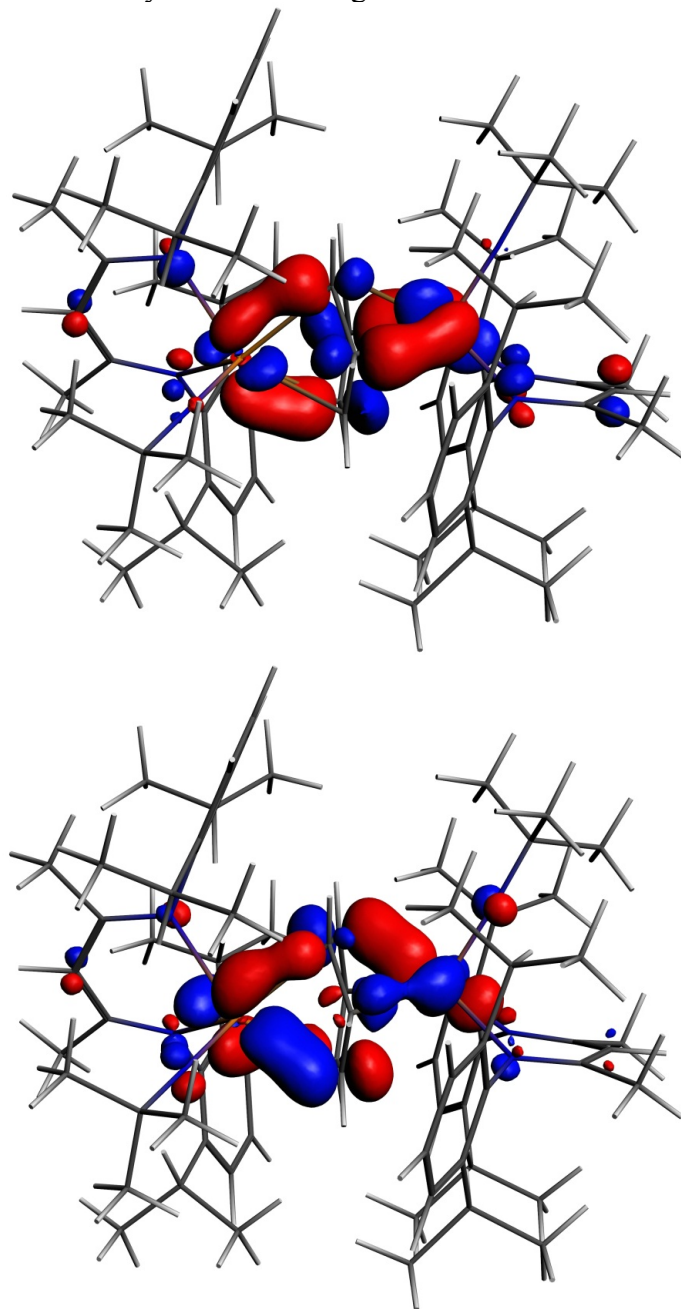


**Figure 3.9** HOMO-1 (-3.934 eV: 13.0% Nb1 d, 17.1% Nb2 d, 1.1% Nb2 s, 38.1% C(benzene) p) and HOMO (-3.875 eV. 20.8% Nb1 d, 17.1% Nb2 d, 35.0% C(benzene) p) of **3.1**. Isosurface value = 0.05.



The benzene ring in complex **3.2** is not in alignment with the Nb – Nb axis as observed in **1**. Interestingly, when geometry optimization of **3.2** was performed by starting from the optimized structure of **3.1**, removing one electron and employing the spin unrestricted approach, the calculation converged to a different geometry than that found when starting from the solid-state structure of **3.2**. The new optimized geometry is only 2.4 kcal.mol<sup>-1</sup> less stable than the previous optimized one and is surprisingly in better agreement with the X-ray structure of **3.2**. This little difference may explain why the CV shows a quasi-reversible wave for the one electron oxidation of **3.1** (the energy of structural rearrangement is very small). Figure 3.10 shows the spin density, the SOMO and  $\alpha$  HOMO of **3.2**. The spin density indicates much greater localization of the unpaired electron on Nb1 (0.66) than Nb(2) (0.06), with significant spin density located on carbons of the benzene ring (0.14 for C3 and 0.15 for C6, respectively). The spin density and SOMO plots are in good agreement with the EPR data. The SOMO is much more localised on Nb(1) than Nb(2), as is the spin density, so that both niobium ions contribute (but not equally) to the overall EPR signal. As an additional note, the calculated EPR data and experimental EPR data were in good agreement. Both the  $\alpha$  and  $\beta$  components of the HOMO show a very strong interaction between two carbon atoms of the benzene and Nb(2) so that the C-Nb(2)-C unit may be described as a metallacyclopropane. This explains the longer distance found for C(1)-C(2) of 1.520(7) Å.

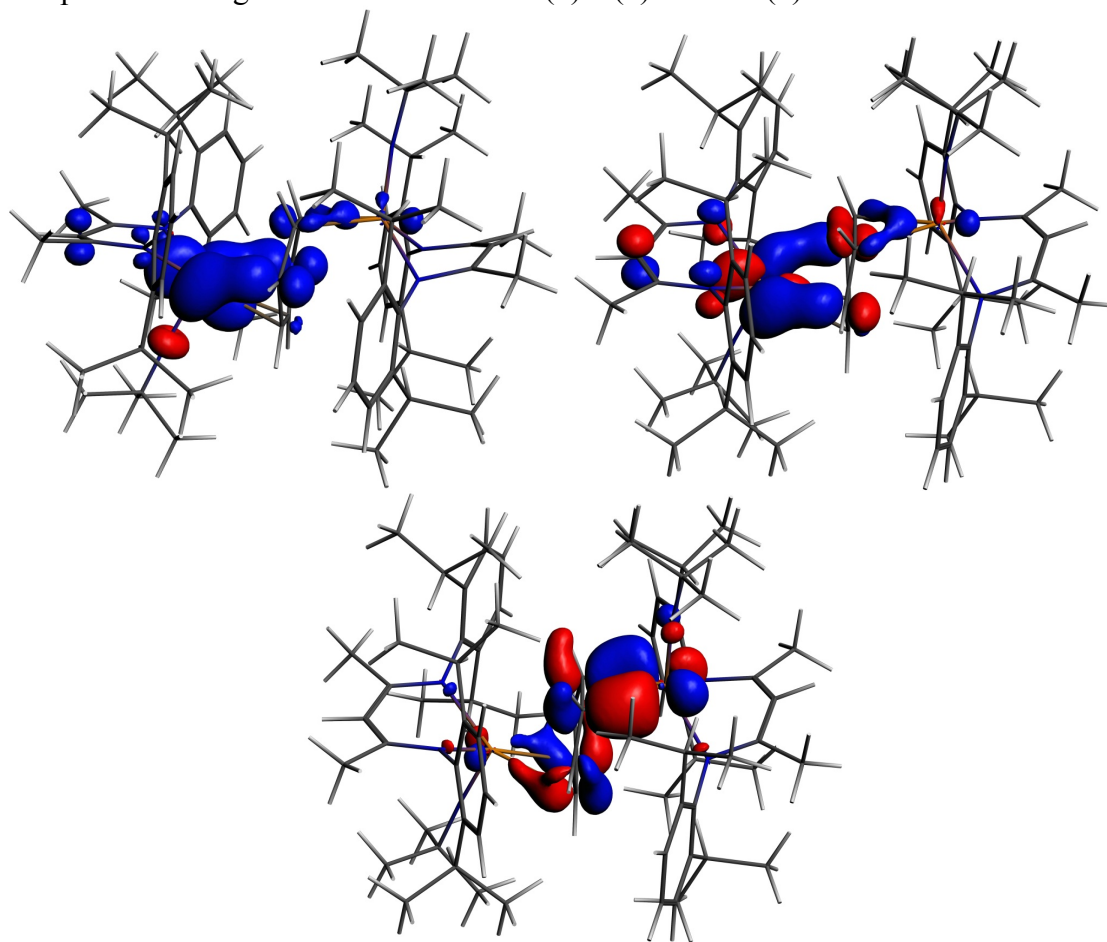
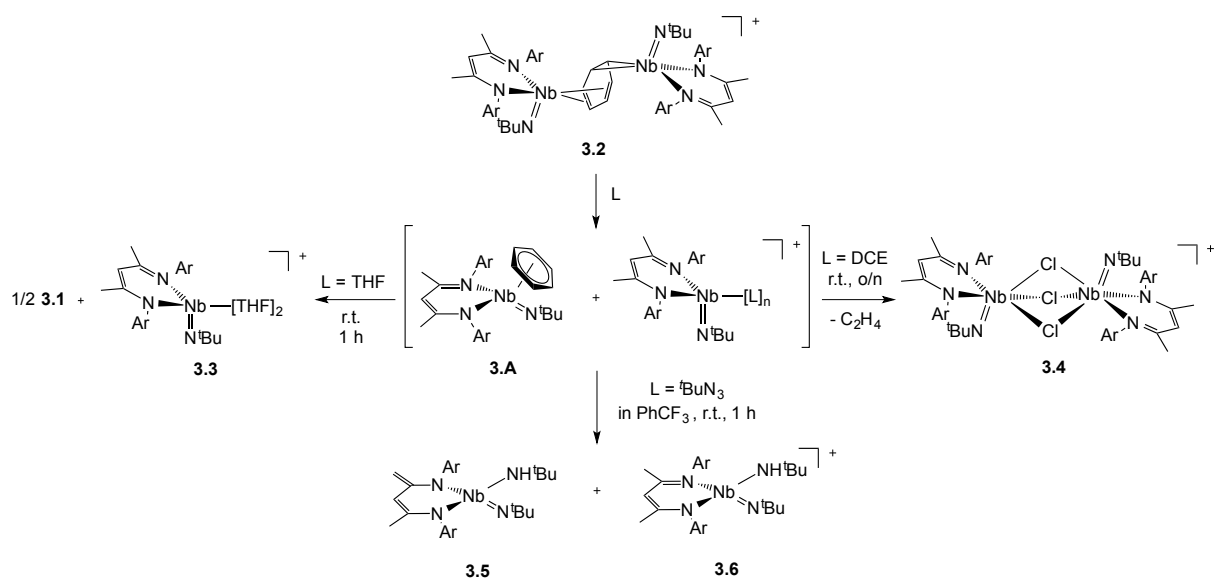


**Figure 3.10** Spin density (left, blue =  $\alpha$ , red =  $\beta$ , isosurface = 0.003), SOMO (middle, -6.349 eV. 41.4% Nb1 d, 1.6% Nb 1 s, 2.5% Nb2 d, 1.4% Nb2 p, 23.0% C(benzene) p) and  $\alpha$  HOMO (right, -6.941 eV. 3.9% Nb1 d, 26.2% Nb2 d, 1.4% Nb2 p, 42.4% C(benzene) p).

Returning to table 3.2, all three charge schemes indicate that the biggest change between **3.1** and **3.2** is for the benzene ring, suggesting that some of the charge build up on the ring arising from d backbonding in the neutral is pulled back in the cation. The Mulliken data suggest that this leads to a reduction in the positive charge of the metals from **3.1** to **3.2**, while the other two methods indicate little change in the metal charge.

**Reactivity studies.** Unlike the neutral sandwich complex **3.1**, which is extremely stable (both chemically and thermally), **3.2** is very reactive at room temperature, even toward coordinating solvents and halocarbons. Dissolution of **3.2** in THF results in a fast exothermic reaction and a color change from deep green to red within 10 min. A red-brown residue is obtained upon removal of the volatile materials. Extraction with hexanes followed by crystallization at -40 °C leads to the formation of red crystals of complex **3.1**. The remaining green powder is highly unstable but can be crystallized from slow diffusion of hexane into THF at room temperature; this species was identified by X-ray diffraction as the Nb(IV) complex,  $\{(\text{BDI})\text{N}^t\text{BuNb}(\text{thf})_2\}^+\{\text{B}(\text{C}_6\text{F}_5)_4\}^-$ , **3.3**. Such reactivity is consistent with the proposed mechanism in Scheme 3.2. Coordination of the solvent to the electron deficient Nb(IV) metal center of the  $\mu$ -benzene complex followed by dissociation results in the formation of the reactive new Nb(IV) cationic species  $\{(\text{BDI})\text{N}^t\text{BuNb}(\text{thf})_2\}^+$ , **3.3**, and the monomeric benzene complex,  $(\text{BDI})\text{N}^t\text{BuNb}(\text{C}_6\text{H}_6)$ ;<sup>22</sup> in solution at room temperature, the latter is known to decompose to form **3.1**.

**Scheme 3.2** Synthesis of complexes **3.3-3.6**.



Complex **3.3** is a rare example of a monomeric  $d^1$  cationic niobium species stabilized by relatively labile ligands (two THFs). Crystallographic analysis of **3.3** (Figure 3.11, top) reveals the presence of a slightly distorted square planar pyramidal geometry ( $\tau = 0.12$ ), with the <sup>t</sup>Bu imido group in the apical position along with the BDI and the two THF ligands in the basal plane. The metal nitrogen bond distances of the imido and BDI ligands are within previously described distances for such ligand platform<sup>37-39</sup> ( $\text{Nb-N}(3) = 1.7531(19) \text{ \AA}$  and  $\text{Nb-N}_{\text{BDI average}} = 2.182 \text{ \AA}$ ), as well as the niobium oxygen bond distances ( $\text{Nb-O}_{\text{average}} = 2.221 \text{ \AA}$ ).

Dissolution of **3.2** in 1,2-dichloroethane (DCE) at room temperature overnight results in color change from deep green to orange from which crystals of  $\{[(\text{BDI})\text{N}^t\text{BuNb}]_2(\mu\text{-Cl})_3\} \{ \text{B}(\text{C}_6\text{F}_5)_4 \}$ , **3.4**, were obtained in good yield (78 %). The X-ray structure of **3.4** consists of a dimeric, cationic molecule in which the two Nb(BDI)N<sup>t</sup>Bu moieties are bridged by three chlorine atoms (Figure 3.11, bottom). The long Nb(1)-Nb(2) bond distance of 3.625 Å supports the absence of metal-metal interaction, consistent with the d<sup>0</sup>/d<sup>0</sup> electronic configuration of **3.4**. The steric hindrance imposed by the BDI ligand results in a non-symmetric coordination of the three chlorines. Thus, Cl(1) aligns with the BDI of Nb(1) and the <sup>t</sup>Bu imido of Nb(2) and is closer to the Nb(2) compared to the other metal center (Cl(1)-Nb(1) = 2.6787(5) Å and Cl(1)-Nb(2) = 2.5119(4) Å). Similar behavior, but with an opposite trend, is noticed with Cl(3), which aligns with the BDI of Nb(2) and the <sup>t</sup>Bu imido of Nb(1) (Cl(3)-Nb(1) = 2.5249(5) Å and Cl(3)-Nb(2) = 2.6963(5) Å). Finally, the third chloride, which is staggered with both BDI ligands, coordinates symmetrically to the two metal centres (Cl(2)-Nb(1) = 2.5559(4) Å and Cl(2)-Nb(2) = 2.5567(4) Å). NMR characterization of this diamagnetic Nb(V)/Nb(V) complex reveals the presence of highly symmetric species in solution. <sup>1</sup>H NMR studies of the reaction between **3.2** and DCE revealed the clean formation of **3.4** and ethene. Formation of **3.4** from **3.2** was also observed in CDCl<sub>3</sub> with d<sub>2</sub>-tetrachloroethane being generated as a side product, albeit at a much slower rate (80 °C, 24 h). The number of chlorine abstracted from DCE (or CDCl<sub>3</sub>) and the formation of ethylene (or C<sub>2</sub>D<sub>2</sub>Cl<sub>4</sub>) is in agreement with the presence of three available electrons in **3.2** to form the oxidized species **3.4**. It is interesting to note that chlorinated volatile organic compounds (VOCs) are among the most ubiquitous environmental pollutants owing to their widespread use as solvents and raw materials in industrial applications, and their poor biodegradability.<sup>40</sup>

Finally, addition of excess <sup>t</sup>BuN<sub>3</sub> (5 equiv.) to a solution of **3.2** in α,α,α-trifluorotoluene and results in a fast color change from green to orange along with vigorous gas evolution. Extraction with toluene yielded  $[(\text{CH}_2\text{C}(\text{NAr})\text{CHC}(\text{NAr})\text{CH}_3)\text{Nb}(\text{N}^t\text{Bu})(\text{NH}^t\text{Bu})]$ , **3.5**.<sup>38</sup> Extraction of the remaining yellow residue with dichloromethane followed by crystallization at -40 °C yielded the new cationic complex  $\{(\text{BDI})\text{Nb}(\text{N}^t\text{Bu})(\text{NH}^t\text{Bu})\} \{ \text{B}(\text{C}_6\text{F}_5)_4 \}$ , **3.6**. X-ray analysis of **3.6** reveals the formation of a tetrahedral complex with two inequivalent <sup>t</sup>BuN moieties, consistent with an imido amide complex (Nb-N(3) = 1.733(3) Å and Nb-N(4) = 1.953(4) Å; Nb-N(3)-C(30) = 172.4 ° and Nb-N(4)-C(34) = 146.4 °, figure 3.11 middle). Interestingly, as observed in complex **3.2**, the BDI backbone appears distorted toward the metal center; however, unlike **3.2**, the metal center appears to be in close contact with the C<sub>alpha</sub> of the imine (Nb-C(4) = 2.694(4) Å), and suggests the presence of an η<sup>2</sup>-imine coordination of one side of BDI to the coordinatively unsaturated and electron poor metal center. Complex **3.5** was previously isolated as a tautomerization product of the bis *tert*-butyl imido niobium BDI complex, which was synthesized either from the reaction of  $[(\text{BDI})\text{Nb}(\text{N}^t\text{Bu})\text{Cl}_2]$  with two equivalents of <sup>t</sup>BuNHLi,<sup>38</sup> or via reaction between a trivalent niobium BDI imido moiety, such as the mono arene niobium complex **3.A**, and <sup>t</sup>BuN<sub>3</sub>.<sup>50</sup>

These latter reactions further confirm that **3.2** can be broken apart with coordinating ligands, leading to Nb(III) and Nb(IV) complexes which further react accordingly to their oxidation state. This is interesting because it gives easy access to stable a cationic Nb(IV) source that could be of high interest for the study of radical based reactions of group 5.

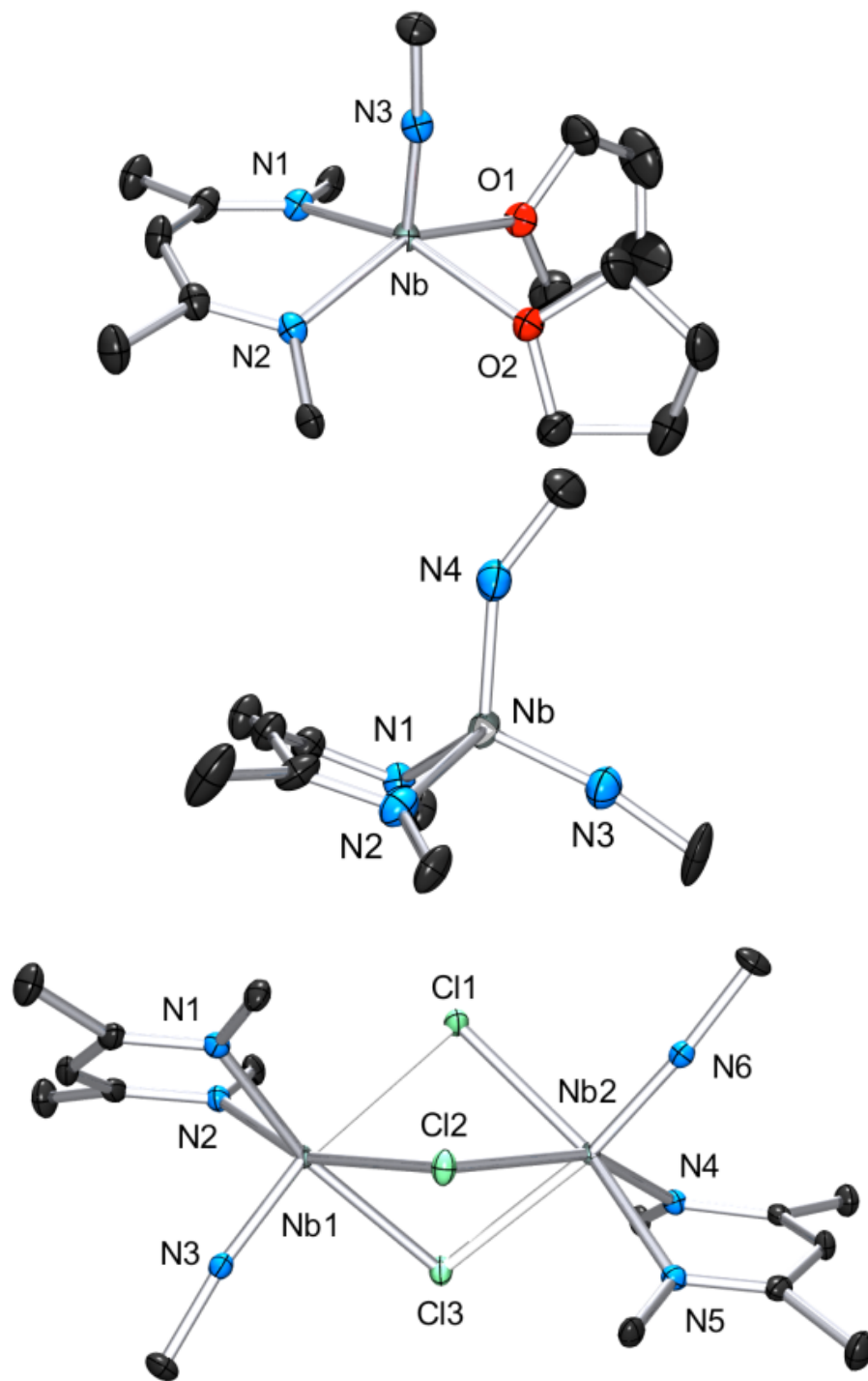


**Figure 3.11.** ORTEP of **3.3** (top left), **3.4** (bottom) and **3.6** (top right).  $i\text{Pr}_2\text{Ar}$  groups of BDI ligand and  $\text{CH}_3$  groups of  $t\text{BuN}$  ligand, counter ion  $[\text{B}(\text{C}_6\text{F}_5)_4]^-$  and hydrogens have been removed for clarity. Thermal ellipsoids are represented at 50 %. Crystallographic parameters are presented in Table 3.3

## Conclusion

In the Nb(III)/Nb(III) inverted sandwich complex **3.1**, the two metal centres each possess two metal-based valence electrons leading to a symmetrical compound. A key feature of the electronic structure of **3.1** is  $\delta$  backbonding between the two niobium centres and the  $\mu$ -benzene ring; in agreement with our previous experimental analysis, DFT calculations confirm the presence of significant charge transfer to the arene. Whereas **3.1** was found to be inert in terms of chemical reactivity, simple 1-electron oxidation leads to a cationic, mixed valence complex, **3.2**, which can be thought of as being generated by removal of an electron from the highest occupied  $\delta$  backbonding orbital of **3.1**. The unpaired electron is principally localized on Nb(1), which interacts with a butadiene-like fragment of the benzene ring. Nb(2) interacts with the remaining  $\pi$  electrons on the benzene ring in what may be described as a metalacyclopropane, based on the structural data and DFT calculations.  $^1\text{H}$  NMR and EPR data are in good agreement with the presence of a Nb(IV) radical species that is mainly localized on one niobium atom but the presence of the  $\mu$ -benzene ring nearby allows partial delocalization and confers stability to the latter. This situation strongly differs from other mixed valence inverted sandwiches in which the C-C distances of the benzene ring remain similar – although elongated – from the neutral benzene averaged C-C distances.<sup>18-20</sup> Encouraged by this unusual behaviour and electronic structure, we studied the reactivity of this complex toward coordinating solvents and ligands and have also found a rare chlorine abstraction from DCE, while the dissolution of **3.2** in THF led to the formation of **3.1** and to an extremely reactive THF adduct of a Nb(IV) species.

## Experimental

**General considerations.** Unless otherwise noted, all reactions were performed either using standard Schlenk line techniques or in an MBraun inert atmosphere glove box under an atmosphere of purified nitrogen (<1 ppm  $\text{O}_2/\text{H}_2\text{O}$ ). Glassware, cannulae, and Celite were stored in an oven at ca. 160 °C for at least 12 hrs prior to use. *n*-Pentane, hexanes,  $\text{Et}_2\text{O}$ , THF, toluene and benzene were purified by passage through a column of activated alumina, stored over 3 or 4 Å molecular sieves, and degassed prior to use.<sup>51</sup>  $\alpha,\alpha,\alpha$ -trifluorotoluene, 1,2-dichloroethane and chlorobenzene were dried over  $\text{P}_2\text{O}_5$ , distilled under reduced pressure, degassed and stored over 4 Å molecular sieves. Deuterated solvents ( $\text{C}_6\text{D}_6$ ,  $\text{C}_7\text{D}_8$  and  $\text{C}_6\text{D}_{12}$ ) were dried over sodium/benzophenone, and  $\text{C}_6\text{D}_5\text{Cl}$  was dried over  $\text{CaH}_2$ . The deuterated solvents were then vacuum transferred to a storage flask and degassed before being stored in the dry box.  $\text{C}_6\text{D}_6$ ,  $\text{C}_7\text{D}_8$  and  $\text{C}_6\text{D}_5\text{Cl}$  were stored over activated molecular sieves.  $\text{N,N}'$ -bis-(2,6-diisopropylphenyl)- $\beta$ -diketiminate (BDI),<sup>52</sup>  $\text{Li}(\text{BDI})\cdot\text{Et}_2\text{O}$ ,<sup>53</sup>  $(\text{BDI})\text{pyCl}_2\text{Nb}(\text{N}^t\text{Bu})$ <sup>54</sup> and  $(\text{BDI})(\text{Me})_2\text{Nb}(\text{N}^t\text{Bu})$ <sup>54</sup> were prepared using literature procedures. All other reagents were acquired from commercial sources and used as received. NMR spectra were recorded on Bruker AV-300, AVQ-400, AVB-400, DRX-500, AV-500, and AV-600 spectrometers. Chemical shifts were measured relative to residual solvent peaks, which were assigned relative to an external TMS standard set at 0.00 ppm.  $^1\text{H}$  and  $^{13}\text{C}$  NMR assignments were routinely confirmed by  $^1\text{H}$ - $^1\text{H}$  (COSY, NOESY) and  $^1\text{H}$ - $^{13}\text{C}$  (HSQC and HMBC) experiments. Samples for UV-vis-NIR spectroscopy were prepared in a Schlenk-adapted quartz cuvette and analyzed on a Varian Cary 50 scanning spectrophotometer. The uncorrected melting points were determined using sealed capillaries prepared under nitrogen on an Optmelt SRS.

Elemental analyses were performed at the College of Chemistry Microanalytical Laboratory, University of California, Berkeley. The X-ray structural determinations were performed at CHEXRAY, University of California, Berkeley on Bruker SMART 1000 or SMART APEX diffractometers.

**[[*(BDI)Nb(N<sup>t</sup>Bu)*]<sub>2</sub>( $\mu$ - $\eta^6$ : $\eta^6$ -C<sub>6</sub>H<sub>6</sub>)]*[B(C<sub>6</sub>F<sub>5</sub>)<sub>4</sub>]* (**3.2**).** A solution of AgB(C<sub>6</sub>F<sub>6</sub>)<sub>4</sub> (384 mg, 0.488 mmol, 1.05 equiv.) in 20 mL of Et<sub>2</sub>O was slowly added to a solution of complex **3.1** (616 mg, 0.465 mmol, 1 equiv.) in 100 mL of hexanes at 273 K in the dark. The red mixture, which quickly turned dark green, was stirred at 273 K for an hour and then at room temperature for another hour from which a large quantity of green microcrystalline powder along with black silver was observed. After removal of the volatile material under reduce pressure and washing with 2 x 20 mL of Et<sub>2</sub>O, the green material was extracted with  $\alpha,\alpha,\alpha$ -trifluorotoluene and crystallized at -20 °C. Dark green crystals of complex **3.2** were thus obtained in good yield (585 mg, 65%). X-ray quality crystals were obtained from recrystallization in DCE at -20 °C, however **3.2** was found to slowly react at room temperature with DCE. <sup>1</sup>H NMR (500 MHz, CDCl<sub>3</sub>, 293 K): 9.4 (2 H), 6.88 (2 H), 4.57 (2 H), 3.12 (7 H), 1.11 (24 H), -0.24 (9 H), -0.95 (4 H). <sup>19</sup>F NMR (470 MHz, CDCl<sub>3</sub>, 293 K):  $\delta$ (ppm) -131.59, -163.14, -166.80 (*[B(C<sub>6</sub>F<sub>6</sub>)<sub>4</sub>]<sup>-</sup>*). Anal. Calcd for C<sub>98</sub>H<sub>110</sub>B<sub>1</sub>Cl<sub>2</sub>F<sub>20</sub>N<sub>6</sub>Nb<sub>2</sub>: C, 58.29; H, 5.49; N, 4.16. Found: C, 58.19; H, 5.55; N, 4.16.

**[[*(BDI)Nb(N<sup>t</sup>Bu)*]<sub>2</sub>( $\mu$ - $\eta^6$ : $\eta^6$ -C<sub>6</sub>D<sub>6</sub>)]*[B(C<sub>6</sub>F<sub>5</sub>)<sub>4</sub>]* (**3.2-d<sub>6</sub>**).** A solution of AgB(C<sub>6</sub>F<sub>6</sub>)<sub>4</sub> (30 mg, 0.04 mmol, 1.05 equiv.) in 5 mL of Et<sub>2</sub>O was slowly added to a solution of complex **3.1-d<sub>6</sub>** (60 mg, 0.04 mmol, 1 equiv.) in 10 mL of hexanes at 273 K in the dark. The reaction mixture was worked up as described in the synthesis of **3.2**. Dark green crystals of complex **3.2-d<sub>6</sub>** were obtained in good yield (51 mg, 62%). The <sup>1</sup>H and <sup>19</sup>F NMR spectra were similar to those of complex **3.2**.

**[*(BDI)Nb(N<sup>t</sup>Bu)*](THF)<sub>2</sub>]*[B(C<sub>6</sub>F<sub>5</sub>)<sub>4</sub>]* (**3.3**).** Complex **3.2** (300 mg, 0.013 mmol) was dissolved in 50 ml of THF, the solution turned rapidly from deep green to red-orange. After stirring at room temperature for 12 hours, the volatile were removed under reduced pressure resulting in a brown powder. The complex **3.1** was extracted and crystallized at -40 °C from hexane affording deep red crystals in moderate yield (95 mg, 42 %). <sup>1</sup>H and <sup>13</sup>C NMR analysis of **3.1** are in agreement with the data reported in the litterature.<sup>ref</sup> The residual green powder was extracted with THF, and crystals were obtained from hexane layering at room temperature. <sup>19</sup>F NMR (470 MHz, CDCl<sub>3</sub>, 293 K):  $\delta$ (ppm) -131.59, -163.14, -166.80 (*[B(C<sub>6</sub>F<sub>6</sub>)<sub>4</sub>]<sup>-</sup>*). Anal. Calcd for C<sub>65</sub>H<sub>66</sub>B<sub>1</sub>F<sub>20</sub>N<sub>3</sub>Nb: C, 55.57; H, 4.74; N, 2.99. Found: C, 55.19; H, 5.12; N, 3.25.

**[[*(BDI)Nb(N<sup>t</sup>Bu)*]<sub>2</sub>( $\mu$ -Cl)<sub>3</sub>]*[B(C<sub>6</sub>F<sub>5</sub>)<sub>4</sub>]* (**3.4**).** Complex **3.2** (500 g, 0.24 mmol) was dissolved in 30 ml of DCE, and the solution turned slowly from deep green to bright orange. After being stirred at room temperature overnight, the solution was concentrated and stored at -20 °C for two days, resulting in the crystallization of **3.4** as orange crystals in good yield (410 mg, 82 %). X-ray quality crystals were obtained by recrystalization from DCE at 0 °C. <sup>1</sup>H NMR (500 MHz, CDCl<sub>3</sub>, 293 K): 7.31 (t, 2 H, *p-Ar*, <sup>3</sup>J<sub>HH</sub> = 7.6 Hz), 7.24 (dd, 2 H, *o-Ar*), 7.10 (dd, 2 H, *o-Ar*), 6.34 (s, 1 H, *HC(C(Me)NAr)*<sub>2</sub>), 3.10 (sept, 2 H, *CHMe*<sub>2</sub>, <sup>3</sup>J<sub>HH</sub> = 6.8 Hz), 2.52 (sept, 2 H, *CHMe*<sub>2</sub>, <sup>3</sup>J<sub>HH</sub> = 6.9 Hz), 2.04 (s, 6 H, *HC(C(Me)NAr)*<sub>2</sub>), 1.31 (d, 6 H, *CHMe*<sub>2</sub>, <sup>3</sup>J<sub>HH</sub> = 6.8 Hz), 1.22 (s, 9 H, *Nb=N<sup>t</sup>Bu*), 1.14 (d, 6 H, *CHMe*<sub>2</sub>, <sup>3</sup>J<sub>HH</sub> = 6.6 Hz), 1.05 (d, 6 H, *CHMe*<sub>2</sub>, <sup>3</sup>J<sub>HH</sub> = 6.9 Hz), 0.61 (m, 6 H, *CHMe*<sub>2</sub>, <sup>3</sup>J<sub>HH</sub> = 6.9 Hz). <sup>13</sup>C NMR (100 MHz, CDCl<sub>3</sub>, 293 K): 172.5

(C, HC(C(Me)NAr)<sub>2</sub>), 144.1 (C, Ar), 140.5 (C, Ar), 140.2 (C, Ar), 127.4 (CH, Ar), 125.6 (CH, Ar), 124.1 (CH, Ar), , 65.9 (CH, HC(C(Me)NAr)<sub>2</sub>), 30.4 (CH<sub>3</sub>, Nb=N<sup>t</sup>Bu, C<sub>a</sub>), 31.4 (CH, CHMe<sub>2</sub> of C=NAr), 31.0 (CH<sub>3</sub>, Nb=NH<sup>t</sup>Bu, C<sub>b</sub>), 29.7 (CH<sub>3</sub>, HC(C(Me)NAr)<sub>2</sub>), 28.9 (CH, CHMe<sub>2</sub> of C=NAr), 24.1 (CH<sub>3</sub>, CHMe<sub>2</sub> of C=NAr), 23.8 (CH<sub>3</sub>, CHMe<sub>2</sub> of C=NAr), 23.6 (CH<sub>3</sub>, CHMe<sub>2</sub> of C=NAr), 22.6 (CH<sub>3</sub>, CHMe<sub>2</sub> of C=NAr). <sup>19</sup>F NMR (470 MHz, CDCl<sub>3</sub>, 293 K): δ(ppm) -131.59, -163.14, -166.80 ([B(C<sub>6</sub>F<sub>6</sub>)<sub>4</sub>]<sup>-</sup>). Anal. Calcd for C<sub>90</sub>H<sub>100</sub>B<sub>1</sub>Cl<sub>3</sub>F<sub>20</sub>N<sub>6</sub>Nb<sub>2</sub>: C, 55.47; H, 5.17; N, 4.31. Found: C, 55.15; H, 5.45; N, 4.06.

**[(BDI<sup>#</sup>)Nb(N<sup>t</sup>Bu)(NH<sup>t</sup>Bu)] (3.5) and [(BDI)Nb(N<sup>t</sup>Bu)(NH<sup>t</sup>Bu)][B(C<sub>6</sub>F<sub>5</sub>)<sub>4</sub>] (3.6).** Complex **3.2** (170 mg, 0.08 mmol) was dissolved in 50 ml of α,α,α-trifluorotoluene, a dilute solution of <sup>t</sup>BuN<sub>3</sub> in α,α,α-trifluorotoluene (40 mg, 0.4 mmol in 5 ml of solvent) was added dropwise and the solution turned rapidly from deep green to light yellow with strong gas evolution. After being stirred at room temperature for 2 hours, the volatile material were removed under reduced pressure. The complex **3.5**, [(BDI<sup>#</sup>)Nb(N<sup>t</sup>Bu)(NH<sup>t</sup>Bu)] (with BDI<sup>#</sup> = H<sub>2</sub>C=C(NAr)CH=C(NAr)Me), was extracted and crystallized at -40 °C from toluene affording orange crystals in moderate yield (54 %). <sup>1</sup>H and <sup>13</sup>C NMR analysis are in agreement with the complex **3.5** previously reported in the literature.<sup>ref</sup> Complex **3.6**, [(BDI)Nb(N<sup>t</sup>Bu)(NH<sup>t</sup>Bu)][B(C<sub>6</sub>F<sub>5</sub>)<sub>4</sub>], was extracted and crystallized at -40 °C from dichloromethane affording colorless crystals in good yield (90 mg, 85 %). X-ray quality crystals of complex **3.6** were obtained by recrystallization from a DCM/hexane layering at room temperature. <sup>1</sup>H NMR (500 MHz, CDCl<sub>3</sub>, 293 K): 7.38 (t, 2 H, *p*-Ar, <sup>3</sup>J<sub>HH</sub> = 7.6 Hz), 7.30 (m, 4 H, *m*- and *o*-Ar), 6.17 (s, 1 H, HC(C(Me)NAr)<sub>2</sub>), 2.60 (sept, 2 H, CHMe<sub>2</sub>, <sup>3</sup>J<sub>HH</sub> = 6.6 Hz), 2.43 (sept, 2 H, CHMe<sub>2</sub>, <sup>3</sup>J<sub>HH</sub> = 6.9 Hz), 1.73 (s, 6 H, HC(C(Me)NAr)<sub>2</sub>), 1.37 (d, 6 H, CHMe<sub>2</sub>, <sup>3</sup>J<sub>HH</sub> = 6.6 Hz), 1.30 (s, 9 H, Nb=N<sup>t</sup>Bu), 1.24 (d, 6 H, CHMe<sub>2</sub>, <sup>3</sup>J<sub>HH</sub> = 6.6 Hz), 1.17 (d, 6 H, CHMe<sub>2</sub>, <sup>3</sup>J<sub>HH</sub> = 6.9 Hz), 1.09 (m, 6 H, CHMe<sub>2</sub>, <sup>3</sup>J<sub>HH</sub> = 6.9 Hz), 0.87 (s, 9 H, Nb=NH<sup>t</sup>Bu). <sup>13</sup>C NMR (100 MHz, CDCl<sub>3</sub>, 293 K): 171.5 (C, HC(C(Me)NAr)<sub>2</sub>), 142.4 (C, Ar), 140.9 (C, Ar), 140.2 (C, Ar), 129.4 (CH, Ar), 125.6 (CH, Ar), 124.6 (CH, Ar), , 65.9 (CH, HC(C(Me)NAr)<sub>2</sub>), 32.4 (CH<sub>3</sub>, Nb=N<sup>t</sup>Bu, C<sub>a</sub>), 31.9 (CH, CHMe<sub>2</sub> of C=NAr), 31.3 (CH<sub>3</sub>, Nb=NH<sup>t</sup>Bu, C<sub>b</sub>), 29.9 (CH<sub>3</sub>, HC(C(Me)NAr)<sub>2</sub>), 28.2 (CH, CHMe<sub>2</sub> of C=NAr), 24.9 (CH<sub>3</sub>, CHMe<sub>2</sub> of C=NAr), 24.7 (CH<sub>3</sub>, CHMe<sub>2</sub> of C=NAr), 24.6 (CH<sub>3</sub>, CHMe<sub>2</sub> of C=NAr), 24.6 (CH<sub>3</sub>, CHMe<sub>2</sub> of C=NAr), 15.4 (C, Nb=N<sup>t</sup>Bu, C<sub>a</sub>), 14.1 (C, Nb=NH<sup>t</sup>Bu, C<sub>a</sub>). <sup>19</sup>F NMR (470 MHz, CDCl<sub>3</sub>, 293 K): δ(ppm) -131.59, -163.14, -166.80 ([B(C<sub>6</sub>F<sub>6</sub>)<sub>4</sub>]<sup>-</sup>). Anal. Calcd for C<sub>61</sub>H<sub>60</sub>B<sub>1</sub>F<sub>20</sub>N<sub>4</sub>Nb<sub>1</sub>: C, 54.97; H, 4.54; N, 4.20. Found: C, 54.89; H, 4.55; N, 4.35.

**Cyclic Voltammetry.** Electrochemical measurements were obtained with a BASi Epsilon potentiostat at room temperature using a glassy carbon working electrode, a platinum counter electrode, and a silver wire floating reference electrode. Cyclic voltammograms were recorded in a glovebox at room temperature in α,α,α-trifluorotoluene solution containing 0.1 M [<sup>n</sup>Bu<sub>4</sub>N][BF<sub>4</sub>] as the supporting electrolyte and 0.001 M of either **1** or **2**. All potentials were referenced against a [Cp<sub>2</sub>Co]<sup>0/+</sup> internal standard, which were then standardized against both [Cp<sub>2</sub>Fe]<sup>0/+</sup> and Ag/Ag<sup>+</sup> (E<sub>1/2</sub>[Cp<sub>2</sub>Co]<sup>0/+</sup> = -1.3 V vs. [Cp<sub>2</sub>Fe]<sup>0/+</sup> and E<sub>1/2</sub>[Cp<sub>2</sub>Co]<sup>0/+</sup> = -1.3 V vs. Ag/Ag<sup>+</sup>).

**Magnetism.** Magnetic susceptibility measurements were made for complex **3.2** at 10 and 40 kOe in a 7 T Quantum Design Magnetic Properties Measurement System, that utilized a superconducting quantum interference device (SQUID). The sample was contained in sealed quartz tube.

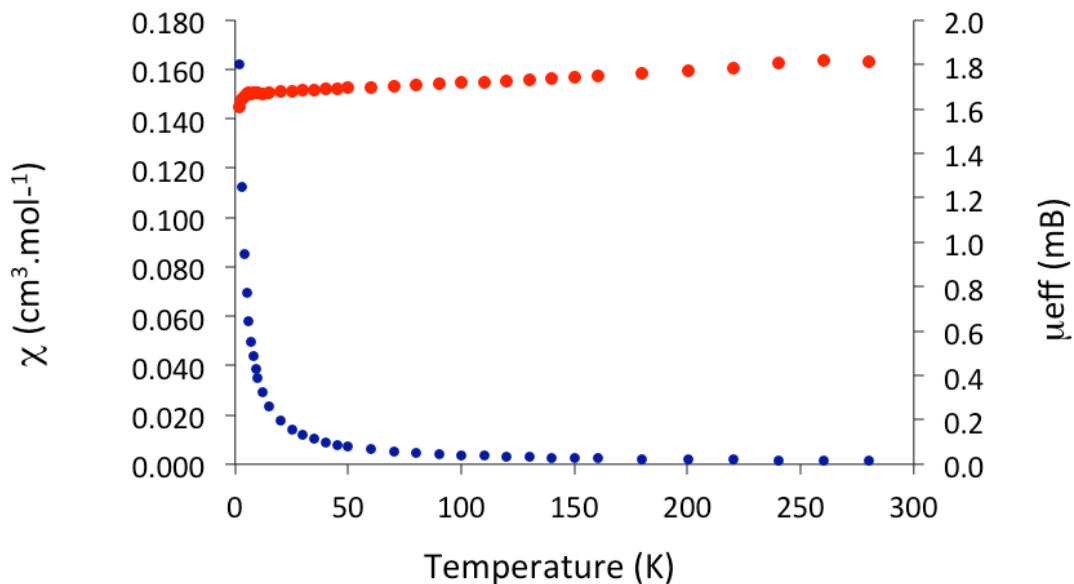


**Figure 3.12**

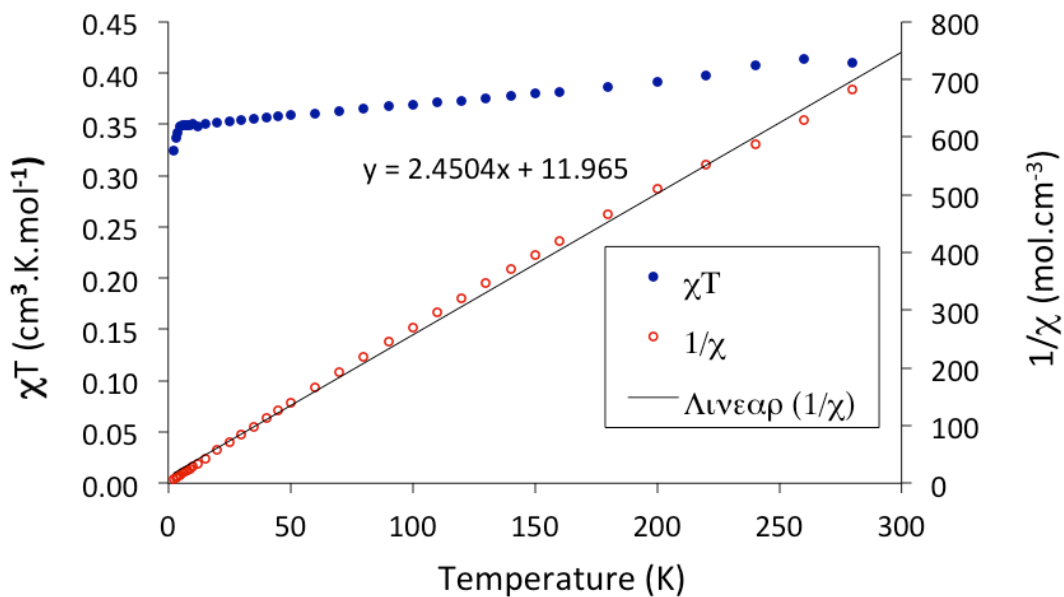


**Figure 3.13**



**EPR spectroscopy** EPR spectra were obtained with a Varian E-12 spectrometer, an EIP-547 microwave frequency counter, and a Varian E-500 gaussmeter, which was calibrated using 2,2-diphenyl-1-picrylhydrazyl (DPPH,  $g = 2.0036$ ). The simulated spectra were obtained using EasySpin.<sup>12</sup>

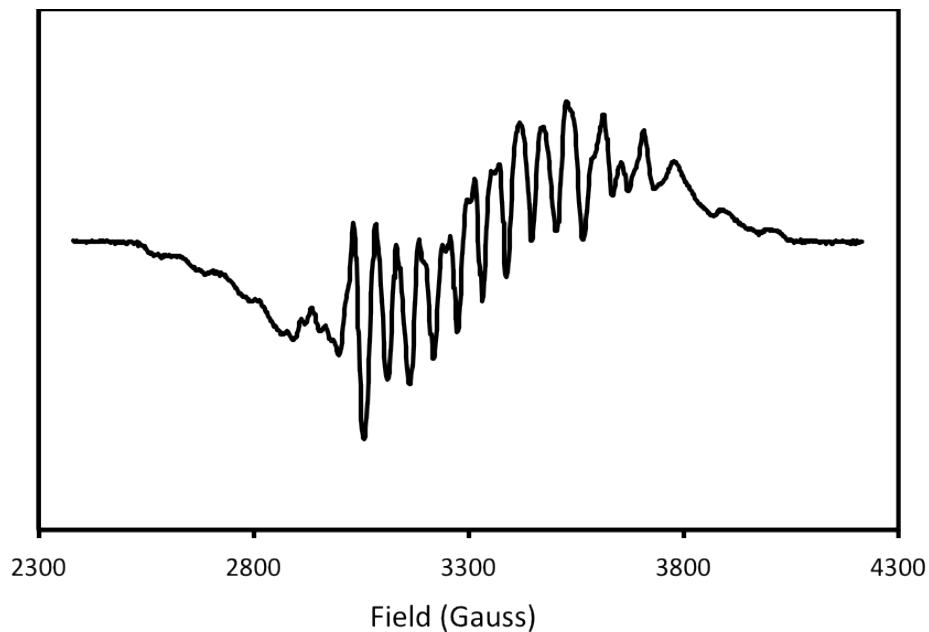


**Figure 3.14** Experimental X-Band EPR of **3.2** recorded in solid state at 300K

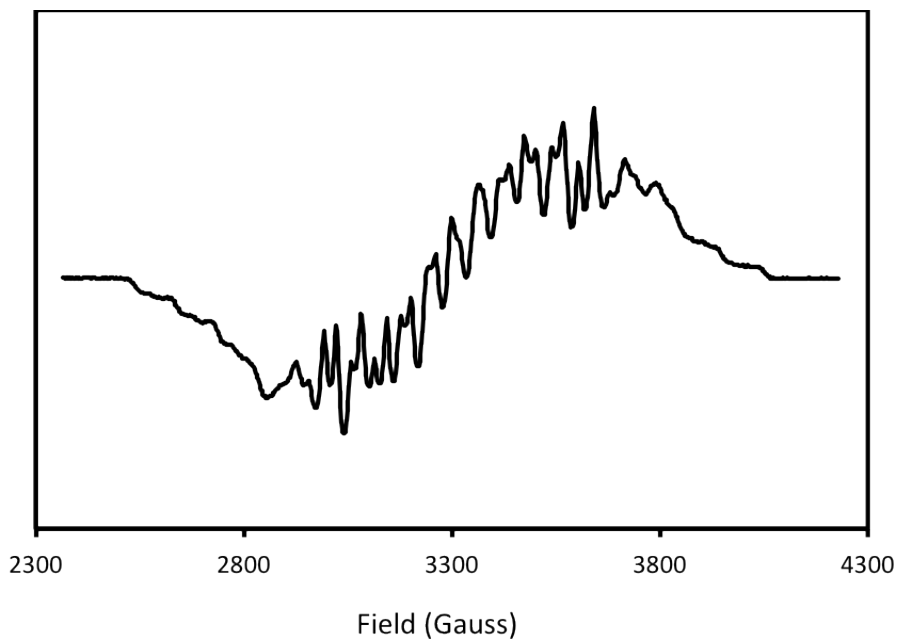


**Figure 3.15** Experimental X-Band EPR of **3.2** recorded in solid state at 4K.

**DFT Calculations.** Gradient-corrected Density Functional Theory calculations were carried out using the PBE functional,<sup>55,56</sup> as implemented in the Amsterdam Density Functional 2012.01<sup>57,58</sup> (ADF) quantum chemistry code. Scalar relativistic effects were incorporated using the Zeroth Order Regular Approximation (ZORA) Hamiltonian. A Slater Type Orbital ZORA basis set of TZP quality was used for Nb, with all other atoms being treated with a DZP ZORA basis. For geometry optimizations, the frozen core approximation was employed; Nb(3d), C(1s), N(1s). The default SCF and geometry convergence criteria were used, together with an integration grid of 4.5.

The EPR *g* matrix and hyperfine coupling constants were obtained from single point calculation using the ORCA program package<sup>59</sup>. Two hybrid functionals B3LYP<sup>60,61</sup> and PBE0 were employed. The TZVP<sup>62</sup> basis set was used for all carbon and hydrogen atoms, while a TZVPP<sup>63</sup> basis set was used for the niobium atoms and an IGLO-III basis set for the nitrogen atoms.<sup>64</sup> For all calculations increased integration grids (Grid4, ORCA convention) and tight SCF convergence were used. Scalar relativistic corrections were included in the valence space via the ZORA formalism.

**X-Ray crystallography studies.** X-ray structural determinations were performed on a Bruker SMART 1000 or SMART APEX diffractometer. Both are 3-circle diffractometers that couple a CCD detector<sup>48</sup> with a sealed-tube source of monochromated Mo K $\alpha$  radiation ( $\lambda = 0.71073$  Å). A crystal of appropriate size was coated in Paratone-N oil and mounted on a Kapton<sup>®</sup> loop. The loop was transferred to the diffractometer, centered in the beam, and cooled by a nitrogen flow low-temperature apparatus that had been previously calibrated by a thermocouple placed at the same position as the crystal. Preliminary orientation matrices and cell constants were determined by collection of 60 10 s frames, followed by spot integration and least-squares refinement. The reported cell dimensions were calculated from all reflections with  $I > 10 \sigma$ . The data were corrected for Lorentz and polarization effects; no correction for crystal decay was applied. An empirical absorption correction based on comparison of redundant and equivalent reflections was applied using SADABS.<sup>49</sup> All software used for diffraction data processing and crystal-structure solution and refinement are contained in the APEX2 program suite (Bruker AXS, Madison, WI).<sup>50</sup> Thermal parameters for all non-hydrogen atoms were refined anisotropically. For all structures,  $R_1 = \Sigma(|F_o| - |F_c|)/\Sigma(|F_o|)$ ;  $wR_2 = [\Sigma\{w(F_o^2 - F_c^2)^2\}/\Sigma\{w(F_o^2)^2\}]^{1/2}$ . Thermal ellipsoid plots were created using the ORTEP-3 software package and POV-ray.<sup>51</sup>

**Table 3.3.** Crystallographic parameters of **3.2** and **3.3**

Compound	<b>3.2-(DCE)</b>	<b>3.3</b>
Formula	C <sub>98</sub> H <sub>110</sub> B <sub>1</sub> Cl <sub>2</sub> F <sub>20</sub> N <sub>3</sub> Nb <sub>1</sub>	C <sub>65</sub> H <sub>66</sub> B <sub>1</sub> F <sub>20</sub> N <sub>3</sub> Nb <sub>1</sub> O <sub>2</sub>
Formula weight	2019.45	1404.93
Space Group	<i>P</i> 2 <sub>1</sub> / <i>c</i>	<i>P</i> 2 <sub>1</sub> / <i>c</i>
<i>a</i> (Å)	14.224(3)	18.1669(5)
<i>b</i> (Å)	21.737(3)	17.1279(5)
<i>c</i> (Å)	31.247(2)	19.7092(5)
$\alpha$ (°)	90	90
$\beta$ (°)	90.83(4)	90.5590(10)
$\gamma$ (°)	90	90
<i>V</i> (Å <sup>3</sup> )	9660.2(2)	6132.4(3)
<i>Z</i>	4	4
$\rho_{\text{calcd}}$ (g/cm <sup>3</sup> )	1.389	1.522
F <sub>000</sub>	4164	2876
$\mu$ (mm <sup>-1</sup> )	0.380	0.305
T <sub>min</sub> /T <sub>max</sub>	0.8508/0.9453	0.9140 /0.9415
No. rflns measured	79928	57885
No. indep. rflns	17729	11263
<i>R</i> <sub>int</sub>	0.0364	0.0347
No. obs. ( <i>I</i> > 2.00σ( <i>I</i> ))	17729	11263
No. variables	1228	842
<i>R</i> <sub>1</sub> , <i>wR</i> <sub>2</sub>	0.0562, 0.0929	0.0363, 0.0946
<i>R</i> <sub>1</sub> (all data)	0.0702	0.0458
GoF	1.056	1.022
Res. peak/hole (e <sup>-</sup> /Å <sup>3</sup> )	1.707/-1.093	0.774/ -0.488

**Table 3.4**

Compound	<b>3.4-(2DCE)</b>	<b>3.6</b>
Formula	C <sub>95</sub> H <sub>110</sub> B <sub>1</sub> Cl <sub>8</sub> F <sub>20</sub> N <sub>6</sub> Nb <sub>2</sub>	C <sub>61</sub> H <sub>59</sub> B <sub>1</sub> F <sub>20</sub> N <sub>3</sub> Nb <sub>1</sub>
Formula weight	2196.12	1331.84
Space Group	<i>P</i> 2 <sub>1</sub> / <i>c</i>	Pn
<i>a</i> (Å)	20.744(2)	15.2666(6)
<i>b</i> (Å)	20.888(2)	16.9177(6)
<i>c</i> (Å)	22.683(3)	25.5770(10)
$\alpha$ (°)	90	90
$\beta$ (°)	90.709(2)	97.658(2)
$\gamma$ (°)	90	90
<i>V</i> (Å <sup>3</sup> )	9827.6(19)	6547.0(4)
<i>Z</i>	4	4
$\rho_{\text{calcd}}$ (g/cm <sup>3</sup> )	1.484	1.351
<i>F</i> <sub>000</sub>	4500	2716
$\mu$ (mm <sup>-1</sup> )	0.537	0.280
<i>T</i> <sub>min</sub> / <i>T</i> <sub>max</sub>	0.8993/0.9892	0.9592 /0.9834
No. rflns measured	157286	66108
No. indep. rflns	17992	23491
<i>R</i> <sub>int</sub>	0.0251	0.0483
No. obs. ( <i>I</i> > 2.00σ( <i>I</i> ))	17992	23491
No. variables	1234	1599
<i>R</i> <sub>1</sub> , <i>wR</i> <sub>2</sub>	0.0257, 0.0621	0.0418, 0.0847
<i>R</i> <sub>1</sub> (all data)	0.0288	0.0559
GoF	1.058	1.016
Res. peak/hole (e <sup>-</sup> /Å <sup>3</sup> )	1.768/-0.665	0.436/ -0.480

## References

- (1) Wilkinson, G., Rosenblum, M., Whiting, M. C., Woodward, R. B. *J. Am. Chem.* **74**, 2225-2226 (1952).
- (2) Astruc, D. *Electron Transfer and Radical Processes in Transition Metal Chemistry*. (VCH Publishers, Inc., 1995).
- (3) Muetterties, E. L., Bleeke, J. R., Wucherer, E. J., Albright, T. *Chem. Rev.* **82**, 499-525 (1982).
- (4) Astruc, D. *Modern Arene Chemistry*. (Willey, 2002).
- (5) Duff, A. W., Jonas, K., Goddard, R., Kraus, H. J. & Kruger, C. *J. Am. Chem.* **105**, 5479-5480 (1983).
- (6) Diaconescu, P. L., Arnold, P. L., Baker, T. A., Mindiola, D. J., Cummins, C. C. *J. Am. Chem.* **122**, 6108-6109 (2000).
- (7) Zabula, A. V., Filatov, A. S., Spisak, S. N., Rogachev, A. Y., Petrukhina, M. A. *Science* **333**, 1008-1011 (2011).
- (8) Robin, M. B. & Day, P. in *Advances in Inorganic Chemistry and Radiochemistry* Vol. Volume 10 (eds H. J. Emeléus & A. G. Sharpe) 247-422 (Academic Press, 1968).
- (9) Creutz, C., Taube, H. *J. Am. Chem. Soc.* **91**, 3988-3989 (1969).
- (10) Taube, H. *Angew. Chem. Int. Ed.* **23**, 329-339 (1984).
- (11) Creutz, C., Ford, P. C., Meyer, T. J. *Inorg. Chem.* **45**, 7059-7068 (2006).
- (12) Demadis, K. D., Hartshorn, C. M., Meyer, T. J. *Chem. Rev.* **101**, 2655-2686 (2001).
- (13) Day, P., Hush, N. S., Clark, R. J. H. *Philos. Trans. Roy. Soc. London Ser. A* **366**, 5-14 (2008).
- (14) Zhang, L. T., Ko, J., Ondrechen, M. *J. Am. Chem. Soc.* **109**, 1666-1671 (1987).
- (15) Kaim, W., Klein, A., Glockle, M. *Acc. chem. res.* **33**, 755-763 (2000).
- (16) Reimers, J. R., Wallace, B. B., Hush, N. S. *Philos. Trans. Roy. Soc. London Ser. A* **366**, 15-31 (2008).
- (17) Bechlars, B. *et al. Nat Chem* **2**, 362-368 (2010).
- (18) Diaconescu, P. L., Cummins, C. C. *Inorg. Chem.* **51**, 2902-2916 (2012).
- (19) Camp, C., Mougél, V., Pécaut, J., Maron, L., Mazzanti, M. *Chem. Eur. J.* **19**, 17528-17540 (2013).
- (20) Nikiforov, G. B., Crewdson, P., Gambarotta, S., Korobkov, I., Budzelaar, P. H. M. *Organometallics* **26**, 48-55 (2006).
- (21) Arnold, P. L., Mansell, S. M., Maron, L., McKay, D. *Nat Chem* **4**, 668-674 (2012).
- (22) Gianetti, T. L. *et al. J. Am. Chem. Soc.* **135**, 3224-3236 (2013).
- (23) Basuli, F., Kilgore, U. J., Brown, D., Huffman, J. C., Mindiola, D. J. *Organometallics* **23**, 6166-6175 (2004).
- (24) Vollmerhaus, R. *et al. Organometallics* **19**, 2161-2169 (2000).
- (25) Rahim, M., Taylor, N. J., Xin, S., Collins, *Organometallics* **17**, 1315-1323 (1998).
- (26) Kakaliou, L. *et al.* Five- and Six-Coordinate Group 4 Compounds Stabilized by  $\beta$ -Ketiminato and Diketiminato Ligands: Syntheses and Comparisons between Solid-State and Solution Structures. *Inorg. Chem.* **38**, 5964-5977 (1999).
- (27) Bonnet, F., Visseaux, M., Barbier-Baudry, D., Vigier, E., Kubicki, M. M. *Chem. Eur. J.* **10**, 2428-2434 (2004).
- (28) Antinolo, A. *et al. J. Chem. Soc., Dalton Tran.s.*, 975-980 (1987).
- (29) Schwarzhaus, K. E. *Angew. Chem. Int. Ed.* **9**, 946-953 (1970).

- (30) La Mar, G. N., Horrocks, W. D., Holm, R. H. *NMR of Paramagnetic Molecules: Principles and Applications*. (Elsevier Inc., 1973).
- (31) D'Alessandr, D. M., Keene, F. R. *Chem. Rev.* **106**, 2270-2298 (2006).
- (32) Bach, D., Schneider, R., Gerthsen, D., Verbeeck, J., Sigle, W. *Microsc. Microanal.* **15**, 505-523 (2009).
- (33) Pearson, D. H., Ahn, C. C., Fultz, B. *Phys. Rev. B* **47**, 8471-8478 (1993).
- (34) Vlasisavljevich, B., Diaconescu, P. L., Lukens, W. L., Gagliardi, L., Cummins, C. C. *Organometallics* **32**, 1341-1352 (2013).
- (35) Kosog, B., La Pierre, H. S., Denecke, M. A., Heinemann, F. W., Meyer, K. *Inorg. Chem.* **51**, 7940-7944 (2012).
- (36) Ziegler, T., Rauk, A. *Inorg. Chem.* **18**, 1558-1565 (1979).
- (37) Tomson, N. C., Arnold, J., Bergman, R. G. *Organometallics* **29**, 2926-2942 (2010).
- (38) Tomson, N. C., Arnold, J., Bergman, R. G. *Organometallics* **29**, 5010-5025 (2010).
- (39) Tomson, N. C., Arnold, J., Bergman, R. G. *Dalton Trans.* **40**, 7718-7729 (2011).
- (40) Krol, M. C. *et al. Nature* **421**, 131-135 (2003).
- (41) Yamazaki, S., Ichikawa, K., Saeki, A., Tanimura, T., Adachi, K. *J. Phys. Chem. A* **114**, 5092-5098 (2010).
- (42) Huang, B., Lsse, A. A., Durante, C., Wei, C., Gennaro, A. *Electrochimica Acta* **70**, 50-61(2012).
- (43) Li, T., Chen, Y., Wan, P., Fan, M., Yang, X. J. *J. Am. Chem. Soc.* **132**, 2500-2510 (2010).
- (44) Heinrichs, B., Delhez, P., Schoebrechts, J. P., Pirard, J. P. in *Preparation of Catalysts VII* Vol. 118 *Studies in Surface Science and Catalysis* (eds B. Delmon *et al.*) 707-716 (1998).
- (45) Holliger, C., Kengen, S. W. M., Schraa, G., Stams, A. J. M., Zehnder, A. J. B. *J. Bacteriol.* **174**, 4435-4443 (1992).
- (46) Coleman, N. V., Mattes, T. E., Gossett, J. M., Spain, J. C. *Appl. Environ. Microbiol.* **68**, 2726-2730 (2002).
- (47) Ohrai, K., Kondo, K., Sodeoka, M., Shibasaki, M. *J. Am. Chem. Soc.* **116**, 11737-11748 (1994).
- (48) Grushin, V. V. *Organometallics* **19**, 1888-1900 (2000).
- (49) McCrindle, R. *et al. Organometallics* **14**, 2741-2748 (1995).
- (50) Obenhuber, A. H., Gianetti, T. L., Berrebi, X., Bergman, R. G., Arnold, J. *J. Am. Chem. Soc.* **136**, 2994-2997 (2014).
- (51) Alaimo, P. J., Peters, D. W., Arnold, J., Bergman, R. G. *J. Chem. Educ.* **78**, 64-64 (2001).
- (52) Feldman, J. *et al. Organometallics* **16**, 1514-1516 (1997).
- (53) M. Budzelaar, P. H., van Oort, A. B., Orpen, A. G. *Eur. J. Inorg. Chem.* **1998**, 1485-1494 (1998)
- (54) Tomson, N. C., Yan, A., Arnold, J., Bergman, R. G. *J. Am. Chem. Soc.* **130**, 11262-11263 (2008).
- (55) Perdew, J. P., Burke, K. & Ernzerhof, M. Generalized Gradient Approximation Made Simple *Phys. Rev. Lett.* **78**, 1396-1396 (1997).
- (56) Fonseca Guerra, C., Snijders, J. G., te Velde, G., Baerends, E. J. *Theor Chem Acc* **99**, 391-403 (1998).
- (58) Velde, G. *et al. J. Comput. Chem.* **22**, 931-967 (2001).
- (59) ORCA - an ab initio, Density Functional and Semiempirical program package v. Version 2.4. (Mülheim and der Ruhr, 2004).
- (60) Becke, A. D. *J. Chem. Physics* **98**, 5648-5652 (1993).

- (61) Lee, C., Yang, W., Parr, R. G. *Phys. Rev. B* **37**, 785-789 (1988).
- (62) Schafer, A., Huber, C., Ahlrichs, R. *J. Chem. Phys.* **100**, 5829-5835 (1994).
- (63) Krishnan, R., Binkley, J. S., Seeger, R., Pople, J. A. *J. Chem. Phys.* **72**, 650-654, doi:10.1063/1.438955 (1980).
- (64) Kutzelnigg, W., Fleischer, U., Schindler, M. *In The IGLO Method: Ab Initio Calculation and Interpretation of NMR Chemical Shifts and Magnetic Susceptibilities*. Vol. 23 (Springer-Verlag, 1990).

## **Chapter IV**

### **Dis-assembly of a Benzylic CF<sub>3</sub> Group Mediated by a Niobium (III) Imido Complex**



## Introduction

The thermodynamic stability of C-F bonds (BDE = [110-130] kcal.mol<sup>-1</sup>), combined with their inherent kinetic inertness, has allowed for many technical applications of fluorocarbons such as the synthesis of resistant polymers and their use in medicinal chemistry.<sup>1-3</sup> However, such strong bonding is also troublesome given that these chemically inert compounds are persistent in the environment.<sup>4,5</sup> Therefore, in recent years, synthetic methods for the activation and functionalization of C-F bonds have attracted growing attention.<sup>1,2,5-16</sup> With the increasing degree of fluorination at carbon, the strength of the C-F bond increases and the C-F bond lengths decrease, resulting in substantial steric shielding of the carbon site.<sup>2</sup> Due to this increased stability, fluorine abstraction from a CF<sub>3</sub> moiety is difficult and rare.<sup>6,9,11,17-20</sup>

An even more challenging transformation is the functionalization of CF<sub>3</sub> groups via triple C-F activation. Recently, significant progress has been made toward reduction of the CF<sub>3</sub> group, leading to hydrodefluorination<sup>16,21-24</sup> and C-C coupling.<sup>21,25</sup> Interestingly, Ar-CF<sub>3</sub> reduction has been achieved with low-valent niobium Nb(0) generated in-situ from NbCl<sub>5</sub>.<sup>19</sup> However, to our knowledge a reaction in which all three fluorine atoms of an organic CF<sub>3</sub> group, as well as the carbon fragment initially bound to them, are directly transferred to a single metal center has not been reported.

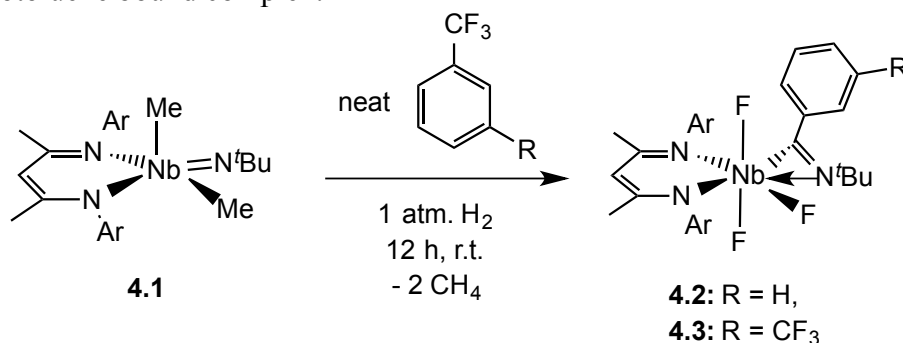
In our effort to develop new semi-hydrogenation catalysts,<sup>26</sup> we reported in chapter I, the efficiency of a trivalent niobium complex toward selective semi-hydrogenation of alkynes.<sup>27</sup> The active catalyst in the mechanism – a transient trivalent tricoordinated “[BDI]Nb=N<sup>*t*</sup>Bu” (BDI = 2,6-diisopropylbenzene-β-diketiminato) – was trapped as a η<sup>6</sup>-bound arene in the absence of CO. We then showed, in chapter II, that this η<sup>6</sup>-bound arene complex can be formed via hydrogenolysis of the dimethyl niobium *t*-Bu imido diketiminato complex ([BDI]Nb(N<sup>*t*</sup>BuN)(CH<sub>3</sub>)<sub>2</sub>) (**4.1**) in neat benzene or toluene.<sup>28</sup> These mono η<sup>6</sup>-bound arene species were found to undergo two-electron reduction chemistry, as well as to form the corresponding bimetallic bridging arene complexes via a dissociative mechanism.<sup>28</sup>

In order to further probe the electronic behavior of these mono- and bimetallic arene complexes, hydrogenolysis of complex **4.1** was studied in fluorinated solvents. This led unexpectedly to a new type of functionalization of a CF<sub>3</sub> group in which all three fluorines are transferred to the Nb center and a new carbon-nitrogen bond is formed between the remaining organic fragment and the *t*-butylimido ligand.

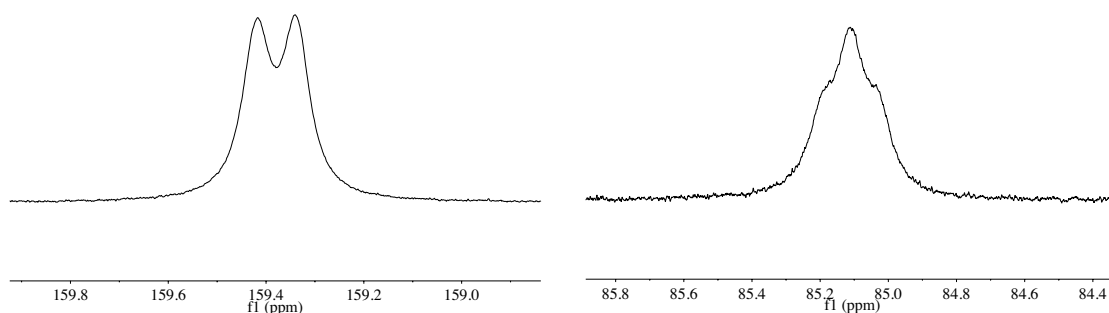
## Results and discussions

**Synthesis.** Hydrogenolysis of **4.1** in neat α,α,α-trifluoromethyl arenes proceeds as shown in Scheme 4.1. As previously observed with benzene and toluene as solvent, the solution quickly changed color from pale yellow to deep red upon H<sub>2</sub> addition at room temperature; after a few hours, the solution lightened to an orange-brown color. Evaporation of the solvent under reduced pressure, followed by extraction and crystallization from Et<sub>2</sub>O, afforded orange blocks of complex **4.2** in good yield (87%). Surprisingly, the <sup>1</sup>H NMR spectrum of **4.2** in d<sub>12</sub>-mesitylene did not show the characteristic resonances of a mono- or bimetallic arene bound complex expected in the 4-2 ppm range. Additionally, <sup>19</sup>F NMR analysis revealed two broad downfield resonances in a 2 : 1 ratio (+162.4 and +92.2 ppm respectively). Lowering the temperature to 243 K led to a sharpening of the two resonances, allowing a better resolution

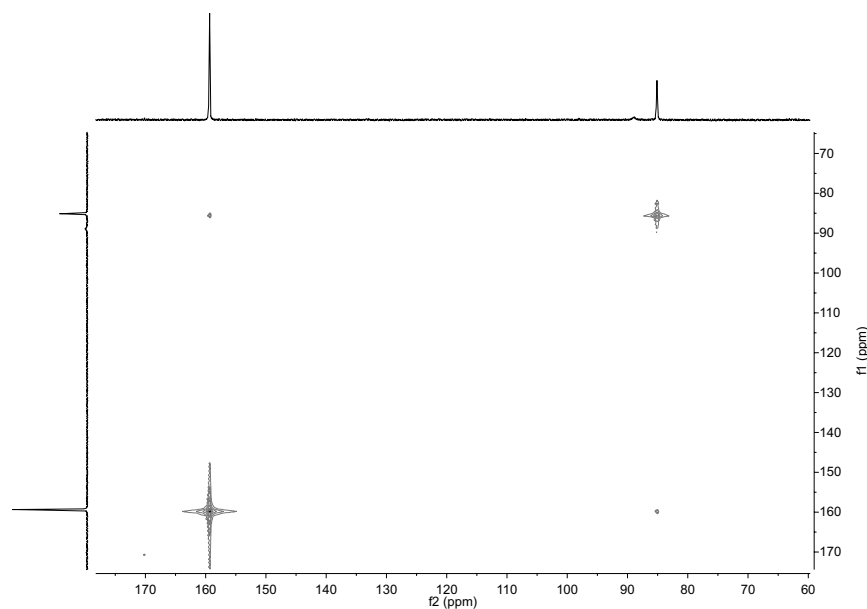
from which a doublet at 159.4 ppm ( $^2J_{F-F} = 45(2)$  Hz) and a poorly resolved triplet at 85.1 ppm ( $^2J_{F-F} = 48(5)$  Hz) were observed (Figure 4.1). Despite the fast relaxation time of these  $^{19}\text{F}$  resonances ( $T_1 = [0.8 - 1.1]$  ms),  $^{19}\text{F}$ - $^{19}\text{F}$  NOESY data obtained at both room- and low-temperature, showed correlation between the two sets of resonances (Figure 4.2). These data strongly indicated the formation of a niobium trifluoride complex rather than an  $\alpha,\alpha,\alpha$ -trifluorotoluene bound complex.



**Scheme 4.1** Hydrogenolysis of complex **4.1** in fluorinated arene solvent.



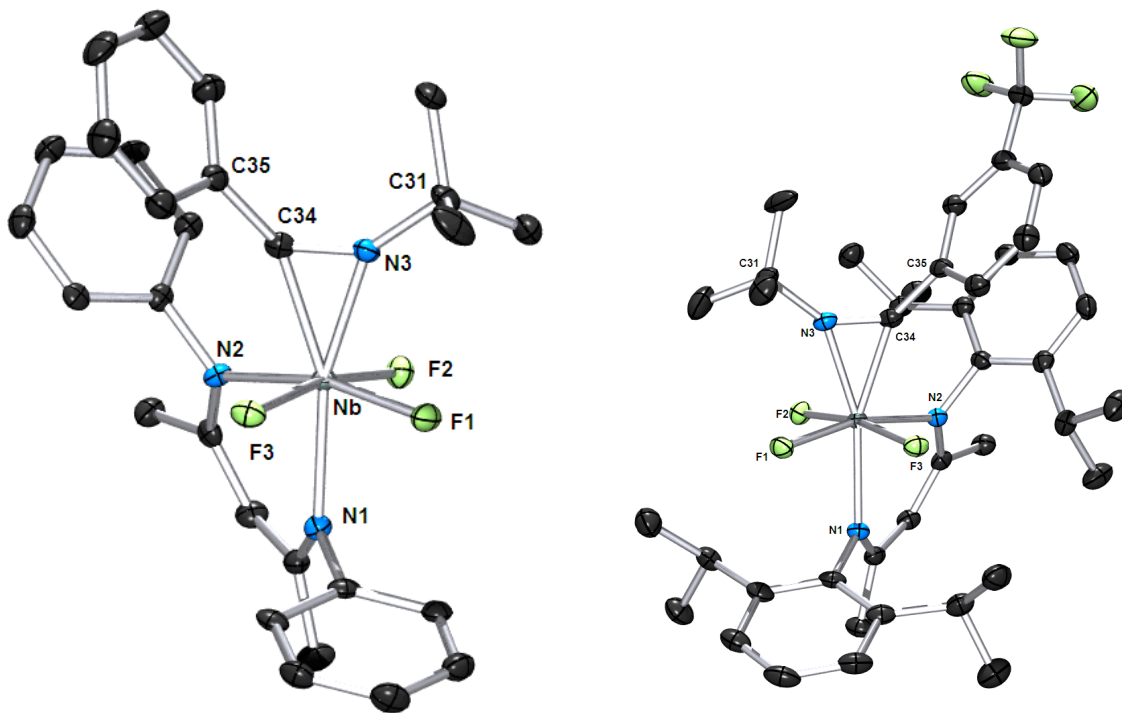
**Figure 4.1**  $^{19}\text{F}$  NMR spectra of **4.2** at 243 K



**Figure 4.2**  $^{19}\text{F}$ - $^{19}\text{F}$  ESXY of complex **4.2** at 243 K.

Crystallographic analysis of **4.2** confirmed the above conclusion, revealing the presence of a bisdiketiminato niobium trifluoride bearing a  $\eta^2$ -bound imine ( $[\text{BDI}]\text{NbF}_3(\text{BuN}=\text{CC}_6\text{H}_5)$ ) in a distorted capped octahedral geometry, with the three fluorines in the basal plane (Figure 4.3). The two *trans* fluorines show similar Nb-F distances (ave. 1.9095(16) Å); the remaining fluorine is *trans* to a nitrogen in the BDI ligand, resulting in a slightly longer Nb-F distance (1.9386(16) Å). One of the apical positions is occupied by the moiety formed from coupling between the imido group and the benzylic carbon of the  $\text{PhCF}_3$ . The C(34)-N(1) bond distance of 1.261(4) Å suggests the presence of a C=N bond, and therefore an imine fragment. The niobium-carbon and niobium-nitrogen bond distances to the imine moiety (Nb-C(34) = 2.170(3) Å and Nb-N(3) = 2.080(3) Å) are within the range of Nb-C<sub>alkyl</sub> and Nb-N<sub>donor</sub> previously observed,<sup>29,30</sup> and are consistent with the view shown in Scheme 1. The large angles observed within the imine moiety (C(35)-C(34)-N(3) = 131.1(3)° and C(34)-N(3)-C(31) = 137.5(3)°) imply  $sp^2$  hybridization of both C(1) and N(3), further supporting the above description.

Conducting a similar experiment using 1,3-bis(trifluoromethyl)benzene afforded dark yellow crystals of **4.3** in very good yield (91%, Scheme 4.1). Both the NMR and X-ray diffraction analyses were analogous to those of complex **4.2** and showed the formation of  $(\text{BDI})\text{NbF}_3(\text{BuN}=\text{CC}_6\text{H}_4\text{CF}_3)$  (Figure 4.3). The  $^{19}\text{F}$  resonance of the remaining  $\text{CF}_3$  group was found as a sharp singlet at - 61.6 ppm. This result provides a second example of selective disassembly of one  $\text{CF}_3$  moiety and supports an intramolecular activation mode.

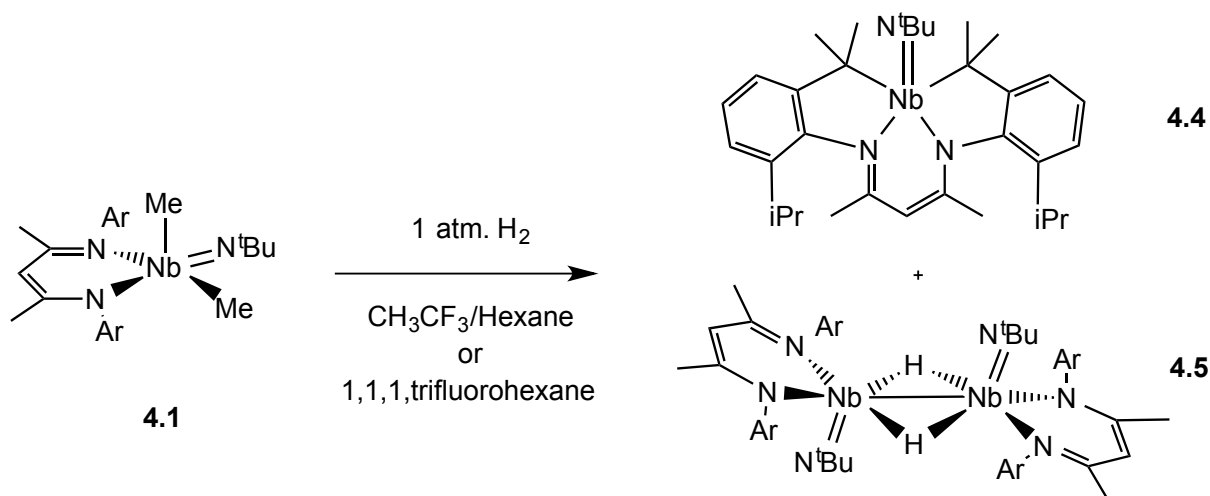


**Figure 4.3** ORTEP diagram of complex **4.2** (left) and **4.3** (right). Hydrogens and *iPr* groups have been removed for clarity. Selected bond distances and angles are presented in Table 4.1.

**Table 4.1** Selected bond distances (Å) and angles (°) for complexes **4.2** and **4.3**

	Compound <b>4.2</b>	Compound <b>4.3</b>
Nb-N <sub>1</sub> (BDI)	2.246(2)	2.2334(14)
Nb-N <sub>2</sub> (BDI)	2.184(2)	2.1880(14)
Nb-N <sub>3</sub> (Imine)	2.080(2)	2.0919(14)
Nb-C <sub>34</sub> (Imine)	2.170(3)	2.1523(17)
Nb-F <sub>1</sub>	1.9386(16)	1.9319(10)
Nb-F <sub>2</sub>	1.9073(16)	1.9004(10)
Nb-F <sub>3</sub>	1.9118(16)	1.9214(10)
C <sub>34</sub> -N <sub>3</sub> (Imine)	1.261(4)	1.261(2)
C <sub>34</sub> -N <sub>3</sub> -C <sub>31</sub>	137.5(3)	136.08(15)
C <sub>35</sub> -C <sub>34</sub> -N <sub>3</sub>	131.1(3)	132.74(16)

Attempts to extend this transformation to non-aromatic CF<sub>3</sub> groups were made by performing the hydrogenolysis of **4.1** in neat 1,1,1-trifluoro-n-hexane or CH<sub>3</sub>CF<sub>3</sub> dissolved in n-hexane. However, the reactivity observed was completely different from that seen with the aromatic CF<sub>3</sub> groups and led to the isolation of two products (Scheme 4.2). Upon H<sub>2</sub> addition, the solution of **4.1** quickly turned red, with the formation of a purple precipitate. After 12 h, evaporation of the solvent under reduced pressure deposited a purple/red powder. The red material was extracted and crystallized from hexane, which afford red crystals of complex **4.4** in 62% yield. The remaining purple powder was extracted with and crystallized from THF, forming dark purple crystals of complex **4.5** in low yield (21%). A control experiment, in which hydrogenolysis of complex **4.1** was performed in hexane alone, afforded the same product distribution. ORTEP views of **4.4** and **4.5** are presented in Figure 4.4.

**Scheme 4.2** Hydrogenolysis of complex **4.1** in fluorinated but non-aromatic solvents.

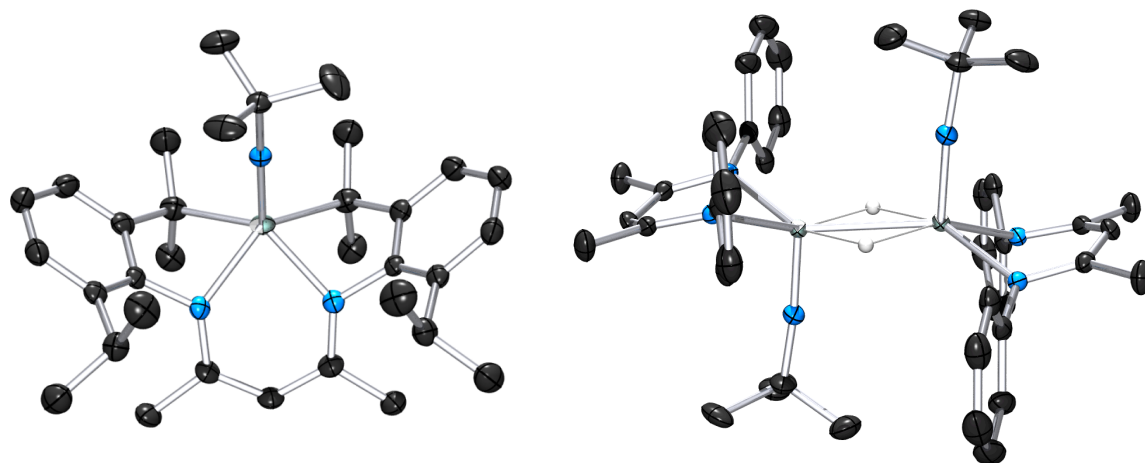


**Figure 4.4** ORTEP diagrams of complexes **4.4** (left) and **4.5** (right). Hydrogens have been removed for clarity in both complexes as well as the *i*-Pr groups in **4.5**. Selected bond distances and angles are presented in Table 4.2.

**Table 4.2** Selected bond distances (Å) for complexes **4.4** and **4.5**

	Compound <b>4.3</b>	Compound <b>4.4</b>
Nb=N <sub>3</sub> <sup>t</sup> Bu	1.7652(18)	1.763(2)
Nb-N <sub>1</sub> (BDI)	2.139(2)	2.2399(13)
Nb-N <sub>2</sub> (BDI)	2.1406(19)	2.2399(13)
Nb <sub>1</sub> -Nb <sub>2</sub>	-	2.7846(4)
Nb <sub>1</sub> -H <sub>1</sub>	-	1.92(2)
Nb-C <sub>15</sub>	2.261(3)	-
Nb-C <sub>27</sub>	2.258(3)	-

Complex **4.4** exhibits a pseudo square-pyramidal geometry in which the BDI group has been transformed into a  $\kappa_4$ -CNNC-ligand via activation of the two isopropyl-methines. The Nb-C bond distances are on average 2.260(3) Å, which is within the range of previously reported Nb(V)-C bonds.<sup>29</sup> Complex **4.5**, on the other hand, was found to be a diamagnetic dihydride bridge complex, with the hydride resonance observed as a broad singlet at - 1.35 ppm in the <sup>1</sup>H NMR spectrum. The hydrides, located in the Fourier difference map and refined isotropically, display a Nb-H distance of 1.92(2) Å. The dimer possesses a center of inversion about a central {Nb<sub>2</sub>(μ-H)<sub>2</sub>} core. The short Nb(1)-Nb(2) distance of 2.7846(4) Å supports metal-metal bonding, and accounts for the observed diamagnetism of **4.5**.<sup>31</sup>

**Mechanistic study.** The reactivity observed in non-aromatic solvent suggests: (i) only benzylic CF<sub>3</sub> groups are activated by this system, (ii) arene coordination to a niobium metal may be a key requirement for C-F activation, (iii) high valent niobium hydrides may be involved as intermediates during the hydrogenolysis. In order to investigate the above hypotheses, hydrogenolysis of **4.1** in the presence and absence of PhCF<sub>3</sub> was followed by <sup>1</sup>H and <sup>19</sup>F NMR spectroscopies. Since both benzene and toluene are known to strongly compete in arene coordination,<sup>28</sup> and the use of neat PhCF<sub>3</sub> could interfere with observation of intermediates, sterically hindered d<sub>12</sub>-mesitylene was used as an NMR solvent.

First, hydrogenolysis of **4.1** alone resulted in the fast formation of **4.4** and **4.5** implying that despite its aromatic character, d<sub>12</sub>-mesitylene is too poor a p-acid ligand to form a persistent arene-bound complex. Following the reaction by <sup>1</sup>H NMR spectroscopy showed the rapid formation and disappearance of an intermediate complex **4.A**, for which a broad resonance at 9.2 ppm is consistent with the presence of a Nb-H bond and (Figure 4.3).<sup>32</sup>

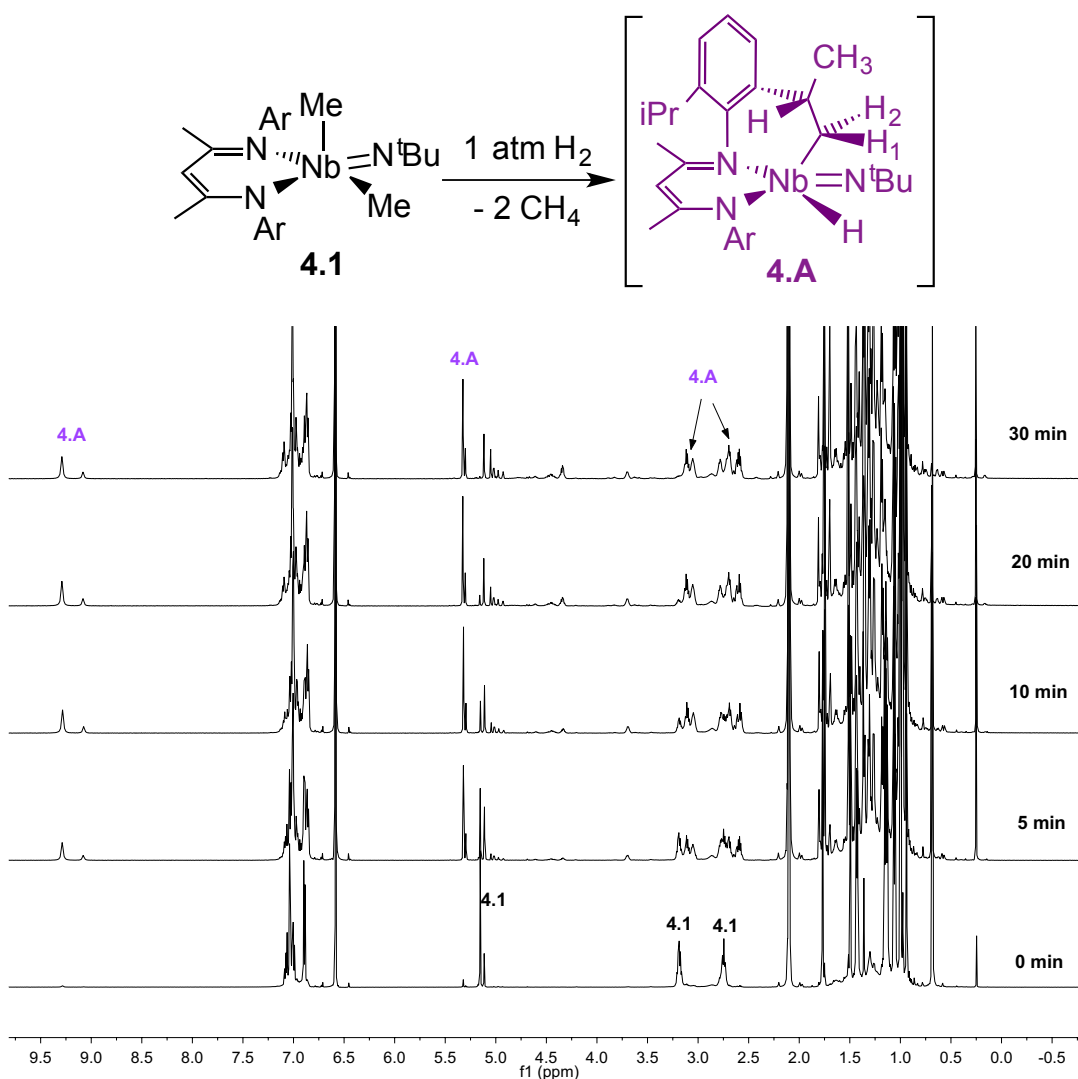


**Figure 4.5** Formation of complexes **4.A** with time. Spectra recorded at 243 K.

In order to gain further structural insight, soon after H<sub>2</sub> addition the sample was placed in a spectrometer cooled to 243 K. The persistence of **4.A** at low temperature allowed for characterization by NMR (Figure 4.6). A DEPT 135 experiment showed the presence of one CH<sub>2</sub> group, consistent with the formation of a metallacyclic niobium hydride (complex **4.A**, Scheme 4.3).<sup>32</sup> The CH<sub>2</sub> carbon was found to bear two inequivalent protons by HSQC (Figure 4.6, top). Additionally, a COSY experiment showed that one of the methylene protons (H<sub>1</sub>) is not correlated to the isopropyl methine (CH<sub>iPr</sub>), while the other methylene (H<sub>2</sub>) is (Figure 4.6, bottom left). Finally, the NOESY spectrum revealed that the methine (CH<sub>iPr</sub>) is strongly correlated to (H<sub>1</sub>) and the CH<sub>3</sub>, but only weakly to (H<sub>2</sub>) (Figure 4.6, bottom right). These 2D experiments further support the assignment of **4.A** and also confirm its stereochemistry, in which the hydride and methine are *cis* to one another. When performed under an atmosphere of D<sub>2</sub>, the hydrogenolysis of **4.1** in hexane formed **4.4** and **4.5** in which deuterium incorporation was observed at all positions of the isopropyl group. Such scrambling suggests a fast equilibrium between **4.A** and the transient “[BDI]Nb=NtBu” **4.B** (Scheme 4.3) and/or successive s-bond metathesis of **4.A**.

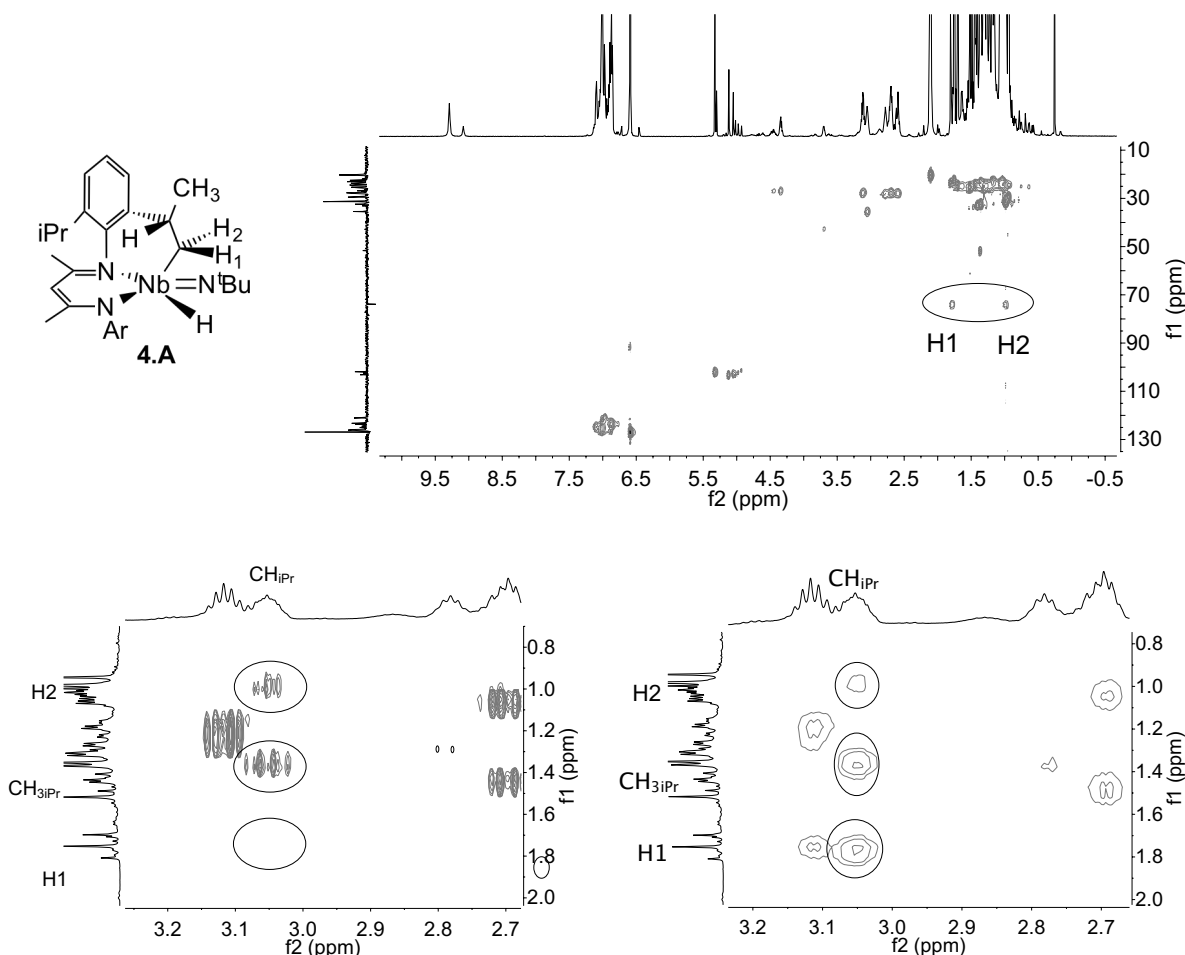


**Figure 4.6** HSQC-<sup>135</sup>DEPT (top), <sup>1</sup>H-<sup>1</sup>H COSY (bottom, left) and <sup>1</sup>H-<sup>1</sup>H NOESY (bottom, right) spectra of complex **4.A** recorded at 243 K.

A similar experiment was then performed in the presence of 10 equivalents of PhCF<sub>3</sub> where the same hydride intermediate **4.A** was observed at low conversion, along with a new complex **4.C** (Figure 4.7). After 10 min at room temperature, a significant amount of **4.C** was formed; cooling the sample to 243 K allowed us to perform its complete NMR characterization (Figure 4.8). The structure of **4.C** is consistent with a PhCF<sub>3</sub> η<sup>6</sup>-bound complex in which the arene protons resonate between 4 and 3 ppm in a 2:3 ratio. Meanwhile, a new singlet in the <sup>19</sup>F NMR appears at δ = -62.4 ppm, slightly upfield from free PhCF<sub>3</sub> (d = -61.4 ppm, Figure 4.7 right). When the solution was allowed to warm to 273 K, **4.C** was quickly converted to the final product **4.2** (Figure 4.9). Additionally, formation of **4.2** and the intermediate **4.C** were observed when the trivalent niobium complex **4.6** was stirred at room temperature in C<sub>9</sub>D<sub>12</sub> with 10 eq of α,α,α-trifluorotoluene (Scheme 4.3, bottom).

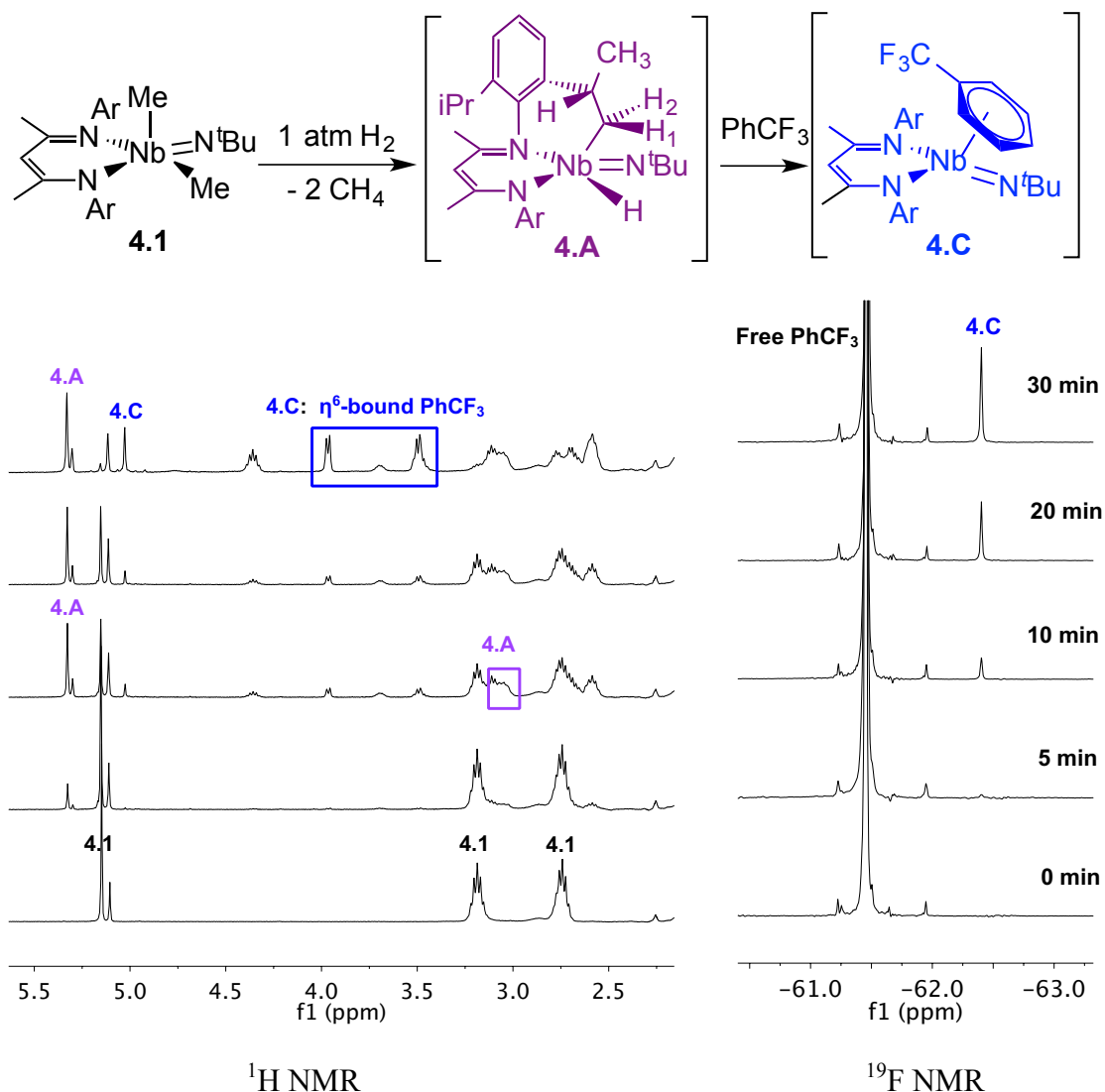


**Figure 4.7** Formation of complex **4.C** with time. <sup>1</sup>H NMR (left) and <sup>19</sup>F NMR (right) spectra recorded at 243 K but NMR sample was warmed and kept at r.t. between acquisition.



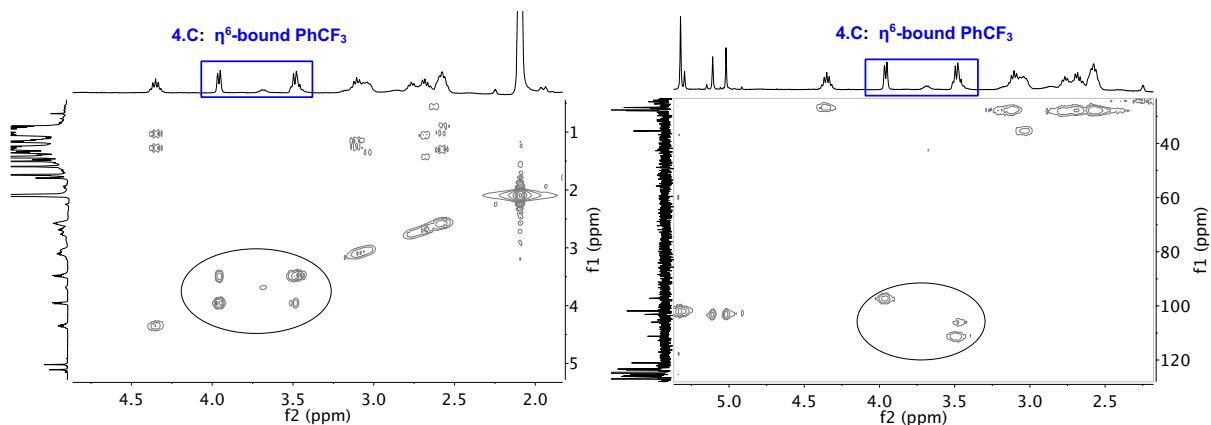


**Figure 4.8** HSCQ-DEPT (top) and  $^1\text{H}$ - $^1\text{H}$  COSY (bottom, left) spectra of complex **4.C** recorded at 243 K.

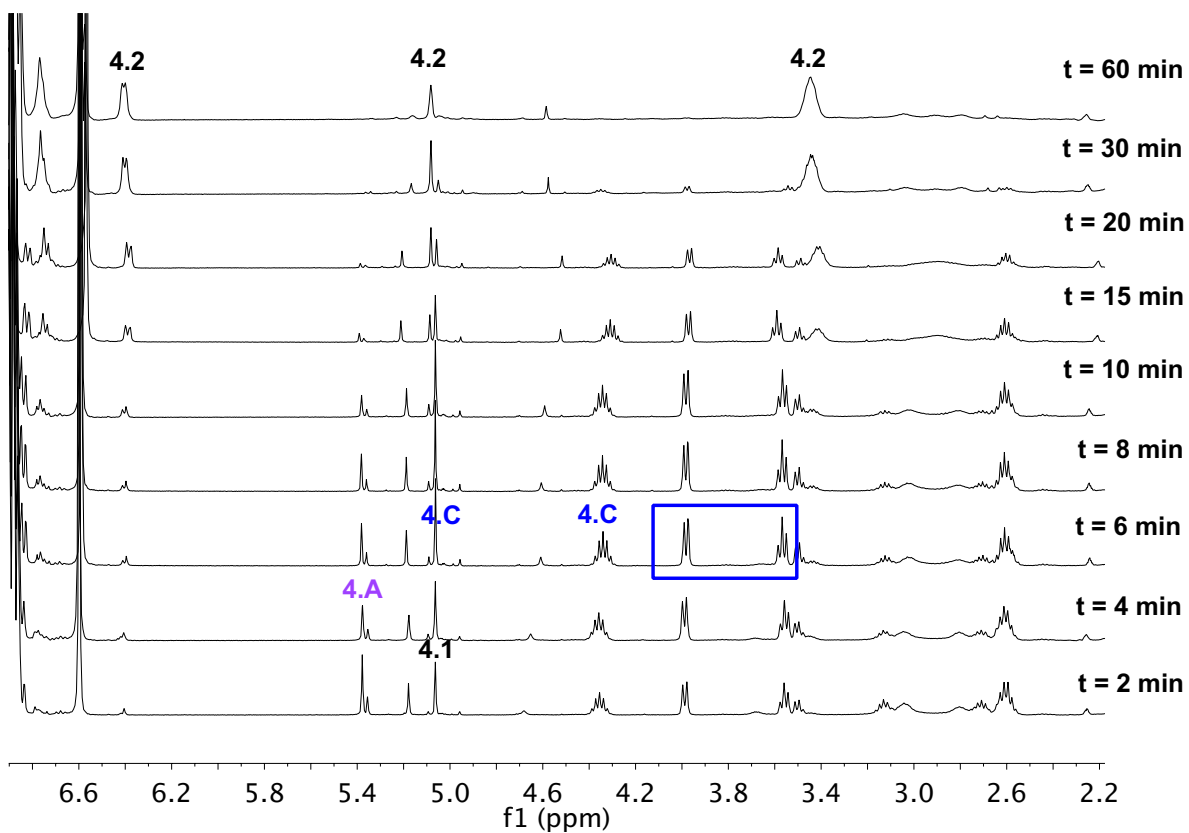
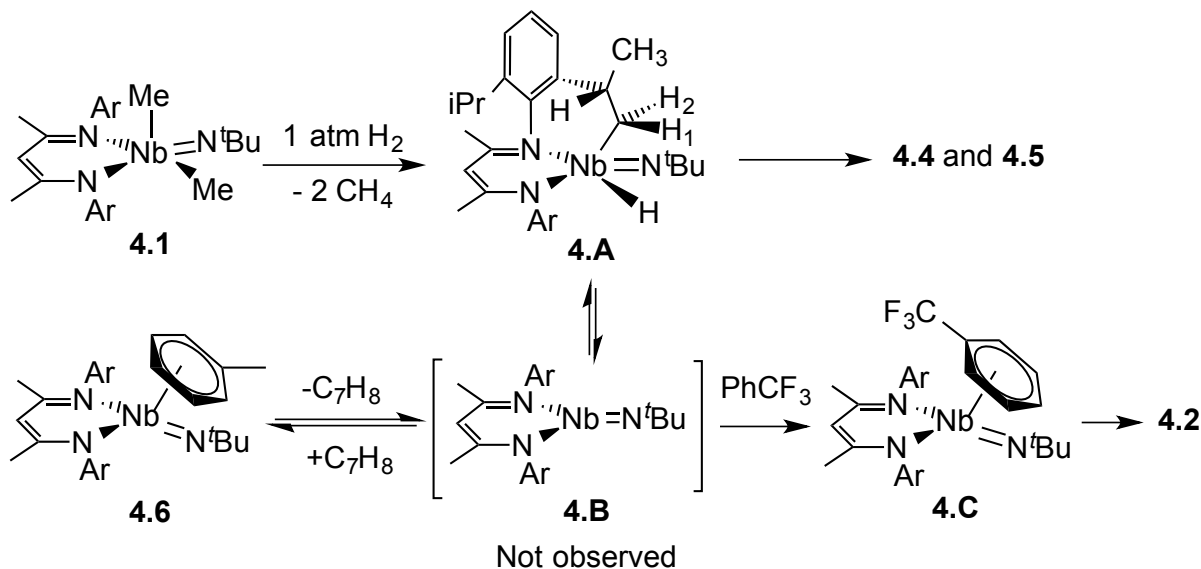


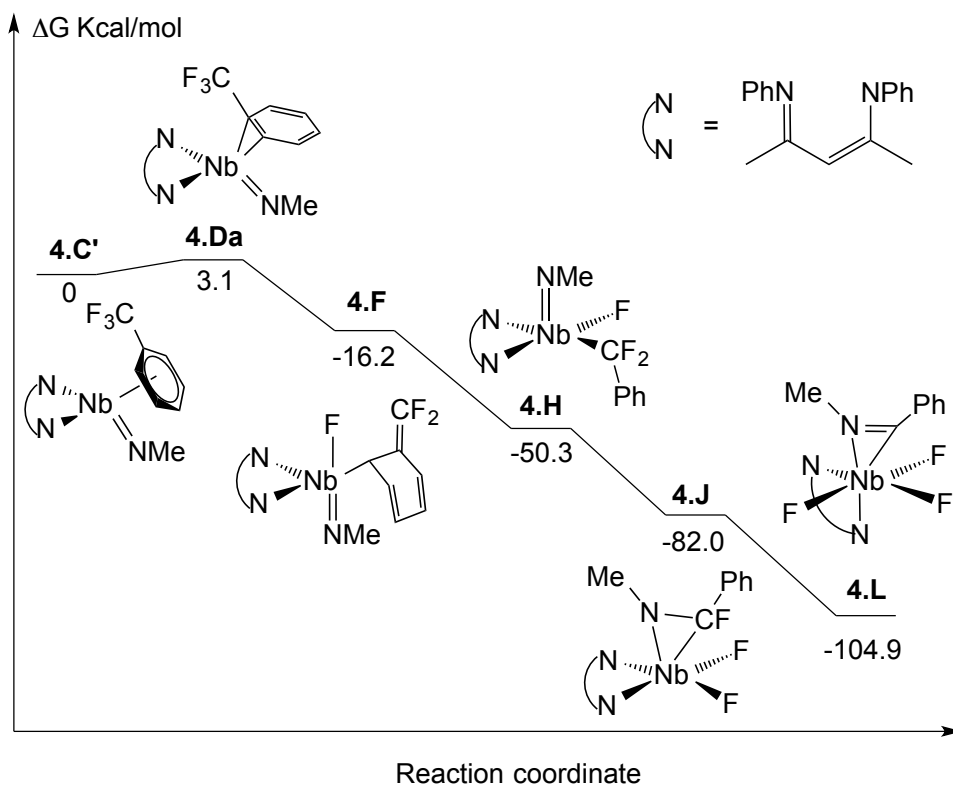
**Figure 4.9** Formation of complex **4.2** and disappearance of **4.C** with time.  $^1\text{H}$  NMR spectra recorded at 273 K.

Taken together, these experiments suggest hydrogenolysis proceeds via the intermediate **4.A**, in equilibrium with the transient tricoordinate Nb(III) species **4.B** illustrated in Scheme 4.3. In the absence of trapping ligands, **4.A** reacts further to form **4.4** and **4.5**, whereas a p-acid ligand such as PhCF<sub>3</sub> traps the low-valent species **4.B**, yielding the d<sup>2</sup> arene intermediate **4.C**. This trivalent intermediate then reacts further to activate the CF<sub>3</sub> moiety.

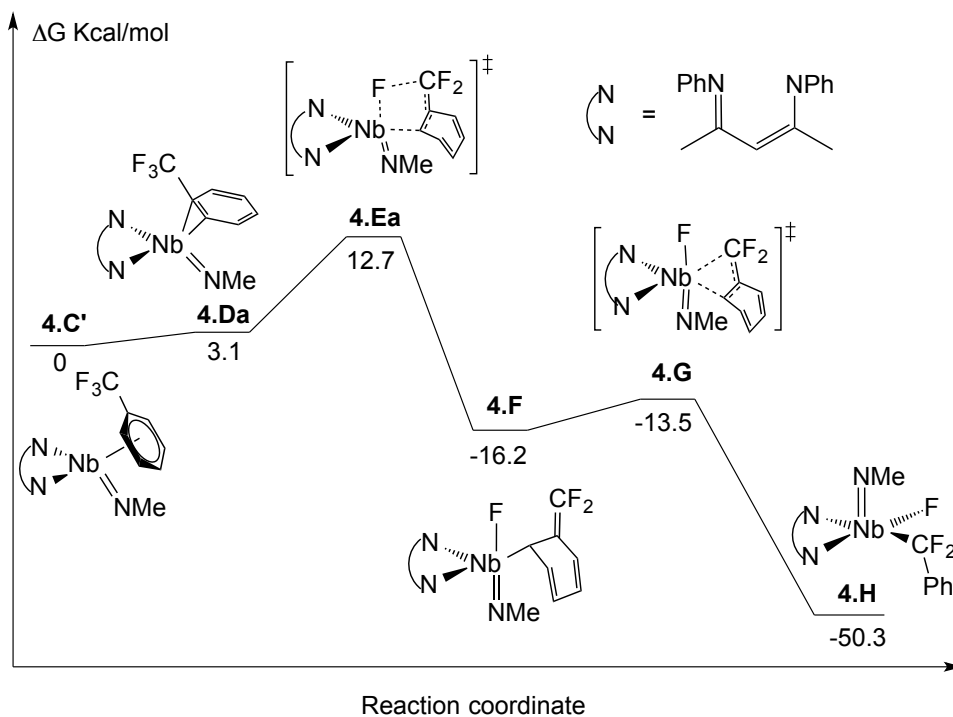


**Scheme 4.3**

**DFT Calculation.** While **4.C** was found experimentally to be a key intermediate in the triple C-F activation of PhCF<sub>3</sub>, the mechanism of its conversion to the final product **4.2** remained unclear. To address this, we turned to DFT calculations for additional mechanistic information (Scheme 4.5). These preliminary calculations showed the presence of a very exergonic overall stepwise C-F activation ( $\Delta H_{4.C \rightarrow 4.L} = -104.8 \text{ kcal.mol}^{-1}$ ), consistent with the formation of strong Nb-F bonds ( $BDE_{\text{Nb-F}} = 137 \text{ kcal.mol}^{-1}$ ).<sup>33</sup> Additionally, no concerted transition state consistent with an oxidative addition was found for the first C-F activation. Instead, DFT suggests a two-step process, with an initial fluorine abstraction leading to sp<sup>2</sup> hybridization at the benzylic carbon (i.e., formation of a coordinated Ph=CF<sub>2</sub> group) with a Nb-C<sub>arene</sub> bond (intermediate **4.F**), followed by a 1,3-shift (Scheme 4.5). Fluorine abstraction in the absence of arene coordination was found to be almost 10 kcal.mol<sup>-1</sup> higher in energy (see Appendix C.1). Finally, the two remaining C-F bonds appear to be activated stepwise. In each step, C-F bond cleavage and nitrene transfer to the benzylic carbon take place in a concerted manner (See Appendix C.1).



**Scheme 4.4** Calculated intermediates involved in  $\text{PhCF}_3$  dis-assembly (energy and structure of transition states are presented in Appendix C.1).



**Scheme 4.5** Calculated intermediates and transition states involved in the first C-F bond activation. (energy and structure of transition states are presented in Appendix C.1).

## Conclusion

To conclude, the selective disassembly of a benzylic CF<sub>3</sub> moiety has been observed in which three fluorine atoms and the resulting carbene fragment are transferred to a single Nb center, with concurrent formation of a new C-N bond. Evidence points to the formation of an h<sup>6</sup>-arene bound niobium complex as a key intermediate in this process. Involvement of arene coordination is apparently essential to stabilize the rate determining transition state since other saturated fluorinated substrates led to intramolecular attack upon other ligands. DFT calculation suggests that the d<sup>2</sup> species **4.C** undergoes stepwise C-F activation to yield the final pentavalent niobium trifluoride/η<sup>2</sup>-bound imine product.

## Experimental

**General Considerations.** Unless otherwise noted, all reactions were performed either using standard Schlenk line techniques or in an MBraun inert atmosphere glove box under an atmosphere of purified nitrogen (<1 ppm O<sub>2</sub>/H<sub>2</sub>O). Glassware, cannulae, and Celite were stored in an oven at *ca.* 160 °C for at least 12 hrs prior to use. Hexanes, Et<sub>2</sub>O, THF and toluene were purified by passage through a column of activated alumina, stored over 3 or 4 Å molecular sieves, and degassed prior to use.<sup>34</sup> α,α,α-trifluorotoluene, 1,3-Bis(trimethyl)benzene, α,α,α-trifluoro-1-hexane were dried over P<sub>2</sub>O<sub>5</sub>, distilled under reduced pressure, degassed and stored over 4 Å molecular sieves. Deuterated solvents (C<sub>6</sub>D<sub>6</sub>, C<sub>7</sub>D<sub>8</sub>, C<sub>9</sub>D<sub>12</sub> and THF-d<sub>8</sub>) were dried over sodium/benzophenone. The deuterated solvents were then vacuum transferred to a storage flask containing activated molecular sieves, and then degassed before being stored in the dry box. *N,N'*-bis-(2,6-diisopropylphenyl)-□-diketiminato (BDI),<sup>35</sup> Li(BDI)·Et<sub>2</sub>O,<sup>36</sup> (BDI)pyCl<sub>2</sub>Nb(N<sup>t</sup>Bu),<sup>29</sup> (BDI)(Me)<sub>2</sub>Nb(N<sup>t</sup>Bu) (**4.1**)<sup>29</sup> and (BDI)(□<sup>6</sup>-C<sub>7</sub>H<sub>8</sub>)<sub>2</sub>Nb(N<sup>t</sup>Bu) (**4.6**)<sup>28</sup> were prepared using literature procedures. All other reagents were acquired from commercial sources and used as received. NMR spectra were recorded on Bruker AV-300, AVQ-400, AVB-400, DRX-500, AV-500, and AV-600 spectrometers. Chemical shifts were measured relative to residual solvent peaks, which were assigned relative to an external TMS standard for <sup>1</sup>H/<sup>13</sup>C and BF<sub>3</sub>·OEt<sub>2</sub> for <sup>19</sup>F set at 0.00 ppm. <sup>1</sup>H and <sup>13</sup>C NMR assignments were routinely confirmed by 135/90 DEPT, <sup>1</sup>H-<sup>1</sup>H (COSY, NOESY) and <sup>1</sup>H-<sup>13</sup>C (HSQC and HMBC) experiments. The uncorrected melting points were determined using sealed capillaries prepared under nitrogen on an Optmelt SRS. Elemental analyses were performed at the College of Chemistry Microanalytical Laboratory, University of California, Berkeley. The X-ray structural determinations were performed at CHEXRAY, University of California, Berkeley on Bruker SMART 1000 or SMART APEX diffractometers.

([BDI]NbF<sub>3</sub>(<sup>t</sup>BuN=CC<sub>6</sub>H<sub>5</sub>)) (**4.2**). α,α,α-trifluorotoluene (30 mL) was added to a 100-mL Schlenk flask containing (BDI)(Me)<sub>2</sub>Nb(N<sup>t</sup>Bu) (**4.1**) (0.300 g, 0.490 mmol, 1.0 equiv.) at room temperature. The clear yellow solution was degassed with two freeze-pump-thaw cycles. While warming the solution during the second cycle, the headspace of the flask was filled with 1 atm of H<sub>2</sub> (70 mL, 2.8 mmol, 10 equiv.) and the solution was stirred vigorously. The color of the solution turned dark red within 15 min, but changed further to brown/orange within a few hours. After 12 h, the volatile materials were removed under reduced pressure to yield a brown residue. Trituration with Et<sub>2</sub>O (2 × 15 ml), extraction with hexane (20 ml), and storage at -40 °C overnight afforded orange crystals, which were collected by filtration. Yield:

310 mg, 0.430 mmol, 87%. X-ray suitable crystals were obtained by recrystallization from Et<sub>2</sub>O. <sup>1</sup>H NMR (500MHz, C<sub>6</sub>D<sub>6</sub>, 293 K): δ (ppm) 7.20 (m, Ar), 7.03 (d, 2 H, Ar, <sup>3</sup>J<sub>HH</sub> = 7.2 Hz), 6.80 (d, 2 H, Ar, <sup>3</sup>J<sub>HH</sub> = 7.2 Hz), 6.70 (m, Ar), 6.62 (m, Ar), 5.13 (s, 1 H, HC(C(Me)NAr)<sub>2</sub>), 3.58 (sept, 2 H, CHMe<sub>2</sub>, <sup>3</sup>J<sub>HH</sub> = 6.6 Hz), 3.51 (sept, 2 H, CHMe<sub>2</sub>, <sup>3</sup>J<sub>HH</sub> = 6.9 Hz), 1.70 (s, 3 H, HC(C(Me)NAr)<sub>2</sub>), 1.66 (d, 6 H, CHMe<sub>2</sub>, <sup>3</sup>J<sub>HH</sub> = 6.9 Hz), 1.42 (s, 3 H, HC(C(Me)NAr)<sub>2</sub>), 1.23 (d, 6 H, CHMe<sub>2</sub>, <sup>3</sup>J<sub>HH</sub> = 6.6 Hz), 1.12 (d, 6 H, CHMe<sub>2</sub>, <sup>3</sup>J<sub>HH</sub> = 6.6 Hz), 1.07 (s, 9 H, <sup>t</sup>Bu), 1.05 (d, 6 H, CHMe<sub>2</sub>, <sup>3</sup>J<sub>HH</sub> = 6.9 Hz). <sup>19</sup>F NMR (470 MHz, C<sub>6</sub>D<sub>6</sub>, 293 K): δ (ppm) 162.28 (b, 2F, Nb-F), 92.20 (b, 1F, Nb-F). <sup>13</sup>C{<sup>1</sup>H} NMR (125.8 MHz, C<sub>6</sub>D<sub>6</sub>, 293 K): δ (ppm) 166.3 (C, HC(C(Me)NAr)<sub>2</sub>), 163.3 (C, HC(C(Me)NAr)<sub>2</sub>), 154.2 (C, Ar), 143.1 (C, Ar), 140.8 (C, Ar), 136.8 (C, Ar), 126.4 (CH, ArCF<sub>3</sub>), 125.9 (CH, ArCF<sub>3</sub>), 124.6 (CH, Ar), 124.3 (CH, Ar), 123.4 (CH, Ar), 120.4 (CH, Ar), 102.4 (CH, HC(C(Me)NAr)<sub>2</sub>), 67.5 (C, Nb-η<sup>2</sup>(ArC=NC(CH<sub>3</sub>)<sub>3</sub>), 65.1 (C, Nb-η<sup>2</sup>(ArC=NC(CH<sub>3</sub>)<sub>3</sub>), 28.9 (CH<sub>3</sub>, Nb-η<sup>2</sup>(ArC=NC(CH<sub>3</sub>)<sub>3</sub>), 28.5 (CH, CHMe<sub>2</sub> of C=NAr), 27.3 (CH, CHMe<sub>2</sub> of C=NAr), 25.9 (CH, CHMe<sub>2</sub> of C=NAr), 25.4 (CH<sub>3</sub>, HC(C(Me)NAr)<sub>2</sub>), 25.0 (CH, CHMe<sub>2</sub> of C=NAr), 24.9 (CH<sub>3</sub>, CHMe<sub>2</sub> of C=NAr), 24.3 (CH<sub>3</sub>, HC(C(Me)NAr)<sub>2</sub>). Anal. Calcd for C<sub>40</sub>H<sub>55</sub>N<sub>3</sub>NbF<sub>3</sub>: C, 66.01; H, 7.62; N, 5.77. Found: C, 66.20; H, 7.74; N, 5.95. m.p.: 200-202 °C (decomp).

Selected NMR resonances in C<sub>9</sub>D<sub>12</sub>: (600MHz, C<sub>9</sub>D<sub>12</sub>, 243 K): δ (ppm) 5.08 (s, 1 H, HC(C(Me)NAr)<sub>2</sub>), 3.44 (m, 4 H, CHMe<sub>2</sub>, <sup>3</sup>J<sub>HH</sub> = 6.9 Hz), 1.69 (s, 3 H, HC(C(Me)NAr)<sub>2</sub>), 1.56 (d, 6 H, CHMe<sub>2</sub>, <sup>3</sup>J<sub>HH</sub> = 6.9 Hz), 1.42 (s, 3 H, HC(C(Me)NAr)<sub>2</sub>), 1.18 (d, 6 H, CHMe<sub>2</sub>, <sup>3</sup>J<sub>HH</sub> = 6.6 Hz), 1.11 (s, 9 H, <sup>t</sup>Bu), 1.05 (d, 6 H, CHMe<sub>2</sub>, <sup>3</sup>J<sub>HH</sub> = 6.9 Hz), 1.01 (d, 6 H, CHMe<sub>2</sub>, <sup>3</sup>J<sub>HH</sub> = 6.9 Hz). <sup>19</sup>F NMR (564 MHz, C<sub>6</sub>D<sub>6</sub>, 243 K): δ (ppm) 159.40 (d, 2F, Nb-F), 85.11 (t, 1F, Nb-F).

**([BDI]NbF<sub>3</sub>(<sup>t</sup>BuN=CC<sub>6</sub>H<sub>4</sub>CF<sub>3</sub>)) (4.3).** 1,3-Bis(trifluoromethyl)benzene (30 mL) was added to a 100-mL Schlenk flask containing **4.1** (0.170 g, 0.278 mmol, 1.0 equiv.) at room temperature. The clear yellow solution was degassed with two freeze-pump-thaw cycles. While warming the solution during the second cycle, the headspace of the flask was filled with 1 atm of H<sub>2</sub> (70 mL, 2.8 mmol, 10 equiv.) and the solution was stirred vigorously. The color of the solution turned to dark red within 15 min, but changed further to brown/orange within a few hours. After 12 h, the volatile materials were removed under reduced pressure to yield a brown residue. Trituration with Et<sub>2</sub>O (2 × 15 ml), extraction with Et<sub>2</sub>O (20 ml), and storage at -40 °C overnight afforded yellow/orange crystals, which were collected by filtration. Yield: 202 mg, 0.253 mmol, 91%. X-ray suitable crystals were obtained by recrystallization from Et<sub>2</sub>O. <sup>1</sup>H NMR (500MHz, C<sub>6</sub>D<sub>6</sub>, 293 K): δ (ppm) 7.2 (m, Ar), 7.03 (d, 1 H, Ar, <sup>3</sup>J<sub>HH</sub> = 7.2 Hz), 6.7 (m, Ar), 6.31 (d, 1 H, Ar, <sup>3</sup>J<sub>HH</sub> = 7.2 Hz), 5.15 (s, 1 H, HC(C(Me)NAr)<sub>2</sub>), 3.58 (sept, 2 H, CHMe<sub>2</sub>, <sup>3</sup>J<sub>HH</sub> = 6.6 Hz), 3.55 (sept, 2 H, CHMe<sub>2</sub>, <sup>3</sup>J<sub>HH</sub> = 6.9 Hz), 1.72 (s, 3 H, HC(C(Me)NAr)<sub>2</sub>), 1.68 (d, 6 H, CHMe<sub>2</sub>, <sup>3</sup>J<sub>HH</sub> = 6.9 Hz), 1.36 (s, 3 H, HC(C(Me)NAr)<sub>2</sub>), 1.24 (d, 6 H, CHMe<sub>2</sub>, <sup>3</sup>J<sub>HH</sub> = 6.6 Hz), 1.14 (d, 6 H, CHMe<sub>2</sub>, <sup>3</sup>J<sub>HH</sub> = 6.6 Hz), 1.09 (s, 9 H, <sup>t</sup>Bu), 1.06 (d, 6 H, CHMe<sub>2</sub>, <sup>3</sup>J<sub>HH</sub> = 6.9 Hz). <sup>19</sup>F NMR (470 MHz, C<sub>6</sub>D<sub>6</sub>, 293 K): δ (ppm) 163.08 (b, 2F, Nb-F), 92.45 (b, 1F, Nb-F), -61.64 (s, 3F, ArCF<sub>3</sub>). <sup>13</sup>C{<sup>1</sup>H} NMR (125.8 MHz, C<sub>6</sub>D<sub>6</sub>, 293 K): δ (ppm) 167.4 (C, HC(C(Me)NAr)<sub>2</sub>), 164.2 (C, HC(C(Me)NAr)<sub>2</sub>), 155.3 (C, Ar), 147.3 (C, ArCF<sub>3</sub>), 145.5 (C, Ar), 141.1 (C, Ar), 137.8 (C, Ar), 127.0 (CH, ArCF<sub>3</sub>), 126.5 (CH, ArCF<sub>3</sub>), 125.6 (CH, Ar), 125.5 (CH, Ar), 124.1 (CH, Ar), 121.2 102.9 (CH, HC(C(Me)NAr)<sub>2</sub>), 68.12 (C, Nb-η<sup>2</sup>(ArC=NC(CH<sub>3</sub>)<sub>3</sub>), 65.9 (C, Nb-η<sup>2</sup>(ArC=NC(CH<sub>3</sub>)<sub>3</sub>), 29.6 (CH<sub>3</sub>, Nb-η<sup>2</sup>(ArC=NC(CH<sub>3</sub>)<sub>3</sub>), 29.1 (CH, CHMe<sub>2</sub> of C=NAr), 27.9 (CH, CHMe<sub>2</sub> of C=NAr), 26.6 (CH, CHMe<sub>2</sub> of C=NAr), 26.1 (CH<sub>3</sub>, HC(C(Me)NAr)<sub>2</sub>), 25.7 (CH, CHMe<sub>2</sub> of C=NAr), 25.0 (CH<sub>3</sub>,

CHMe<sub>2</sub> of C=NAr), 24.3 (CH<sub>3</sub>, HC(C(Me)NAr)<sub>2</sub>). Anal. Calcd for C<sub>41</sub>H<sub>54</sub>N<sub>3</sub>Nb<sub>1</sub>F<sub>6</sub>: C, 61.88; H, 6.84; N, 5.28. Found: C, 61.90; H, 7.02; N, 5.36. m.p.: 202 - 204 °C (decomp).

([κ<sub>4</sub>-CNCC-BDI]Nb(<sup>t</sup>BuN)) (4.4) and ([BDI]Nb(<sup>t</sup>BuN)(μ-H))<sub>2</sub> (4.5). Hexanes (30 mL) were added to a 100-mL Schlenk flask containing 4.1 (0.200 g, 0.33 mmol, 1.0 equiv.) at room temperature. The clear yellow solution was degassed with two freeze-pump-thaw cycles. While warming the solution during the second cycle, the headspace of the flask was filled with 1 atm of H<sub>2</sub> (70 mL, 2.8 mmol, 8.0 equiv.) and the solution was stirred vigorously. The color of the solution turned to dark red within 15 min, and a purple precipitate started to appear after 30 mins. After 12 h, the volatile materials were removed under reduced pressure to yield a red and purple powder. The red powder was extracted with hexanes (10 ml), and storage at -40 °C overnight afforded red crystals of complex 4.4, which were collected by filtration. Yield: 116 mg, 62%. The purple powder was extracted with THF (20 ml), and storage at -40 °C overnight afforded dark purple crystals of complex 4.5, which were collected by filtration Yield: 90 mg, 21%.

**Complex 4.4:** X-ray suitable crystals were obtained by recrystallization from Et<sub>2</sub>O. <sup>1</sup>H NMR (500MHz, C<sub>6</sub>D<sub>6</sub>, 293 K): δ (ppm) 7.34 (t, 2 H, *p*-Ar, <sup>3</sup>J<sub>HH</sub> = 7.6 Hz), 7.30 (dd, 4 H, *m*-Ar, <sup>3</sup>J<sub>HH</sub> = 7.2 Hz), 7.00 (dd, 4 H, *o*-Ar, <sup>3</sup>J<sub>HH</sub> = 7.2 Hz), 5.19 (s, 1 H, HC(C(Me)NAr)<sub>2</sub>), 2.85 (sept, 2 H, CHMe<sub>2</sub>, <sup>3</sup>J<sub>HH</sub> = 6.9 Hz), 2.34 (s, 6 H, Nb-CMe<sub>2</sub>), 1.96 (s, 6 H, HC(C(Me)NAr)<sub>2</sub>), 1.33 (s, 6 H, Nb-CMe<sub>2</sub>), 1.21 (d, 6 H, CHMe<sub>2</sub>, <sup>3</sup>J<sub>HH</sub> = 6.9 Hz), 0.87 (d, 6 H, CHMe<sub>2</sub>, <sup>3</sup>J<sub>HH</sub> = 6.6 Hz), 0.68 (s, 9 H, <sup>t</sup>Bu). <sup>13</sup>C{<sup>1</sup>H} NMR (125.8 MHz, C<sub>6</sub>D<sub>6</sub>, 293 K): δ (ppm) 168.56 (C, HC(C(Me)NAr)<sub>2</sub>), 153.15 (C, Ar), 143.08 (C, Ar), 141.31 (C, Ar), 125.71 (CH, Ar), 125.63 (CH, Ar), 124.06 (CH, Ar), 105.21 (broad, CH, C<sub>6</sub>H<sub>6</sub>), 103.56 (CH, HC(C(Me)NAr)<sub>2</sub>), 33.04 (CH<sub>3</sub>, Nb=N<sup>t</sup>Bu, C<sub>β</sub>), 28.46 (CH, CHMe<sub>2</sub> of C=NAr), 27.39 (CH, CHMe<sub>2</sub> of C=NAr), 25.92 (CH<sub>3</sub>, CHMe<sub>2</sub> of C=NAr), 25.71 (CH<sub>3</sub>, CHMe<sub>2</sub> of C=NAr), 25.07 (CH<sub>3</sub>, CHMe<sub>2</sub> of C=NAr), 24.79 (CH<sub>3</sub>, CHMe<sub>2</sub> of C=NAr), 24.70 (CH<sub>3</sub>, HC(C(Me)NAr)<sub>2</sub>). Anal. Calcd for C<sub>32</sub>H<sub>48</sub>N<sub>3</sub>Nb<sub>1</sub> powders: C, 67.71; H, 8.85; N, 7.40. Found: C, 69.61; H, 8.45; N, 6.33. m.p.: 165-166 °C.

**Complex 4.5:** X-ray suitable crystals were obtained by slowly diffusing H<sub>2</sub> at room temperature through a diluted solution of hexane (40 ml) containing 20 mg of 1. Due to its poor solubility, only a <sup>1</sup>H NMR spectrum was recorded. <sup>1</sup>H NMR (500MHz, THF-d<sub>8</sub>, 293 K): δ (ppm) 7.07 (d, 4 H, *o*-Ar, <sup>3</sup>J<sub>HH</sub> = 7.1 Hz), 7.01 (t, 4 H, *p*-Ar, <sup>3</sup>J<sub>HH</sub> = 7.2 Hz), 6.88 (2, 4 H, *m*-Ar, <sup>3</sup>J<sub>HH</sub> = 7.1 Hz), 4.74 (s, 2 H, HC(C(Me)NAr)<sub>2</sub>), 3.84 (sept, 4 H, CHMe<sub>2</sub>, <sup>3</sup>J<sub>HH</sub> = 6.6 Hz), 2.95 (sept, 4 H, CHMe<sub>2</sub>, <sup>3</sup>J<sub>HH</sub> = 6.6 Hz), 1.61 (d, 12 H, CHMe<sub>2</sub>, <sup>3</sup>J<sub>HH</sub> = 6.9 Hz), 1.49 (s, 18 H, <sup>t</sup>Bu), 1.31 (s, 6 H, HC(C(Me)NAr)<sub>2</sub>), 1.10 (d, 12 H, CHMe<sub>2</sub>, <sup>3</sup>J<sub>HH</sub> = 6.6 Hz), 0.92 (d, 12 H, CHMe<sub>2</sub>, <sup>3</sup>J<sub>HH</sub> = 6.6 Hz), 0.14 (m, 12 H, CHMe<sub>2</sub>, <sup>3</sup>J<sub>HH</sub> = 6.9 Hz), -1.35 (b, 2H, Nb-H). Anal. Calcd for C<sub>66</sub>H<sub>102</sub>N<sub>6</sub>Nb<sub>2</sub> powders: C, 68.02; H, 8.82; N, 7.21. Found: C, 68.31; H, 8.95; N, 7.33. m.p.: 195-196 °C.

**NMR analysis of intermediate 4.A.** A solution of C<sub>9</sub>D<sub>12</sub> containing (BDI)(Me)<sub>2</sub>Nb(N<sup>t</sup>Bu) (4.1) (0.011 M, 1 equiv.) was added to a J-Young NMR tube with a Teflon cap. A <sup>1</sup>H NMR spectrum was taken at T = 243 K and corresponds to t = 0. The solution was freeze-pump-thawed three times and then refilled with 1 atm of H<sub>2</sub>. The NMR tube with the thawing solution was placed in the spectrometer, cooled to 243 K and several <sup>1</sup>H NMR spectra were recorded. Between each spectrum, the NMR tube was ejected from the spectrometer and was shaken at room temperature for 1-2 mins before being brought back to 243 K. Figure 4.5 shows the formation of the intermediate 4.A after several minutes at room temperature. The

tube was then repeatedly brought to room temperature in order to observe the further conversion of **4.A**.

**Characterization of 4.A:** (600MHz, C<sub>9</sub>D<sub>12</sub>, 243 K):  $\delta$  (ppm) 9.29 (b, 1 H, Nb-*H*), 5.32 (s, 1 H, HC(C(Me)NAr)<sub>2</sub>), 3.12 (sept, 1 H, CHMe<sub>2</sub>, <sup>3</sup>J<sub>HH</sub> = 6.9 Hz), 3.05 (m, 1 H, Nb-CH<sub>2</sub>CH(Ar)CH<sub>3</sub>), 2.70 (sept, 1 H, CHMe<sub>2</sub>), 2.61 (sept, 1 H, CHMe<sub>2</sub>, <sup>3</sup>J<sub>HH</sub> = 6.9 Hz), 1.78 (m, 1 H, Nb-CH<sub>2</sub>CH(Ar)CH<sub>3</sub>), 1.75 (s, 3 H, HC(C(Me)NAr)<sub>2</sub>), 1.52 (s, 3 H, HC(C(Me)NAr)<sub>2</sub>), 1.44 (d, 3 H, CHMe<sub>2</sub>), 1.36 (d, 3 H, Nb-CH<sub>2</sub>CH(Ar)CH<sub>3</sub>), 1.31 (d, 3 H, CHMe<sub>2</sub>), 1.26 (d, 3 H, CHMe<sub>2</sub>), 1.18 (d, 3 H, CHMe<sub>2</sub>), 1.06 (d, 3 H, CHMe<sub>2</sub>), 1.02 (d, 3 H, CHMe<sub>2</sub>), 0.99 (s, 9 H, <sup>t</sup>Bu), 0.98 (m, 1 H, Nb-CH<sub>2</sub>CH(Ar)CH<sub>3</sub>). <sup>13</sup>C NMR (125 MHz, C<sub>6</sub>D<sub>6</sub>, 243 K):  $\delta$  (ppm) 73.8 (CH<sub>2</sub>, Nb-CH<sub>2</sub>CH(Ar)CH<sub>3</sub>), 35.5 (CH, Nb-CH<sub>2</sub>CH(Ar)CH<sub>3</sub>).

**NMR analysis of intermediate 4.C.** A solution of C<sub>9</sub>D<sub>12</sub> containing a,a,a-trifluorotoluene (6.8 ml, 0.055 mmol, 5 equiv.) and **4.1** (0.011 M, 1 equiv.) was added to a J-Young NMR tube with a Teflon cap. A <sup>1</sup>H NMR spectrum was taken at T = 243 K and corresponds to t = 0 (spectrum 1, Figure 4.7). The solution was freeze-pump-thawed three times and then refilled with 1 atm of H<sub>2</sub>. The NMR tube with the thawing solution was placed in the spectrometer, cooled to 243 K and several <sup>1</sup>H NMR spectra were recorded. Between each spectrum, the NMR tube was ejected from the spectrometer and was shaken at room temperature for 1-2 mins before being brought back to 243 K. Figure 4.7 shows the quick formation of the intermediate **4.A**, followed by the formation of **4.C**. Once again, the persistency of these intermediates at 243 K allowed for their complete characterization. The tube was then repeatedly brought back to room temperature in order to observe the further conversion of **4.C** to the final product **4.1** (Figure 4.9).

**Characterization of 4.C:** <sup>1</sup>H NMR (600 MHz, C<sub>9</sub>D<sub>12</sub>, 243 K):  $\delta$ (ppm) 5.03 (s, 1 H, HC(C(Me)NAr)<sub>2</sub>), 4.36 (m, 2 H, CHMe<sub>2</sub>, <sup>3</sup>J<sub>HH</sub> = 6.9 Hz), 3.96 (d, 2 H, PhCF<sub>3</sub>), 3.50 (d, 3 H, PhCF<sub>3</sub>). <sup>19</sup>F NMR (564 MHz, C<sub>6</sub>D<sub>6</sub>, 243 K):  $\delta$ (ppm) -62.4 (s, 3F, PhCF<sub>3</sub>). <sup>13</sup>C NMR (125 MHz, C<sub>9</sub>D<sub>12</sub>, 243 K):  $\delta$ (ppm) 103 (s, 1 H, HC(C(Me)NAr)<sub>2</sub>), 4.36 (m, 2 H, CHMe<sub>2</sub>, <sup>3</sup>J<sub>HH</sub> = 6.9 Hz), 97, 106 and 111 (CH, PhCF<sub>3</sub>).

**Deuterium scrambling.** A solution of C<sub>9</sub>D<sub>12</sub> containing (BDI)(Me)<sub>2</sub>Nb(N<sup>t</sup>Bu) (0.011 M, 1 equiv.) was added to a J-Young NMR tube with a Teflon cap. The solution was freeze-pump-thawed three times and then refilled with 1 atm of D<sub>2</sub>. The NMR tube was left at room temperature for 12 hrs, and the C<sub>9</sub>D<sub>12</sub> was then removed under reduced pressure and replaced by C<sub>6</sub>D<sub>6</sub>.

**General remarks for DFT Calculations.** All structures and energies were calculated using the Gaussian09 suite of programs.<sup>37</sup> Self-consistent field computations were performed with tight convergence criteria on ultrafine grids, while geometry optimizations were converged to tight geometric convergence criteria for all compounds. Spin expectation values  $\langle S \rangle^2$  indicated that spin contamination was not significant in any result. Frequencies were calculated analytically at 298.15 K and 1 atm. Structures were considered true minima if they did not exhibit imaginary vibration modes and were considered as transition states when only one imaginary vibration mode was found. Intrinsic Reaction Coordinates (IRC) calculations were performed to ensure the transition state geometries connected the reactants and the products. Optimized geometries were compared using the sum of their electronic and zero-point energies. In order to reduce the computational time, the system was structurally

simplified by replacing 2,6-diisopropylphenyl groups by phenyl groups and the N<sup>t</sup>Bu imido group by a NMe imido group.

The B3LYP hybrid functional was used throughout this computational study.<sup>38,39</sup> For geometry optimizations and frequency calculations, the light atoms (H, C, N and F) were treated with Pople's 6-31G(d,p) double- $\zeta$  split-valence basis,<sup>40,41</sup> while the niobium atom was treated with a Stuttgart/Dresden ECPs pseudopotential (SDD).<sup>42,43</sup>

**X-Ray crystallography studies.** X-ray structural determinations were performed on a Bruker SMART 1000 or SMART APEX diffractometer. Both are 3-circle diffractometers that couple a CCD detector<sup>44</sup> with a sealed-tube source of monochromated Mo K $\alpha$  radiation ( $\lambda = 0.71073$  Å). A crystal of appropriate size was coated in Paratone-N oil and mounted on a Kapton<sup>®</sup> loop. The loop was transferred to the diffractometer, centered in the beam, and cooled by a nitrogen flow low-temperature apparatus that had been previously calibrated by a thermocouple placed at the same position as the crystal. Preliminary orientation matrices and cell constants were determined by collection of 60 x 10 s frames, followed by spot integration and least-squares refinement. The reported cell dimensions were calculated from all reflections with  $I > 10 \sigma$ . The data were corrected for Lorentz and polarization effects; no correction for crystal decay was applied. An empirical absorption correction based on comparison of redundant and equivalent reflections was applied using SADABS.<sup>45</sup> All software used for diffraction data processing and crystal-structure solution and refinement are contained in the APEX2 program suite (Bruker AXS, Madison, WI).<sup>46</sup> Thermal parameters for all non-hydrogen atoms were refined anisotropically. For all structures,  $R_1 = \Sigma(|F_o| - |F_c|)/\Sigma(|F_o|)$ ;  $wR_2 = [\Sigma\{w(F_o^2 - F_c^2)^2\}/\Sigma\{w(F_o^2)^2\}]^{1/2}$ . Thermal ellipsoid plots were created using the ORTEP-3 software package and POV-ray.<sup>47</sup>



**Table 4.3** Crystallographic parameters for complexes **4.2** and **4.3**

Compound	<b>4.2</b>	<b>4.3</b>
Formula	C <sub>40</sub> H <sub>55</sub> F <sub>3</sub> N <sub>3</sub> Nb	C <sub>41</sub> H <sub>54</sub> F <sub>6</sub> N <sub>3</sub> Nb
Formula weight (amu)	727.78	795.78
Space Group	P2 <sub>1</sub> /c	<i>Pbca</i>
<i>a</i> (Å)	20.1958(9)	20.9710(16)
<i>b</i> (Å)	20.5403(10)	16.6536(13)
<i>c</i> (Å)	18.1628(9)	22.7371(17)
$\alpha$ (°)	90°	90°
$\beta$ (°)	96.318(3)°	90°
$\gamma$ (°)	90°	90°
<i>V</i> (Å <sup>3</sup> )	7488.7(6)	7940.8(11)
<i>Z</i>	8	8
$\rho_{\text{calcd}}$ (g/cm <sup>3</sup> )	1.291	1.331
<i>F</i> <sub>000</sub>	3072	3328
$\mu$ (mm <sup>-1</sup> )	0.367	0.363
<i>T</i> <sub>min</sub> / <i>T</i> <sub>max</sub>	0.8583/0.9875	0.8835/0.9084
No. rflns measured	81947	194464
No. indep. rflns	13712	7298
<i>R</i> <sub>int</sub>	0.0609	0.0317
No. obs. ( <i>I</i> > 2.00σ( <i>I</i> ))	13712	7298
No. variables	873	473
<i>R</i> <sub>1</sub> , <i>wR</i> <sub>2</sub>	0.0400/0.0951	0.0262/0.0611
<i>R</i> <sub>1</sub> (all data)	0.0604	0.0307
GoF	1.029	1.074
Res. peak/hole (e <sup>-</sup> /Å <sup>3</sup> )	0.482/-1.154	0.417/-0.465

**Table 4.4** Crystallographic parameters for complexes **4.4** and **4.5**

Compound	<b>4.4</b>	<b>4.5</b>
Formula	C <sub>33</sub> H <sub>48</sub> N <sub>3</sub> Nb	C <sub>66</sub> H <sub>102</sub> N <sub>6</sub> Nb <sub>2</sub>
Formula weight (amu)	579.65	1165.36
Space Group	P <sub>2</sub> <sub>1</sub>	C <sub>2</sub> /m
<i>a</i> (Å)	9.2011(4)	17.7537(15)
<i>b</i> (Å)	18.8526(9)	19.0483(16)
<i>c</i> (Å)	9.5779(4)	11.5495(9)
$\alpha$ (°)	90°	90°
$\beta$ (°)	111.256(2)°	120.0960(10)°
$\gamma$ (°)	90°	90°
<i>V</i> (Å <sup>3</sup> )	1548.40(12)	3379.2(5)
<i>Z</i>	2	2
$\rho_{\text{calcd}}$ (g/cm <sup>3</sup> )	1.243	1.145
<i>F</i> <sub>000</sub>	616	1244
$\mu$ (mm <sup>-1</sup> )	0.413	0.379
<i>T</i> <sub>min</sub> / <i>T</i> <sub>max</sub>	0.9183/0.9756	0.9140/0.9218
No. rflns measured	12610	30549
No. indep. rflns	4997	3204
<i>R</i> <sub>int</sub>	0.0213	0.0215
No. obs. ( <i>I</i> > 2.00σ( <i>I</i> ))	4997	3204
No. variables	378	206
<i>R</i> <sub>1</sub> , <i>wR</i> <sub>2</sub>	0.0312/0.0708	0.0244/0.0668
<i>R</i> <sub>1</sub> (all data)	0.0355	0.0253
GoF	1.025	1.070
Res. peak/hole (e <sup>-</sup> /Å <sup>3</sup> )	0.406/-0.471	0.519/-0.423

## References

- (1) Osterberg, C.; Richmond, T. G.; Kiplinger, J. L. *Chem. Rev.* **1994**, *94*, 373–431.
- (2) Burdeniuc, J.; Jedicka, B.; Crabtree, R. H. *Eur. J. Inorg. Chem.* **1997**, *130*, 145–154.
- (3) Richmond, T. in *Activation of Unreactive Bonds and Organic Synthesis*; Murai, S. Eds; Springer-Verlag Berlin Heidelberg **1999**, 243–269.
- (4) Shine, K. P.; Sturges, W. T. *Science* **2007**, *315*, 1804–1805.
- (5) Amii, H.; Uneyama, K. *Chem. Rev.* **2009**, *109*, 2119–2183.
- (6) Uneyama, K.; Amii, H. *J. Fluorine Chem.* **2002**, *114*, 127–131.
- (7) Torrens, H. *Coord. Chem. Rev.* **2005**, *249*, 1957–1985.
- (8) Clot, E.; Eisenstein, O.; Jasim, N.; Macgregor, S. A.; McGrady, J. E.; Perutz, R. N. *Acc. Chem. Res.* **2011**, *44*, 333–348.
- (9) Braun, T.; Wehmeier, F. *Eur. J. Inorg. Chem.* **2011**, *2011*, 613–625.
- (10) Jones, W. D. *Dalton Trans.* **2003**, 3991–3995
- (11) Klahn, M.; Rosenthal, U. *Organometallics* **2012**, *31*, 1235–1244.
- (12) Nova, A.; Mas-Ballesté, R.; Lledós, A. *Organometallics* **2012**, *31*, 1245–1256.
- (13) Yow, S.; Gates, S. J.; White, A. J. P.; Crimmin, M. R. *Angew. Chem. Int. Ed.* **2012**, *51*, 12559–12563.
- (14) Lv, H.; Cai, Y.-B.; Zhang, J.-L. *Angew. Chem. Int. Ed.* **2013**, *52*, 3203–3207.
- (15) Yang, X.; Sun, H.; Zhang, S.; Li, X. *J. Organomet. Chem.* **2013**, *723*, 36–42.
- (16) Kuehnel, M. F.; Holstein, P.; Kliche, M.; Krüger, J.; Matthies, S.; Nitsch, D.; Schutt, J.; Sparenberg, M.; Lentz, D. *Chem. Eur. J.* **2012**, *18*, 10701–10714.
- (17) Lentz, D. *J. Fluorine Chem.* **2004**, *125*, 853–861.
- (18) Barrett, A. G. M.; Crimmin, M. R.; Hill, M. S.; Hitchcock, P. B.; Procopiou, P. A. *Angew. Chem. Int. Ed.* **2007**, *46*, 6339–6342.
- (19) Driver, T. G. *Angew. Chem. Int. Ed.* **2009**, *48*, 7974–7976.
- (20) Azhakar, R.; Roesky, H. W.; Wolf, H.; Stalke, D. *Chem. Commun.* **2013**, *49*, 1841.
- (21) Fuchibe, K.; Akiyama, T. *J. Am. Chem. Soc.* **2006**, *128*, 1434–1435.
- (22) Douvris, C.; Ozerov, O. V. *Science* **2008**, *321*, 1188–1190.
- (23) Douvris, C.; Nagaraja, C. M.; Chen, C.-H.; Foxman, B. M.; Ozerov, O. V. *J. Am. Chem. Soc.* **2010**, *132*, 4946–4953.
- (24) Janjetovic, M.; Träff, A. M.; Ankner, T.; Wettergren, J.; Hilmersson, G. *Chem. Commun.* **2013**, *49*, 1826.
- (25) Fuchibe, K.; Mitomi, K.; Suzuki, R.; Akiyama, T. *Chem. Asian J.* **2008**, *3*, 261–271.
- (26) La Pierre, H. S.; Arnold, J.; Toste, F. D. *Angew. Chem. Int. Ed.* **2011**, *50*, 3900–3903.
- (27) Gianetti, T. L.; Tomson, N. C.; Arnold, J.; Bergman, R. G. *J. Am. Chem. Soc.* **2011**, *133*, 14904–14907.
- (28) Gianetti, T. L.; Nocton, G.; Minasian, S. G.; Tomson, N. C.; Kilcoyne, A. L. D.; Kozimor, S. A.; Shuh, D. K.; Tyliszczak, T.; Bergman, R. G.; Arnold, J. *J. Am. Chem. Soc.* **2013**, *135*, 3224–3236.
- (29) Tomson, N. C.; Arnold, J.; Bergman, R. G. *Organometallics* **2010**, *29*, 2926–2942.
- (30) Tomson, N. C.; Arnold, J.; Bergman, R. G. *Organometallics* **2010**, *29*, 5010–5025.
- (31) Akagi, F.; Matsuo, T.; Kawaguchi, H. *Angew. Chem. Int. Ed.* **2007**, *46*, 8778–8781.
- (32) Figueroa, J. S.; Piro, N. A.; Mindiola, D. J.; Fickes, M. G.; Cummins, C. C. *Organometallics* **2010**, *29*, 5215–5229.
- (33) Drobot, D. V.; Pisarev, E. A. *Russ. J. Inorg. Chem.* **1981**, *26*, 1–13.
- (34) Alaimo, P. J.; Peters, D. W.; Arnold, J.; Bergman, R. G. *J. Chem. Educ.* **2001**, *78*, 64.

- (35) Feldman, J.; McLain, S. J.; Parthasarathy, A.; Marshall, W. J.; Calabrese, J. C.; Arthur, S. D. *Organometallics* **1997**, *16*, 1514.
- (36) Budzelaar, P. H. M.; van Oort, A. B.; Orpen, A. G. *Eur. J. Inorg. Chem.* **1998**, *10*, 1485.
- (37) Frisch, M. J.; Trucks, G. W.; Schlegel, H. B.; Scuseria, G. E.; Robb, M. A.; Cheeseman, J. R.; Scalmani, G.; Barone, V.; Mennucci, B.; Petersson, G. A.; Nakatsuji, H.; Caricato, M.; Li, X.; Hratchian, H. P.; Izmaylov, A. F.; Bloino, J.; Zheng, G.; Sonnenberg, J. L.; Hada, M.; Ehara, M.; Toyota, K.; Fukuda, R.; Hasegawa, J.; Ishida, M.; Nakajima, T.; Honda, Y.; Kitao, O.; Nakai, H.; Vreven, T.; J. A. Montgomery, J.; Peralta, J. E.; Ogliaro, F.; Bearpark, M.; Heyd, J. J.; Brothers, E.; Kudin, K. N.; Staroverov, V. N.; Kobayashi, R.; Normand, J.; Raghavachari, K.; Rendell, A.; Burant, J. C.; Iyengar, S. S.; Tomasi, J.; Cossi, M.; Rega, N.; Millam, J. M.; Klene, M.; Knox, J. E.; Cross, J. B.; Bakken, V.; Adamo, C.; Jaramillo, J.; Gomperts, R.; Stratmann, R. E.; Yazyev, O.; Austin, A. J.; Cammi, R.; Pomelli, C.; Ochterski, J. W.; Martin, R. L.; Morokuma, K.; Zakrzewski, V. G.; Voth, G. A.; Salvador, P.; Dannenberg, J. J.; Dapprich, S.; Daniels, A. D.; Farkas, Ö.; Foresman, J. B.; Ortiz, J. V.; Cioslowski, J.; Fox, D. J. Gaussian09, Revision A.2; Gaussian, Inc.: Wallingford, CT, 2009.
- (38) Becke, A. D. *Phys. Rev. A* **1988**, *38*, 3098.
- (39) Lee, C. T.; Yang, W. T.; Parr, R. G. *Phys. Rev. B* **1988**, *37*, 785.
- (40) Harihara.Pc; Pople, J. A. *Theor. Chim. Acta.* **1973**, *28*, 213.
- (41) Harihara.Pc; Pople, J. A. *Mol. Phys.* **1974**, *27*, 209.
- (42) P. Fuentealba, P.; H. Preuss, H.; H. Stoll, H.; Szentpaly, L. V. *Chem. Phys. Lett.*, **1989**, *89*, 418.
- (43) *Quantum Chemistry: The Challenge of Transition Metals and Coordination Chemistry*, Wedig, U.; Dolg, M.; Stoll, H.; Preuss, H. Ed. A. Veillard, Reidel, and Dordrecht, **1986**, 79.
- (44) SMART: Area-Detector Software Package; Bruker Analytic X-ray Systems, I., Madison, WI, 2001-2003, Ed.
- (45) SADABS: Bruker-Nonius Area Detector Scaling and Absorption V2.05 Bruker Analytical X-ray Systems, I., Madison, WI, 2003.
- (46) Sheldrick, G. M. *Acta. Crystallogr. A* **2008**, *64*, 112.
- (47) Farrugia, L. J., *J. Appl. Crystallogr.* **1997**, *30*, 565, Ed.

## Chapter V

### **Carbon-Fluorine Bond Cleavage in Fluoroarenes via a Niobium (III) Imido Complex: From Stoichiometric to Catalytic Hydrodefluorination**

## Introduction

Due to their high bond strength and inherent kinetic inertness, C-F bonds are among the most difficult bonds to functionalize.<sup>1</sup> Additionally, recent studies have shown that chemically inert fluorinated compounds are persistent in nature, causing environmental issues.<sup>2</sup> The activation and functionalization of C-F bonds has received increasing interest over the past two decades;<sup>3,4</sup> such processes, especially hydrodefluorination, have been mediated by complexes involving metals from across the periodic table.<sup>5-8</sup> The metal-mediated cleavage of a C-F bond can occur via different pathways, depending on the type of C-F bond and the metal.<sup>9</sup> These include oxidative addition,<sup>3i-h,10</sup> metal-fluorine bond formation via hydrodefluorination from a metal hydride,<sup>4,5d,6c,7,8,11</sup> metal-carbon bond formation via elimination of HF,<sup>3f-i,12</sup> Si-F,<sup>6a-b,13</sup> B-F,<sup>14</sup> and Al-F bonds,<sup>5c,7c,15</sup> and nucleophilic attack by an electron-rich metal.<sup>16</sup>

The oxidative addition pathway is commonly seen in systems containing electron-rich transition metals. In the case of fluoroarene activation, it is known that the inertness of the C<sub>sp2</sub>-F bond toward most reagents increases when the degree of fluorination decreases; with complexes of precious metals, C-H activation is often kinetically preferred over C-F activation.<sup>3j-h,6a,17</sup> Due to these limitations, reports of catalytic transformation are often restricted to perfluorinated and/or heteroperfluorinated arene substrates. Additionally, these mechanisms often involve formation of  $\eta^2$ -arene-bound metal complexes,<sup>3j</sup> a coordination mode retained during the C-F activation transition state. The strong affinity between the electron-rich metal center and the electron-poor, highly fluorinated arenes further contributes to the scarce examples of monofluoroarene activation.<sup>3j</sup>

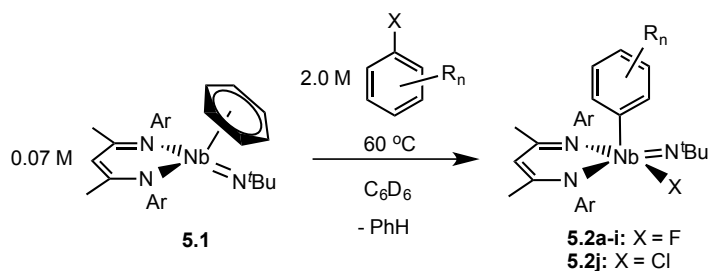
Although several heterogeneous systems can activate the strong C<sub>sp2</sub>-F bond of a less fluorinated arene, such as fluorobenzene, via either hydrodefluorination<sup>18</sup> or cross-coupling reactions,<sup>19</sup> in most cases the mechanism is not fully understood, and homogenous systems capable of performing such transformations remain rare.<sup>15a,20</sup> Therefore, mechanistic information involving fluorobenzene activation with well-defined molecular systems is required to improve our understanding of this activation process and allow for better catalyst design. Due to their propensity to favor coordination to electron-rich arenes, as well as the strength of their M-F bonds, reduced early transition metal systems could overcome the above-mentioned thermodynamic and kinetic limitations of C-F activation as well as allow the observation of arene-bound intermediates.

In our effort to develop new group 5 catalysts,<sup>21</sup> we reported the combination of an imido group and diketiminate ligand (BDI = 2,6-diisopropylbenzene- $\beta$ -diketiminate) as a successful platform to support both low and high valent niobium complexes<sup>22</sup> which engender some interesting stoichiometric and catalytic reactivity.<sup>22a,23</sup> Several reports have shown that in-situ reduction of NbCl<sub>5</sub> in the presence of fluorinated substrates leads to C-F activation.<sup>12b,24</sup> Driven by these results, we reported in chapter IV, remarkable reactivity of a reduced niobium species, resulting in triple C-F bond activation of benzylic CF<sub>3</sub> groups.<sup>25</sup> Experimental data revealed the intermediacy of an  $\eta^6$ -bound arene niobium (III) complex, from which C-F bond cleavage occurred stepwise. Further rearrangement involving the imido functionality led to a coordinated imine moiety.

We have now extended these studies to fluoroarene substrates, which result in the clean formation of formally oxidized niobium (V) aryl fluoride complexes. As mentioned above, activation of non-perfluorinated arenes, particularly mono- and di-fluorinated arenes is known, but remains rare and not well understood, especially with early transition metals. Additionally, previously reported systems often involve very expensive catalysts,<sup>20</sup> especially compared to the low price of niobium. In contrast to previous reports, selectivity toward substrates involving arenes with one or two C-F bonds over highly fluorinated arenes is observed, suggesting a novel approach from which a counter-intuitive trend of selective C-F activation could be obtained. The homogeneous and well-defined character of the organometallic species involved allowed for intensive spectroscopic analyses, which, supported by DFT calculations, sheds light on the mechanism of this unusual selectivity. Importantly, we have been able to characterize an arene bound intermediate of the type implicated in fluoroarene activation with late transition metals but never observed in early transition metal systems or prior fluorobenzene activation.<sup>20</sup> Additionally, we describe herein the homogenous catalytic hydrodefluorination of mono- and di-fluoroarenes, which is enabled through the use of a stoichiometric quantity of a silane reagent to abstract the fluoride from niobium.

## Results and discussion

**C-F bond activation of fluoroarenes.** The reaction of the niobium benzene complex **5.1**, [(BDI)NbN<sup>t</sup>Bu(C<sub>6</sub>H<sub>6</sub>)], with fluorobenzene resulted in efficient C-F activation to form a niobium (V) phenyl fluoride complex **5.2a**, under mild conditions (Table 5.1, entry 1). Qualitatively, the rate of C-F activation was dependent on the solvent, substrate, and substrate concentration: the transformation of fluorobenzene was much faster in neat fluorobenzene (entry 2) or 2.0 M fluorobenzene in mesitylene-*d*<sub>12</sub> (entry 3) as compared to 2.0 M in a C<sub>6</sub>D<sub>6</sub> solution (entry 1). Examination of a range of fluoroarenes showed that similar C-F activation occurs in most cases (see Table 5.1). Substrates allowing for different regioisomers, such as 1,2,3-trifluorobenzene (Table 5.1, entry 8), resulted in formation of a 2:1 mixture of the 2,3-difluorophenyl- and 2,6-difluorophenylniobium fluoride complexes **5.2f<sub>A</sub>** and **5.2f<sub>B</sub>**. However, with the 1,2,3,4-tetrafluorobenzene substrate, selective formation of the 2,3,6-trifluorophenylniobium fluoride regioisomer **5.2h** was observed (Table 5.1, entry 10 and Figure 5.1). Surprisingly, the reaction of 1,2,4,5-tetrafluorobenzene was relatively sluggish, with poor yields; and no conversion was observed with perfluorobenzene (Table 5.1, entry 11-12). In these cases, dimerization of complex **5.1** to form the previously reported dinobium inverted sandwich complex was found to be competitive with C-F activation.<sup>23c</sup> These results were unexpected since perfluorination typically results in more reactive C-F bonds.<sup>1</sup>

**Table 5.1** C-F bond activation of fluoroarenes

Entry	Complex	Substrate	Time	Yield <sup>[a]</sup> (%)	$r_{\text{relative}}$ <sup>[b]</sup>
1			3 h	98(1)	1
2 <sup>[c]</sup>	<b>5.2a</b>		½ h	100(1)	-
3 <sup>[d]</sup>			½ h	99(1)	-
4	<b>5.2b</b>		4 h	62(1)	0.54
5	<b>5.2c</b>		¼ h	98(1)	16
6	<b>5.2d</b>		¼ h	96(1)	11
7	<b>5.2e</b>		2 h	95(1)	1.3
8	<b>5.2f<sub>A/B</sub></b>		½ h	97(1)	4.0
9	<b>5.2g</b>		4 h	84(1) <sup>[e]</sup>	0.44
10	<b>5.2h</b>		6 h	79(1) <sup>[e]</sup>	0.36
11	<b>5.2i</b>		12 h	26(1) <sup>[e]</sup>	0.04
12	-		12 h	<1 <sup>[e]</sup>	<0.04 <sup>[f]</sup>
13	<b>5.2j</b>		¼ h	97(1)	>16 <sup>[f]</sup>

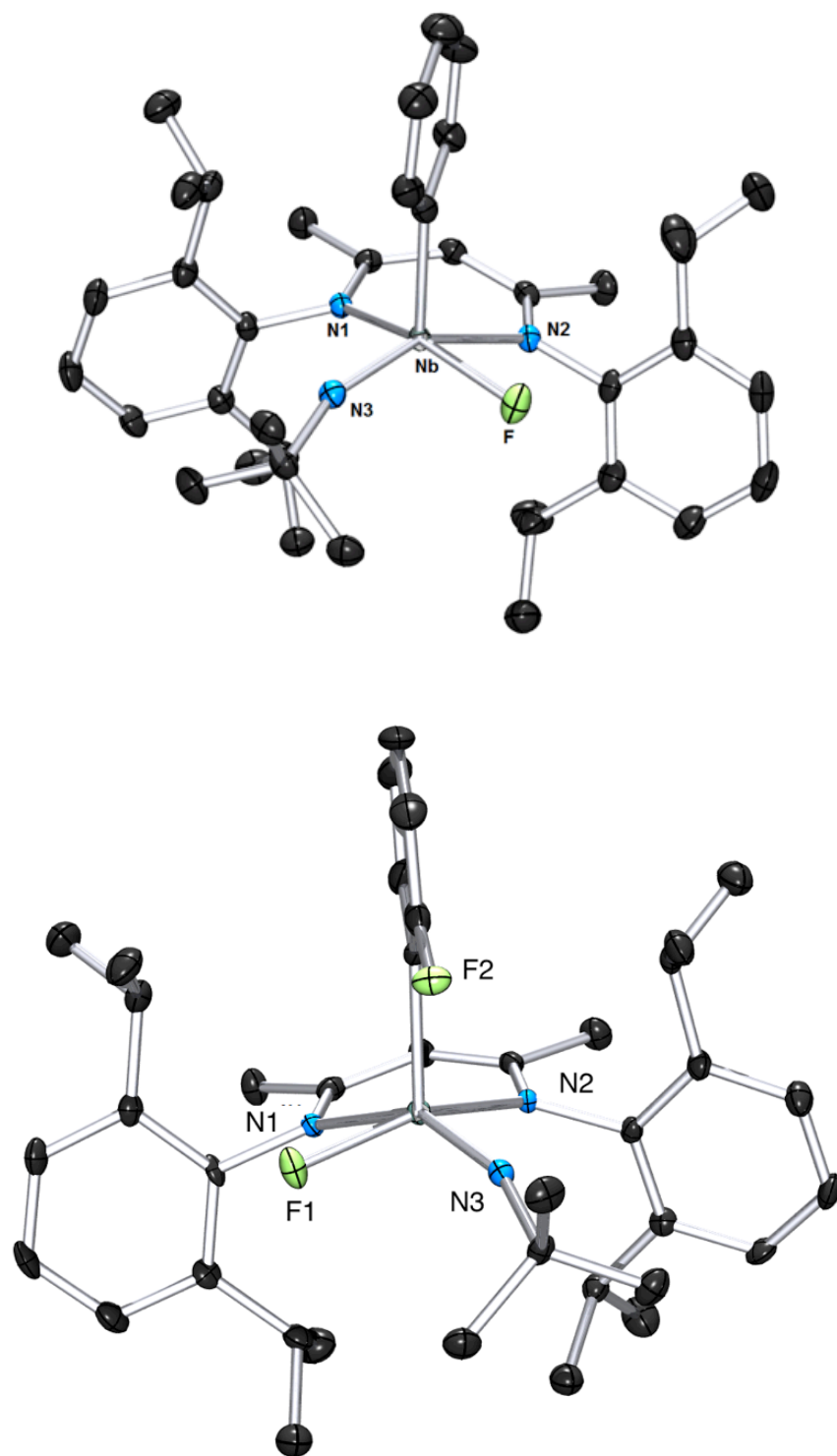
[a] Yields were calculated by integration of <sup>1</sup>H NMR spectra using 0.02 M of trimethoxybenzene as internal standard. [b] Relative rates were estimated via competition experiments between fluorobenzene and other fluoroarenes at 60 °C. [c] Sample in neat fluorobenzene with capillary containing a 0.02 M of trimethoxybenzene in C<sub>6</sub>D<sub>6</sub>. [d] 2.0 M fluorobenzene in mesitylene-*d*<sub>12</sub>. [e] The reaction was stopped at 100% conversion of complex **5.1**. [f] Due to the absence of either **5.2a** or **5.2x**,  $r_{\text{relative}}$  are estimated to be higher or lower than the faster or slower  $r_{\text{relative}}$  calculated.



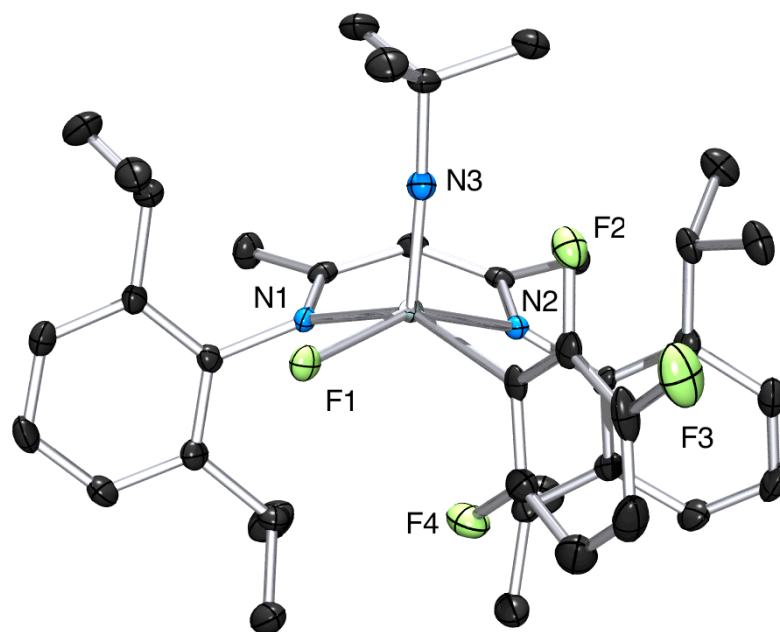
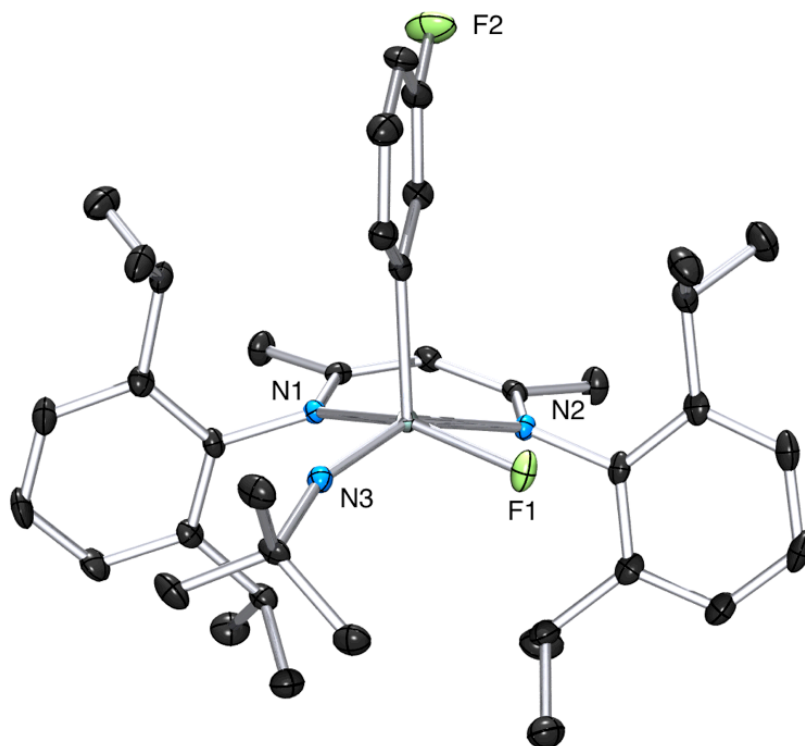
**Crystallographic analysis.** Complexes **5.2a-h** and **5.2j** were each isolated as yellow or orange crystals from Et<sub>2</sub>O, from reactions with neat fluoroarenes at 40 °C, in reasonable yields (47-91%). In the case of **5.2f**, a mixture of **5.2f<sub>A</sub>** and **5.2f<sub>B</sub>** was crystallized. Crystallographic analyses of **5.2a,c-d,h** confirmed the atom connectivity, revealing the presence of a diketimate niobium aryl fluoride in a square-based pyramidal geometry with the aryl group in the apical position for **5.2a,c-d** (Figure 5.1 and 5.2). The more sterically demanding trifluoroaryl moiety of **5.2h** occupies a basal position (Figure 5.2, bottom). The Nb-F distances (avg. 1.936(5) Å) and Nb-C<sub>Ar</sub> (avg. 2.167(4) Å) are similar to Nb-F and Nb-C<sub>aryl</sub> bonds previously observed in Nb(V) complexes (see Table 5.2).<sup>22b-c,25</sup> Although broad at room temperature, NMR resonances for **5.2a-h** became well resolved at T = 353 K, suggesting pseudorotation of the 5-coordinate species and/or hindered rotation of the aryl ligand.

**Table 5.2** Selected distances and bond angles for complexes **5.2a**, **5.2c-d,h**

	<b>5.2a</b>	<b>5.2c</b>	<b>5.2d</b>	<b>5.2h</b>
Nb-N <sub>1</sub> (BDI)	2.1422(14)	2.134(2)	2.1333(17)	2.194(2)
Nb-N <sub>2</sub> (BDI)	2.2968(14)	2.301(2)	2.3061(16)	2.180(2)
Nb-N <sub>3</sub> (Imido)	1.7659(14)	1.758(2)	1.7631(17)	1.746(3)
Nb-C <sub>1</sub> (Aryl)	2.1580(18)	2.176(3)	2.167(2)	2.246(2)
Nb-F <sub>1</sub>	1.93225(11)	1.9336(17)	1.9411(12)	1.946(2)
C-F <sub>2</sub>	-	1.246(4)	1.363(3)	1.359(3)
C <sub>1</sub> -Nb-F <sub>1</sub>	101.27(6)	100.74(9)	100.96(7)	85.33(7)
τ <sup>11</sup>	0.05	0.07	0.04	0.02



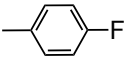
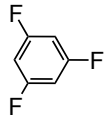
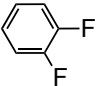
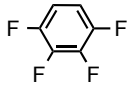
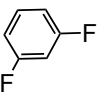
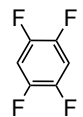
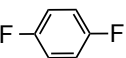
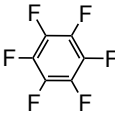
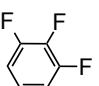
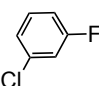
**Figure 5.1** ORTEP diagram of complexes **5.2a** (top) and **5.2c** (bottom). H atoms have been removed for clarity. Selected bond distances and angles are presented in Table 5.2.



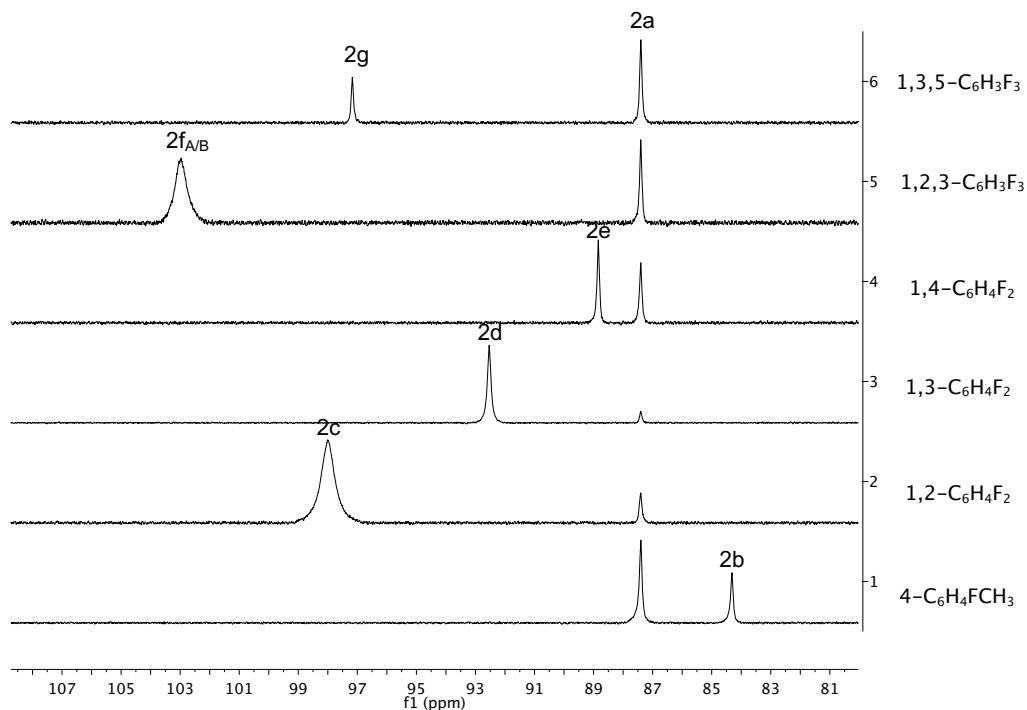
**Figure 5.2** ORTEP diagram of complexes **5.2d** (top) and **5.2h** (bottom). H atoms have been removed for clarity. Selected bond distances and angles are presented in Table 5.2.

**Mechanistic investigation.** While the above reactions were clean and quantitative in  $C_6D_6$ , a small amount of unidentified side product was observed, in either cyclohexane- $d_{12}$  or mesitylene- $d_{12}$ , preventing accurate kinetic analysis. Thus, to obtain further insight, relative rate ratios ( $r_{\text{relative}}$ ) were obtained via competition experiments carried out on mixtures containing equimolar concentrations of fluorobenzene and other fluoroarenes:  $r_{\text{relative}}$  corresponds to the product ratios **5.2x/5.2a** (see Tables 5.1 and 5.3, **5.2x = 5.2b-i**). These  $r_{\text{relative}}$  data revealed an unusual and non-linear trend. In spite of the low reactivity of more highly fluorinated aromatics, *ortho*- and *meta*-fluorination resulted in significant rate enhancement, with *ortho*-F having the biggest impact (Table 5.1, entry 5 and 6). This observation was further confirmed in a competition experiment between equimolar concentrations of 1,2- and 1,3-difluorobenzene, which led to formation of **2c** as the major product. On the other hand, *para*-fluorination resulted in a moderate rate enhancement (Table 5.1, entry 7). On the other hand, further fluorination of the ring affected the C-F activation, as shown by the significantly slower rates for the tetrafluorinated arene (Table 5.1, entry 10-11) and complete inhibition of activation for the perfluorinated substrate (Table 5.1, entry 12). As expected, a slower rate compared to those of fluorobenzene and difluorobenzene (but higher than that for the tetrafluorinated arene) is observed with the 1,3,5-trifluorobenzene ( $r_{\text{relative}} = 0.44$ , Table 5.1, entry 9). However, the significant rate enhancement of C-F activation of 1,2,3-trifluorobenzene is surprising and implies that the degree of fluorination is not the only factor governing the kinetics of C-F activation ( $r_{\text{relative}} = 3.95$ , an order of magnitude higher than 1,3,5-trifluorobenzene, Table 5.1, entry 8). A similar trend was observed in the tetrafluoroarenes, in which the relative rate of 1,2,3,4-tetrafluorobenzene was an order of magnitude higher than the 1,2,4,5-isomer (Table 5.1, entry 10-11,  $r_{\text{relative}} = 0.36$  and 0.04 respectively). Finally, when the mixed halogenated substrate 1-chloro-3-fluorobenzene was employed (Table 5.1, entry 13), selective activation of C-Cl bond was observed, with the largest  $r_{\text{relative}}$  consistent with both the weaker C-Cl vs. C-F,<sup>27</sup> bonds and the favorability of *meta*-fluorination.

**Table 5.3** Competition experiments and  $R_{\text{relative}}$  calculation.

Substrate	Integral 2a	Integral 2x	$R_{\text{relative}}$	Substrate	Integral 2a	Integral 2x	$R_{\text{relative}}$
	1	0.54	0.54		1	0.44	0.44
	1	16.2	16.2		1	0.36	0.36
	1	11.3	11.3		1	0.04	0.04
	1	1.30	1.30		1	nd	< 0.1 <sup>[a]</sup>
	1	3.95	3.95		nd	1	> 16 <sup>[a]</sup>

nd: not detected by NMR spectroscopy, [a]: Due to the non-detection of one complex,  $R_{\text{relative}}$  is estimated to be higher or lower than the faster or slower  $R_{\text{relative}}$  respectively.

**Figure 5.3**  $^{19}\text{F}$  NMR spectrum of the competition experiment between 1M of fluorobenzene and 1 M of other fluoroarenes.

Further mechanistic information was obtained by following the conversion of **5.1** to **5.2a** in mesitylene- $d_{12}$  via  $^1\text{H}$  and  $^{19}\text{F}$  NMR spectroscopies, which revealed the presence of several intermediates, although under these conditions their low concentrations hampered characterization. Thus, in an effort to avert competition from benzene coordination we carried out hydrogenolysis of **5.3** in the presence of fluorobenzene in mesitylene- $d_{12}$  and monitored the reaction at low temperature by  $^1\text{H}$  and  $^{19}\text{F}$  NMR. Under these conditions, the previously reported cyclometallated hydride **5.A** was first observed. Over time, the concentration of a second intermediate increased, allowing its assignment as the  $\eta^6$ -fluorobenzene-bound complex **5.B** (Scheme 5.1 and Figure 5.4). Upon warming the sample, conversion to the final product **5.2a** was observed (see Figures 5.5 and 5.6).

To further understand the lack of reactivity of highly fluorinated substrates, hydrogenolysis of **5.3** was carried out in mesitylene- $d_{12}$  in the presence of  $\text{C}_6\text{F}_6$ . While intermediate **5.A** was observed, we saw no evidence for an arene-bound intermediate or C-F activation. Instead, the same mixture of products previously observed during hydrogenolysis in hexanes was formed (Scheme 5.1,  $[(\text{BDI})\text{Nb}(\text{N}^t\text{Bu})(\text{H})]_2$  complex **5.4** and  $(\kappa_4\text{-CNNC-BDI})\text{Nb}(\text{N}^t\text{Bu})$  complex **5.5**).<sup>25</sup> Taken together, the nature of the observed intermediates with fluorobenzene, the solvent dependence, and the lack of C-F activation of highly fluorinated arenes suggest that arene coordination to form **5.B**, an interaction that is maintained in the subsequent transition state, is a critical requirement for C-F activation.

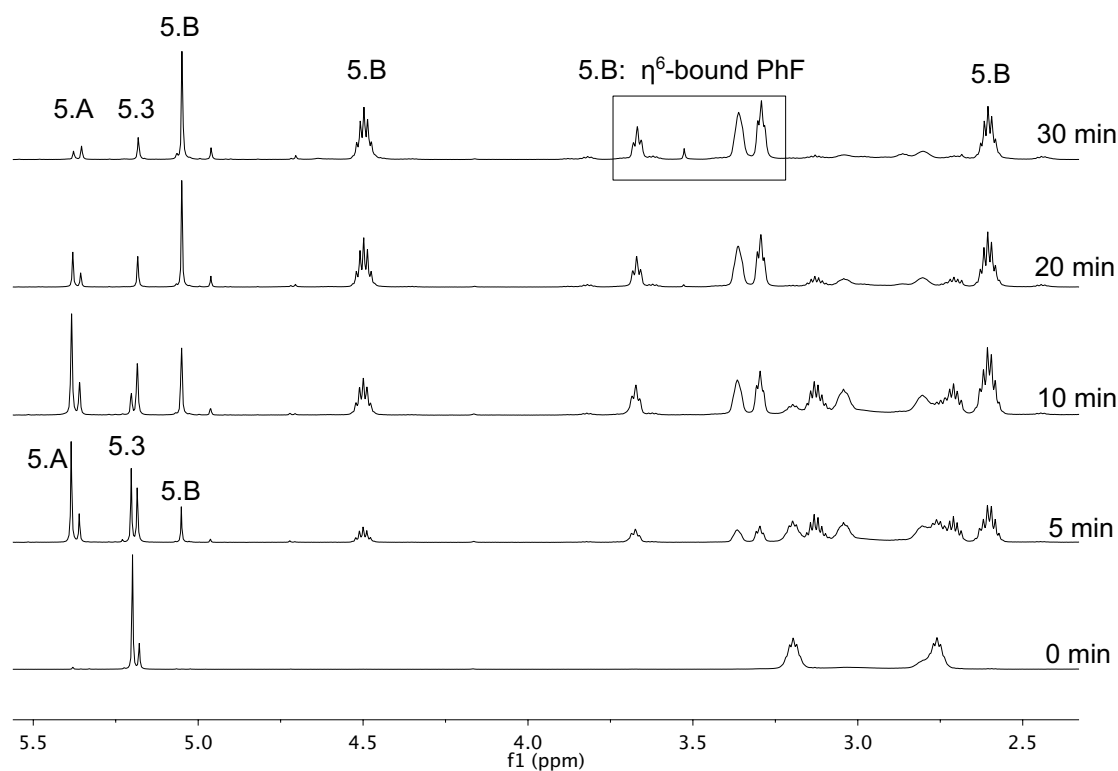


**Figure 5.4**  $^1\text{H}$  NMR monitoring upon time of the formation of complex **5.B** from hydrogenolysis of **5.3** at 263 K in the 2.4-5.5 ppm range.

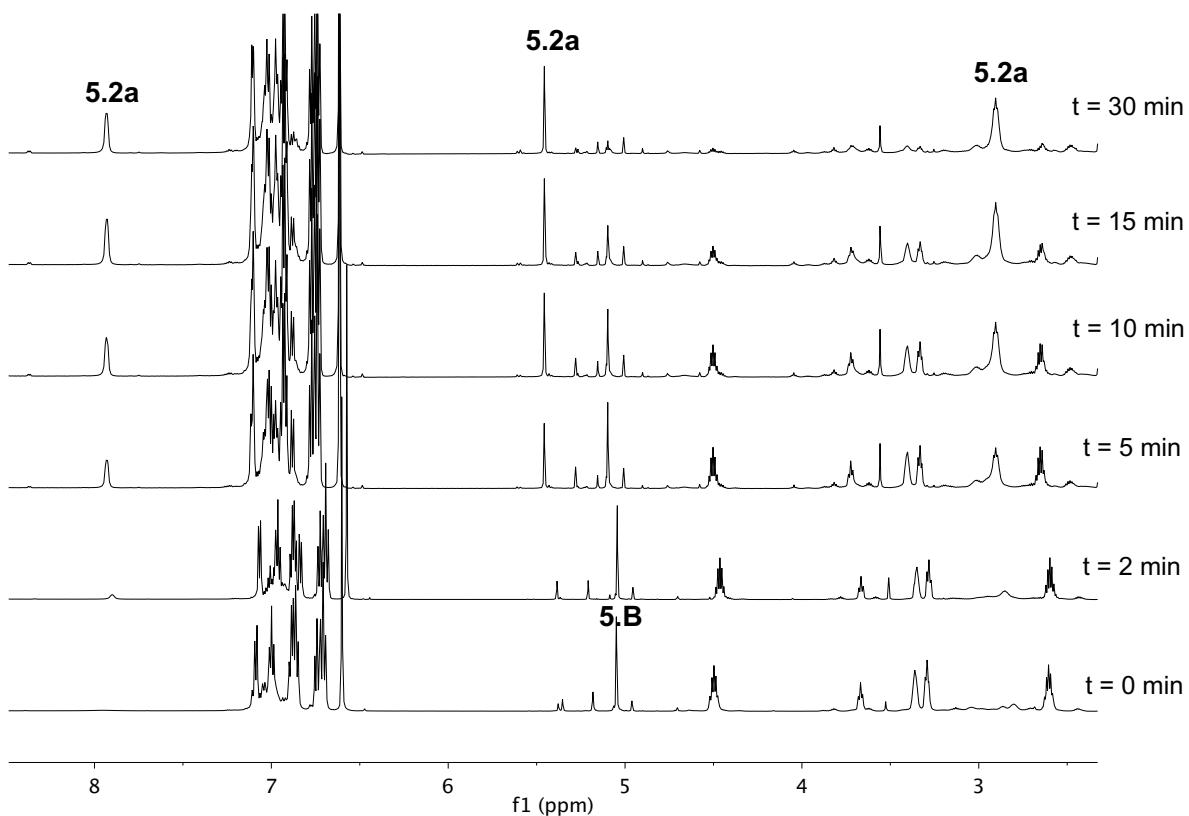


**Figure 5.5** Formation of complex **5.2a** and disappearance of **5.B** with time.  $^1\text{H}$  NMR spectra recorded at 313 K.

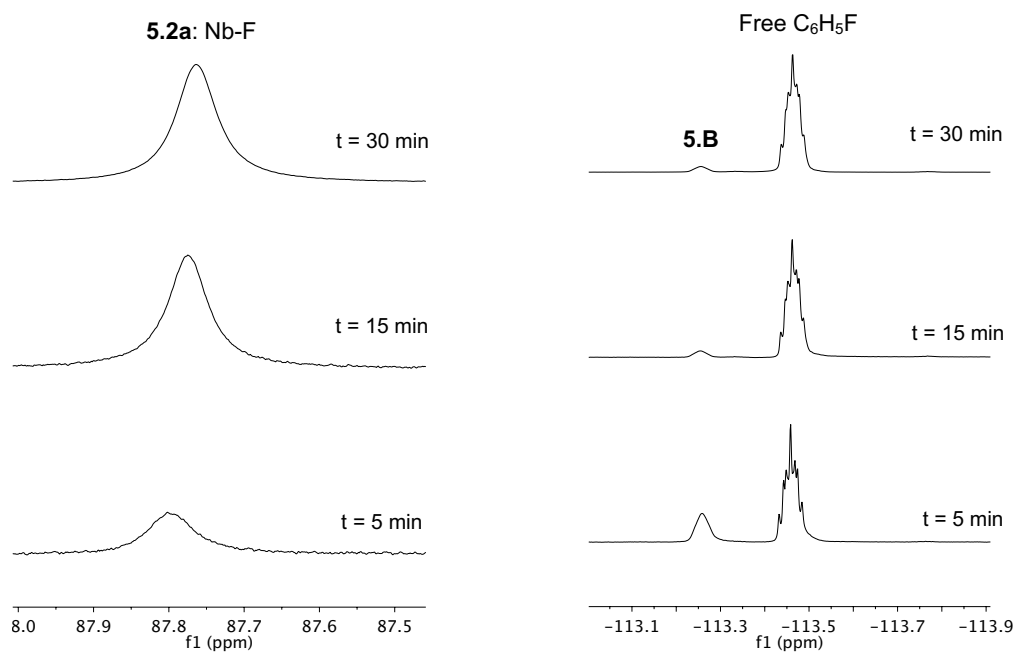
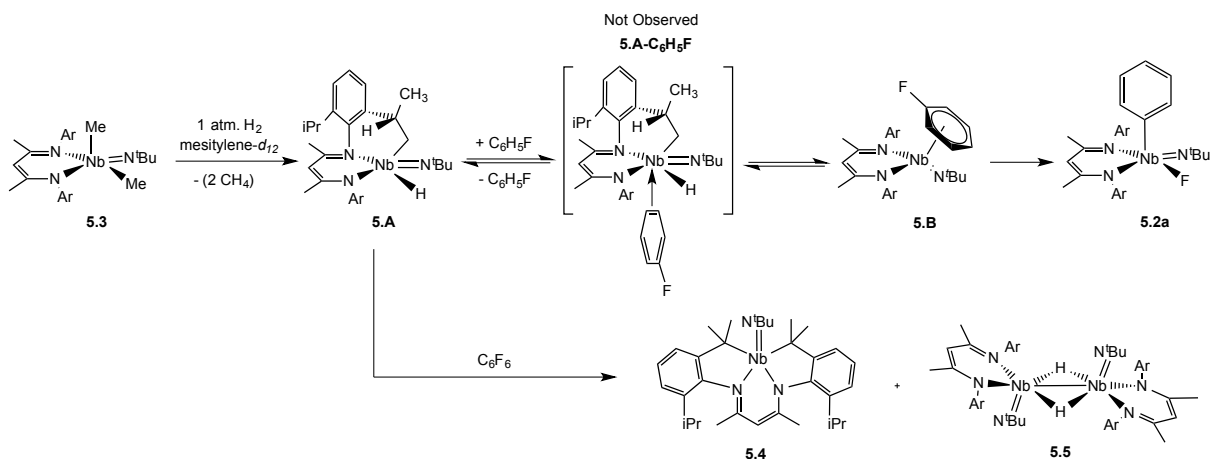


**Figure 5.6** Formation of complex **5.2a** (left) and disappearance of **5.B** (right) with time.  $^{19}\text{F}$  NMR spectra recorded at 313 K.



**Scheme 5. 1** Proposed mechanism for the selective activation of non-perfluorinated arenes.

**DFT calculation.** While **5.B** was found experimentally to be a key intermediate in the C-F activation of fluoroarene, the mechanism of its conversion to the final product **5.2a** remained unclear (Scheme 5.1). To address this, we turned to DFT calculations for additional mechanistic information (Scheme 5.2). These calculations showed the presence of a very exergonic C-F activation (Scheme 5.6,  $\Delta G_{5.B' \rightarrow 5.2a'} = -45 \text{ kcal.mol}^{-1}$ ), consistent with the formation of strong Nb-F bonds ( $\text{BDE}_{\text{Nb-F}} = 137 \text{ kcal.mol}^{-1}$ ).<sup>28</sup> In the first path, the arene-bound complex slips from its  $\eta^6$ -mode in **5.B'**, to an  $\eta^2$ -mode (in **5.C**). This reorganization allows the C-F bond to be held closer to the metal center leading to transition state, **5.D**, which maintains coordination to the arene and leads to oxidative addition of the C-F bond. The structure of **5.D** is best described as involving  $\eta^3$ -coordination, with a single C-F moiety. Transition state **5.D** was found to be relatively high energy for a room-temperature transformation ( $\Delta G = 33 \text{ kcal.mol}^{-1}$  relative to **5.B'**). This high activation energy can be attributed to the strong arene distortion required to allow orbital overlap between the metal center and the C-F  $\sigma$ -bond leading to the oxidative addition step. Attempts to locate a more conventional concerted oxidation addition transition state were unsuccessful, collapsing either on **5.C** or **5.D**. Still, DFT calculations suggest that a less energetically demanding pathway is possible in which the distorted arene is stabilized via formation of an arene-bridged inverted sandwich complex. From **5.F**, C-F bond cleavage followed by dissociation of the second metal center leads to the fluoroaryl complex **5.2a'** and reformation of an equivalent of **5.B'** (see Scheme 5.2). Larrosa *et. al.* have recently reported that C-H arylation of unreactive arenes was rendered possible via  $\pi$ -complexation of a  $\text{Cr}(\text{CO})_3$  unit, greatly enhancing the reactivity of the aromatic C-H bonds.<sup>29</sup> Along our bimetallic pathway, dissociation of fluorobenzene from one molecule of **5.C** generates a 3-coordinate species **5.E** which reacts with another equivalent of **5.B'** to form complex **5.F**. Although arene dissociation from the metal center is energetically demanding, formation of the bimetallic intermediate **5.F** is thermodynamically favored ( $\Delta G = -10.9 \text{ kcal.mol}^{-1}$ , with a  $\Delta H = -9.57 \text{ kcal.mol}^{-1}$ , and a  $\Delta S = +4.3 \text{ cal.mol}^{-1}.\text{K}^{-1}$ ). Such a transformation is analogous to (and in accord with) the isolated benzene- and toluene-bridged complexes that we recently reported.<sup>23c</sup> At transition state **5.G**, coordination of a second “BDINb=NtBu” moiety resulted in a



stabilization of 13 kcal/mol of the C-F activation step itself. Similarly to the ortho-, meta-, and para-fluorination trend observed experimentally, the coordination of second Nb moiety may stabilize the partial negative charge that builds up on the ring via  $\pi$ -back donation, thereby lowering the C-F activation barrier.

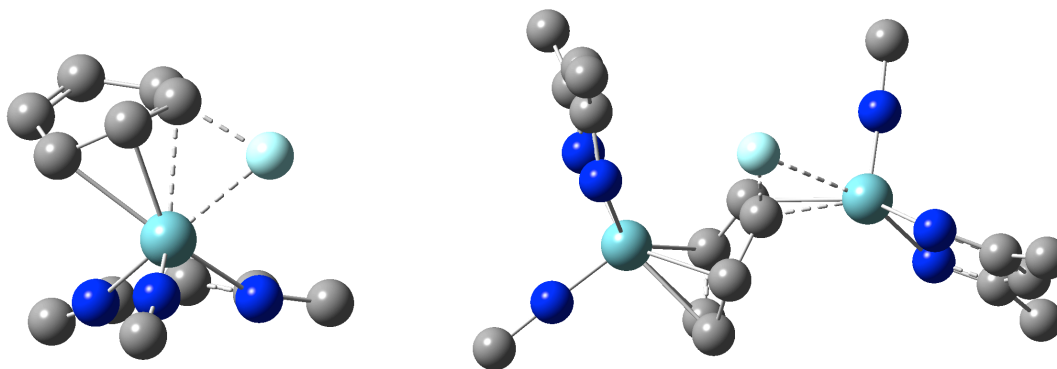
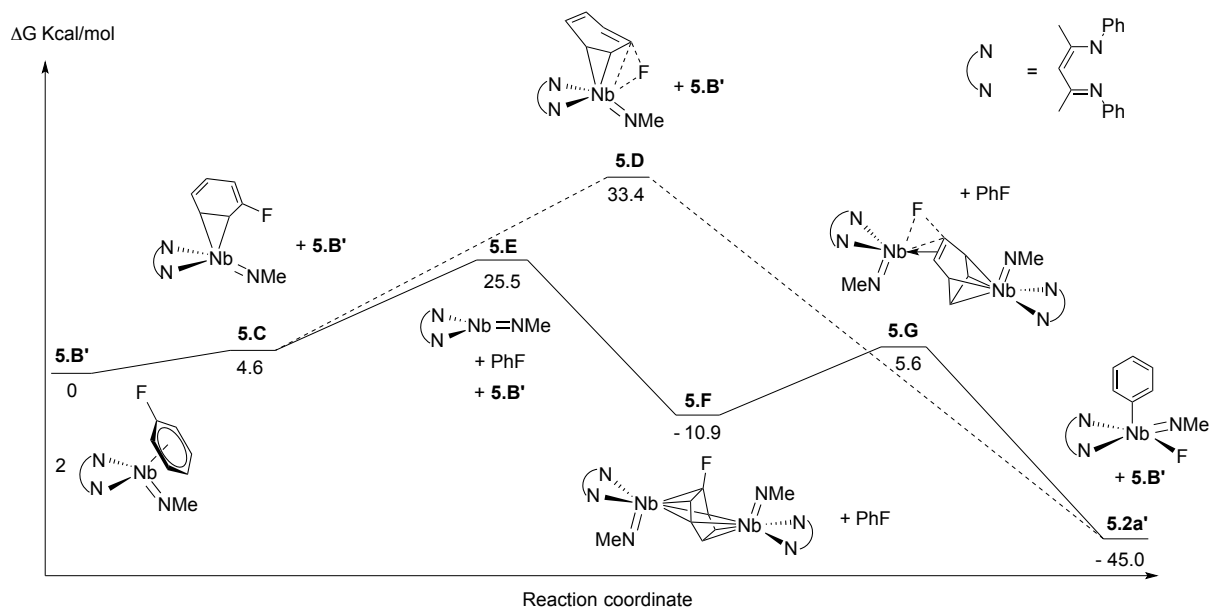


**Figure 5.7** Optimized structures of transition states **5.D** (left) and **5.G** (right). Hydrogen atoms and phenyl groups are removed for clarity.

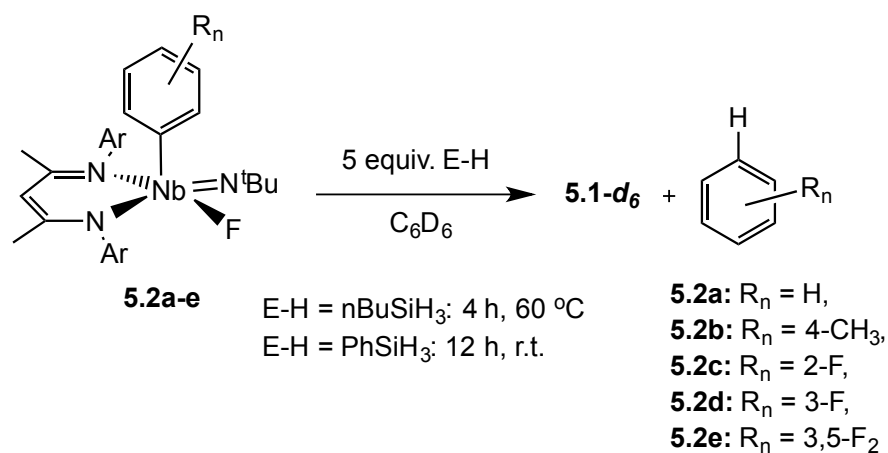
An alternative path was also investigated, in which oxidative addition of the ortho C-H bond occurs first, followed by  $\beta$ -F elimination and C-H recombination (see Appendix C.2). Nevertheless, the significant amount of Nb-X character present in the transition state involving C-X bond activation (X = F, H) results in a lower activation barrier (by 10 kcal/mol) for the thermodynamically-favored Nb-F bond formation compared to the Nb-H interaction.



**Scheme 5.2** DFT calculation on the conversion from **5.B'** to **5.2a'** using PBE1PBE hybrid functional, 6-311G(d,p) basis for light atoms (H, C, N and F) and Stuttgart/Dresden ECPs pseudopotential basis (SDD) for niobium (see Appendix C.2).

Regardless of the above insights, the nonlinear rate dependence of differently fluorinated arenes is still perplexing. Although other factors are undoubtedly also involved, we find it significant that qualitatively the arenes capable of undergoing reasonably efficient C-F activation are those in which the metal can first coordinate to a non-fluorinated C2 moiety in the arene. When only mono-fluorinated (1,3,5-trifluoroarene) or doubly fluorinated (1,2,4,5-tetrafluoroarene, and hexafluorobenzene) C2 moieties are available, the rate decreases substantially. As noted above, we have experimental evidence that reversible  $\pi$ -coordination precedes the C-F activation rate-determining step. NMR monitoring of the reaction in mesitylene- $d_{12}$  showed that the conversion from the metallacyclic hydride intermediate **5.A** to the arene adducts is dependent on the nature of fluoroarene. We believe that coordination to the hydride **5.A**, to form **5.A-C<sub>6</sub>H<sub>5</sub>F** (see Scheme 5.1), is required to induce reductive elimination to form a niobium (III) arene adduct.<sup>30</sup> Coordination of fluoroarenes that lack a non-fluorinated C2 moiety (Table 5.1, entry 11-12) will be in competition with the formation of the inverted sandwich complex in C<sub>6</sub>D<sub>6</sub> (or with the ligand activation species in mesitylene- $d_{12}$ ) (Scheme 5.1). Additionally, our computations indicate that the arene pre-coordination interaction of the metal center with a non-fluorinated C2 moiety of the arene appears to be energetically favored (see Scheme 5.2). These calculations also indicate that in the more energetically favored bimetallic pathway, arene dissociation (required for formation of the bimetallic species) is the rate-limiting step, suggesting that the nature of the arene (i.e. its steric and electronic properties) governs the kinetics of the reaction. Finally, the intramolecular selectivity (with 1,2,3,4-C<sub>6</sub>H<sub>2</sub>F<sub>4</sub>, Table 5.1 entry 10) and lack of selectivity (with 1,2,3-C<sub>6</sub>H<sub>3</sub>F<sub>3</sub>, Table 5.1 entry 8) is perplexing. However, it suggests that a non-fluorinated C2 moiety, not only facilitate the formation of the arene bound intermediate **5.B**, but its position on the ring influence the rate of C-F activation.

**Hydrodefluorination of fluoroarenes.** Stoichiometric hydrodefluorination was observed when **5.2a-d,g** were treated with 5 equiv. of nBuSiH<sub>3</sub> in C<sub>6</sub>D<sub>6</sub> at 60 °C for 4 h. NMR spectroscopy and GC/MS are in agreement with clean and quantitative formation of the C<sub>6</sub>D<sub>6</sub> bound complex **5.1-d<sub>6</sub>**, along with the free organic product and nBuSiF<sub>3</sub> (Scheme 5.3 and SI). No reaction between the fluorinated organic product and complex **5.1-d<sub>6</sub>** was detected during the course of the reaction, consistent with the concentration dependence in substrate and its coordinative competition with solvent (e.g. C<sub>6</sub>D<sub>6</sub>) in the C-F activation step. Similar reactivity was observed using 5 equiv. of PhSiH<sub>3</sub> within several hours at room temperature. Faster hydrodefluorination was achieved at higher temperature, although some decomposition of complex **5.1-d<sub>6</sub>** was observed above 50 °C.



**Scheme 5.3** Stoichiometric hydrodefluorination of fluoroarenes.

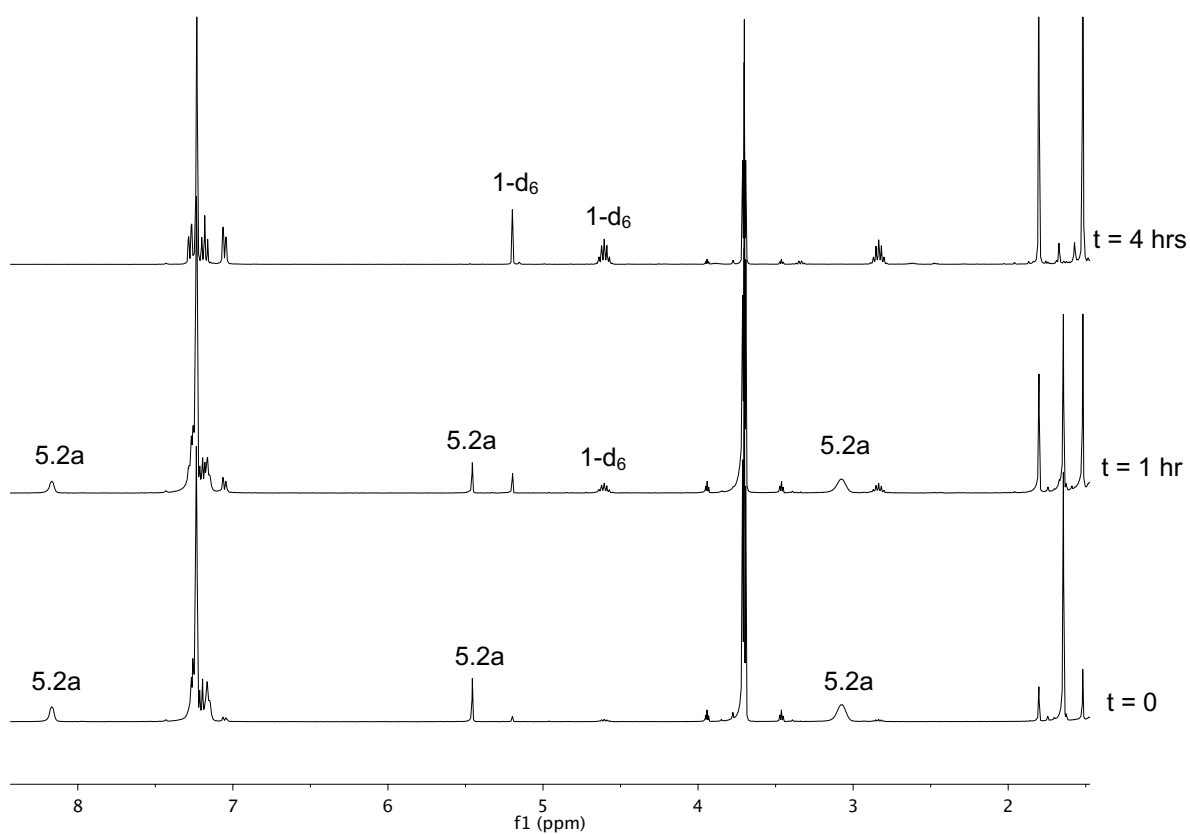
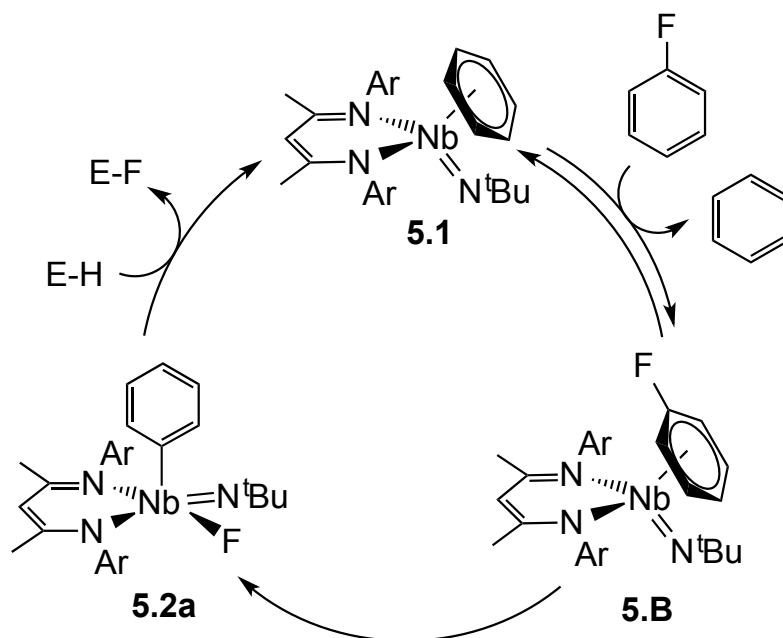


**Figure 5.8** Example of <sup>1</sup>H monitoring of stoichiometric hydrodefluorination of fluorobenzene with nBuSiH<sub>3</sub>.

The data presented above suggested to us that, under appropriate conditions, hydrodefluorination using catalytic loadings of niobium might be possible (Scheme 5.4). Accordingly, preliminary catalytic activity was investigated by  $^{19}\text{F}$  NMR spectroscopy on a solution containing 3.0 M of substrates in mesitylene, 0.05 M of catalyst and 0.11-0.33 M silanes (5-15 mol % catalyst loading relative to the concentration of one hydride, Table 5.4 and Tables 5.6-5.7). Yields and TON were calculated by integrating the peaks of the  $\text{RSiF}_3$  formed as compared to 0.07 M of  $\text{C}_6\text{F}_6$  used as internal standard. For the 1,2- and 1,3-difluorobenzenes, the yields were further confirmed by integrating the peak of the fluorobenzene product compared to that of 1.0 M of 2-fluorobiphenyl in mesitylene in a capillary tube (see experimentals for calibration).

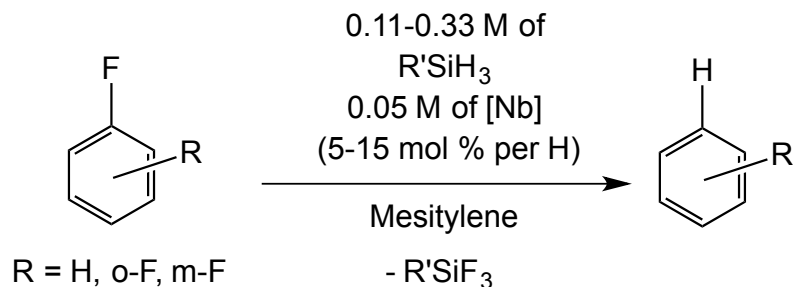


**Scheme 5.4** Proposed mechanism for catalytic hydrodefluorination of fluorobenzene.

First, catalytic activity of **5.1** was tested toward fluorobenzene, which showed limited conversion (Table 5.4, entry 1). The low conversion was attributed to catalyst degradation by the hydride source, since extended reaction times, concentration of silanes higher than 0.11 M and higher temperature resulted in little to no conversion (Table 5.6, entries 1-4). Meanwhile, in neat substrates, in which C-F activation is faster, higher conversion was observed (Table 5.4, entry 2). These data suggest that the nature of the catalyst resting state (**5.1** vs. **5.2a**) and its stability under catalytic conditions, have a pronounced effect on catalysis. Consistent with the above data, catalytic activity was improved when complex **5.2a** was formed in-situ by treating **5.1** with fluorobenzene for 30 min at 60 °C, prior to silane addition (Table 5.4, entry 3). Under these conditions, high catalyst activity was observed. Additionally, using  $\text{PhSiH}_3$  as the hydride source resulted in poor conversion, also consistent with catalyst degradation since this silane was found to react readily with **5.1** at elevated temperature. Extending this reactivity to other poorly activated fluorobenzenes such as 1,2- and 1,3-difluorobenzenes using **5.1** as a precatalyst also resulted in good catalytic

activity with both silanes, even at higher silane concentration (Table 5.4, entries 5-8,  $[\text{R}'\text{SiH}_3] = 0.33 \text{ M}$ ). This is in accord with a faster C-F activation of difluorinated arenes relative to fluorobenzene ( $r_{\text{relative}} = 42$  and  $23$ , for 1,2- and 1,3-difluorobenzene respectively), resulting in a faster conversion of the reactive Nb(III) species to the more stable Nb(V) resting state, effectively competing with catalyst degradation.

**Table 5.4** Catalytic monodefluorination of fluoroarenes.



Entry	ArF (3.0 M)	Product	[Nb]	R'SiH <sub>3</sub>	T (°C)	TON <sup>[a]</sup>	
1			<b>5.1</b>	R = nBu	70	<1	
2 <sup>[b]</sup>							4
3				R = nBu	70	5	
4				R = Ph	40	1	
5			<b>5.2<sup>[c]</sup></b>	R = nBu	70	18	
6				R = Ph	40	16	
7				R = nBu	70	19	
8				R = Ph	40	17	

[a] Turnover numbers (TON) were determined, after 16 h, relative to the concentration of  $\text{R}'\text{SiF}_3$  formed. [b] In neat fluorobenzene. [c] Complexes **5.2a-c** were generated in-situ by reacting **5.1** with the corresponding fluoroarene for 30 min at 60 °C prior to hydride addition.

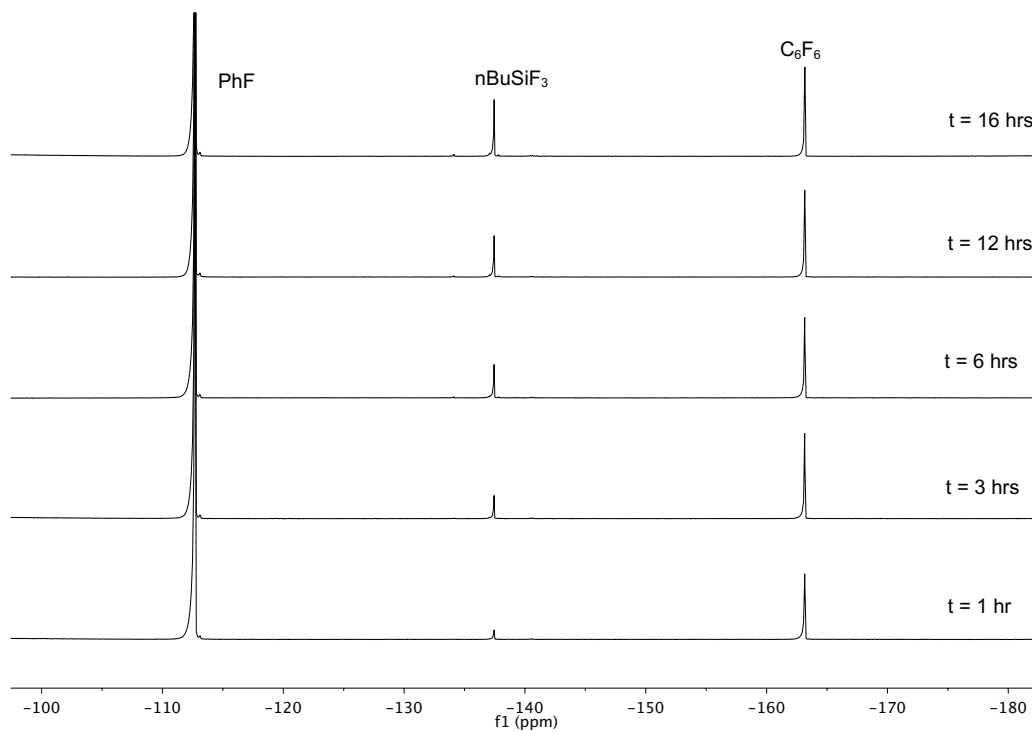


**Figure 5.9** Example of  $^{19}\text{F}$  NMR monitoring of catalytic hydrodefluorination of fluorobenzene with  $\text{nBuSiH}_3$  using  $\text{C}_6\text{F}_6$  as internal standard

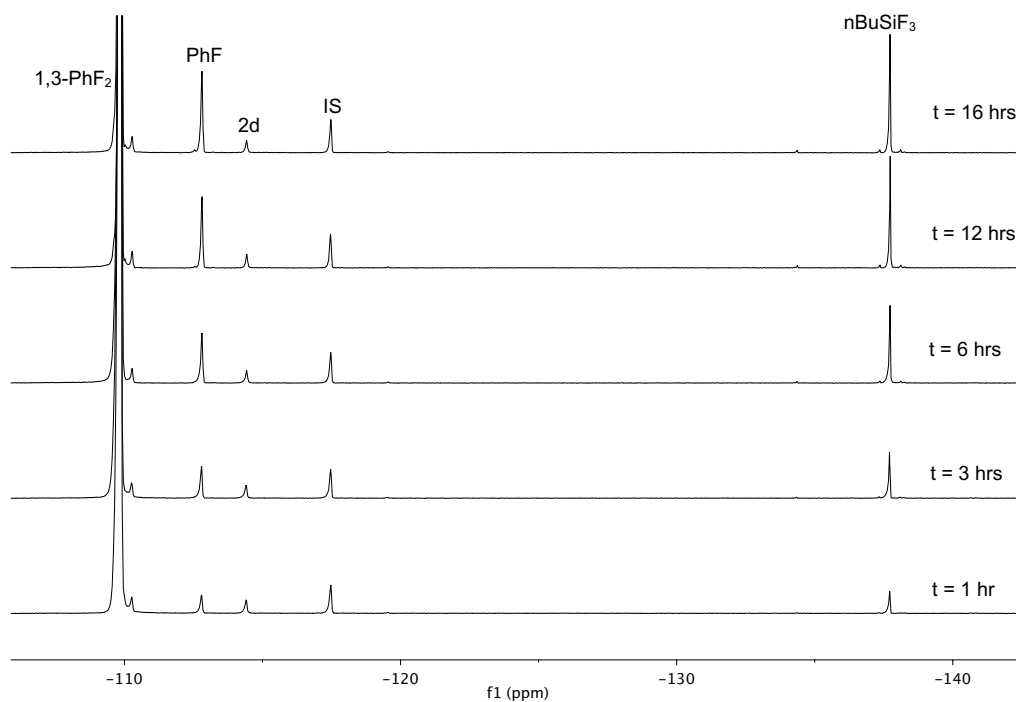


**Figure 5.10** Example of  $^{19}\text{F}$  NMR monitoring of catalytic hydrodefluorination of 1,3-difluorobenzene with  $\text{nBuSiH}_3$

## Conclusions

In this report we provide the first experimental evidence implicating  $\eta^6$ -arene-bound complexes in C-F bond activation reactions of fluoroarenes. These  $\pi$  interactions are maintained in the rate-determining transition-state and thus play a vital role in promoting this reactivity. To allow the formation of these arene bound species, coordination of the fluoroarene to the metallacyclic hydride intermediate **5.A** is required to induce reductive elimination; indeed, their involvement is crucial to understanding the very specific selectivity observed. Additionally, DFT calculations suggest that a bimolecular process facilitates the transformation by stabilizing the arene distortion required during the C-F oxidative addition rate-limiting transition state. Finally, challenging stoichiometric and catalytic hydrodefluorinations of mono- and difluorinated arenes under mild conditions have been achieved. Work is in progress to further probe the mechanism and to optimize and extend the scope of catalysis.

## Experimental

**General Considerations** Unless otherwise noted, all reactions were performed either using standard Schlenk line techniques or in an MBraun inert atmosphere glove box under an atmosphere of purified nitrogen (<1 ppm O<sub>2</sub>/H<sub>2</sub>O). Glassware, cannulae, and Celite were stored in an oven at *ca.* 160 °C for at least 12 hrs prior to use. Hexanes, Et<sub>2</sub>O, THF, DCM and toluene were purified by passage through a column of activated alumina, stored over 3 or 4 Å molecular sieves, and degassed prior to use.<sup>31</sup> Benzyl fluoride, fluorobenzene, 1,2-, 1,3- and 1,4-fluorobenzenes, 1,2,3- and 1,3,5-trifluorobenzenes, 1,2,4,5-tetrafluorobenzene, pentafluorobenzene, and perfluorobenzene were dried and stored over 4 Å molecular sieves. Deuterated solvents (C<sub>6</sub>D<sub>6</sub>, C<sub>7</sub>D<sub>8</sub> and mesitylene-*d*<sub>12</sub>) and mesitylene were dried over sodium/benzophenone; and then vacuum transferred to a storage flask containing activated molecular sieves. *N,N'*-bis-(2,6-diisopropylphenyl)- $\beta$ -diketiminate (BDI),<sup>32</sup> Li(BDI)·Et<sub>2</sub>O,<sup>33</sup> (BDI)pyCl<sub>2</sub>Nb(N<sup>*t*</sup>Bu),<sup>34</sup> (BDI)(Me)<sub>2</sub>Nb(N<sup>*t*</sup>Bu),<sup>34</sup> (BDI)( $\eta^6$ -benzene)<sub>2</sub>Nb(N<sup>*t*</sup>Bu),<sup>35</sup> were prepared using literature procedures. All other reagents were acquired from commercial sources and used as received. NMR spectra were recorded on Bruker AV-300, AVQ-400, AVB-400, DRX-500, AV-500, and AV-600 spectrometers. Chemical shifts were measured relative to residual solvent peaks, which were assigned relative to an external TMS standard for <sup>1</sup>H/<sup>13</sup>C and BF<sub>3</sub>·OEt<sub>2</sub> for <sup>19</sup>F set at 0.00 ppm. <sup>1</sup>H and <sup>13</sup>C NMR assignments were routinely confirmed by 135/90 DEPT, <sup>1</sup>H-<sup>1</sup>H (COSY, NOESY) and <sup>1</sup>H-<sup>13</sup>C (HSQC and HMBC) experiments. GC/MS analyses were performed using a Agilent 6890 N Network GC system coupled to a 5973 Network mass selective detector. The uncorrected melting points were determined using sealed capillaries prepared under nitrogen on an Optmelt SRS. Elemental analyses were performed at the School of Human Sciences, Science Center, London Metropolitan University. The X-ray structural determinations were performed at CHEXRAY, University of California, Berkeley on Bruker SMART APEX or SMART QUAZAR diffractometers.

**NMR scale reactions.** Complex **5.1**, (BDI)( $\eta^6$ -C<sub>6</sub>H<sub>6</sub>)Nb(N<sup>*t*</sup>Bu) (18.5 mg, 0.028 mmol, 0.07 M) was dissolved in 0.4 ml of C<sub>6</sub>D<sub>6</sub> containing 2.0 M of fluoroarene and 0.02 M of trimethoxybenzene as internal standard, and the resulting solution was added to a J-Young NMR tube with a Teflon cap. The NMR tube was either stored at room temperature or heated

at 60 °C depending on the condition described in table 1 of the manuscript. The yield of each reaction was calculated by integrating the peak corresponding to the CH of the BDI backbone ( $HC(C(Me)NAr)_2$ ) of the new complex, commonly observed in the 5.5-5.0 ppm range, relative to the peak at 6.25 ppm of the internal standard ( $C_6H_3(OCH_3)_3$ ) by  $^1H$  NMR. In the case of 1,3,5-trifluorobenzene, the overlap between the substrates and the internal standard forced us to use the signal at 3.42 ppm corresponding to the methoxy group of the internal standard ( $C_6H_3(OCH_3)_3$ ). Due to the strong signals of the substrates, the yields were further confirmed by removing the volatile materials under high vacuum, adding 0.4 mL of fresh  $C_6D_6$  to the J-Young NMR tube, and reanalyzing the solution by NMR.

**Competition experiment 1,2- vs 1,3- difluorobenzene:** Complex **5.1** ( $(BDI)(\eta^6-C_6H_6)Nb(N^tBu)$ ) (18.5 mg, 0.028 mmol, 0.07 M) was dissolved in 0.4 ml of  $C_6D_6$  containing 1.0 M of 1,2-difluorobenzene, 1.0 M of 1,3-difluorobenzene and 0.02 M of trimethoxybenzene as internal standard. The resulting solution was added to a J-Young NMR tube with a Teflon cap. The NMR tube was heated at 60 °C for 30 min. The yield of each complex, **5.2c** and **5.2d**, was calculated relative to the amount of internal standard by  $^1H$  NMR

**Determination of relative rates:** Complex **5.1** ( $(BDI)(\eta^6-C_6H_6)Nb(N^tBu)$ ) (18 mg, 0.027 mmol, 0.07 M) was dissolved in 0.4 ml of  $C_6D_6$  containing 1.0 M of fluorobenzene (45 mL), 1.0 M of fluoroarene and 0.02 M of trimethoxybenzene as internal standard. The resulting solution was added to a J-Young NMR tube with a Teflon cap. The NMR tube was heated at 60 °C and monitored every 30 min. The relative rate between the two complexes, **5.2a** : **5.2x** (x= b-h), was calculated using the integral ratio of  $^{19}F$  NMR resonance of Nb-F (Table 5.3 and Figure S.2, bottom) and further confirmed by the integral ratio of the CH backbond of the BDI ligand in the  $^1H$  spectrum.

**General method for the synthesis of complexes 5.2a-f,h.** Each fluoroarene (10 mL) was added to a 25-mL Schlenk flask containing ( $(BDI)(\eta^6-C_6H_6)Nb(N^tBu)$ ) (0.120 g, 0.182 mmol, 1.0 equiv.) at room temperature. The dark red solution was heated to 60 °C. The color of the solution turned from dark red to yellow/orange within 15 to 45 min depending on the substrate. After 3 h, the volatile materials were removed under reduced pressure to yield a yellow/orange residue. Trituration with  $Et_2O$  ( $2 \times 5$  ml), extraction with hexane (20 ml), and storage at -40 °C overnight afforded yellow crystals, which were collected by filtration.

**[(BDI)Nb( $N^tBu$ )(Ph)(F)], 5a.** Yield: 97 mg, 0.143 mmol, 79%. X-ray suitable crystals were obtained by recrystallization from hexanes at -40 °C.  $^1H$  NMR (500 MHz,  $C_7D_8$ , 293 K):  $\delta$  (ppm) 8.05 (b, 2 H, *Ph*-Nb), 7.18-6.96 (broad, Ar), 5.39 (s, 1 H,  $HC(C(Me)NAr)_2$ ), 2.96 (broad sept, 4 H,  $CHMe_2$ ), 1.58 (s, 6 H,  $HC(C(Me)NAr)_2$ ), 1.21 (b, 6 H,  $CHMe_2$ ), 1.08 (d, 12 H,  $CHMe_2$ ,  $^3J_{HH}=6.6$  Hz), 1.0 (b, 6 H,  $CHMe_2$ ), 0.94 (s, 9 H,  $tBu$ ).  $^1H$  NMR (500 MHz,  $C_7D_8$ , 353 K):  $\delta$  (ppm) 7.97 (dd, 2 H, *Ph*-Nb), 7.14-6.96 (Ar +  $C_7D_8$ ), 5.47 (s, 1 H,  $HC(C(Me)NAr)_2$ ), 2.96 (sept, 4 H,  $CHMe_2$ ,  $^3J_{HH}=6.6$  Hz), 1.63 (s, 6 H,  $HC(C(Me)NAr)_2$ ), 1.08 (b, 12 H,  $CHMe_2$ ), 1.04 (d, 12 H,  $CHMe_2$ ,  $^3J_{HH}=6.6$  Hz), 0.91 (s, 9 H,  $tBu$ ).  $^{19}F$  NMR (470 MHz,  $C_7D_8$ , 293 K):  $\delta$  (ppm) 87.4 (s, Nb-F).  $^{19}F$  NMR (470 MHz,  $C_7D_8$ , 353 K):  $\delta$  (ppm) 89.4 (s, Nb-F).  $^{13}C\{^1H\}$  NMR (125.8 MHz,  $C_7D_8$ , 353 K):  $\delta$  (ppm) 132.5 (CH, *Ph*-Nb), 103.2 (CH,  $HC(C(Me)NAr)_2$ ), 30.6 ( $CH_3$ , Nb=NC( $CH_3$ ) $_3$ ), 28.5 (CH,  $CHMe_2$  of C=NAr), 25.3 ( $CH_3$ ,  $HC(C(Me)NAr)_2$ ), 24.8 ( $CH_3$ ,  $CHMe_2$  of C=NAr), 24.3 ( $CH_3$ ,  $CHMe_2$  of C=NAr),



23.2 (CH<sub>3</sub>, CHMe<sub>2</sub> of C=NAr). Anal. Calcd for C<sub>39</sub>H<sub>55</sub>F<sub>1</sub>N<sub>3</sub>Nb<sub>1</sub>: C, 69.11; H, 8.18; N, 6.20. Found: C, 68.89; H, 8.35; N, 6.16.

**[(BDI)Nb(N<sup>t</sup>Bu)(4-CH<sub>3</sub>Ph)(F)], 5.b.** Yield: 85 mg, 0.123 mmol, 68%. <sup>1</sup>H NMR (500 MHz, C<sub>6</sub>D<sub>6</sub>, 293 K): δ (ppm) 8.09 (d, 2 H, *pTol*-Nb), 7.18-6.96 (broad, Ar), 5.49 (s, 1 H, HC(C(Me)NAr)<sub>2</sub>), 3.1 (b, 4 H, CHMe<sub>2</sub>), 1.71 (s, 6 H, HC(C(Me)NAr)<sub>2</sub>), 1.31 (b, 6 H, CHMe<sub>2</sub>), 1.22 (d, 12 H, CHMe<sub>2</sub>, <sup>3</sup>J<sub>HH</sub> = 6.6 Hz), 1.15 (b, 6 H, CHMe<sub>2</sub>), 1.07 (s, 9 H, <sup>t</sup>Bu). <sup>19</sup>F NMR (470 MHz, C<sub>6</sub>D<sub>6</sub>, 293 K): δ (ppm) 82.3 (s, Nb-F). <sup>13</sup>C{<sup>1</sup>H} NMR (125.8 MHz, C<sub>6</sub>D<sub>6</sub>, 293 K): δ (ppm) 132.5 (CH, *Ph*-Nb), 103.2 (CH, HC(C(Me)NAr)<sub>2</sub>), 30.6 (CH<sub>3</sub>, Nb=NC(CH<sub>3</sub>)<sub>3</sub>), 28.5 (CH, CHMe<sub>2</sub> of C=NAr), 25.3 (CH<sub>3</sub>, HC(C(Me)NAr)<sub>2</sub>), 24.8 (CH<sub>3</sub>, CHMe<sub>2</sub> of C=NAr), 24.3 (CH<sub>3</sub>, CHMe<sub>2</sub> of C=NAr), 23.2 (CH<sub>3</sub>, CHMe<sub>2</sub> of C=NAr). Anal. Calcd for C<sub>40</sub>H<sub>58</sub>F<sub>1</sub>N<sub>3</sub>Nb<sub>1</sub>: C, 69.34; H, 8.44; N, 6.07. Found: C, 69.70; H, 8.77; N, 6.41.

**[(BDI)Nb(N<sup>t</sup>Bu)(2-C<sub>6</sub>H<sub>4</sub>F)(F)], 5.c.** Yield: 94 mg, 0.134 mmol, 74%. X-ray suitable crystals were obtained by recrystallization from hexanes at -40 °C. <sup>1</sup>H NMR (500 MHz, C<sub>7</sub>D<sub>8</sub>, 293 K): δ (ppm) 7.85 (b, 2 H, 2-C<sub>6</sub>H<sub>4</sub>F-Nb), 7.18-6.96 (broad, Ar), 5.39 (s, 1 H, HC(C(Me)NAr)<sub>2</sub>), 2.99 (broad, 4 H, CHMe<sub>2</sub>), 1.59 (s, 6 H, HC(C(Me)NAr)<sub>2</sub>), 1.24 (b, 12 H, CHMe<sub>2</sub>), 1.15 (b, 12 H, CHMe<sub>2</sub>), 1.01 (s, 9 H, <sup>t</sup>Bu). <sup>1</sup>H NMR (500 MHz, C<sub>7</sub>D<sub>8</sub>, 353 K): δ (ppm) 7.82 (dd, 2 H, 2-C<sub>6</sub>H<sub>4</sub>F-Nb), 7.14-6.96 (Ar + C<sub>7</sub>D<sub>8</sub>), 6.86 (t, 2 H, 2-C<sub>6</sub>H<sub>4</sub>F-Nb), 6.79 (t, 2 H, Ar), 5.46 (s, 1 H, HC(C(Me)NAr)<sub>2</sub>), 2.99 (sept, 4 H, CHMe<sub>2</sub>, <sup>3</sup>J<sub>HH</sub> = 6.6 Hz), 1.63 (s, 6 H, HC(C(Me)NAr)<sub>2</sub>), 1.11 (d, 12 H, CHMe<sub>2</sub>, <sup>3</sup>J<sub>HH</sub> = 6.6 Hz), 1.07 (d, 12 H, CHMe<sub>2</sub>, <sup>3</sup>J<sub>HH</sub> = 6.6 Hz), 0.92 (s, 9 H, <sup>t</sup>Bu). <sup>19</sup>F NMR (470 MHz, C<sub>7</sub>D<sub>8</sub>, 293 K): δ (ppm) 98.0 (s, Nb-F), -84.2 (b, o-F). <sup>19</sup>F NMR (470 MHz, C<sub>7</sub>D<sub>8</sub>, 353 K): δ (ppm) 99.9 (s, Nb-F), -85.2 (s, o-F). <sup>13</sup>C{<sup>1</sup>H} NMR (125.8 MHz, C<sub>7</sub>D<sub>8</sub>, 353 K): δ (ppm) 131.3 (CH, *Ph*-Nb), 103.9 (CH, HC(C(Me)NAr)<sub>2</sub>), 29.9 (CH<sub>3</sub>, Nb=NC(CH<sub>3</sub>)<sub>3</sub>), 28.3 (CH, CHMe<sub>2</sub> of C=NAr), 25.0 (CH<sub>3</sub>, HC(C(Me)NAr)<sub>2</sub>), 24.8 (CH<sub>3</sub>, CHMe<sub>2</sub> of C=NAr), 24.0 (CH<sub>3</sub>, CHMe<sub>2</sub> of C=NAr), 23.9 (CH<sub>3</sub>, CHMe<sub>2</sub> of C=NAr). Anal. Calcd for C<sub>39</sub>H<sub>54</sub>F<sub>2</sub>N<sub>3</sub>Nb<sub>1</sub>: C, 67.32; H, 7.82; N, 6.04. Found: C, 67.49; H, 8.05; N, 6.19.

**[(BDI)Nb(N<sup>t</sup>Bu)(3-C<sub>6</sub>H<sub>4</sub>F)(F)], 5.2d.** Yield: 112 mg, 0.160 mmol, 91%. X-ray suitable crystals were obtained by recrystallization from hexanes at -40 °C. <sup>1</sup>H NMR (500 MHz, C<sub>7</sub>D<sub>8</sub>, 293 K): δ (ppm) 7.84 (d, 1 H, 3-C<sub>6</sub>H<sub>4</sub>F-Nb, <sup>3</sup>J<sub>HH</sub> = 6.7 Hz), 7.74 (d, 1 H, 3-F*Ph*-Nb, <sup>3</sup>J<sub>HH</sub> = 6.8 Hz), 7.18-6.96 (broad, Ar), 6.84 (dt, 1 H, 3-C<sub>6</sub>H<sub>4</sub>F-Nb, <sup>3</sup>J<sub>HH</sub> = 6.7 Hz, <sup>4</sup>J<sub>HH</sub> = 1.7 Hz), 5.34 (s, 1 H, HC(C(Me)NAr)<sub>2</sub>), 2.91 (sept, 4 H, CHMe<sub>2</sub>, <sup>3</sup>J<sub>HH</sub> = 6.6 Hz), 1.53 (s, 6 H, HC(C(Me)NAr)<sub>2</sub>), 1.20 (b, 6 H, CHMe<sub>2</sub>), 1.06 (d, 12 H, CHMe<sub>2</sub>, <sup>3</sup>J<sub>HH</sub> = 6.6 Hz), 1.02 (b, 6 H, CHMe<sub>2</sub>), 0.89 (s, 9 H, <sup>t</sup>Bu). <sup>1</sup>H NMR (500 MHz, C<sub>7</sub>D<sub>8</sub>, 353 K): δ (ppm) 7.80 (dd, 1 H, 3-C<sub>6</sub>H<sub>4</sub>F-Nb, <sup>3</sup>J<sub>HH</sub> = 6.7 Hz, <sup>4</sup>J<sub>HH</sub> = 1.7 Hz), 7.72 (d, 1 H, 3-C<sub>6</sub>H<sub>4</sub>F-Nb, <sup>3</sup>J<sub>HH</sub> = 6.8 Hz), 7.18-6.96 (broad, Ar), 6.83 (dt, 1 H, 3-C<sub>6</sub>H<sub>4</sub>F-Nb, <sup>3</sup>J<sub>HH</sub> = 6.7 Hz, <sup>4</sup>J<sub>HH</sub> = 1.7 Hz), 5.39 (s, 1 H, HC(C(Me)NAr)<sub>2</sub>), 2.91 (sept, 4 H, CHMe<sub>2</sub>, <sup>3</sup>J<sub>HH</sub> = 6.6 Hz), 1.56 (s, 6 H, HC(C(Me)NAr)<sub>2</sub>), 1.09 (d, 12 H, CHMe<sub>2</sub>, <sup>3</sup>J<sub>HH</sub> = 6.8 Hz), 1.06 (d, 12 H, CHMe<sub>2</sub>, <sup>3</sup>J<sub>HH</sub> = 6.6 Hz), 0.88 (s, 9 H, <sup>t</sup>Bu). <sup>19</sup>F NMR (470 MHz, C<sub>7</sub>D<sub>8</sub>, 293 K): δ (ppm) 92.1 (s, Nb-F), -113.6 (s, m-F). <sup>19</sup>F NMR (470 MHz, C<sub>7</sub>D<sub>8</sub>, 353 K): δ (ppm) 94.3 (s, Nb-F), -113.9 (s, m-F). <sup>13</sup>C{<sup>1</sup>H} NMR (125.8 MHz, C<sub>7</sub>D<sub>8</sub>, 353 K): δ (ppm) 103.8 (CH, HC(C(Me)NAr)<sub>2</sub>), 29.7 (CH<sub>3</sub>, Nb=NC(CH<sub>3</sub>)<sub>3</sub>), 28.1 (CH, CHMe<sub>2</sub> of C=NAr), 25.4 (CH<sub>3</sub>, HC(C(Me)NAr)<sub>2</sub>), 24.6 (CH<sub>3</sub>, CHMe<sub>2</sub> of C=NAr), 24.1 (CH<sub>3</sub>, CHMe<sub>2</sub> of C=NAr), 23.7 (CH<sub>3</sub>, CHMe<sub>2</sub> of C=NAr). Anal. Calcd for C<sub>39</sub>H<sub>54</sub>F<sub>2</sub>N<sub>3</sub>Nb<sub>1</sub>: C, 67.32; H, 7.82; N, 6.04. Found: C, 67.53; H, 8.00; N, 6.21.

**[(BDI)Nb(N<sup>t</sup>Bu)(4-C<sub>6</sub>H<sub>4</sub>F)(F)], 5.2e.** Yield: 100 mg, 0.150 mmol, 87%. <sup>1</sup>H NMR (500 MHz, C<sub>7</sub>D<sub>8</sub>, 293 K): δ (ppm) 8.00 (b, 2 H, 4-C<sub>6</sub>H<sub>4</sub>F-Nb), 7.18-6.96 (broad, Ar), 5.38 (s, 1 H, HC(C(Me)NAr)<sub>2</sub>), 2.90 (broad, 4 H, CHMe<sub>2</sub>), 1.56 (s, 6 H, HC(C(Me)NAr)<sub>2</sub>), 1.21 (b, 12 H, CHMe<sub>2</sub>), 1.05 (b, 12 H, CHMe<sub>2</sub>), 0.92 (s, 9 H, <sup>t</sup>Bu). <sup>19</sup>F NMR (470 MHz, C<sub>7</sub>D<sub>8</sub>, 293 K): δ (ppm) 97.2 (s, 1 F, Nb-F), -108.3 (s, 1 F, p-F). <sup>13</sup>C{<sup>1</sup>H} NMR (125.8 MHz, C<sub>7</sub>D<sub>8</sub>, 298 K): δ (ppm) 103.5 (CH, HC(C(Me)NAr)<sub>2</sub>), 29.1 (CH<sub>3</sub>, Nb=NC(CH<sub>3</sub>)<sub>3</sub>), 28.6 (CH, CHMe<sub>2</sub> of C=NAr), 24.9 (CH<sub>3</sub>, HC(C(Me)NAr)<sub>2</sub>), 24.5 (CH<sub>3</sub>, CHMe<sub>2</sub> of C=NAr), 23.1 (CH<sub>3</sub>, CHMe<sub>2</sub> of C=NAr), 22.6 (CH<sub>3</sub>, CHMe<sub>2</sub> of C=NAr). Anal. Calcd for C<sub>39</sub>H<sub>54</sub>F<sub>2</sub>N<sub>3</sub>Nb<sub>1</sub>: C, 67.32; H, 7.82; N, 6.04. Found: C, 67.10; H, 7.52; N, 6.29.

**[(BDI)Nb(N<sup>t</sup>Bu)(2,x-C<sub>6</sub>H<sub>3</sub>F<sub>2</sub>)(F)], x = 3 or 6, 5.2f<sub>A/B</sub>:** Yield: 83 mg, 0.116 mmol, 65%. Anal. Calcd for C<sub>39</sub>H<sub>53</sub>F<sub>3</sub>N<sub>3</sub>Nb<sub>1</sub>: C, 65.63; H, 7.48; N, 5.89. Found: C, 65.87; H, 7.81; N, 6.12.

Main resonances for complex 5.2f<sub>A</sub>, [(BDI)Nb(N<sup>t</sup>Bu)(2,3-C<sub>6</sub>H<sub>3</sub>F<sub>2</sub>)(F)]: (500 MHz, C<sub>7</sub>D<sub>8</sub>, 293 K): δ (ppm) 5.34 (s, 1 H, HC(C(Me)NAr)<sub>2</sub>), 2.93 (b, 4 H, CHMe<sub>2</sub>, <sup>3</sup>J<sub>HH</sub> = 6.6 Hz), 1.54 (s, 6 H, HC(C(Me)NAr)<sub>2</sub>). <sup>1</sup>H NMR (500 MHz, C<sub>7</sub>D<sub>8</sub>, 353 K): δ (ppm) 5.44 (s, 1 H, HC(C(Me)NAr)<sub>2</sub>), 2.98 (sept, 4 H, CHMe<sub>2</sub>, <sup>3</sup>J<sub>HH</sub> = 6.6 Hz), 1.61 (s, 6 H, HC(C(Me)NAr)<sub>2</sub>). <sup>19</sup>F NMR (470 MHz, C<sub>7</sub>D<sub>8</sub>, 293 K): δ (ppm) 103.2 (b, Nb-F). <sup>19</sup>F NMR (470 MHz, C<sub>7</sub>D<sub>8</sub>, 353 K): δ (ppm) 104.4 (s, Nb-F).

Main resonances for complex 5.2f<sub>B</sub>, [(BDI)Nb(N<sup>t</sup>Bu)(2,6-C<sub>6</sub>H<sub>3</sub>F<sub>2</sub>)(F)]: (500 MHz, C<sub>7</sub>D<sub>8</sub>, 293 K): δ (ppm) 5.32 (s, 1 H, HC(C(Me)NAr)<sub>2</sub>), 3.18 (b, 4 H, CHMe<sub>2</sub>, <sup>3</sup>J<sub>HH</sub> = 6.6 Hz), 1.61 (s, 6 H, HC(C(Me)NAr)<sub>2</sub>). <sup>1</sup>H NMR (500 MHz, C<sub>7</sub>D<sub>8</sub>, 353 K): δ (ppm) 5.39 (s, 1 H, HC(C(Me)NAr)<sub>2</sub>), 3.22 (sept, 4 H, CHMe<sub>2</sub>, <sup>3</sup>J<sub>HH</sub> = 6.6 Hz), 1.66 (s, 6 H, HC(C(Me)NAr)<sub>2</sub>). <sup>19</sup>F NMR (470 MHz, C<sub>7</sub>D<sub>8</sub>, 293 K): δ (ppm) 103.2 (b, Nb-F). <sup>19</sup>F NMR (470 MHz, C<sub>7</sub>D<sub>8</sub>, 353 K): δ (ppm) 109.5 (s, 1 F, Nb-F).

Accurate assignment of 2,x-C<sub>6</sub>H<sub>4</sub>F<sub>2</sub>, with x = 3 or 6, was challenging due to the broadness of the signals and the resulting difficulty of integration. Three resonances in a roughly 1:1:1 ratio were observed, consistent with the three inequivalent C-F bonds expected (two resonances for the non-symmetric 2,3-C<sub>6</sub>H<sub>4</sub>F<sub>2</sub> group of 5.2f<sub>A</sub> and one resonance for the symmetric 2,6-C<sub>6</sub>H<sub>4</sub>F<sub>2</sub> moiety of 5.2f<sub>B</sub>), and the 2:1 ratio between 5.2f<sub>A</sub> and 5.2f<sub>B</sub>. <sup>19</sup>F NMR (470 MHz, C<sub>7</sub>D<sub>8</sub>, 353 K): -80.2 (vb, 2 F, 2,6-F<sub>2</sub>C<sub>6</sub>H<sub>4</sub> of 5.2f<sub>B</sub>), -109.9 (b, 1 F, 2-F<sub>2</sub>C<sub>6</sub>H<sub>4</sub> of 2f<sub>A</sub>), -136.1 (d, 1 F, 3-F<sub>2</sub>C<sub>6</sub>H<sub>4</sub> of 5.2f<sub>A</sub>).

**[(BDI)Nb(N<sup>t</sup>Bu)(3,5-C<sub>6</sub>H<sub>3</sub>F<sub>2</sub>)(F)], 5.2g.** Yield: 60 mg, 0.082 mmol, 47%. <sup>1</sup>H NMR (500 MHz, C<sub>7</sub>D<sub>8</sub>, 293 K): δ (ppm) 7.61 (dd, 2 H, 3,5-C<sub>6</sub>H<sub>3</sub>F<sub>2</sub>-Nb, <sup>3</sup>J<sub>HH</sub> = 6.7 Hz, <sup>4</sup>J<sub>HH</sub> = 1.6 Hz), 7.18-6.96 (broad, Ar), 6.59 (dt, 1 H, 3,5-C<sub>6</sub>H<sub>3</sub>F<sub>2</sub>-Nb, <sup>3</sup>J<sub>HH</sub> = 6.8 Hz, <sup>4</sup>J<sub>HH</sub> = 1.5 Hz), 5.32 (s, 1 H, HC(C(Me)NAr)<sub>2</sub>), 2.86 (broad, 4 H, CHMe<sub>2</sub>), 1.51 (s, 6 H, HC(C(Me)NAr)<sub>2</sub>), 1.10 (b, 12 H, CHMe<sub>2</sub>), 1.05 (b, 12 H, CHMe<sub>2</sub>), 0.84 (s, 9 H, <sup>t</sup>Bu). <sup>19</sup>F NMR (470 MHz, C<sub>7</sub>D<sub>8</sub>, 293 K): δ (ppm) 97.2 (s, 1 F, Nb-F), -111.1 (b, 2 F, m-F). <sup>13</sup>C{<sup>1</sup>H} NMR (125.8 MHz, C<sub>7</sub>D<sub>8</sub>, 298 K): δ (ppm) 103.5 (CH, HC(C(Me)NAr)<sub>2</sub>), 30.3 (CH<sub>3</sub>, Nb=NC(CH<sub>3</sub>)<sub>3</sub>), 28.7 (CH, CHMe<sub>2</sub> of C=NAr), 25.6 (CH<sub>3</sub>, HC(C(Me)NAr)<sub>2</sub>), 24.3 (CH<sub>3</sub>, CHMe<sub>2</sub> of C=NAr), 24.1 (CH<sub>3</sub>, CHMe<sub>2</sub> of C=NAr), 23.8 (CH<sub>3</sub>, CHMe<sub>2</sub> of C=NAr). Anal. Calcd for C<sub>39</sub>H<sub>53</sub>F<sub>3</sub>N<sub>3</sub>Nb<sub>1</sub>: C, 65.63; H, 7.48; N, 5.89. Found: C, 65.39; H, 7.75; N, 6.01.

**[(BDI)Nb(N<sup>t</sup>Bu)(2,3,6-C<sub>6</sub>H<sub>2</sub>F<sub>3</sub>)(F)], 5.2h.** Yield: 71 mg, 0.100 mmol, 55%. <sup>1</sup>H NMR (500 MHz, C<sub>7</sub>D<sub>8</sub>, 293 K): δ (ppm) 7.18-6.96 (broad, Ar), 6.41 (b, 1 H, 2,3,6-C<sub>6</sub>H<sub>2</sub>F<sub>3</sub>), 6.15 (b, 1 H, 2,3,6-C<sub>6</sub>H<sub>2</sub>F<sub>3</sub>), 5.29 (s, 1 H, HC(C(Me)NAr)<sub>2</sub>), 3.34 (b, 2 H, CHMe<sub>2</sub>), 3.14 (b, 2 H,

*CHMe*<sub>2</sub>), 1.59 (s, 3 H, HC(C(*Me*)NAr)<sub>2</sub>), 1.58 (s, 3 H, HC(C(*Me*)NAr)<sub>2</sub>), 1.38 (d, 6 H, *CHMe*<sub>2</sub>, <sup>3</sup>*J*<sub>HH</sub> = 6.8 Hz), 1.32 (d, 6 H, *CHMe*<sub>2</sub>, <sup>3</sup>*J*<sub>HH</sub> = 6.6 Hz), 1.16 (s, 9 H, <sup>t</sup>Bu), 1.10 (d, 12 H, *CHMe*<sub>2</sub>, <sup>3</sup>*J*<sub>HH</sub> = 6.6 Hz). <sup>1</sup>H NMR (500 MHz, C<sub>7</sub>D<sub>8</sub>, 353 K): δ (ppm) 7.18-6.96 (broad, Ar), 6.52 (b, 1 H, 2,3,6-C<sub>6</sub>H<sub>2</sub>F<sub>3</sub>), 6.23 (b, 1 H, 2,3,6-C<sub>6</sub>H<sub>2</sub>F<sub>3</sub>), 5.37 (s, 1 H, HC(C(*Me*)NAr)<sub>2</sub>), 3.20 (b, 4 H, *CHMe*<sub>2</sub>), 1.65 (s, 3 H, HC(C(*Me*)NAr)<sub>2</sub>), 1.21 (d, 12 H, *CHMe*<sub>2</sub>, <sup>3</sup>*J*<sub>HH</sub> = 6.8 Hz), 1.19 (d, 12 H, *CHMe*<sub>2</sub>, <sup>3</sup>*J*<sub>HH</sub> = 6.6 Hz), 1.07 (s, 9 H, <sup>t</sup>Bu). <sup>19</sup>F NMR (470 MHz, C<sub>7</sub>D<sub>8</sub>, 293 K): δ (ppm) 120.3 (s, 1F, Nb-*F*), -90.1 (s, 1F, 6-*F*), -103.7 (s, 1F, 2-*F*), -142.1 (s, 1F, 3-*F*). <sup>19</sup>F NMR (470 MHz, C<sub>7</sub>D<sub>8</sub>, 353 K): δ (ppm) 116.6 (s, 1F, Nb-*F*), -94.3 (s, 1F, 6-*F*), -108.4 (s, 1F, 2-*F*), -144.9 (s, 1F, 3-*F*). Anal. Calcd for C<sub>39</sub>H<sub>52</sub>F<sub>4</sub>N<sub>3</sub>Nb<sub>1</sub>: C, 64.01; H, 7.16; N, 5.74. Found: C, 64.37; H, 7.02; N, 6.02.

**[(BDI)Nb(<sup>t</sup>Bu)(3-C<sub>6</sub>H<sub>5</sub>F)(Cl)], 5.2j.** Yield: 113 mg, 0.158 mmol, 88%. <sup>1</sup>H NMR (500 MHz, C<sub>6</sub>D<sub>6</sub>, 293 K): δ (ppm) 7.82 (b, 2 H, *Ph*-Nb), 7.18-6.96 (broad, Ar), 5.66 (s, 1 H, HC(C(*Me*)NAr)<sub>2</sub>), 2.75 (broad, 4 H, *CHMe*<sub>2</sub>), 1.74 (s, 3 H, HC(C(*Me*)NAr)<sub>2</sub>), 1.57 (s, 3 H, HC(C(*Me*)NAr)<sub>2</sub>), 1.35 (b, 6 H, *CHMe*<sub>2</sub>), 1.05 (d, 12 H, *CHMe*<sub>2</sub>, <sup>3</sup>*J*<sub>HH</sub> = 6.7 Hz), 1.01 (s, 9 H, <sup>t</sup>Bu), 0.65 (b, 6 H, *CHMe*<sub>2</sub>). <sup>19</sup>F NMR (470 MHz, C<sub>6</sub>D<sub>6</sub>, 293 K): δ (ppm) -113.8 (b, 1F, *m-F*-Ar). Anal. Calcd for C<sub>39</sub>H<sub>54</sub>Cl<sub>1</sub>F<sub>1</sub>N<sub>3</sub>Nb<sub>1</sub>: C, 65.77; H, 7.64; N, 5.90. Found: C, 65.45; H, 7.83; N, 6.11.

**Characterization of intermediate 5.B.** A solution of C<sub>9</sub>D<sub>12</sub> containing fluorobenzene (10 ml, 0.107 mmol, 2 equiv.) and (BDI)(Me)<sub>2</sub>Nb(<sup>t</sup>Bu) (35 mg, 0.057 mmol, 1 equiv.) was added to a J-Young NMR tube with a Teflon cap. The solution was freeze-pump-thawed three times and then refilled with 1 atm of H<sub>2</sub>. The NMR tube with the thawing solution was placed in the spectrometer, with the probe pre-cooled to 263 K, and several <sup>1</sup>H NMR spectra were recorded. Between each spectrum, the NMR tube was ejected from the spectrometer and was shaken at room temperature for 1-2 mins before being brought back to 263 K. Figure 5.4 shows the quick formation of the intermediate **5.A**, followed by the formation of **5.B**, also observed by <sup>19</sup>F NMR spectroscopy. The persistence of these intermediates at 263 K allowed for their complete characterization. The spectrometer probe was then warmed to 313 K in order to observe the further conversion of **5.B** to the final product **5.2a** (Figures 5.5 and 5.6).

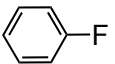
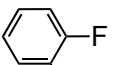
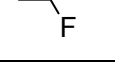
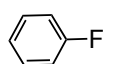
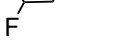
**Characterization of 5.B:** <sup>1</sup>H NMR (600 MHz, C<sub>9</sub>D<sub>12</sub>, 263 K): δ(ppm) 5.05 (s, 1 H, HC(C(*Me*)NAr)<sub>2</sub>), 4.50 (m, 2 H, *CHMe*<sub>2</sub>, <sup>3</sup>*J*<sub>HH</sub> = 6.9 Hz), 3.67 (t, 1 H, *p-PhF*, <sup>3</sup>*J*<sub>HH</sub> = 6.6 Hz), 3.36 (broad, 2 H, *m-PhF*), 3.29 (t, 2 H, *o-PhF*, <sup>3</sup>*J*<sub>HH</sub> = 6.2 Hz), 2.61 (m, 2 H, *CHMe*<sub>2</sub>, <sup>3</sup>*J*<sub>HH</sub> = 6.9 Hz), 1.68 (s, 6 H, HC(C(*Me*)NAr)<sub>2</sub>), 1.34 (s, 9 H, <sup>t</sup>Bu), 1.31 (d, 6 H, *CHMe*<sub>2</sub>, <sup>3</sup>*J*<sub>HH</sub> = 6.9 Hz), 1.10 (d, 6 H, *CHMe*<sub>2</sub>, <sup>3</sup>*J*<sub>HH</sub> = 6.6 Hz), 0.96 (d, 6 H, *CHMe*<sub>2</sub>, <sup>3</sup>*J*<sub>HH</sub> = 6.6 Hz), 0.94 (d, 6 H, *CHMe*<sub>2</sub>, <sup>3</sup>*J*<sub>HH</sub> = 6.9 Hz). <sup>19</sup>F NMR (564 MHz, C<sub>9</sub>D<sub>12</sub>, 263 K): δ(ppm) -113.4 (s, 3 F, *PhF*). <sup>13</sup>C NMR (125 MHz, C<sub>9</sub>D<sub>12</sub>, 263 K): δ(ppm) 116 (CH, *m-PhF*), 115 (CH, *p-PhF*), 102 (CH, HC(C(*Me*)NAr)<sub>2</sub>), 84 (CH, *o-PhF*)

**Stoichiometric hydrodefluorination.** A solution of  $C_6D_6$  containing each complex **2a-e** (10-15 mg, 0.107 mmol, 1 equiv.) and  $RSiH_3$  (R = nBuSiH<sub>3</sub>: 35 mL, 0.057 mmol, 5 equiv., R = Ph: 35 mL, 0.057 mmol, 5 equiv.) was added to a J-Young NMR tube with a Teflon cap. The solution was either stored at room temperature (R = Ph) or heated to 60 °C (R = nBu) for several hours. The yellow-orange solution slowly turned dark red, the color characteristic of the arene bound complex. <sup>1</sup>H NMR spectra were then recorded, revealing the presence of complex **5.1-d<sub>6</sub>** as the only organometallic species (example for complex **5.2a** and nBuSiH<sub>3</sub>, Figure 5.8). After completion, the volatile materials were vacuum-transferred away from the organometallic compound and analyzed by <sup>1</sup>H, <sup>19</sup>F NMR in  $C_6D_6$  and further analyzed by GC-MS showing the presence of the mono-hydrodefluorinated arene and  $RSiF_3$ .

- nBuSiF<sub>3</sub>: <sup>1</sup>H NMR (600 MHz,  $C_6D_6$ , 293 K):  $\delta$ (ppm) 1.13 (m, 2 H,  $CH_3(CH_2)_2CH_2SiF_3$ ), 1.06 (m, 2 H,  $CH_3(CH_2)_2CH_2SiF_3$ ), 0.76 (t, 3 H,  $CH_3(CH_2)_2CH_2SiF_3$ , <sup>3</sup>J<sub>HH</sub> = 8.2 Hz), 0.40 (m, 2 H,  $CH_3(CH_2)_2CH_2SiF_3$ ). <sup>19</sup>F NMR (564 MHz,  $C_6D_6$ , 293 K):  $\delta$ (ppm) -136.2 (s, 3F, nBuSiF<sub>3</sub>).
- PhSiF<sub>3</sub>: <sup>19</sup>F NMR (564 MHz,  $C_6D_6$ , 293 K):  $\delta$ (ppm) -141.8 (s, 3F, PhSiF<sub>3</sub>).

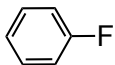
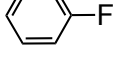
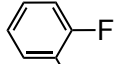
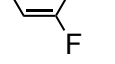
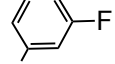
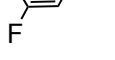
**Catalytic hydrodefluorination. Complex 5.1 as a catalyst:** A solution of 0.4 ml mesitylene containing complex **5.1** (13.5 mg, 0.020 mmol, 0.05 M), fluoroarene and silane, as well as a solution of mesitylene containing  $C_6F_6$  as internal standard (0.10 M), was added to a J-Young NMR tube with a Teflon cap (see Table 5.5). The reaction mixture was heated in an oil bath for several hours (70 °C for nBuSiH<sub>3</sub> and 40 °C nBuSiH<sub>3</sub>) and the conversion was frequently monitored by <sup>19</sup>F NMR spectroscopy, performing 2 scans with a delay time  $d_1$  of 20 s.

**Table 5.5**

Entry	ArF	[ArF] (M)	V (mL)	[nBuSiH <sub>3</sub> ] (M)	V (mL)	mol % of <b>1</b> <sup>[a]</sup>	C <sub>9</sub> H <sub>12</sub> (mL)	[C <sub>6</sub> F <sub>6</sub> ] (M)	Time	T (°C)	Yield (%)
1		3.0	113	0.11	5.7	15	281	0.070	12 h	70	7(2)
2		3.0	113	0.11	5.7	15	281	0.070	24 h	70	9(2)
3		3.0	113	0.11	5.7	15	281	0.070	12 h	90	<1
4		3.0	113	0.33	17.1	5	270	0.068	12 h	70	<1
5		neat	0.390	0.11	5.7	15	-	0.110	12 h	70	63(2)
6		3.0	118	0.11	5.7	15	276	0.069	12 h	70	42(3)
7		3.0	118	0.33	17.1	5	255	0.064	12 h	70	24(2)
8		3.0	118	0.11	5.7	15	276	0.069	12 h	70	34(4)
9		3.0	118	0.33	17.1	5	255	0.064	12 h	70	19(2)

**Complex 5.1 as a precatalyst:** A solution of 0.4 ml containing complex **5.1** (13.5 mg, 0.020 mmol, 0.05 M), fluoroarene, as well as a solution of mesitylene containing C<sub>6</sub>F<sub>6</sub> as internal standard (0.10 M) (see Table 5.6), was added to a J-Young NMR tube with a Teflon cap. For the run involving 1,2- and 1,3-difluorobenzene, a capillary tube containing 0.1 M of fluorobiphenyl in mesitylene was added and used as a 2<sup>nd</sup> internal standard (see calibration). The reaction mixture was heated at 50 °C in an oil bath for 30 min, which resulted in a color change from red to yellow, characteristic of the Nb(V) aryl fluoride complex. A 0.11 M solution of silane (corresponding to 15 mol% catalyst loading per H, see Table 5.6) was then added and the NMR tube, which was heated in an oil bath for several hours (70 °C for nBuSiH<sub>3</sub> and 40 °C PhSiH<sub>3</sub>). The conversion was frequently monitored by <sup>19</sup>F NMR spectroscopy and the yield calculated using the internal standard peak (see example of monitored conversion for fluorobenzene, Figure 5.9, and 1,3-difluorobenzene, Figure 5.10). Each of the following experiments has been repeated twice, affording very similar yields; the yields presented are an average of the two runs.

**Table 5.6**

Entry	ArF (3.0 M)	V (mL)	E-H (0.11 M)	V (mL)	C <sub>9</sub> H <sub>12</sub> (mL)	[C <sub>6</sub> F <sub>6</sub> ] (M)	Time	T (°C)	Yield (%)
1		113	nBuSiH <sub>3</sub>	5.7	281	0.070	16 h	70	71(4)
2		113	PhSiH <sub>3</sub>	5.4	281	0.070	12 h	40	12(4)
3		118	nBuSiH <sub>3</sub>	17.1	255	0.069	16 h	70	90(4)
4		118	PhSiH <sub>3</sub>	16.9	254	0.069	16 h	40	82(4)
5		118	nBuSiH <sub>3</sub>	17.1	255	0.069	16 h	70	97(4)
6		118	PhSiH <sub>3</sub>	16.9	254	0.069	16 h	40	85(4)

**Calibration curve:** A capillary tube containing 1.0 M of fluorobiphenyl in mesitylene was added to an NMR tube containing 0.25, 0.5, 0.75 and 1.0 M of fluorobenzene in mesitylene. <sup>19</sup>F NMR spectra were recorded by performing 2 scans with a delay time d<sub>1</sub> of 20 s. The ratio of fluorobenzene/fluorobiphenyl peaks were then plotted as a function of fluorobenzene concentration.

**DFT calculations.** All structures and energies were calculated using the Gaussian09 suite of programs.<sup>36</sup> Self-consistent field computations were performed with tight convergence criteria on ultrafine grids, while geometry optimizations were converged to tight geometric convergence criteria for all compounds. Spin expectation values  $\langle S \rangle^2$  indicated that spin contamination was not significant in any result. Frequencies were calculated analytically at 298.15 K and 1 atm. Structures were considered true minima if they did not exhibit imaginary vibration modes and were considered as transition states when only one imaginary vibration mode was found. Intrinsic Reaction Coordinates (IRC) calculations were performed to ensure the transition state geometries connected the reactants and the products. Optimized geometries were compared using the sum of their electronic and zero-point energies. In order to reduce the computational time, the system was structurally simplified by replacing 2,6-diisopropylphenyl groups by phenyl groups and the N<sup>t</sup>Bu imido group by a NMe imido group. The PBE1PBE hybrid functional was used throughout this computational study.<sup>37</sup> For geometry optimizations and frequency calculations, the light atoms (H, C, N and F) were treated with the 6-311G(d,p) basis,<sup>38</sup> while the niobium atom was treated with a Stuttgart/Dresden ECPs pseudopotential (SDD).<sup>39,40</sup>

**X-Ray crystallography studies.** X-ray structural determinations were performed on a Bruker SMART 1000 or SMART APEX diffractometer. Both are 3-circle diffractometers that couple a CCD detector<sup>41</sup> with a sealed-tube source of monochromated Mo K $\alpha$  radiation ( $\lambda = 0.71073$  Å). A crystal of appropriate size was coated in Paratone-N oil and mounted on a Kapton<sup>®</sup> loop. The loop was transferred to the diffractometer, centered in the beam, and cooled by a nitrogen flow low-temperature apparatus that had been previously calibrated by a thermocouple placed at the same position as the crystal. Preliminary orientation matrices and cell constants were determined by collection of 60 x 10 s frames, followed by spot integration and least-squares refinement. The reported cell dimensions were calculated from all reflections with  $I > 10 \sigma$ . The data were corrected for Lorentz and polarization effects; no correction for crystal decay was applied. An empirical absorption correction based on comparison of redundant and equivalent reflections was applied using SADABS.<sup>42</sup> All software used for diffraction data processing and crystal-structure solution and refinement are contained in the APEX2 program suite (Bruker AXS, Madison, WI).<sup>43</sup> Thermal parameters for all non-hydrogen atoms were refined anisotropically. For all structures,  $R_1 = \Sigma(|F_o| - |F_c|)/\Sigma(|F_o|)$ ;  $wR_2 = [\Sigma\{w(F_o^2 - F_c^2)^2\}/\Sigma\{w(F_o^2)^2\}]^{1/2}$ . Thermal ellipsoid plots were created using the ORTEP-3 software package and POV-ray.<sup>4</sup>

**Table 5.7** Crystallographic parameters for complexes **5.2a** and **5.2c**

Compound	<b>5.2a</b>	<b>5.2c</b>
Formula	C <sub>39</sub> H <sub>55</sub> FN <sub>3</sub> Nb	C <sub>39</sub> H <sub>54</sub> F <sub>2</sub> N <sub>3</sub> Nb
Formula weight (amu)	677.77	695.75
Space Group	P <sub>-1</sub>	P <sub>-1</sub>
<i>a</i> (Å)	10.795(5)	10.8194(10)
<i>b</i> (Å)	12.323(5)	12.3148(12)
<i>c</i> (Å)	13.680(5)	13.7249(13)
$\alpha$ (°)	79.363(5)°	79.695(6)°
$\beta$ (°)	87.377(5)°	87.396(6)°
$\gamma$ (°)	88.428(5)°	88.376(6)°
<i>V</i> (Å <sup>3</sup> )	1786.3(13)	1797.0(3)
<i>Z</i>	2	2
$\rho_{\text{calcd}}$ (g/cm <sup>3</sup> )	1.260	1.284
F <sub>000</sub>	720	734
$\mu$ (mm <sup>-1</sup> )	0.372	0.375
T <sub>min</sub> /T <sub>max</sub>	0.8654/0.8966	0.9458/0.9706
No. rflns measured	27323	26452
No. indep. rflns	6588	6544
<i>R</i> <sub>int</sub>	0.0168	0.0659
No. obs. ( <i>I</i> > 2.00σ( <i>I</i> ))	6588	6544
No. variables	410	429
<i>R</i> <sub>1</sub> , <i>wR</i> <sub>2</sub>	0.0224/0.0587	0.0445/0.0829
<i>R</i> <sub>1</sub> (all data)	0.0240	0.0677
GoF	1.066	1.036
Res. peak/hole (e <sup>-</sup> /Å <sup>3</sup> )	0.349/-0.326	0.756/-0.469

**Table 5.8** Crystallographic parameters for complexes **5.2d** and **5.2h**

Compound	<b>5.2d</b>	<b>5.2h</b>
Formula	C <sub>39</sub> H <sub>54</sub> F <sub>2</sub> N <sub>3</sub> Nb	C <sub>39</sub> H <sub>52</sub> F <sub>4</sub> N <sub>3</sub> Nb
Formula weight (amu)	695.76	731.74
Space Group	P <sub>1</sub>	P2 <sub>1/c</sub>
<i>a</i> (Å)	10.9151(4)	12.7898(5)
<i>b</i> (Å)	12.3010(4)	11.5223(4)
<i>c</i> (Å)	13.7072(5)	24.9612(9)
<i>α</i> (°)	79.714(6)°	90°
<i>β</i> (°)	87.243(6)°	91.2170(10)°
<i>γ</i> (°)	88.804(6)°	90°
<i>V</i> (Å <sup>3</sup> )	1808.60(11)	3677.7(2)
<i>Z</i>	2	4
$\rho_{\text{calcd}}$ (g/cm <sup>3</sup> )	1.278	1.322
F <sub>000</sub>	736	1536
$\mu$ (mm <sup>-1</sup> )	0.373	0.378
T <sub>min</sub> /T <sub>max</sub>	0.9427/0.9708	0.9717/0.9802
No. rflns measured	42043	26888
No. indep. rflns	6684	6733
<i>R</i> <sub>int</sub>	0.0493	0.0468
No. obs. ( <i>I</i> > 2.00σ( <i>I</i> ))	6684	6733
No. variables	419	437
<i>R</i> <sub>1</sub> , <i>wR</i> <sub>2</sub>	0.0302/0.0702	0.0368/0.0862
<i>R</i> <sub>1</sub> (all data)	0.0371	0.0522
GoF	1.055	1.017
Res. peak/hole (e <sup>-</sup> /Å <sup>3</sup> )	0.469/-0.356	0.963/-0.325



## References

- (1) T. Richmond, T. *Activation of Unreactive Bonds and Organic Synthesis* **1999**, 243.
- (2) Shine, K. P.; Sturges, W. T. *Science* **2007**, *315*, 1804.
- (3) For review articles on C-F activation and functionalization see: (a) Osterberg, C.; Richmond, T. G.; Kiplinger, J. L. *Chem. Rev.* **1994**, *94*, 373. (b) Burdeniuc, J.; Jedicka, B.; Crabtree, R. H. *Eur. J. Inorg. Chem.* **1997**, *130*, 145. (c) Braun, T.; Perutz, R. N. *Chem. Commun.* **2002**, 2749. (d) Uneyama, K.; Amii, H. *Journal of Fluorine Chemistry* **2002**, *114*, 127. (e) Torrens, H. *Coord. Chem. Rev.* **2005**, *249*, 1957; (f) Amii, H.; Uneyama, K. *Chem. Rev.* **2009**, *109*, 2119. (g) Meier, G.; Braun, T. *Angew. Chem. Int. Ed.* **2009**, *48*, 1546. (h) Hughes, R. P. *Eur. J. Inorg. Chem.* **2009**, 4591. (i) Sun, A. D.; Love, J. A. *Dalton Trans.* **2010**, *39*, 10362.
- (4) For review articles specific to early transition and f-block metals, see: (a) Jones, W. D. *Dalton Trans.* **2003**, 3991. (b) Driver, T. G. *Angew. Chem. Int. Ed.* **2009**, *48*, 7974. (c) Klahn, M.; Rosenthal, U. *Organometallics* **2012**, *31*, 1235.
- (5) For examples of main-group-catalyzed or mediated hydrode-fluorination of fluoroarenes, see: (a) Scott, V. J.; Çelenligil-Çetin, R.; Ozerov, O. V. *J. Am. Chem. Soc.* **2005**, *127*, 2852. (b) Panisch, R.; Bolte, M.; Müller, T. *J. Am. Chem. Soc.* **2006**, *128*, 2852. (c) Terao, J.; Begum, S. A.; Shinohara, Y.; Tomita, M.; Naitoh, Y.; Kambe, N. *Chem. Commun.* **2007**, 855. (d) Douvris, C.; Ozerov, O. V. *Science* **2008**, *321*, 1188–1190. (e) Gu, W.; Haneline, M. R.; Douvris, C.; Ozerov, O. V. *J. Am. Chem. Soc.* **2009**, *131*, 11203. (f) Douvris, C.; Nagaraja, C. M.; Chen, C. H.; Foxman, B. M.; Ozerov, O. V. *J. Am. Chem. Soc.* **2010**, *132*, 4946. (g) Caputo, C. B.; Stephan, D. W. *Organometallics* **2012**, *31*, 27.
- (6) For selected recent examples of late-transition-metal-catalyzed hydro- defluorination of fluoroarenes, see: (a) Vela, J.; Smith, J. M.; Yu, Y.; Ketterer, N. A.; Flaschenriem, C. J.; Lachicotte, R. J.; Holland, P. L. *J. Am. Chem. Soc.* **2005**, *127*, 7857. (b) Schaub, T.; Fischer, P.; Steffen, A.; Braun, T.; Radius, U.; Mix, A. *J. Am. Chem. Soc.* **2008**, *130*, 9304. (c) Reade, S. P.; Mahon, M. F.; Whittlesey, M. K. *J. Am. Chem. Soc.* **2009**, *131*, 1847. (d) Clot, E.; Eisenstein, O.; Jasim, N.; Macgregor, S. A.; McGrady, J. E.; Perutz, R. N. *Acc. Chem. Res.* **2011**, *44*, 333. (e) Lv, H.; Cai, Y.-B.; Zhang, J.-L. *Angew. Chem. Int. Ed. Engl.* **2013**, *52*, 3203.
- (7) For selected examples of early-transition-metal-catalyzed hydro- defluorination of fluoroarenes, see: (a) Kiplinger, J. L.; Richmond, T. G. *J. Am. Chem. Soc.* **1996**, *118*, 1805. (b) Kraft, B. M.; Jones, W. D. *J. Organomet. Chem.* **2002**, *658*, 132. (c) Jäger-Fielder, U.; Klahn, M.; Arndt, P.; Baumann, W.; Spannenberg, A.; Burlakov, V. V.; Rosenthal, U. *J. Mol. Catal. A* **2007**, *261*, 184. (d) Kühnel, M. F.; Lentz, D. *Angew. Chem. Int. Ed.* **2010**, *49*, 2933. (e) Kühnel, M. F.; Holstein, P.; Kliche, M.; Krueger, J.; Matthies, S.; Nitsch, D.; Schutt, J.; Sparenberg, M.; Lentz, D. *Chem. Eur. J.* **2012**, *18*, 10701. (f) Yow, S.; Gates, S. J.; White, A. J. P.; Crimmin, M. R. *Angew. Chem. Int. Ed. Engl.* **2012**, *51*, 12559.
- (8) (a) Werkema, E. L.; Andersen, R. A. *J. Am. Chem. Soc.* **2008**, *130*, 7153. (b) Janjetovic, M.; Träff, A. M.; Ankner, T.; Wettergren, J.; Hilmersson, G. *Chem. Commun.* **2013**, *49*, 1826.
- (9) Braun, T.; Perutz, R. N. Transition- Metal Mediated C-F Bond Activation. In *Comprehensive Organo-metallic Chemistry III*; R. H. Crabtree, D. M. P. Mingos, Eds.; Elsevier: Amsterdam, 2006.
- (10) Osterberg, C. E.; Richmond, T. G. Activation of Carbon-Fluorine Bonds by Oxidative Addition to Low-Valent Transition Metals. In *Inorganic Fluorine Chemistry*; Oxford

University Press: London, 1994.

(11) For recent selected examples of metal-fluorine bond formation from a metal hydride, see: (a) B. M. Kraft, R. J. Lachicotte, W. D. J. Jones, *J. Am. Chem. Soc.*, 2000, **122**, 8559; (b) R. P. Hughes, R. B. Laritchev, R. A. Williamson, C. D. Incarvito, L. N. Zakharov, A. L. Rheingold, *Organometallics*, 2003, **22**, 2134; (c) P. A. Deck, A. M. M. Konate, B. V. Kelly, C. Slebodnick, *Organometallics*, 2004, **23**, 1089; (d) L. Bareille, S. Becht, J. L. Cui, P. Le Gendre, C. Moïse, *Organometallics*, 2005, **24**, 5802. (e) B. C. Bailey, J. C. Huffman, D. H. Mindiola, *J. Am. Chem. Soc.*, 2007, **129**, 5302; (f) R. D. Rieth, W. W. Brennessel, W. D. Jones, *Eur. J. Inorg. Chem.*, 2007, 2839; (g) S. A. Johnson, E. T. Taylor, S. J. Cruise, *Organometallics* 2009, **28**, 3842;

(12) (a) T. G. Richmond, *Angew. Chem., Int. Ed.*, 2000, **39**, 3241. (b) T. G. Driver, *Angew. Chem., Int. Ed.*, 2009, **48**, 7974.

(13) (a) D. Noveski, T. Braun, M. Schulte, B. Neumann, H.-H. Stammeler, *Dalton Trans.*, 2003, 4075. (b) T. Braun, F. Wehmeier, K. Altenhöner, *Angew. Chem., Int. Ed.*, 2007, **46**, 5321. (c) R. J. Lindup, T. B. Marder, R. N. Perutz, A. C. Whitwood, *Chem. Commun.*, 2007, 3664. (d) J. Yang, M. Brookhart, *J. Am. Chem. Soc.*, 2007, **129**, 12656.

(14) (a) T. Braun, M. Ahijado-Salomon, K. Altenhöner, M. Teltewskoi, S. Hinze, *Angew. Chem., Int. Ed.*, 2009, **48**, 1818. (b) M. Teltewskoi, J. A. Panetier, S. A. Macgregor, T. Braun, *Angew. Chem., Int. Ed.*, 2010, **49**, 3947.

(15) (a) M. Klahn, C. Fischer, A. Spannenberg, U. Rosenthal, I. Krossing, *Tetrahedron Lett.*, 2007, **48**, 8900; (b) M. Ali, L-P Liu, G. B. Hammond, B. Xu, *Tetrahedron Lett.*, 2009, **50**, 4078.

(16) (a) R. B. King, M. B. Bisnette, *J. Organomet. Chem.*, 1964, **2**, 38; (b) P. W. Jolly, M. I. Bruce, F. G. A. Stone, *J. Chem. Soc.*, 1965, 5830; (c) S. J. Doig, R. P. Hughes, R. E. Davis, S. M. Gadol, K. D. Holland, *Organometallics*, 1984, **3**, 1921; (d) B. L. Edelbach, W. D. Jones, *J. Am. Chem. Soc.*, 1997, **119**, 7734; (e) M. Rausch, C. Bruhn, D. Steinborn, *J. Organomet. Chem.*, 2001, **622**, 172.

(17) (a) M. Aizenberg, D. Milstein, *J. Am. Chem. Soc.*, 1995, **117**, 8674. (b) R. Bosque, E. Clot, S. Fantacci, F. Maseras, O. Eisenstein, R. N. Perutz, K. B. Renkema, K. G. Caulton, *J. Am. Chem. Soc.*, 1998, **120**, 12634.

(18) For examples of heterogenous catalytic hydrodefluorination and hydrogenation of fluorobenzene see: (a) R. J. Young, Jr., V. V. Grushin, *Organometallics*, 1999, **18**, 294; (b) H. Yang, H. R. Gao, R. J. Angelici, *Organometallics* 1999, **18**, 2285; (c) J. Blum, A. Rosenfeld, F. Gelman, H. Schumann, D. Avnir, *J. Mol. Catal. A*, 1999, **146**, 117; (d) C. Desmarets, S. Kuhl, R. Schneider, Y. Fort, *Organometallics*, 2002, **21**, 1554; (e) K. J. Stanger, R. J. Angelici, *J. Mol. Catal. A*, 2004, **207**, 59; (f) M. L. Buil, M. A. Esteruelas, S. Niembro, M. Olivan, L. Orzechowski, C. Pelayo, A. Vallribera, *Organometallics*, 2010, **29**, 4375; (g) R. Baumgartner, K. McNeill, *Environ. Sci. Technol.*, 2012, **46**, 10199. (h) J. Xiao, J. Wu, W. Zhao, S. Cao, *J. Fluorine Chem.*, 2013, **146**, 76.

(19) For examples of heterogenous catalytic cross-coupling reaction with fluorobenzene see: (a) Y. Kiso, K. Tamao, M. Kumada, *J. Organomet. Chem.*, 1973, **50**, C12; (b) V. P. W. Böhm, C. W. K. Gstöttmayr, T. Weskamp, W. A. Herrmann, *Angew. Chem. Int. Ed.*, 2001, **40**, 3387; (c) P. P. Cellier, J-F. Spindler, M. Teaillefer, H-J. Cristau, *Tetrahedron Lett.*, 2003, **44**, 7191; (d) L. Ackermann, R. Born, J. H. Spatz, D. Meyer, *Angew. Chem. Int. Ed.*, 2005, **44**, 7216.

(20) (a) M. Booij, B. Deelman, R. Duchateau, D. S. Postma, A. Meetsma, J. H. Teuben, *Organometallics*, 1993, **12**, 3535; (b) B. M. Kraft, R. J. Lachicotte, W. D. Jones, *J. Am.*

*Chem. Soc.*, 2001, **123**, 10973; (c) W. Liu, K. Welch, C. O. Trindle, M. Sabat, W. H. Myers, W. D. Harman, *Organometallics*, 2007, **26**, 2589; (d) A. R. Fout, J. Scott, D. L. Miller, B. Bailey, M. Pink, D. J. Mindiola, *Organometallics*, 2009, **28**, 331; (e) S. Duttwyler, C. Douvris, N. L. P. Fackler, F. S. Tham, C. A. Reed, K. K. Baldrige, J. S. Siegel, *Angew. Chem. Int. Ed. Engl.*, 2010, **49**, 7519; (f) T. R. Dugan, X. Sun, E. V. Rybak-Akimova, O. Olatunji-Ojo, T. R. Cundari, P. L. Holland, *J. Am. Chem. Soc.*, 2011, **133**, 12418; (g) M. Tobisu, T. Xu, T. Shimasaki, N. Chatani, *J. Am. Chem. Soc.*, 2011, **133**, 19505. (h) T. R. Dugan, J. M. Goldberg, W. W. Brennessel, P. L. Holland, *Organometallics* **2012**, *31*, 1349.

(21) (a) H. S. La Pierre, J. Arnold, F. D. Toste, *Angew. Chem. Int. Ed.* 2011, **50**, 3900; (b) T. L. Gianetti, H. S. La Pierre, J. Arnold, *Eur. J. Inorg. Chem.*, 2013, **22-23**, 3771; (c) H. S. La Pierre, J. Arnold, R. G. Bergman, F. D. Toste, *Inorg. Chem.*, 2012, **51**, 13334; (d) H. S. La Pierre, S. G. Minasian, M. Abubekerev, S. A. Kozimor, D. K. Shuh, T. Tyliszczak, J. Arnold, R. G. Bergman, F. D. Toste, *Inorg. Chem.*, 2013, **52**, 11650.

(22) (a) N. C. Tomson, A. Yan, J. Arnold, R. G. Bergman, *J. Am. Chem. Soc.*, 2008, **130**, 11262; (b) N. C. Tomson, J. Arnold, R. G. Bergman, *Organometallics*, 2010, **29**, 2926; (c) N. C. Tomson, J. Arnold, R. G. Bergman, *Organometallics* 2010, **29**, 5010;

(23) (a) N. C. Tomson, J. Arnold, R. G. Bergman, *Dalton Trans.* **2011**, *40*, 7718. (b) T. L. Gianetti, N. C. Tomson, J. Arnold, R. G. Bergman, *J. Am. Chem. Soc.*, 2011, **133**, 14904; (c) T. L. Gianetti, G. Nocton, S. G. Minasian, N. C. Tomson, A. L. D. Kilcoyne, S. A. Kozimor, D. K. Shuh, T. Tyliszczak, R. G. Bergman, J. Arnold, *J. Am. Chem. Soc.*, 2013, **135**, 3224.

(24) (a) K. Fuchibe, T. Akiyama, *Syn. Lett.*, 2004, **7**, 1282; (b) K. Fuchibe, T. Akiyama, *J. Am. Chem. Soc.*, 2006, **128**, 1434.

(25) T. L. Gianetti, R. G. Bergman, J. Arnold, *J. Am. Chem. Soc.*, 2013, **135**, 8145.

(26) C. Hansch, A. Leo, R. W. Taft, *Chem. Rev.*, 1991, **91**, 165.

(27) S. J. Blanksby, G. B. Ellison, *Acc. Chem. Res.*, 2003, **36**, 255.

(28) D. V. Drobot, E. A. Pisarev, *Russ. J. Inorg. Chem.*, 1981, **26**, 1.

(29) P. Ricci, K. Kramer, X. C. Cambeiro, I. Larrossa, *J. Am. Chem. Soc.*, 2013, **135**, 13258.

(30) We recently isolated and characterized the metallacyclic hydride of the kinetically more inert tantalum analogue, and observed that addition of Lewis bases is required to induce reductive elimination. Kriegel, B., *personal communication*.

(31) Alaimo, P. J.; Peters, D. W.; Arnold, J.; Bergman, R. G. *J. Chem. Educ.* **2001**, *78*, 64.

(32) Feldman, J.; McLain, S. J.; Parthasarathy, A.; Marshall, W. J.; Calabrese, J. C.; Arthur, S. D. *Organometallics* **1997**, *16*, 1514.

(33) Budzelaar, P. H. M.; van Oort, A. B.; Orpen, A. G. *Eur. J. Inorg. Chem.* **1998**, *10*, 1485.

(34) Tomson, N. C.; Yan, A.; Arnold, J.; Bergman, R. G. *J. Am. Chem. Soc.* **2008**, *130*, 11262.

(35) Gianetti, T. L.; Nocton, G.; Minasian, S. G.; Tomson, N. C.; Kilcoyne, A. L. D.; Kozimor, S. A.; Shuh, D. K.; Tyliszczak, T.; Bergman, R. G.; Arnold, J. *J. Am. Chem. Soc.* **2013**, *135*, 3224.

(36) Frisch, M. J.; Trucks, G. W.; Schlegel, H. B.; Scuseria, G. E.; Robb, M. A.; Cheeseman, J. R.; Scalmani, G.; Barone, V.; Mennucci, B.; Petersson, G. A.; Nakatsuji, H.; Caricato, M.; Li, X.; Hratchian, H. P.; Izmaylov, A. F.; Bloino, J.; Zheng, G.; Sonnenberg, J. L.; Hada, M.; Ehara, M.; Toyota, K.; Fukuda, R.; Hasegawa, J.; Ishida, M.; Nakajima, T.; Honda, Y.; Kitao, O.; Nakai, H.; Vreven, T.; J. A. Montgomery, J.; Peralta, J. E.; Ogliaro, F.; Bearpark, M.; Heyd, J. J.; Brothers, E.; Kudin, K. N.; Staroverov, V. N.; Kobayashi, R.; Normand, J.; Raghavachari, K.; Rendell, A.; Burant, J. C.; Iyengar, S. S.; Tomasi, J.; Cossi, M.; Rega, N.;

- Millam, J. M.; Klene, M.; Knox, J. E.; Cross, J. B.; Bakken, V.; Adamo, C.; Jaramillo, J.; Gomperts, R.; Stratmann, R. E.; Yazyev, O.; Austin, A. J.; Cammi, R.; Pomelli, C.; Ochterski, J. W.; Martin, R. L.; Morokuma, K.; Zakrzewski, V. G.; Voth, G. A.; Salvador, P.; Dannenberg, J. J.; Dapprich, S.; Daniels, A. D.; Farkas, Ö.; Foresman, J. B.; Ortiz, J. V.; Cioslowski, J.; Fox, D. J. Gaussian09, Revision A.2; Gaussian, Inc.: Wallingford, CT, 2009.
- (37) C. Adamo and V. Barone, *J. Chem. Phys.*, **1999**, *110*, 6158-69.
- (38) A. D. McLean and G. S. Chandler, "Contracted Gaussian-basis sets for molecular calculations. 1. 2nd row atoms, Z=11-18," *J. Chem. Phys.*, **72** (1980) 5639-48.
- (39) P. Fuentealba, P.; H. Preuss, H.; H. Stoll, H.; Szentpaly, L. V. *Chem. Phys. Lett.*, **1989**, *89*, 418.
- (40) *Quantum Chemistry: The Challenge of Transition Metals and Coordination Chemistry*, Wedig, U.; Dolg, M.; Stoll, H.; Preuss, H. Ed. A. Veillard, Reidel, and Dordrecht, **1986**, 79.
- (41) SMART: Area-Detector Software Package; Bruker Analytic X-ray Systems, I., Madison, WI, 2001-2003, Ed.
- (42) SADABS: Bruker-Nonius Area Detector Scaling and Absorption V2.05 Bruker Analytical X-ray Systems, I., Madison, WI, 2003.
- (43) Sheldrick, G. M. *Acta. Crystallogr. A* **2008**, *64*, 112.
- (44) Farrugia, L. J., *J. Appl. Crystallogr.* 1997, *30*, 565, Ed.

## **Appendix A**

### **DFT Calculation for Chapter I**

## A.1 Calculated stereochemistry configuration of 1.2

The most stable stereochemistry for **1.2** is a capped, square-based pyramidal geometry with the alkenyl-methyl group oriented toward the CO moiety (Figure A.1). This result is supported by the X-ray crystal structures of complexes **1.3** and **1.4** which both exhibit a capped, square-based pyramidal geometry. Additionally, the preferred stereochemistry of the alkyne of **1-2a** is in agreement with the X-ray structure of **1.4** in which the methyl group is oriented toward the <sup>t</sup>BuNC group.

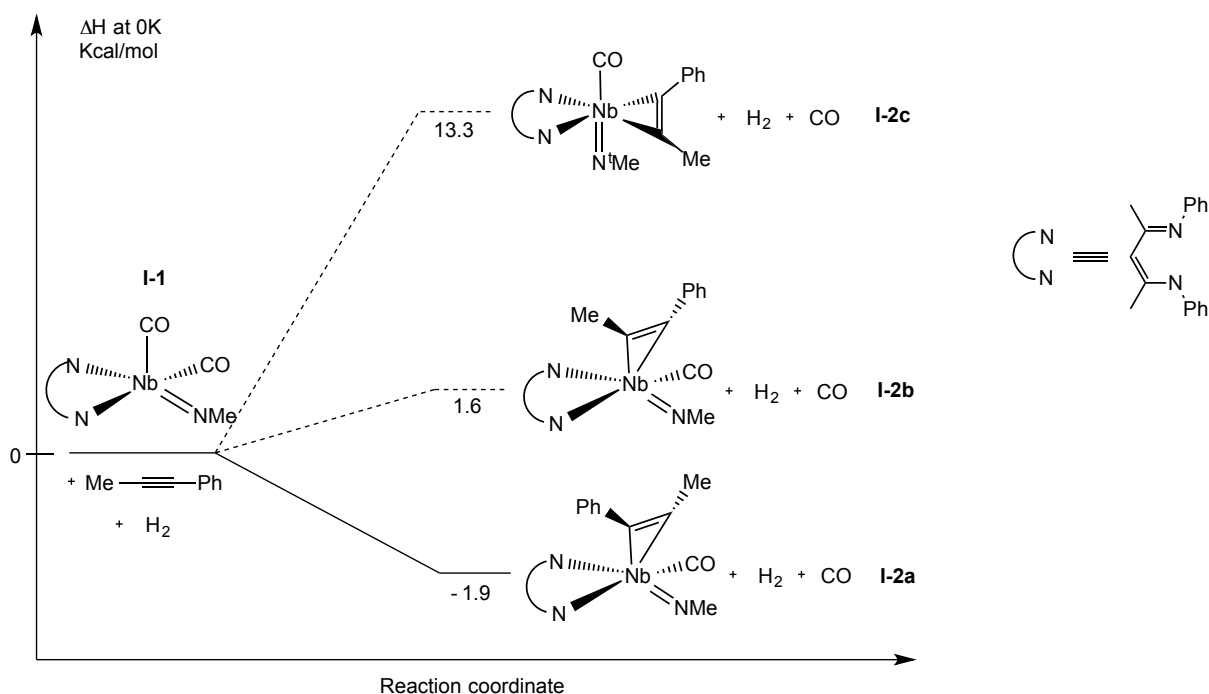


**Figure A.1** Comparison of the energy of the three different possible stereochemistry configurations of **1.2**

## A.2 Calculated transition states for four different activation modes of H<sub>2</sub> by 1.2

Among the four possible transition states studied ( $\sigma$ -bond metathesis, **TS-3a-1**; [3+2] imido activation, **TS-3b-1**; [1,2] imido addition, **TS-3c**; and [3+2] CO activation, **TS-3d**), the sigma bond metathesis transition state was favored by 16.4 - 30.3 kcal/mol (Figure A.2).

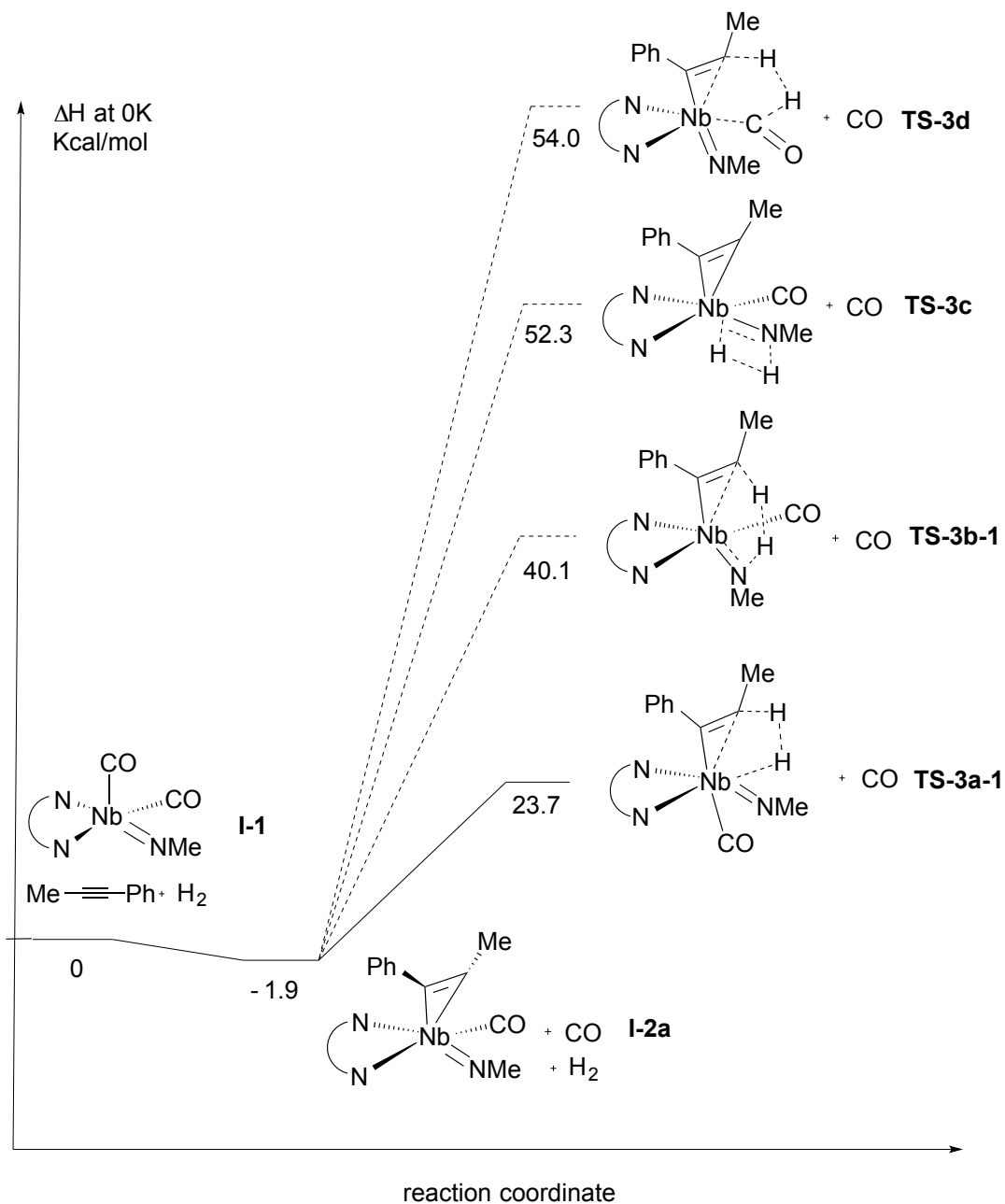


**Figure A.2** Energy comparison of the four different transition states considered for H<sub>2</sub> activation.

### A.3 Regioselectivity of the transition states for the activation of H<sub>2</sub> by 1.2

For the two most energetically favored transition states described in A.2 (**TS-3a** and **TS-3b**), the activation of both Nb-C<sub>(alkyne)</sub> bonds were considered. The cleavage of the Nb-C<sub>(aCH<sub>3</sub>)</sub> bond was found to be more favorable than the cleavage of the Nb-C<sub>(aPh)</sub> in all cases (Figure A.3).

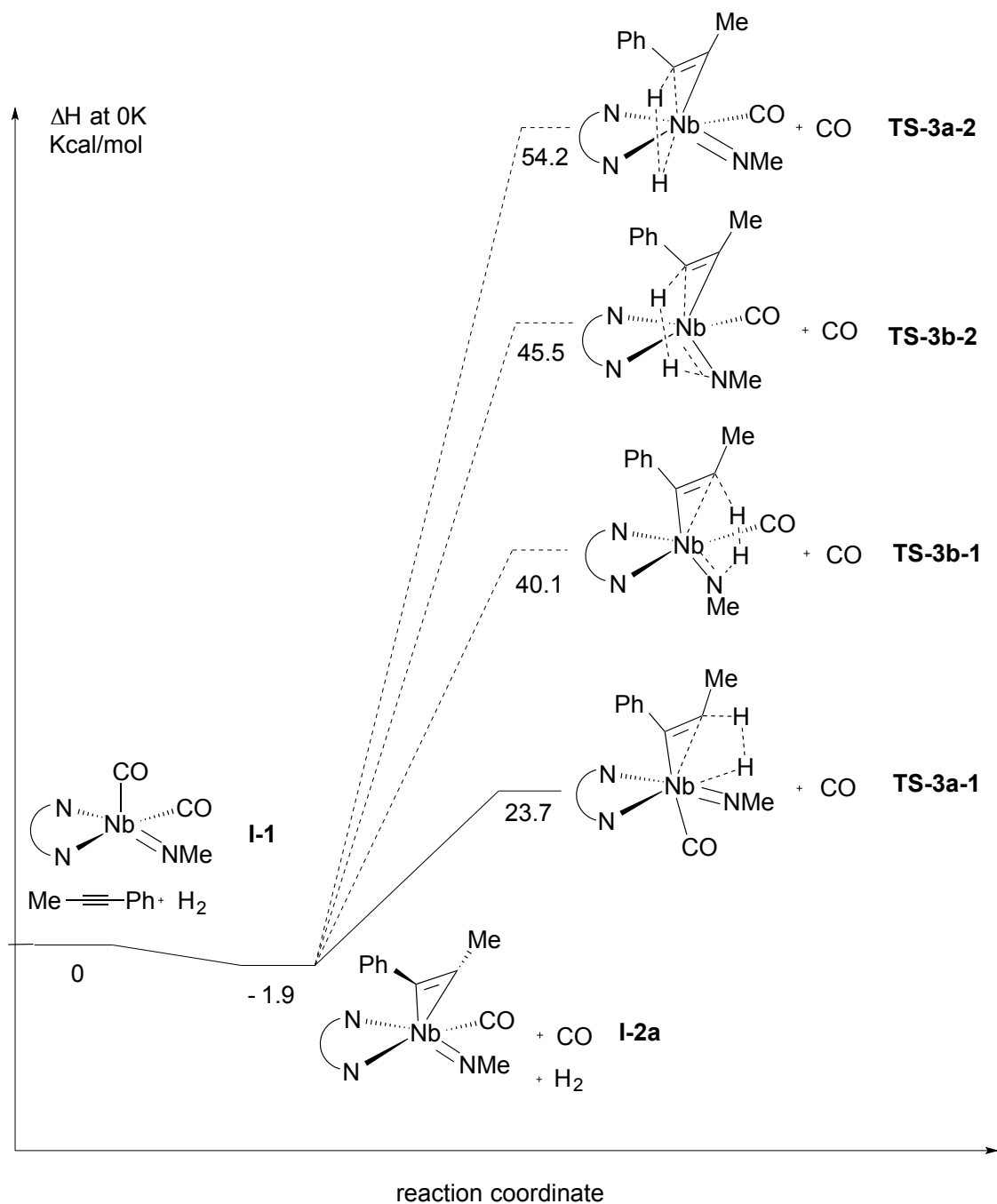


**Figure A.3** Energy calculation of each Nb-C bond for the transition states **TS-3a** and **TS-3b**



#### A.4 Determination of the most favorable final intermediate of the hydrogenation reaction

Two final intermediates were considered for this reaction. The first is the catalyst-product adduct **1.B** observed by  $^1\text{H}$  NMR spectroscopy during hydrogenation in the absence of CO and represented as **I-7** in this theoretical study. The alkene must be displaced by a molecule of CO to reform the catalyst and restart the cycle. In order to estimate the mechanism of CO coordination (associative vs. dissociative) the  $d^2$  four-coordinate complex **I-9** was also considered as a potential intermediate. Both singlet and triplet states were considered for this  $d^2$  species, and the singlet state (**I-9s**) was found to be more stable than the triplet by 9.6 kcal/mol (**I-9t**, Figure A.4). Moreover, the product-catalyst complex **I-7** was found to be slightly more stable than the four-coordinate species **I-9s** (Figure A.4), albeit by only 0.2 kcal/mol at this level of theory.

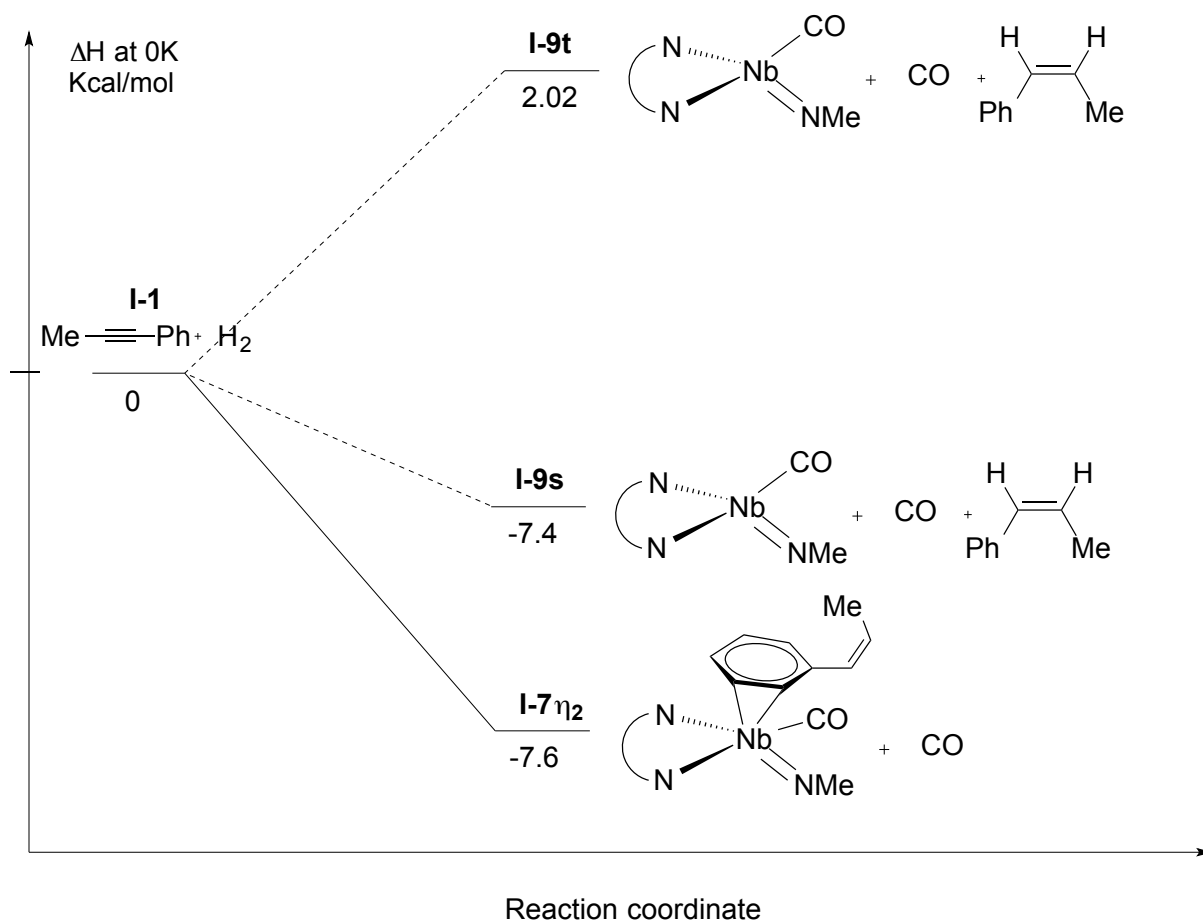


**Figure A.4** Investigation of potential final intermediates of the hydrogenation reaction

## A.5 Calculated reaction coordinates for the hydrogenation reaction via the $\sigma$ -bond metathesis transition state TS-3a-1:

Two reaction pathways were found for the reaction following s-bond metathesis. The first (Figure A.5) involves direct reductive elimination from the octahedral intermediate **I-4**. In the second path, the intermediate **I-4** reorganizes to isomer **I-5** before the reductive elimination step (Figure A.6).

### A.5.1 Reductive elimination directly from **I-4**

Having identified the final product, the first transition state (**TS-3a-1**) and an intermediate between the two (**I-4**), the reductive elimination transition state (**TS-6a**) was easily found. We note that the activation energy associated with this transition state is reasonable for a reaction that proceeds within the observed time frame at room temperature (Figure A.5).

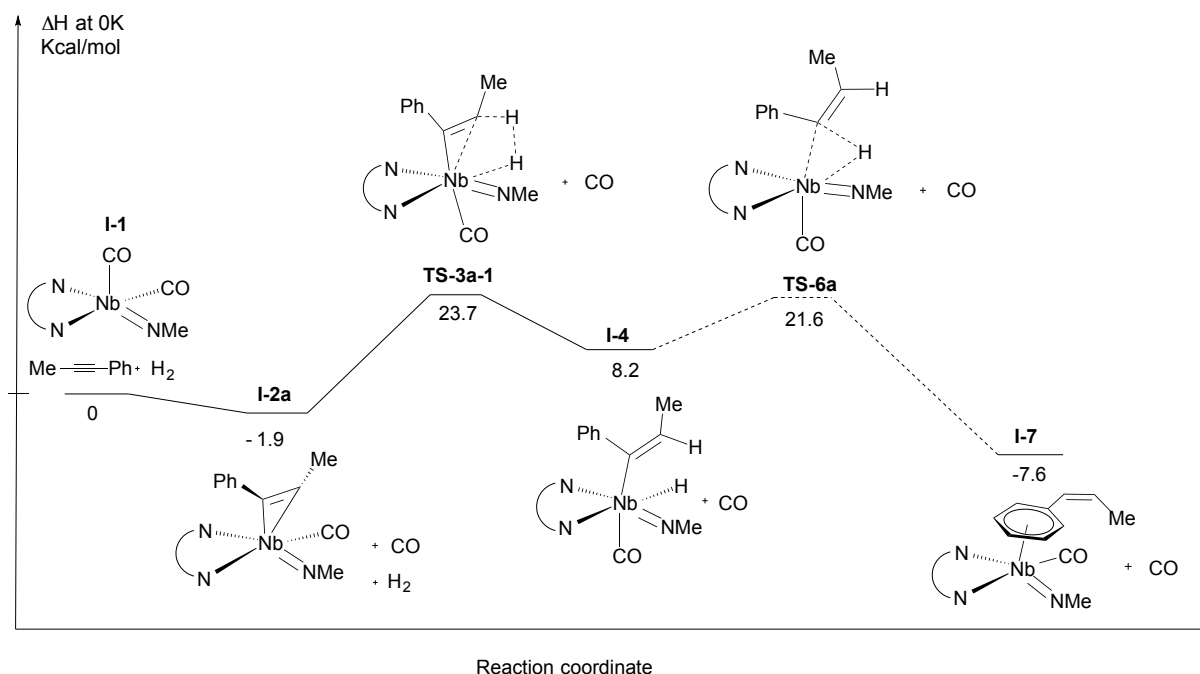


**Figure A.5** Reaction coordinate involving reductive elimination from the intermediate **I-4**

### A.5.2 Reductive elimination after geometrical change from **I-4** to **I-5**.

Still, a more energetically favorable pathway connecting **I-4** and **I-7** was found. Instead of undergoing immediate reductive elimination, the intermediate **I-4** was found to be stabilized by a geometrical change from octahedral to a pentagonal-based pyramidal geometry (intermediate **I-5**, Figure A.6). From this structure, the reductive elimination activation energy leading to the transition state **I-6b** is at only +5.3 kcal/mol. Interestingly, a competitive pathway leading to the formation of a formyl species (**I-8b**) via hydride transfer was found from intermediate **I-5**. However, as mentioned in the paper, no hydroformylation of the alkyne was observed under the catalytic conditions.

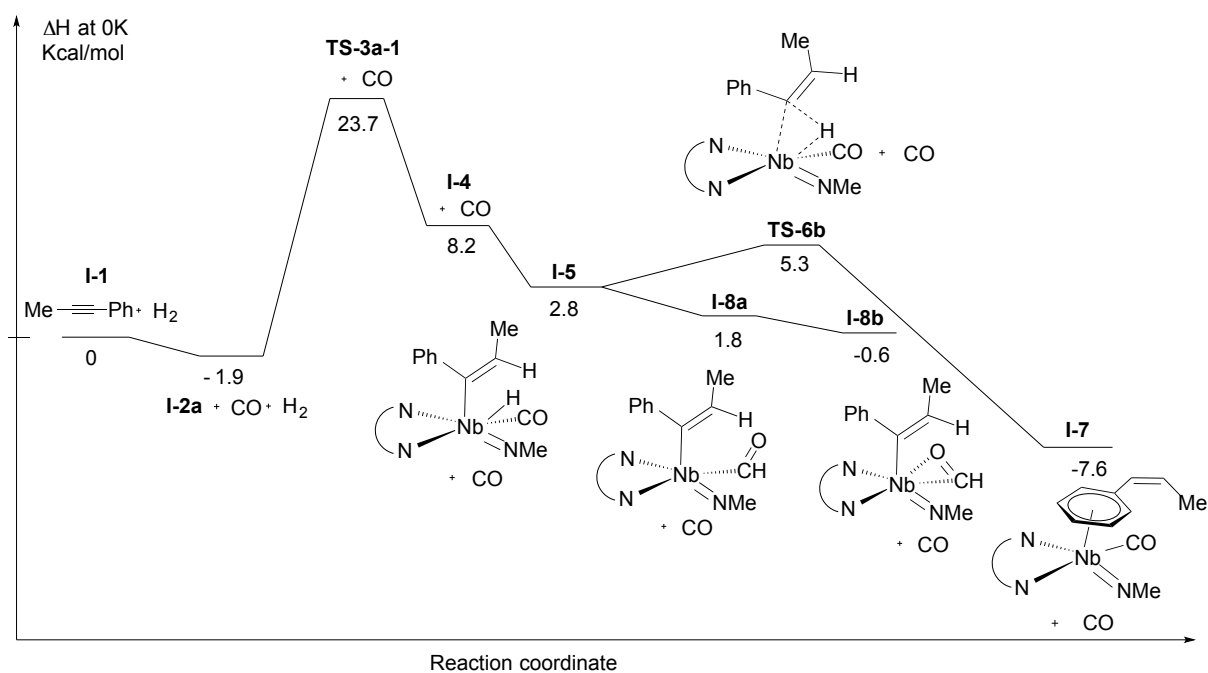


**Figure A.6** The most energetically favored reaction coordinate pathway.

## A.6 Calculated reaction coordinates for the oxidative addition of H<sub>2</sub>

Lastly, the oxidative addition of H<sub>2</sub> to form a dihydride species was studied. However, the dihydride intermediate **I-10** was found to be +3.8 kcal/mol from the  $\sigma$ -bond transition state **TS-3a-1** (Figure A.7). This result further supports the absence of a mechanism involving the oxidative addition of H<sub>2</sub> in this system.

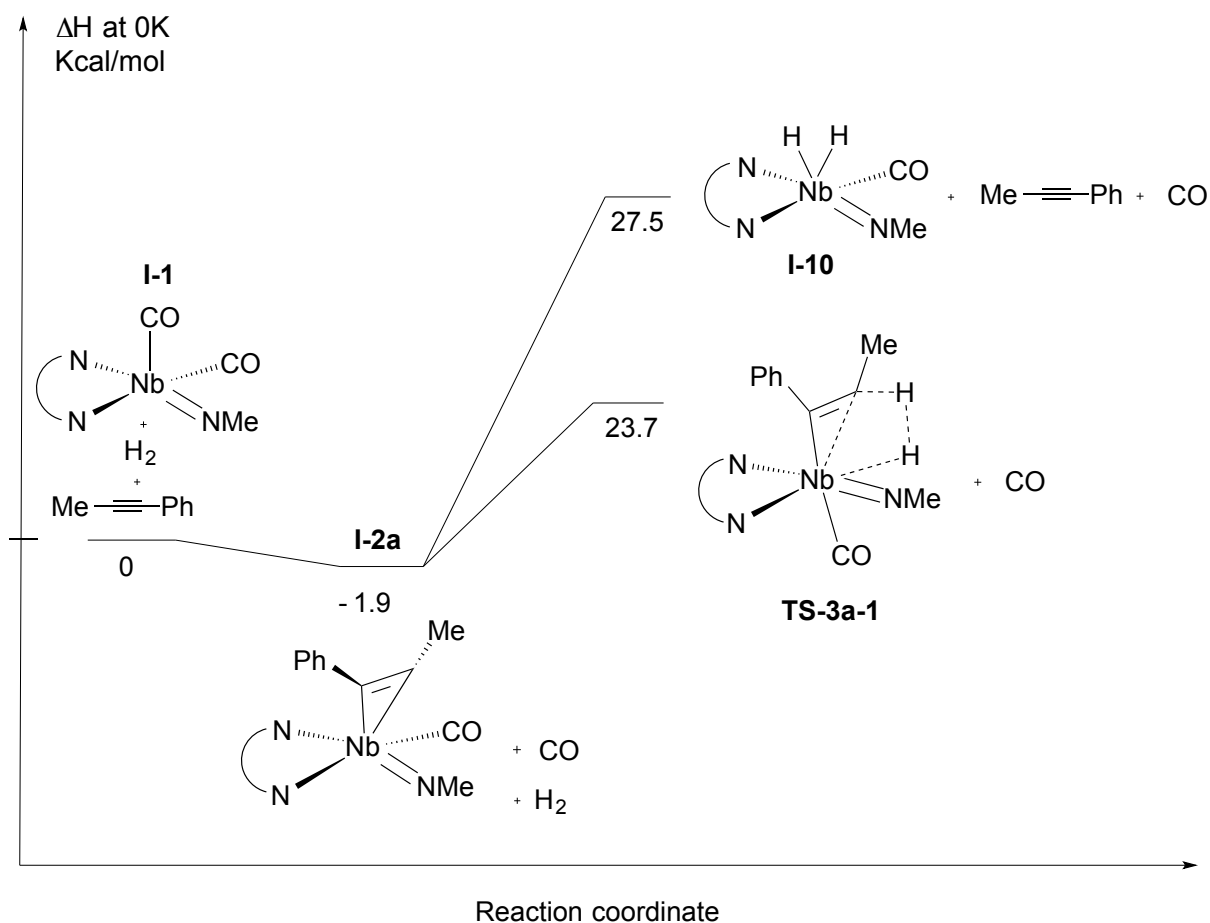


**Figure A.7** Reaction coordinate involving oxidative addition of H<sub>2</sub> to form a dihydride complex **I-10**

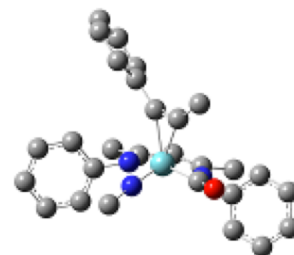
## A.7 Geometry of intermediates and transition states

Color code: carbon = grey, hydrogen = white, nitrogen = blue, niobium = green, oxygen = red.

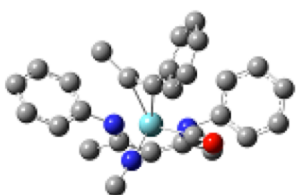
I-1:



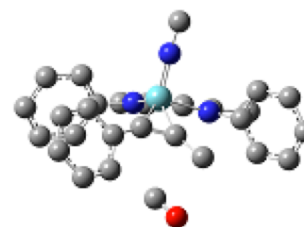
I-2a:



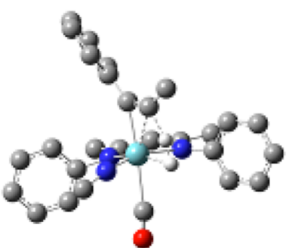
I-2b:



I-2c:



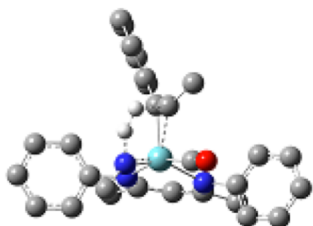
TS-3a-1:



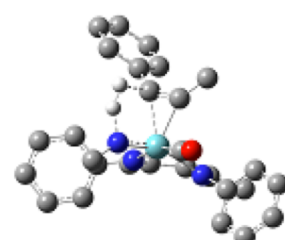
TS-3a-2:



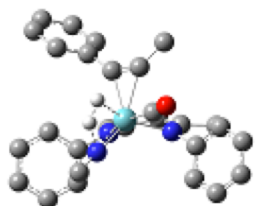
TS-3b-1:



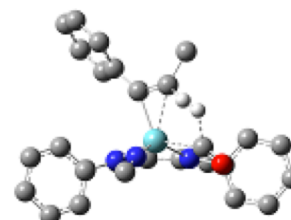
TS-3b-2:



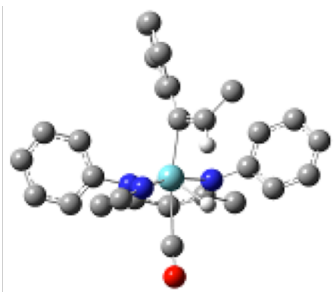
TS-3c:



TS-3d:



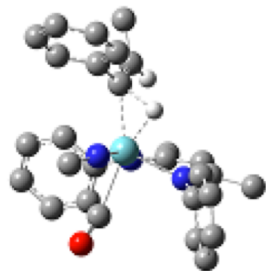
I-4:



I-5:



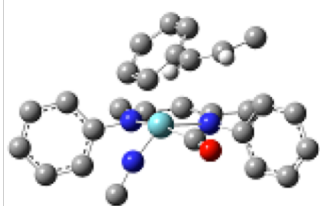
TS-6a:



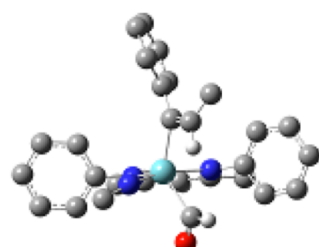
TS-6b:



I-7:



I-8a:



I-8b:



I-9s:



I-9t:



I-10:



## A.8 Calculated energies

### **H<sub>2</sub>**

E (a.u.) = -1.165337  
ZPE (a.u.) = 0.010145

### **CO**

E (a.u.) = -113.301875  
ZPE (a.u.) = 0.005037

### **PhC≡CMe**

E (a.u.) = -347.574536  
ZPE (a.u.) = 0.138264

### **Z-PhCH=CHMe**

E (a.u.) = -348.794080  
ZPE (a.u.) = 0.162443

### **I-1**

E (a.u.) = -1144.891968  
ZPE (a.u.) = 0.357700

### **I-2a**

E (a.u.) = -1379.166498  
ZPE (a.u.) = 0.489485

### **I-2b**

E (a.u.) = -1379.162021  
ZPE (a.u.) = 0.489753

### **I-2c**

E (a.u.) = -1379.143428  
ZPE (a.u.) = 0.489521

### **TS-3a-1**

E (a.u.) = -1380.292207  
ZPE (a.u.) = 0.503167

### **TS-3a-2**

E (a.u.) = -1380.243593  
ZPE (a.u.) = 0.502854

### **TS-3b-1**

E (a.u.) = -1380.266142  
ZPE (a.u.) = 0.503890

### **TS-3b-2**

E (a.u.) = -1380.257544  
ZPE (a.u.) = 0.502720

### **TS-3c**

E (a.u.) = -1380.245726  
ZPE (a.u.) = 0.502062

### **TS-3d**

E (a.u.) = -1380.243974  
ZPE (a.u.) = 0.501717

### **I-4**

E (a.u.) = -1380.316851  
ZPE (a.u.) = 0.507262

### **I-5**

E (a.u.) = -1380.325570  
ZPE (a.u.) = 0.509727

### **TS-6a**

E (a.u.) = -1380.295556  
ZPE (a.u.) = 0.506095

### **TS-6b**

E (a.u.) = -1380.321491  
ZPE (a.u.) = 0.507322

### **I-7**

E (a.u.) = -1380.342005  
ZPE (a.u.) = 0.512890

### **I-8a**

E (a.u.) = -1380.327054  
ZPE (a.u.) = 0.511468

### **I-8b**

E (a.u.) = -1380.330962  
ZPE (a.u.) = 0.511861

### **I-9s, S = 0**

E (a.u.) = -1031.547669  
ZPE (a.u.) = 0.348878

### **I-9t, S = 1**

E (a.u.) = -1031.532662  
ZPE (a.u.) = 0.347734

### **I-10**

E (a.u.) = -1032.712023  
ZPE (a.u.) = 0.363715

## **Appendix B**

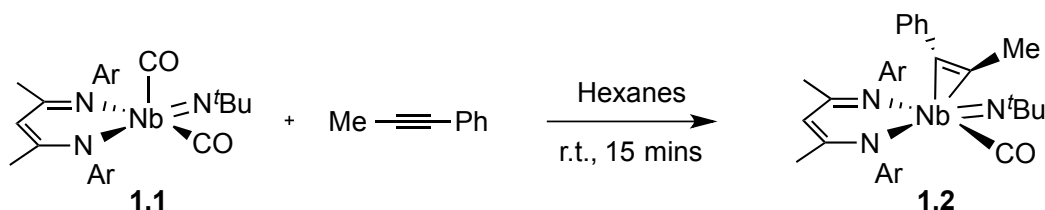
### **Stoichiometric Carbon-Carbon Bond Formation Mediated by Well Defined Nb(III) Complexes**



## Introduction

The use of  $d^2$  early-transition metal complexes as reducing agents is a powerful tool in synthetic organic chemistry.<sup>1</sup> The ability to form C–C bonds *via* the reductive coupling of unsaturated organic molecules (alkenes, alkynes, ketones and ketimines) provides alternative routes to dienes, amino alcohols, diols, and bicyclic products. However, the small number of coordinatively unsaturated  $d^2$  complexes has limited the development of new coupling chemistry and these transformations are mainly observed with  $d^2$  metallocenes of group IV.<sup>2</sup> The most common reaction reported is the coupling of two alkynes, via the formation of a metallacyclopentadiene, to form a diene moiety that is released via acidic work-up.<sup>3</sup> Hydroformylation and hydroiminylation of alkenes and alkynes involving coupling with carbon monoxide or isocyanide to form an enone or enamine products is also known.<sup>4</sup> However, the coupling of a carbon monoxide and two alkynes,<sup>5</sup> as well as the formation of an a,b-unsaturated imine from a metal-mediated reaction of alkyne and isocyanide,<sup>6</sup> remains rare.

In our effort to develop new group 5 catalysts,<sup>7</sup> we presented in chapter I the selective semi-hydrogenation of alkynes under  $H_2:CO$  atmosphere, catalyzed by a dicarbonyl niobium(III) imido supported by a BDI ligand (BDI = N,N-diisopropylphenyl-b-diketiminate, **1.1**, Scheme A.1).<sup>8</sup> Our mechanistic investigations revealed the involvement of an  $h^2$ -alkyne bound monocarbonyl intermediate, (BDI)Nb(N<sup>t</sup>Bu)( $h^2$ -MeC≡CPh)(CO) **1.2**, which is rapidly formed via displacement of one equivalent of carbon monoxide. This species, which was isolated and characterized, then interacts with a molecule of  $H_2$  to release the cis-alkene organic product and reform the dicarbonyl niobium catalyst.<sup>6</sup>



### Scheme B.1

In this chapter is reported the reaction between the dicarbonyl complex **1.1** and a terminal alkyne leading to an unusual coupling product, as well as hydrogenolysis of the NC<sup>t</sup>Bu bound analog of **1.2**, resulting in both *Z*-alkene and a,b-unsaturated imine formation.

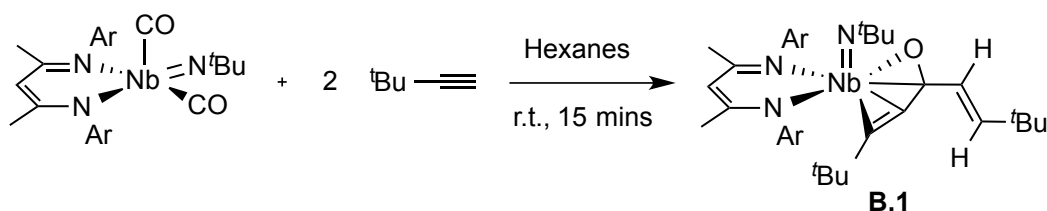
## Results and discussion

### *Reactivity of terminal alkyne*

Reaction of **1.1** with 5 equivalents of <sup>t</sup>butylacetylene led to a fast color change from deep yellow green to orange. Subsequent workup provided orange crystals of **B.1** in 87 % yield (Scheme B.2). The absence of a terminal carbonyl band in the IR spectrum suggests that a new species, different from **1.1** and **1.2**, was formed (**1.1**:  $\nu_{CO} = 1988$  and  $1999$   $cm^{-1}$ , and **1.2**:  $\nu_{CO} = 2031$   $cm^{-1}$  respectively). Instead, an intense band at  $1522$   $cm^{-1}$  was observed, which suggests the presence of highly reduced CO moiety. <sup>1</sup>H NMR spectroscopic analysis reveals the formation of a low-symmetry complex displaying three singlets in the alkyl region integrating for 9 H each, consistent with three inequivalent tert-butyl groups (one from the

imido and two from the alkyne moieties). This observation implies coupling of the alkynes, a reaction that is well known in low-valent early transition metal chemistry.<sup>3</sup>

Coupling of terminal alkynes can form two metallacyclopentadiene regioisomers, the head to head product (M-(RC=CH-CH=CR-)) or the head to tail isomer (M-(HC=CR-CH=CR-)). The b-Hs of the first regioisomer are often observed as singlets in <sup>1</sup>H NMR spectroscopy,<sup>3c-e</sup> while the a-H / b-H set of the second regioisomer exhibits two doublets with a small coupling constant (<sup>4</sup>J<sub>H-H</sub> = 1 to 3 Hz),<sup>3f,g</sup> both within the aromatic region (6.5 to 7.5 ppm). In the present case, two doublets, integrating for one proton each, are observed. COSY and HSQC experiments reveal that these two resonances are not attributable to diastereotopic hydrogens and are coupled to each other, which imply the formation of a metallacyclopentadiene in a head to tail fashion. However, their downfield chemical shifts (6.0 to 6.5 ppm) along with their large coupling constants (<sup>3</sup>J<sub>H,H</sub> = 16.2 Hz) are inconsistent with the formation of a metallacyclopentadiene.



**Scheme B.2** Synthesis of complex **B.1**

The structure of **B.1** was revealed using X-ray crystallography (Figure B.1), which shows the unprecedented coupling of two alkynes and one carbon monoxide to form an ene-one-yne moiety bound in a  $k^4$ -fashion. Complex **B.1** exhibits a pseudo square-based pyramidal geometry ( $t = 0.42$ ),<sup>13</sup> in which both the BDI ligand and the ene-one-yne moiety occupy the basal position, while the imido group is in apical position. Both the metal-BDI nitrogen and metal-imido distances are within the range of distances previously reported for this system (Nb-N<sub>BDI</sub> = 2.22 Å and Nb-N<sub>imido</sub> = 1.757(4) Å). The bond distances of the moiety formed by alkyne-carbonyl coupling as well as the distance between this fragment and the metal center are presented in Figure B.2, left. The long C(1)-C(2) and C(3)-O(1) bond distances of 1.283(3) Å and 1.337(4) Å respectively, compared to 1.20 Å for alkynes and 1.23 Å for ketones, along with the short C(2)-C(3) of 1.386(2) Å, suggest a delocalization of the p-system within the  $k^4$ -yne-one ligand along with formal oxidation of the metal center to Nb(V). Additionally, the Nb-C and Nb-O bond distances (Nb(1)-C(1) = 2.356(3) Å, Nb(1)-C(2) = 2.272(3) Å, Nb(1)-C(3) = 2.308(3) Å and Nb(1)-O(1) = 2.116(2) Å) are within the range of Nb(V)-C(alkyl) and Nb(V)-C(alkoxide) bonds reported previously for this system. <sup>13</sup>C NMR spectroscopy reveals a significant formal reduction of the  $k^4$ -moiety (Figure B.2, right). Both C1 and C2 possess significantly downfield shifted <sup>13</sup>C resonances (C1 = 155 ppm and C2 = 150 ppm) compared to those observed in free t-butyl acetylene (92 and 67 ppm), or compared to signals for a free ynone such as but-3-yn-2-one (82 and 78 ppm). Similarly C3 has a chemical shift of 135 ppm, upfield compared to that of a free ynone molecule (185 ppm), and consistent with the low stretching frequency observed by IR spectroscopy (see above). Both the <sup>1</sup>H and <sup>13</sup>C chemical shifts of H1, H2, C4 and C5 are within expected values for an enone moiety

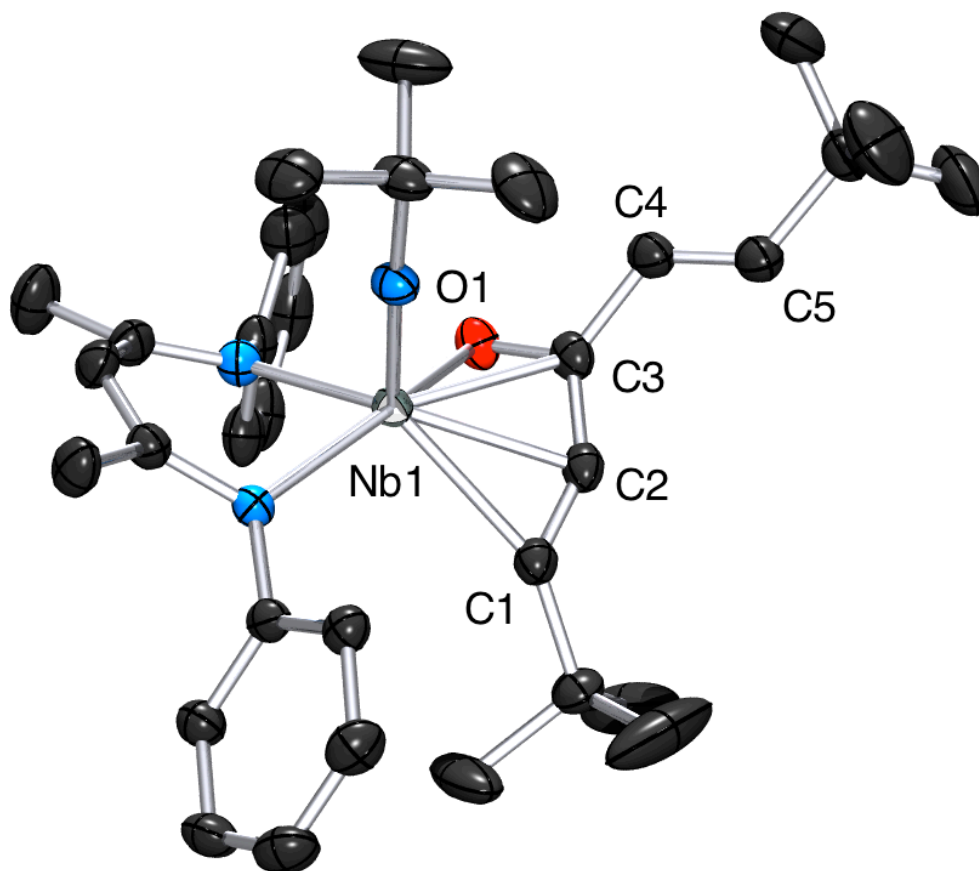


**Figure B.8** ORTEP diagram of **B.1**. Hydrogen atoms and isopropyl of the arene groups have been omitted for clarity.

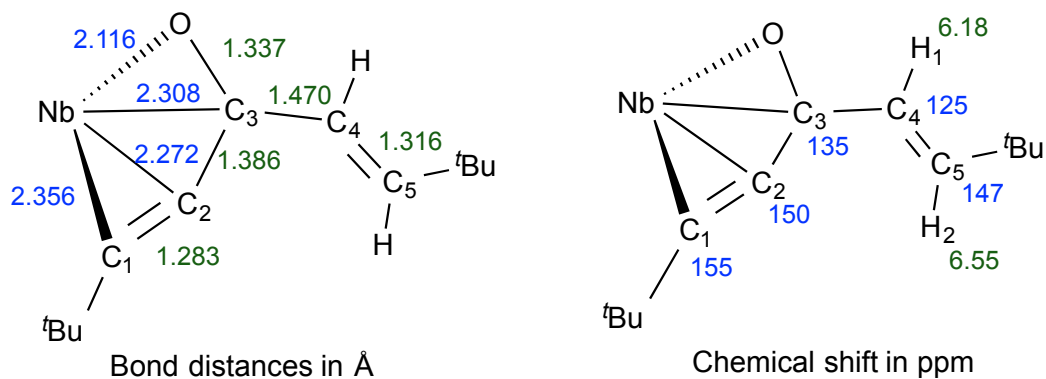
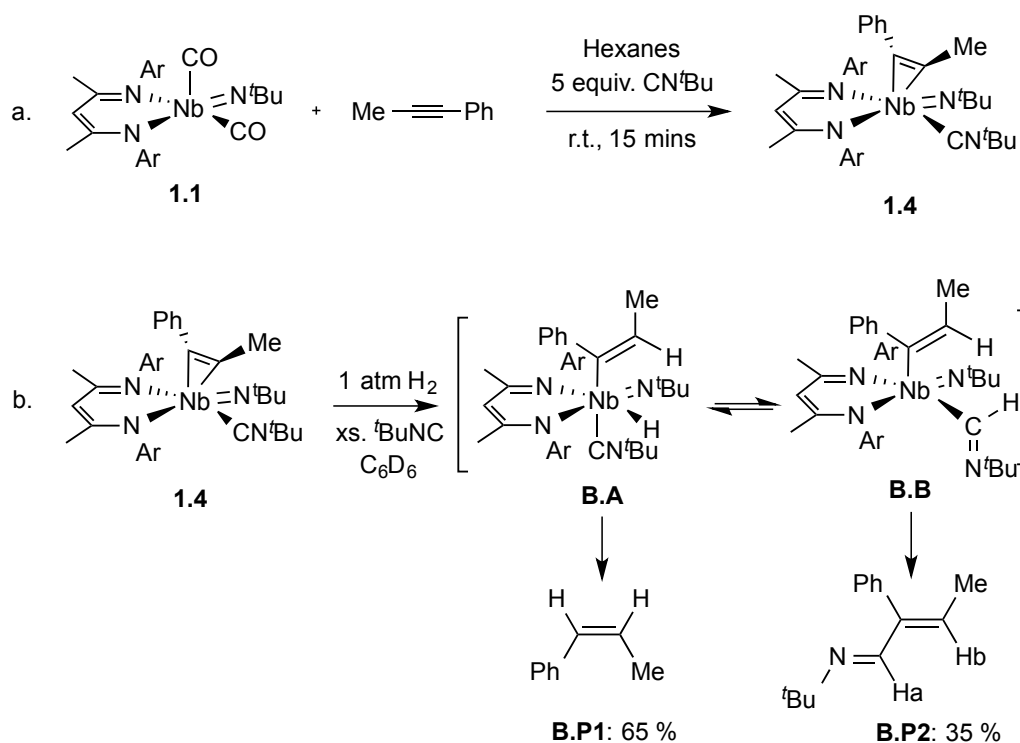


**Figure B.9** Selected bond distances (in Å, left) and chemical shifts (in ppm, right) for the ynone-ene moiety of **B.1**.

## Reactivity of internal alkyne

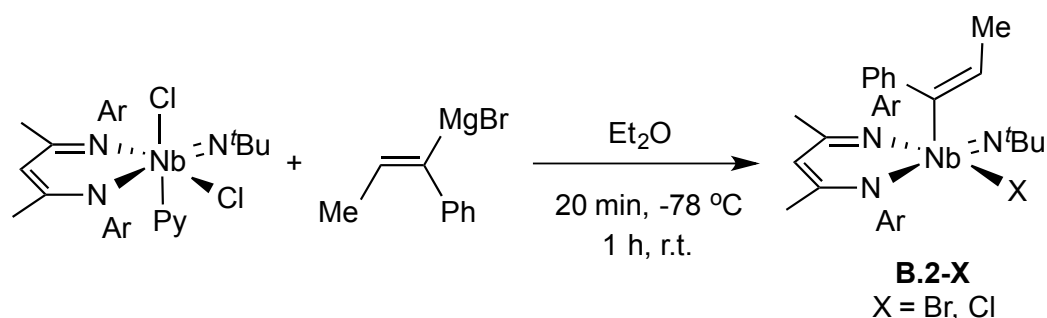
While the mechanism of this unusual terminal alkyne transformation is not yet understood, C-C bond formation involving internal alkynes was also observed within this system. In chapter I, we reported that addition of 1-phenylpropyne to **1.1** in presence of 5 equivalents of CN<sup>t</sup>Bu led to the formation of the alkyne bound complex **1.4**, the isocyanide bound analog of (BDI)Nb(N<sup>t</sup>Bu)(*h*<sup>2</sup>-MeC≡CPh)(CO) (Scheme B.3a). We now present the stoichiometric hydrogenation of **1.4** with an excess of <sup>t</sup>BuNC, which led to a mixture of two organic products in a 1.6 : 1 ratio (**B.P1** and **B.P2**, Scheme B.3b), along with the formation of an organometallic species, which is believed to be the bis- or tris-<sup>t</sup>BuNC niobium analog of (BDI)Nb(N<sup>t</sup>Bu)(CO)<sub>2</sub> (**1.1**). The thermal instability of this complex hampered its isolation and characterization. NMR spectroscopy and GC/MS analysis revealed the formation of the expected cis-alkene (**B.P1**) along with *N*-(<sup>t</sup>butyl)-2-phenylbut-2-en-1-imine (**B.P2**). The formation of the second organic product is believed to have occurred via an alkenyl iminyl intermediate **B.B** (Scheme B.3b). Monitoring of this transformation by <sup>1</sup>H NMR spectroscopy revealed the presence of an organometallic intermediate that exhibits a quartet at 5.56 ppm (<sup>3</sup>J<sub>H,H</sub> = 6.5 Hz) integrating for 1 H relative to the BDI ligand backbone proton (d = 5.18 ppm). The similarity with the <sup>1</sup>H NMR chemical shift of the free organic product (singlet at 7.95 ppm for Ha and quartet at 5.95 ppm for Hb with <sup>3</sup>J<sub>H,H</sub> = 6.8 Hz, Scheme B.3b) suggests that the species observed can be assigned to one of the two intermediates **B.A** and **B.B** proposed in Scheme B.3b or a product-bound species. However, the complexity of the spectrum along with the short lifetime of this compound hampered its complete solution characterization.



**Scheme B.3** Synthesis and hydrogenation of complex **1.4**

Interestingly, during the reported catalytic semi-hydrogenation of 1-phenylpropyne with **1.1** and under high concentration of CO, no hydroformylation products were observed. However, the DFT calculations we reported suggested that an alkenyl formyl complex (the analog of the proposed intermediate **B.B**) was energetically accessible; but such a species was not experimentally observed. Thus, we believe that the reactivity differences observed between **1.2** (hydrogenation only, see chapter I) vs. **1.4** (hydrogenation and C-C coupling) toward H<sub>2</sub>, is governed by the relative rates of the hydride transfer from Nb to the alkenyl moiety vs. the CX ligand (X = O or N<sup>t</sup>Bu).

In order to obtain further structural information on this alkenyl intermediate, the halide analog was synthesized by reaction between (BDI)(Cl)<sub>2</sub>PyNb(N<sup>t</sup>Bu), and one equivalent of the *E*-alkenyl Grignard (Scheme B.4). After workup, yellow crystals of **B.2-X** were isolated in moderate yield (45%). In the first attempt, incomplete halide transfer between Mg and Nb was observed leading to the isolation of a halide mixture, **B.2-Br** and **B.2-Cl**, in a 9:1 ratio. Pure **B.2-Br** was formed by adding an excess of anhydrous MgBr<sub>2</sub>·Et<sub>2</sub>O once the reaction reached room temperature.



**Scheme B.4** Synthesis of complex **B.2-X** (X = Br : Cl in a 9 : 1 ratio).

An ORTEP diagram derived from the single crystal X-ray analysis of **B.2-Br** along with selected bond distances and angles are presented in Figure B.3. This complex exhibits a distorted square pyramidal geometry ( $t = 0.28$ )<sup>13</sup> with the alkenyl moiety in the apical position. The C(2)-C(3) bond distance is within the values reported for other niobium alkenyl complexes and consistent with a carbon-carbon double bond. However, the Nb(1)-C(3) bond distance of 2.155(3) Å is shorter than other reported distances (between 2.25 and 2.40 Å).<sup>14</sup> <sup>1</sup>H NMR spectroscopy showed that the BDI proton backbone can be found at 5.51 ppm, and that the alkenyl proton is coupled to the methyl group resulting in a quartet (<sup>3</sup>J<sub>H,H</sub> = 6.4. Hz) at 6.73 ppm. Although the chemical shifts are more downfield than those obtained for the intermediate observed during hydrogenation of **1.4** (see above), these data support its assignment as an alkenyl complex; however, they are insufficient to allow further structural elucidation. Unfortunately, treatment with hydride sources (*e.g.* super hydride, red-Al, NaH) in the presence or absence of CN<sup>t</sup>Bu resulted in either no conversion, or rapid formation of an intractable mixture, respectively.

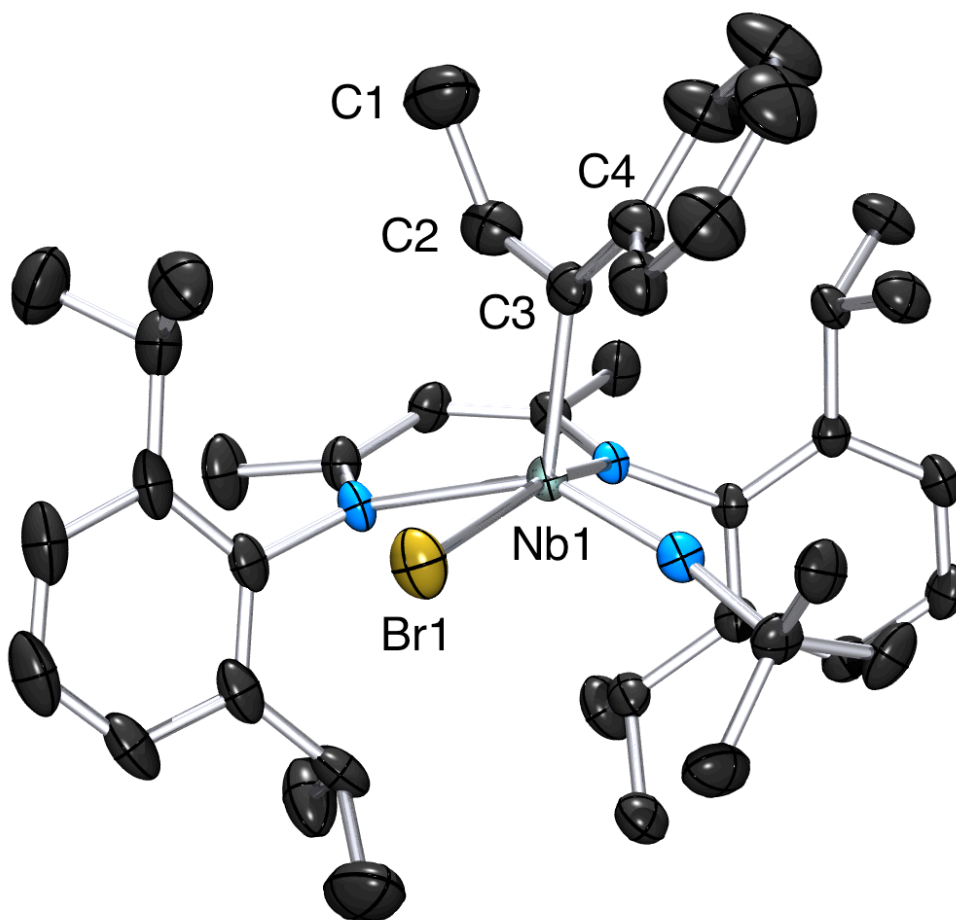


**Figure B.10** ORTEP diagram of **B.2-Br**. Hydrogen atoms have been omitted for clarity. Selected bond lengths (Å): C(1)-C(2): 1.497(6); C(2)-C(3): 1.330(6); C(3)-C(4): 1.487(6), Nb(1)-C(3): 2.155(6), Nb(1)-Br(1): 2.588(4). Selected angles (°): C(1)-C(2)-C(3): 130.1(3), C(2)-C(3)-C(4): 123.5(4), Nb(1)-C(3)-C(2): 102.0(3), Nb(1)-C(3)-C(4): 133.9(3).

## Conclusions

We have described the unusual coupling between two terminal alkynes and one carbon monoxide molecule to form an yne-one-ene bound moiety mediated by a well-defined dicarbonyl niobium (III) complex **1.1**. We have also shown that hydrogenation of the alkyne adduct **1.4** in presence of isocyanide leads to the formation of the expected *Z*- $\beta$ -methylstyrene along with an  $\alpha,\beta$ -unsaturated imine product formed by coupling between the alkyne, H<sub>2</sub> and the isocyanide. <sup>1</sup>H NMR monitoring along with the synthesis of an alkenyl niobium bromide complex suggests that an alkenyl iminyl species is involved in the C-C coupling. In our previous report, in which CO was used in place of CN<sup>t</sup>Bu, related coupling chemistry was not observed, which shows the sensitivity of the system toward modest changes in reaction conditions. We are currently performing further synthetic and mechanistic studies in order to understand the mechanism involved in these transformations as well as their scope and catalytic potential.

## Experimental

**General methods.** Unless otherwise noted, all reactions were performed using standard Schlenk line techniques or in an MBraun inert atmosphere box under an atmosphere of purified nitrogen (<1 ppm O<sub>2</sub>/H<sub>2</sub>O). Glassware, cannulae, and Celite were stored in an oven at *ca.* 160 °C. *n*-Pentane, *n*-hexane, Et<sub>2</sub>O and toluene, were purified by passage through a column of activated alumina, stored over 3 or 4 Å molecular sieves, and degassed prior to use.<sup>9</sup> Deuterated solvents (C<sub>6</sub>D<sub>6</sub>, C<sub>7</sub>D<sub>8</sub>) were dried over sodium/benzophenone, vacuum transferred to a storage flask containing activated molecular sieves, and degassed by three freeze-pump-thaw cycles before being stored in the dry box. PhC≡CMe and <sup>t</sup>BuC≡CH were stored over 4 Å activated molecular sieves and degassed by three freeze-pump-thaw cycles. 1,3,5-trimethoxybenzene was sublimed under static vacuum. (BDI)(CO)<sub>2</sub>Nb(N<sup>t</sup>Bu) (**1.1**),<sup>10a</sup> (BDI)(Cl)<sub>2</sub>PyNb(N<sup>t</sup>Bu),<sup>10b</sup> (BDI)Nb(N<sup>t</sup>Bu)(PhC≡CMe)(L) with (**1.3**: L = CO and **1.4**: L = CN<sup>t</sup>Bu),<sup>8</sup> and Ph(MgBr)C=C(H)Me<sup>11</sup> were prepared using literature procedures. All other reagents were acquired from commercial sources and used as received. NMR spectra were recorded on Bruker AV-300, AVQ-400, AVB-400, DRX-500, AV-500, and AV-600 spectrometers. Chemical shifts were measured relative to residual solvent peaks, which were assigned relative to an external TMS standard set at 0.00 ppm. <sup>1</sup>H and <sup>13</sup>C NMR assignments were routinely confirmed by <sup>1</sup>H-<sup>1</sup>H (COSY, NOESY) or <sup>1</sup>H-<sup>13</sup>C (HSQC and HMBC) experiments. The uncorrected melting points were determined on an Optmelt SRS using sealed capillaries prepared under nitrogen. Elemental analyses were determined at the College of Chemistry, University of California, Berkeley. The X-ray structural determinations were performed at CHEXRAY, University of California, Berkeley on Bruker SMART 1000 or SMART APEX diffractometers. GC/MS analyses were performed using a Agilent 6890 N Network GC system coupled to a 5973 Network mass selective detector.

**(BDI)(<sup>t</sup>BuCCC(O)(C(H)=C(H)<sup>t</sup>Bu)Nb(N<sup>t</sup>Bu) (B.1).** <sup>t</sup>BuC≡CH (48 mL, 3.90 mmol, 5 equiv.) was added to a solution of **1.1** (0.51 g, 0.78 mmol, 1 equiv.) in hexane at room temperature. The solution immediately changed color from yellow-green to orange. The solution was stirred for 15 min at room temperature, the volatile materials were removed under vacuum and the orange residue was extracted with hexanes (40 mL). Crystallization from hexane at -40 °C resulted in the formation of orange crystals of **B.1** (68 %). X-ray quality crystals were obtained by recrystallization from toluene at -20 °C. <sup>1</sup>H NMR (400 MHz, C<sub>6</sub>D<sub>6</sub>, 293 K): δ(ppm) 7.36 (d, 1H, Ar, <sup>3</sup>J<sub>HH</sub> = 7.2 Hz), 7.27 (m, 2H, Ar), 7.21 (m, 2H, Ar), 7.12 (m, 2H, Ar), 7.06 (d, 1H, Ar, <sup>3</sup>J<sub>HH</sub> = 7.0 Hz), 7.01 (d, 1H, Ar, <sup>3</sup>J<sub>HH</sub> = 6.8 Hz), 6.55 (d, 1H, RCH=CH<sup>t</sup>Bu, <sup>3</sup>J<sub>HH</sub> = 16.4 Hz), 6.18 (d, 1H, RCH=CH<sup>t</sup>Bu, <sup>3</sup>J<sub>HH</sub> = 16.4 Hz), 5.28 (s, 1 H, HC(C(Me)NAr)<sub>2</sub>), 4.50 (sept, 1 H, CHMe<sub>2</sub>, <sup>3</sup>J<sub>HH</sub> = 7.0 Hz), 3.83 (sept, 1 H, CHMe<sub>2</sub>, <sup>3</sup>J<sub>HH</sub> = 7.0 Hz), 3.11 (sept, 1 H, CHMe<sub>2</sub>, <sup>3</sup>J<sub>HH</sub> = 6.9 Hz), 2.76 (sept, 1 H, CHMe<sub>2</sub>, <sup>3</sup>J<sub>HH</sub> = 6.9 Hz), 1.77 (s, 3 H, HC(C(Me)NAr)<sub>2</sub>), 1.71 (s, 3 H, HC(C(Me)NAr)<sub>2</sub>), 1.65 (d, 3 H, CHMe<sub>2</sub>, <sup>3</sup>J<sub>HH</sub> = 6.8 Hz), 1.53 (d, 3 H, CHMe<sub>2</sub>, <sup>3</sup>J<sub>HH</sub> = 6.8 Hz), 1.40 (d, 3 H, CHMe<sub>2</sub>, <sup>3</sup>J<sub>HH</sub> = 7.2 Hz), 1.37 (d, 3 H, CHMe<sub>2</sub>, <sup>3</sup>J<sub>HH</sub> = 6.8 Hz), 1.27 (d, 3 H, CHMe<sub>2</sub>, <sup>3</sup>J<sub>HH</sub> = 6.8 Hz), 1.25 (s, 9 H, Nb=N<sup>t</sup>Bu), 1.15 (d, 6 H, CHMe<sub>2</sub>, <sup>3</sup>J<sub>HH</sub> = 7.2 Hz), 1.11 (d, 3 H, CHMe<sub>2</sub>, <sup>3</sup>J<sub>HH</sub> = 6.8 Hz), 0.96 (s, 9 H, RCH=CH<sup>t</sup>Bu), 0.88 (d, 3 H, CHMe<sub>2</sub>, <sup>3</sup>J<sub>HH</sub> = 6.8 Hz), 0.81 (s, 9 H, <sup>t</sup>BuCCC(O)R'). <sup>13</sup>C NMR (100 MHz, C<sub>6</sub>D<sub>6</sub>, 293 K): 171.3 and 169.3 (C, HC(C(Me)NAr)<sub>2</sub>), 155.3 (C, <sup>t</sup>BuCCC(O)R'), 150.2 (C, <sup>t</sup>BuCCC(O)R'), 147.5 (CH, RCH=CH<sup>t</sup>Bu), 145-140 (4 peaks, C, Ar<sub>N</sub>), 135.4 (C, <sup>t</sup>BuCCC(O)R'), 125.3 (CH, RCH=CH<sup>t</sup>Bu), 127-123 (6 peaks, CH, Ar), 103.5 (CH, HC(C(Me)NAr)<sub>2</sub>), 72.5 (C, Nb=NC(CH<sub>3</sub>)<sub>3</sub>), 34.2 and 33.5 (C and CH<sub>3</sub>, <sup>t</sup>BuCCC(O)R'), 32.5

(CH<sub>3</sub>, Nb=NC(CH<sub>3</sub>)<sub>3</sub>), 29.4 and 29.0 (CH<sub>3</sub> and C, RCH=CH<sup>t</sup>Bu), 29.0-27.9 (4 peaks, CH, CHMe<sub>2</sub>), 26.3 and 26.0 (CH<sub>3</sub>, HC(C(Me)NAr)<sub>2</sub>), 26-24 (8 peaks, CH<sub>3</sub>, CHMe<sub>2</sub>). To simplify the assignment R and R' were used to describe the yne-one-ene moiety with R = <sup>t</sup>BuCCC(O) and R' = RCH=CH<sup>t</sup>Bu. IR (nujol): 1522 cm<sup>-1</sup>. Anal. Calcd for C<sub>50</sub>H<sub>71</sub>N<sub>3</sub>NbO: C, 71.38; H, 9.12; N, 5.43; found: C, 71.14; H, 9.36; N, 5.65. Mp: 185-190 °C (decomp).

**(BDI)(PhC=C(H)Me)(X)Nb(N<sup>t</sup>Bu) (B.2-X)** (X = Br : Cl, in a 9:1 ratio). To a stirred suspension of (BDI)pyCl<sub>2</sub>Nb(N<sup>t</sup>Bu) (0.369 g, 0.490 mmol, 1 equiv.) in 20 mL Et<sub>2</sub>O cooled to -78 °C was added dropwise the *trans*-Grignard Ph(MgBr)C=C(H)Me in Et<sub>2</sub>O (1.2 mL, 0.38 M, 0.45 mmol, 0.9 equiv.). The resulting mixture was stirred for 20 min at -78 °C. The solution was allowed to warm to room temperature, resulting in a color change from deep red to green. The mixture was stirred for 1 h at room temperature, and then the volatile materials were removed under vacuum. The residue was extracted with pentane (3 x 30 mL) and the extracts were concentrated to 50 mL, at which time yellow crystals started to form on the walls of the flask. The flask was stored at -40 °C for 2 days, resulting in isolation of yellow crystals of B.2-X. Analysis by <sup>1</sup>H NMR spectroscopy revealed a mixture of two complexes: 90 % of the bromide and 10 % of the analogous chloride. Yield: 152 mg, 64 %. <sup>1</sup>H NMR (400 MHz, C<sub>6</sub>D<sub>6</sub>, 293 K): δ(ppm) Bromide complex: 7.58 (d, 2 H, PhC=C(H)Me, <sup>3</sup>J<sub>HH</sub> = 7.2 Hz), 7.26-7.20 (m, 5 H, Ar and PhC=C(H)Me), 7.11-7.00 (m, 5 H, Ar and PhC=C(H)Me), 6.73 (q, 1 H, PhC=C(H)Me, <sup>3</sup>J<sub>HH</sub> = 6.4 Hz), 5.51 (s, 1 H, HC(C(Me)NAr)<sub>2</sub>), 3.24 (sept, 1 H, CHMe<sub>2</sub>, <sup>3</sup>J<sub>HH</sub> = 6.8 Hz), 3.15 (sept, 1 H, CHMe<sub>2</sub>, <sup>3</sup>J<sub>HH</sub> = 6.8 Hz), 3.08 (sept, 1 H, CHMe<sub>2</sub>, <sup>3</sup>J<sub>HH</sub> = 6.8 Hz), 2.86 (sept, 1 H, CHMe<sub>2</sub>, <sup>3</sup>J<sub>HH</sub> = 6.8 Hz), 1.75 (d, 3 H, PhC=C(H)Me, <sup>3</sup>J<sub>HH</sub> = 6.4 Hz), 1.71 (s, 3 H, HC(C(Me)NAr)<sub>2</sub>), 1.47 (s, 3 H, HC(C(Me)NAr)<sub>2</sub>), 1.39 (m, 9 H, CHMe<sub>2</sub>), 1.23 (d, 3 H, CHMe<sub>2</sub>, <sup>3</sup>J<sub>HH</sub> = 6.8 Hz), 1.20 (d, 6 H, CHMe<sub>2</sub>, <sup>3</sup>J<sub>HH</sub> = 7.2 Hz), 1.11 (d, 3 H, CHMe<sub>2</sub>, <sup>3</sup>J<sub>HH</sub> = 6.8 Hz), 1.07 (d, 3 H, CHMe<sub>2</sub>, <sup>3</sup>J<sub>HH</sub> = 6.8 Hz), 0.93 (s, 9 H, <sup>t</sup>Bu). Chloride complex: 7.53 (d, 2 H, PhC=C(H)Me, <sup>3</sup>J<sub>HH</sub> = 7.2 Hz), 6.62 (q, 1 H, PhC=C(H)Me, <sup>3</sup>J<sub>HH</sub> = 6.4 Hz), 5.46 (s, 1 H, HC(C(Me)NAr)<sub>2</sub>), 1.80 (d, 3 H, PhC=C(H)Me, <sup>3</sup>J<sub>HH</sub> = 6.4 Hz), 1.62 (s, 3 H, HC(C(Me)NAr)<sub>2</sub>), 1.49 (s, 3 H, HC(C(Me)NAr)<sub>2</sub>), 0.85 (s, 9 H, <sup>t</sup>Bu). No further characterization was performed due to the mixed composition of this sample.

**(BDI)(PhC=C(H)Me)(Br)Nb(N<sup>t</sup>Bu) (B.2-Br)**. MgBr<sub>2</sub>·Et<sub>2</sub>O was added to a solution of **B.2-X** (X = Br : Cl, in a 9:1 ratio, 0.220 g, 0.282 mmol, 1 equiv.) in ether (20 mL) and the mixture was stirred overnight. The volatile material was removed under vacuum and the residue was extracted with pentane (3 x 30 mL). The extracts were concentrated to 50 mL to afford orange crystals after storage at -40 °C for two days. Yield: 164 mg, 75 %. X-ray quality crystals were obtained by recrystallization from hexanes at -20 °C. The <sup>1</sup>H NMR spectrum was completely identical to that of the bromide complex described previously. <sup>13</sup>C NMR (100 MHz, C<sub>6</sub>D<sub>6</sub>, 293 K): 171.3 and 169.3 (C, HC(C(Me)NAr)<sub>2</sub>), 143.1 (CH, Nb-C(Ph)=CHMe), 145-140 (CH, Nb-C(Ph)=CHMe), 141 (C, Nb-C(Ph)=CHMe), 145-140 (4 peaks, C, Ar<sub>N</sub>), 121.3 (C, Nb-C(Ph)=CHMe), 127-123 (6 peaks, CH, Ar), 105.5 (CH, HC(C(Me)NAr)<sub>2</sub>), 70.5 (C, Nb=NC(CH<sub>3</sub>)<sub>3</sub>), 30.5 (CH<sub>3</sub>, Nb=NC(CH<sub>3</sub>)<sub>3</sub>), 34.5 (CH<sub>3</sub>, Nb-C(Ph)=CHMe), 29.6-28.5 (4 peaks, CH, CHMe<sub>2</sub>), 25.3 and 25.0 (CH<sub>3</sub>, HC(C(Me)NAr)<sub>2</sub>), 27-25 (8 peaks, CH<sub>3</sub>, CHMe<sub>2</sub>). Anal. Calcd for C<sub>42</sub>H<sub>59</sub>BrN<sub>3</sub>Nb: C, 64.78; H, 7.64; N, 5.40; found: C, 65.13; H, 7.93; N, 5.55. Mp: 160-165 °C (decomp).



**Stoichiometric hydrogenation of 1.4.** To a J-Young NMR tube with a Teflon cap containing 0.5 mL of C<sub>6</sub>D<sub>6</sub> and trimethoxybenzene (0.011 M, 1 equiv.) was added complex **1.4** (51 mg, 0.078 mmol, 1 equiv), and *t*-butyl isocyanide (44 mL, 0.390 mmol, 5 equiv.). The solution was freeze-pump-thawed three times and then refilled with H<sub>2</sub> (1 atm, 2.5 mL, 0.102 mmol, 10 equiv). The mixture was allowed to warm to room temperature. The transformation was then monitored by <sup>1</sup>H NMR spectroscopy until completion (4 h). NMR yields were calculated by integration of the vinyl protons of the *cis*-β-methylstyrene and *N*-(*t*-butyl)-2-phenylbut-2-en-1-imine. <sup>1</sup>H NMR (500MHz, C<sub>6</sub>D<sub>6</sub>, 293 K), δ(ppm), **trimethoxybenzene**: 6.26 (s, 3 H, benzene ring); ***cis*-β-methylstyrene (B.P1)**: 6.42 (dd, 1 H, PhC(*H*)=C(*H*)Me, <sup>3</sup>J<sub>HHvinyl</sub> = 11.5 Hz, <sup>3</sup>J<sub>HHphenyl</sub> = 2 Hz); ***N*-(*t*-butyl)-2-phenylbut-2-en-1-imine (B.P2)**: 5.95 (q, 1 H, MeCHC(Ph)N<sup>t</sup>Bu, <sup>3</sup>J<sub>HH</sub> = 6.8 Hz). Once the reaction was complete, the organic products were analysed by GC/MS further confirming the nature of the a,b-unsaturated imine product. (m/z): P(2) = 201.

**X-ray crystallography study.** A crystal of appropriate size was coated in Paratone-N oil and mounted on a Kapton<sup>®</sup> loop. The loop was transferred to a diffractometer equipped with a CCD area detector,<sup>12a</sup> centered in the beam, and cooled by a nitrogen flow low-temperature apparatus that had been previously calibrated by a thermocouple placed at the same position as the crystal. Preliminary orientation matrices and cell constants were determined by collection of 3x20 10 s frames, followed by spot integration and least-squares refinement. An arbitrary hemisphere of data was collected, and the raw data were integrated using SAINT.<sup>12b</sup> Cell dimensions reported were calculated from all reflections with *I* > 10 σ. The data were corrected for Lorentz and polarization effects; no correction for crystal decay was applied. Data were analyzed for agreement and possible absorption using XPREP.<sup>12c</sup> An empirical absorption correction based on comparison of redundant and equivalent reflections was applied using SADABS.<sup>12d</sup> Structures were solved by direct methods with the aid of successive difference Fourier maps and were refined on *F*<sup>2</sup> using the SHELXTL 5.0 software package. Thermal parameters for all non-hydrogen atoms were refined anisotropically. For all structures,  $R_1 = \Sigma(|F_o| - |F_c|)/\Sigma(|F_o|)$ ;  $wR_2 = [\Sigma\{w(F_o^2 - F_c^2)^2\}/\Sigma\{w(F_o^2)^2\}]^{1/2}$ .

**Table B.2** Crystallographic parameters of **B.1** and **B.2-Br**

<b>Compound</b>	<b>B.1.C<sub>7</sub>H<sub>8</sub></b>	<b>B.2-Br</b>
Formula	C <sub>50</sub> H <sub>70</sub> N <sub>3</sub> NbO	C <sub>42</sub> H <sub>59</sub> BrN <sub>3</sub> Nb
Formula weight	822.00	778.74
Space Group	<i>P</i> 2 <sub>1</sub> / <i>c</i>	<i>P</i> 2 <sub>1</sub> / <i>n</i>
<i>a</i> (Å)	9.377(5)	13.268(2)
<i>b</i> (Å)	22.177(5)	19.718(3)
<i>c</i> (Å)	22.588(5)	15.667(3)
$\alpha$ (°)	90	90
$\beta$ (°)	90.240(5)	98.086(2)
$\gamma$ (°)	90	90
<i>V</i> (Å <sup>3</sup> )	4697(3)	4058.0(12)
<i>Z</i>	4	4
$\rho_{\text{calcd}}$ (g/cm <sup>3</sup> )	1.162	1.275
F <sub>000</sub>	1760	1632
$\mu$ (mm <sup>-1</sup> )	0.294	1.312
T <sub>min</sub> /T <sub>max</sub>	0.8940/0.9328	0.7267/0.8800
No. rflns measured	55745	23885
No. indep. Rflns	8591	7386
<i>R</i> <sub>int</sub>	0.0255	0.0577
No. obs. ( <i>I</i> > 2.00σ( <i>I</i> ))	8591	7386
No. variables	581	438
<i>R</i> <sub>1</sub> , <i>wR</i> <sub>2</sub>	0.0287, 0.0716	0.0471, 0.1010
<i>R</i> <sub>1</sub> (all data)	0.0363	0.0919
GoF	1.046	1.011
Res. peak/hole (e <sup>-</sup> /Å <sup>3</sup> )	0.349/-0.285	0.555/-0.793

## References:

- (1) Sato, F.; Urabe, H.; Okamoto, S. *Chem. Rev.*, **2000**, *100*, 2835.
- (2) (a) Demerseman, B.; Bouquet, G.; Bigorgne, M. *J. Organomet. Chem.*, **1976**, *107*, C19. (b) Demerseman, B.; Bouquet, G.; Bigorgne, M. *J. Organomet. Chem.*, **1977**, *132*, 223. (c) Fachinetti, G.; Fochi, G.; Floriani, C. *J. Chem. Soc., Chem. Comm.*, **1976**, 230. (d) Gell, K. I.; Schwartz, J. *J. Am. Chem. Soc.*, **1981**, *103*, 2687. (e) Thomas, J. L.; Brown, J. K. T. *J. Organomet. Chem.* **1976**, *111*, 297.
- (3) For selected examples with early transition metals: (a) Miller, A. D.; McBee, J. L.; Tilley, T. D. *J. Am. Chem. Soc.*, **2008**, *130*, 4992. (b) García-Yebra, C.; Carrero, F.; López-Mardomingo, C.; Fajardo, M.; Rodríguez, A.; Antiñolo, A.; Otero, A.; Lucas, D.; Mugnier, Y. *Organometallics*, **1999**, *18*, 1287. (c) Chao, Y-W; Wexler, P. A.; Wigley, D. E. *Inorg. Chem.*, **1989**, *28*, 3860. (d) Guérin, F.; McConville, D. H.; Vittal, J. J. *Organometallics*, **1997**, *16*, 1491. (e) Smith, D. P.; Gray, S. D.; Bruck, M. A.; Holmes, R. S.; Wigley, D. E. *Organometallics*, **1992**, *11*, 1275. (f) Strickier, J. R.; Wexler, P. A.; Wigley, D. E. *Organometallics*, **1991**, *10*, 118.
- (4) For selected examples with niobium complexes: (a) Wakgari, H.; Curtis, M. D. *Organometallics*, **1994**, *13*, 2706. (b) Etienne, M.; White, P. S.; Templeton, J. L. *Organometallics*, **1993**, *12*, 4010.
- (5) Selected examples: (a) Allen, S. R.; Green, M.; Norman, N. C.; Paddick, K. E.; Orpen, A. G. *J. Chem. Soc., Dalton Trans.*, **1983**, 1625. (b) Adams, R. D.; Chen, G.; Chen, L.; Wu, W.; Yin, J. *Organometallics*, **1993**, *12*, 3431.
- (6) Selected examples: (a) Cao, C.; Shi, Y.; Odom, A. L. *J. Am. Chem. Soc.*, **2003**, *125*, 2880. (b) Adams, C. J.; Anderson, K. M.; Bartlett, I. M.; Connelly, N. G.; Orpen, A. G.; Paget, T. J. *Organometallics*, **2002**, *21*, 3454.
- (7) (a) Tomson, N. C.; Yan, A.; Arnold, J.; Bergman, R. G. *J. Am. Chem. Soc.*, **2008**, *130*, 11262. (b) La Pierre, H. S.; Arnold, J.; Bergman, R. B.; Toste, F. D. *Angew. Chem. Int. Ed.*, **2011**, *50*, 3900. (d) Gianetti, T. L.; La Pierre, H. S.; Arnold, J. *Eur. J. Inorg. Chem.*, **2013**, 22-23, 3771. (e) Gianetti, T. L.; Nocton, G.; Minasian, S. G.; Tomson, N. C.; Kilcoyne, A. L. D.; Kozimor, S. A.; Shuh, D. K.; Tyliszczak, T.; Bergman, R. G.; Arnold, J. *J. Am. Chem. Soc.*, **2013**, *135*, 3224. (f) Gianetti, T. L.; Bergman, R. G.; Arnold, J. *J. Am. Chem. Soc.*, **2013**, *135*, 8145. (g) Gianetti, T. L.; Bergman, R. G.; Arnold, J. *Chem. Science*, **2014**, DOI: 10.1039/c4sc00006d.
- (8) Gianetti, T. L.; Tomson, N. C.; Arnold, J.; Bergman, R. G. *J. Am. Chem. Soc.*, **2011**, *133*, 14904.
- (9) Alaimo, P. J.; Peters, D. W.; Arnold, J.; Bergman, R. G. *J. Chem. Educ.*, **2001**, *78*, 64.
- (10) (a) Tomson, N. C.; Arnold, J.; Bergman, R. G. *Organometallics*, **2010**, *29*, 5010. (b) Tomson, N. C.; Arnold, J.; Bergman, R. G. *Organometallics*, **2010**, *29*, 2926.
- (11) (a) Sato, F. *J. Organomet. Chem.*, **1985**, *285*, 53. (b) Sato, F.; Ishikawa, H.; Sato, M. *Tetrahedron Lett.*, **1981**, *22*, 85.
- (12) (a) SMART: Area-Detector Software Package; Bruker Analytical X-ray Systems, I. M., WI, 2001-2003. (b) SAINT: SAX Area-detector Integration Program; Bruker Analytical X-ray Systems, I. M., WI, 2003. (c) XPREP; Bruker Analytical X-ray Systems, I. M., WI, 2003. (d) SADABS: Bruker-Nonius Area Detector Scaling and Absorption v. 2.05; Bruker Analytical X-ray Systems, I. M., WI, 2003.
- (13) As determined using the continuous symmetry parameter  $t = (a - b)/60$ , where a and b

are the largest and second-largest angles about the metal center, respectively, See: Addison, A. W.; Rao, T. N.; Reedijk, J.; van Rijn, J.; Verschoor, G. C. *J. Chem. Soc., Dalton Trans.*, **1984**, 1349.

(14) (a) Amaudrut, J.; Sala-Pala, J.; Guerchais, J. E.; Mercier, R. *J. of Organomet. Chem.*, **1990**, *391*, 61. (b) Herberich, G. E.; Mayer, H. *Organometallics*, **1990**, *9*, 2655. (c) Etienne, M.; Mathieu, R.; Donnadiou, B. *J. Am. Chem. Soc.*, **1997**, *119*, 3218.

## Appendix C

### **DFT Calculation for Chapter IV and V**

## C.1 DFT calculations for chapter IV

### C.2.1 Calculated reaction coordinates

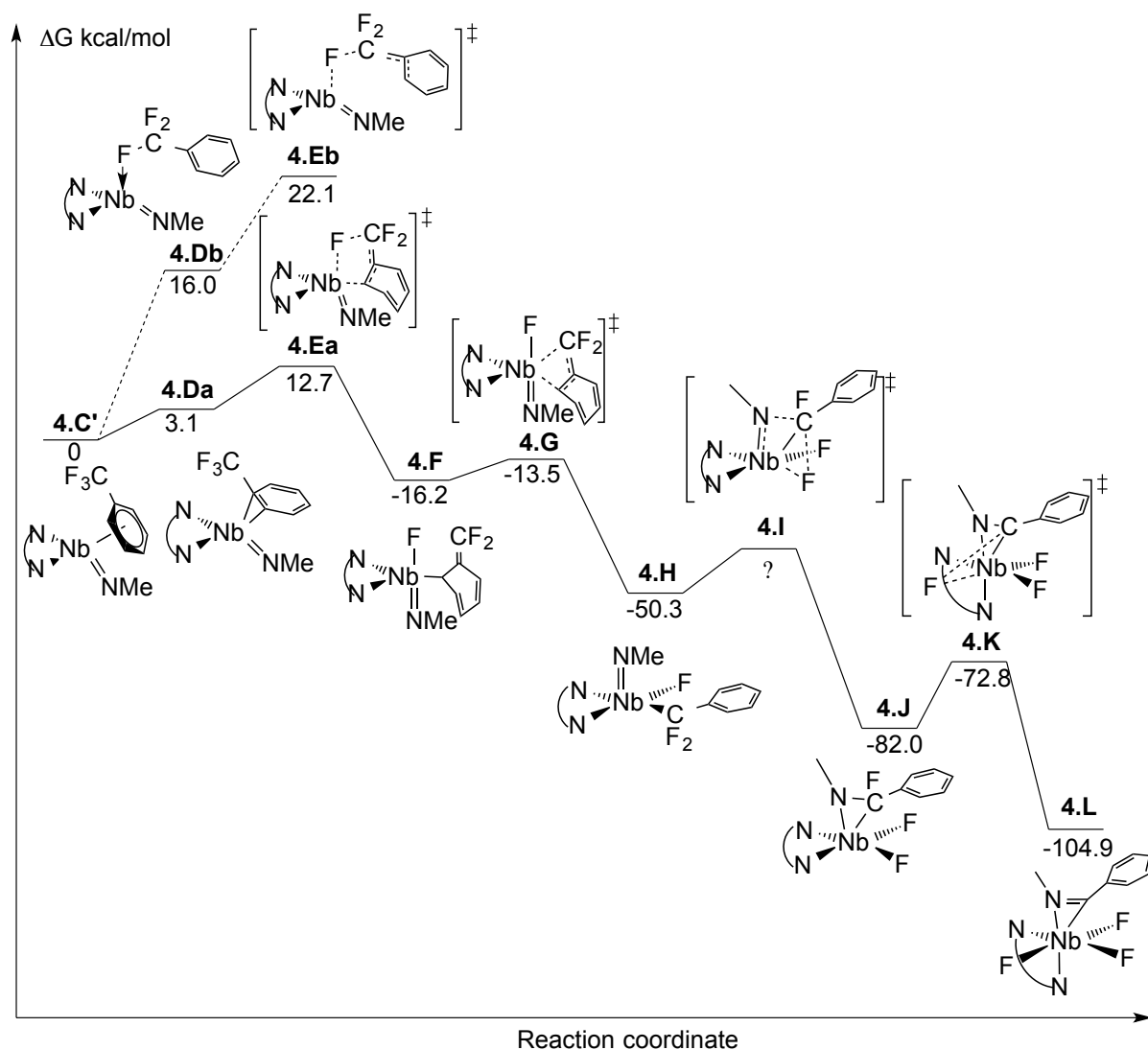
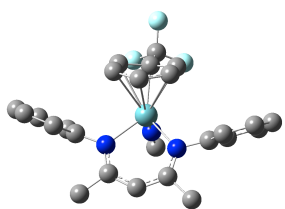


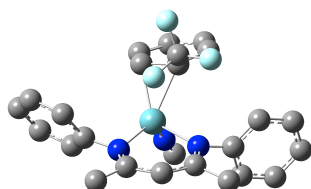
**Figure E.1** DFT calculations of the full transformation

Several attempts were made in order to find the transition state **4.I**. However, none of the calculation submitted was successful, and either converged back to **4.H** or to **4.J**, suggesting a rather flat surface between these two intermediates. Several transition states were found in which the coupling of imido/ $C_{\text{benzylic}}$  happens first to form Nb(III)/imine complex, then followed by C-F activation via oxidative addition. However this pathway was too high in energy to be considered (over  $60 \text{ kcal}\cdot\text{mol}^{-1}$  when compare to **4.H**).

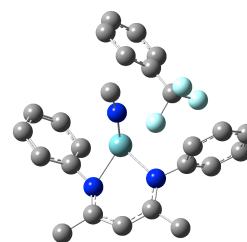
## C.1.2 Intermediates and transition states



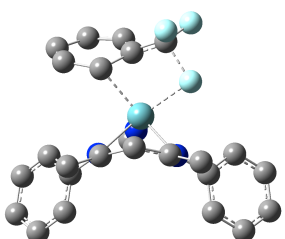
**4.C'**



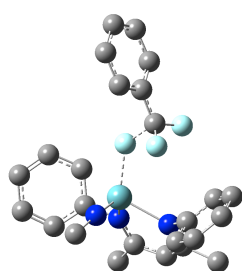
**4.Da**



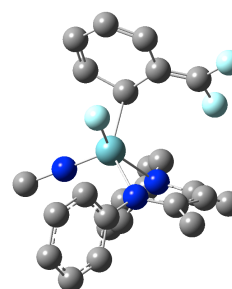
**4.Db**



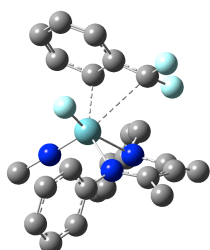
**4.Ea**



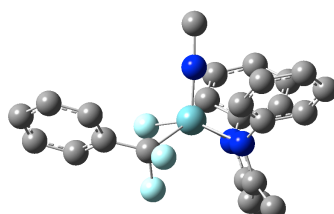
**4.Eb**



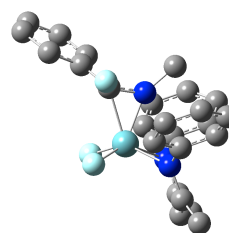
**4.F**



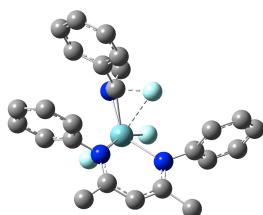
**4.G**



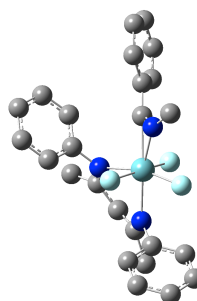
**4.H**



**4.J**



**4.K**



**4.L**

### C.1.3 Energis of intermediates and transition states

**Intermediate 4.C':**

$$G(\text{a.u.}) = -1488.188068$$

**Intermediate 4.Da:**

$$G(\text{a.u.}) = -1488.182111$$

**Intermediate 4.Db:**

$$G(\text{a.u.}) = -1488.162656$$

**Transition state 4.Ea:**

$$G(\text{a.u.}) = -1488.166753$$

$$n = -333.8 \text{ cm}^{-1}$$

**Transition state 4.Eb:**

$$G(\text{a.u.}) = -1488.152645$$

$$n = -402.3 \text{ cm}^{-1}$$

**Intermediate 4.F:**

$$G(\text{a.u.}) = -1488.214388$$

**Transition state 4.G:**

$$G(\text{a.u.}) = -1488.209404$$

$$n = -135.5 \text{ cm}^{-1}$$

**Intermediate 4.H:**

$$G(\text{a.u.}) = -1488.270457$$

**Intermediate 4.J:**

$$G(\text{a.u.}) = -1488.318791$$

**Transition state 4.K:**

$$G(\text{a.u.}) = -1488.302140$$

$$n = -127.0 \text{ cm}^{-1}$$

**Intermediate 4.L:**

$$G(\text{a.u.}) = -1488.355252$$



## C.2 DFT calculations for chapter V

### C.2.1 C-F bond activation

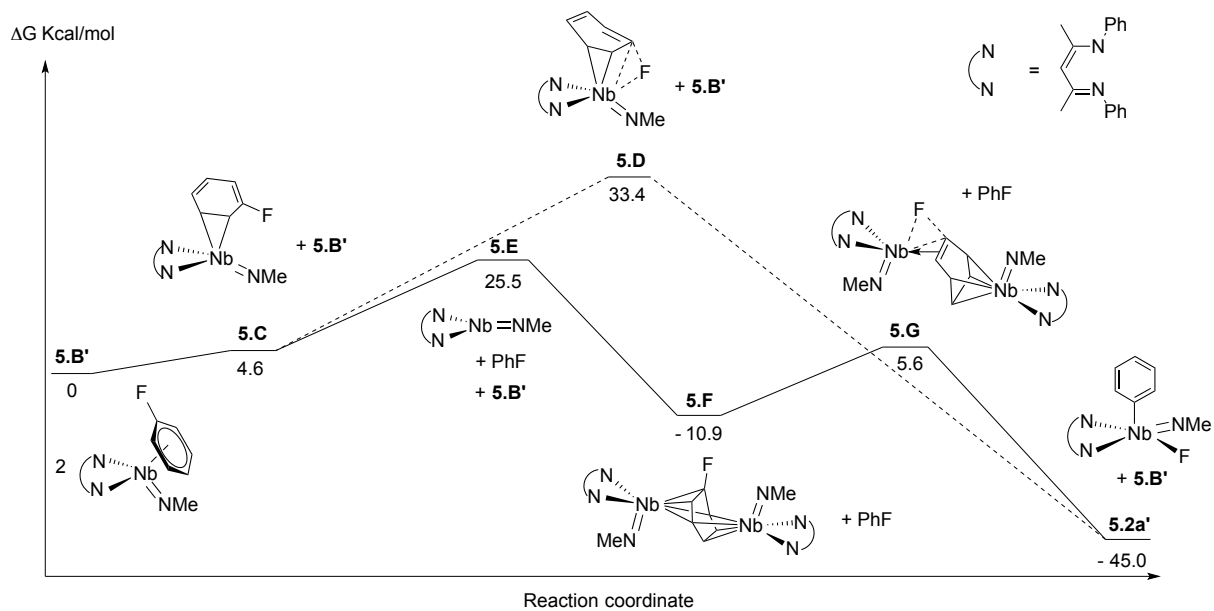
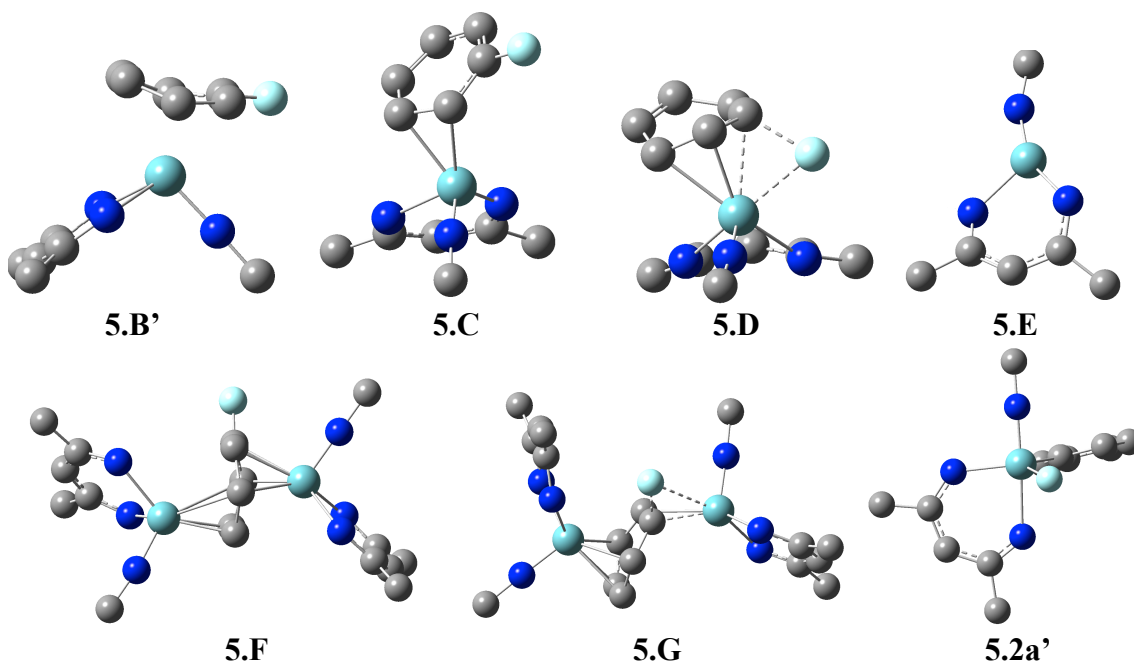


Figure C. 2



## C.2.2 C-F vs C-H bond activation

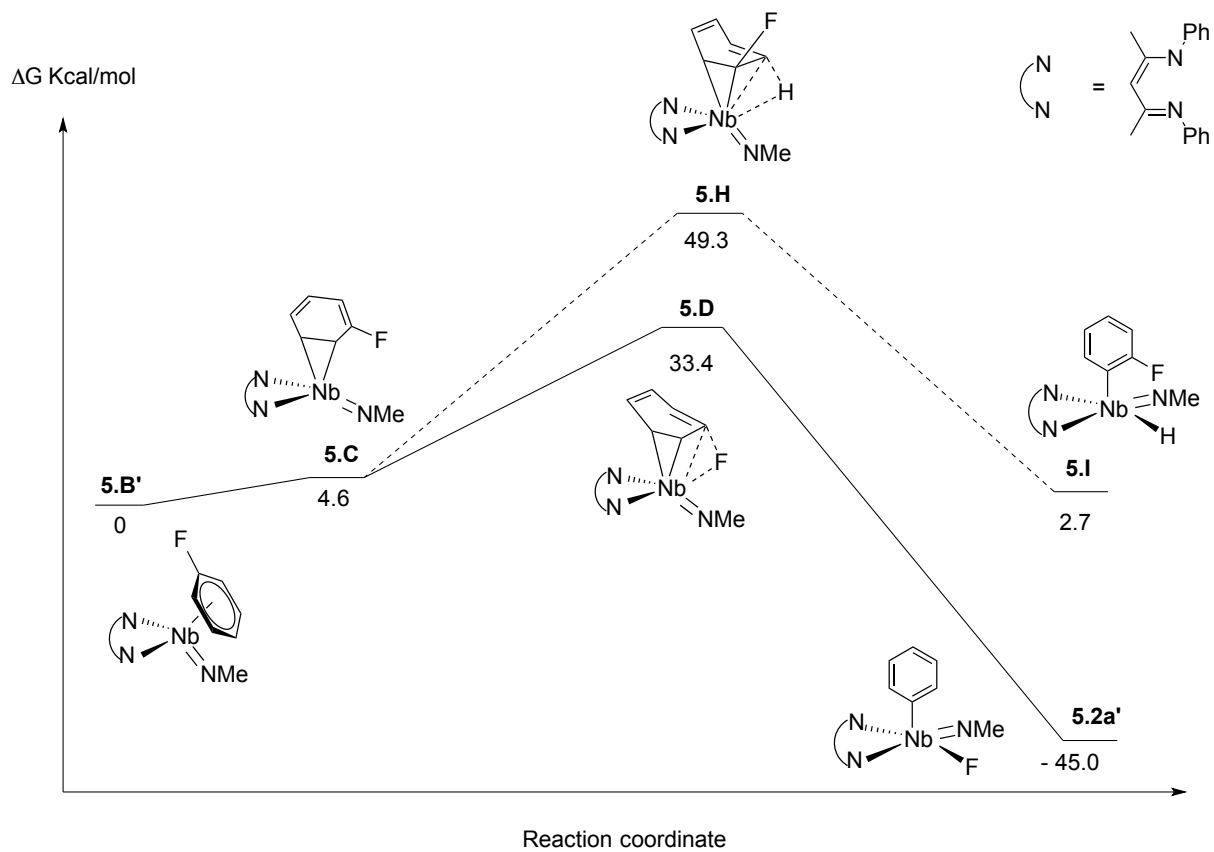
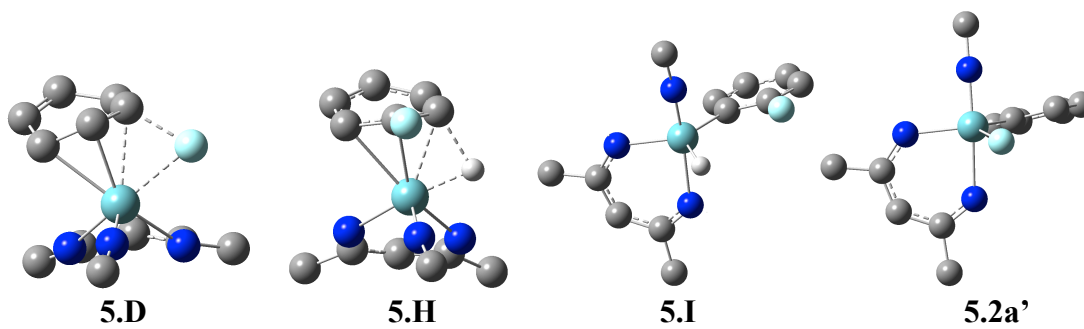


Figure C. 3



### C.2.3 Energies of intermediates and transition states

**C<sub>6</sub>H<sub>5</sub>F:**

$$G(\text{a.u.}) = -331.11256$$

**Intermediate 5.B':**

$$G(\text{a.u.}) = -1249.208739$$

**Intermediate 5.C:**

$$G(\text{a.u.}) = -1249.201423$$

**Transition state 5.D:**

$$G(\text{a.u.}) = -1249.155525$$
$$n = -271.57 \text{ cm}^{-1}$$

**Intermediate 5.E:**

$$G(\text{a.u.}) = -918.055493$$

**Intermediate 5.F:**

$$G(\text{a.u.}) = -2167.322205$$

**Transition state 5.G:**

$$G(\text{a.u.}) = -2167.296004$$
$$n = -234.12 \text{ cm}^{-1}$$

**Transition state 5.H:**

$$G(\text{a.u.}) = -1249.130173$$
$$n = -271.59 \text{ cm}^{-1}$$

**Intermediate 5.I:**

$$G(\text{a.u.}) = -1249.204473$$

**Intermediate 5.2a':**

$$G(\text{a.u.}) = -1249.280496$$